RADIOLOŠKI VJESNIK
RADIOLOGICAL JOURNAL

radiology • radiotherapy • nuclear medicine

Godina: XLIX | Broj: 1/2025 | ISSN 0352-9835 (Tisak) | ISSN 2671-0781 (Online)



Availability of magnetic resonance imaging during the COVID-19 pandemic at the Children's disease clinic in Zagreb

Comparison of magnetic resonance imaging of the prostate 1.5T and 3T

The Efficiency of Artificial Intelligence in Distinguishing Malignant from Benign Ultrasound Features of Breast Tumors

Radiological Management of Infections in Immunocompromised Patients

HRVATSKO DRUŠTVO RADIOLOŠKE TEHNOLOGIJE

RADIOLOŠKI VJESNIK
Radiological Journal
1/2025
ISSN 0352-9835 (Tisak)
ISSN 2671-0781 (Online)

Publisher / Nakladnik
HRVATSKO DRUŠTVO
RADIOLOŠKE TEHNOLOGIJE
Mlinarska cesta 38
10000 Zagreb
e-mail: info@hdrt.hr

Editor in Chief / Glavni urednik
Damir Ciprić

Deputy editors / Zamjenici glavnog urednika
Velimir Karadža,
Frane Mihanović

Secretary / Tajnik
Branko Kovalisko

Editorial Board / Uredički odbor
Vladimir Bahun, Andrija Čop, Dražen Horvatinec, Matija Hranić, Maja Karić, Vedran Manestar, Tatjana Matijaš, Rita Simões, Enis Tinjak

Scientific Advisory Council / Uredički savjet
Dario Faj, Marija Frković, Hrvoje Hršak, Melita Kukuljan, Ivana Kralik, Goran Roić, Tamer Salha, Klaudija Višković

For publisher / Za nakladnika
Damir Ciprić
damir.cipric@gmail.com
Velimir Karadža
karadzav@gmail.com

Graphic design / Grafičko uređenje
Željko Podoreški

Riječ urednika

Dragi čitatelji Radiološkog Vjesnika,

Prvo izdanje Radiološkog vjesnika u 2025. godini, baš kao i sezona virusa i gripe u zimi koja je upravo iza nas, podsjeća na važnost radiološke obrade infektivnih bolesti dišnog sustava.

Iako je COVID-19 pandemija iza nas, koronavirus kao i virus gripe su se pokazali kao vrlo aktualan, pa i vrlo ozbiljan zdravstveni problem krajem 2024. i početkom 2025. godine.

Na tom tragu, u ovom broju Vjesnika vrlo zanimljivi članci nas podsjećaju na suvremene dijagnostičke mogućnosti kao i na dostupnost radiološke dijagnostike u vrijeme epidemije te rad sa imunokompromitiranim pacijentima. Tu je sada neizostavno i korištenje dubokih neuronskih mreža i umjetne inteligencije u dijagnostičkoj obradi infekcija, ali i sve naglašenija potreba za korištenjem dubokog učenja u dijagnostici, interpretaciji i evaluaciji malignih bolesti. Kroz ovo nas sve vode izvorni znanstveni radovi, pregledi dostupne literature i stručni članci, koji nadalje daju i uvid u korištenje magnetske rezonancije u dijagnostici određenih onkoloških bolesti, a potom i u planiranju i provođenju radioterapije, za sve skupine pacijenata i one najmlađe, u pedijatrijskoj onkologiji.

Sa zadovoljstvom najavljujemo i neka stručna događanja koja su pred nama u ovoj godini, poput Radionice Hrvatskog društva radiološke tehnologije – OKRT 9 u prvoj i 6. Kongresa radiološke tehnologije u drugoj polovici godine.

U ime Uredničkog odbora Radiološkog vjesnika, Tatjana Matijaš.

A word from the Editor

Dear readers of Radiological Journal,

The first issue of the Radiological Journal in 2025, much like the flu season in the winter that is just behind us, reminds us of the importance of radiological treatment of infectious diseases of the respiratory system.

Although the COVID-19 pandemic is behind us, the coronavirus and the influenza virus have proven to be very current, and even a very serious health problem at the end of 2024 and the beginning of 2025.

Along these lines, in this issue of the Journal, very interesting articles remind us of modern diagnostic capabilities as well as the availability of radiological diagnostics during the epidemic and work with immunocompromised patients. The use of deep neural networks and artificial intelligence in the diagnostic treatment of infections is now indispensable, but also the increasingly pronounced need for the use of deep learning in the diagnosis, interpretation and evaluation of malignant diseases. We are guided through all of this by original scientific papers, reviews of available literature and professional articles, which also provide insight into the use of magnetic resonance imaging in the diagnosis of certain oncological diseases, as well as in the planning and delivery of radiation therapy, for all groups of patients, including the youngest, in paediatric oncology.

We are very pleased to announce some professional events that are ahead of us this year, such as the Workshop of the Croatian Association of Radiation Technology – QART 9 in the first, and the 6th Congress of Radiological Technology in the second half of the year.

On behalf of the Editorial Board of the Radiological Journal, Tatjana Matijaš.

Hrčak doi EBSCO

SADRŽAJ

2 **Availability of magnetic resonance imaging during the COVID-19 pandemic at the Children's disease clinic in Zagreb**
Jurica Folnožić, Nada Tomasović-Mrčela
Original scientific paper (Izvorni znanstveni rad)

10 **Učinkovitost umjetne inteligencije u razlikovanju malignih od benignih ultrazvučnih osobina tumora dojki**
Filip Marković, Damir Štimac
Izvorni znanstveni članak (Original scientific paper)

16 **Radiological Management of Infections in Immunocompromised Patients**
Domagoj Babić, Sanja Lovrić Kojundžić
Review article (Pregledni rad)

26 **Present and future role of MRI in radiotherapy**
Endira Al-Khazae, Frane Mihanović
Review article (Pregledni rad)

38 **Comparison of magnetic resonance imaging of the prostate 1.5T and 3T**
Goran Kutlić, Krešimir Dolić
Review paper (Pregledni rad)

48 **HyperSight Spotlight: Larger Field of View**
Promotivni članak (Promotional article)

50 **Advantages and limitations of artificial intelligence tools in the analysis of thoracic computed tomography images in patients with COVID-19 pneumonia – a review**
Nina Mrvoš, Melita Kukuljan, Maja Karić, Klaudija Višković
Review article (Pregledni rad)

66 **Radiological modalities in the detection, assessment and monitoring of COVID-19 infection**
Nives Grepo, Maja Marinović Guić
Review paper (Pregledni rad)

78 **Radioterapija kod djece**
Marta Pekvarić, Velimir Karadža
Stručni rad (Professional paper)

84 **Implementation and Practice for Image-guided Stereotactic Body Radiotherapy**
Ivan Balentović
Sažetak sa skupa (Meeting abstract)

88 **Osvrt na Kongres "Dani radiološke tehnologije" i I. Simpozij studenata radiološke tehnologije**
Sažetak sa skupa (Meeting abstract)

95 **Zaštita od zračenja u različitim područjima radiološke tehnologije u Republici Hrvatskoj**
9. Radionica OKRT
Program radionice

Autori/ce pridržavaju sva prava. Tekstovi u časopisu odražavaju stavove autora/ica i nisu nužno stavovi uredništva niti Hrvatskog društva radiološke tehnologije.

ORIGINAL SCIENTIFIC PAPER (IZVORNI ZNANSTVENI RAD)

Availability of magnetic resonance imaging during the COVID-19 pandemic at the Children's disease clinic in Zagreb

Jurica Folnožić[1,2], **Nada Tomasović-Mrčela**[2,3]

[1] Zagreb Clinic for Children's Diseases, Department of Pediatric Radiology

[2] University of Split, University Department of Health Studies, Split, Croatia

[3] Teaching Institute for Public Health 'Dr. Andrija Štampar', Zagreb, Croatia

Corresponding author: Jurica Folnožić, email: folnozic@gmail.com

DOI: https://doi.org/10.55378/rv.49.1.1

Abstract

The study analyzed the impact of the COVID-19 pandemic on the availability of MRI services for pediatric patients in five diagnostic groups according to ICD-10 that were most prevalent in the pediatric diagnostics of the Children's Disease Clinic in Zagreb from January 1, 2018, to December 31, 2021.

There were no statistically significant differences regarding the age of patients ordered for MRI scans in the most frequent diagnostic groups between the pre-pandemic years (2018, 2019) and the pandemic years (2020, 2021) at the clinic's outpatient and inpatient departments. Likewise, no statistically significant differences were found in the average waiting time, which was 17 weeks, for patients referred for MRIs in the pre-pandemic (2018, 2019) and pandemic (2020, 2021) years.

The negative trend of decreasing the number of scans can be linked to longer intervals between individual scans, as a result of the applicable epidemiological guidelines, as well as concerns from parents about infection, who voluntarily postponed elective check-ups, as well as due to their own or their child's positive PCR test for coronavirus.

In the case of an increase in the number of scans, it can be attributed to a higher number of patients referred from other institutions for MRI scans, especially oncology patients.

Keywords: children; quality; MRI; pandemic; imaging

Introduction

The COVID-19 pandemic in the 21st century led to numerous changes and phenomena such as isolation and self-isolation, high numbers of daily deaths, the conversion of departments and entire hospitals into COVID departments, and then COVID hospitals, as well as the redistribution of healthcare workers to work in COVID wards. Patient associations and the Ombudsperson for Children warned in the media about the inaccessibility of certain healthcare services during the pandemic (1).

At the Children's Disease Clinic 'Klaićeva', almost all Magnetic Resonance Imaging (MRI) diagnostics for children in Croatia are performed, especially for children who require general anesthesia (GA). At the beginning of the pandemic and with the introduction of epidemiological measures, there were demanding changes for healthcare workers at the Radiology Department and the need for various adjustments to the new situation, including shifting the time between individual scans of young patients, ventilating the space between scans, and increased disinfection of the space.

MRI is not considered a dangerous or harmful examination for health (2,3). The procedure typically lasts from 20 to 60 minutes. The main advantages of MRI are the better contrast representation of soft tissues (water, fat, muscles, and other soft tissues are more distinctly differentiated compared to CT scans). It is especially an important method for diagnosing diseases of the central nervous system (brain and spinal cord), pelvic organs, joints, and soft tissues. MRI images provide important information to doctors in diagnosing various diseases and conditions (4). Due to the absence of radiation risk, this method can be repeated if there is dissatisfaction with the image quality or if the child is restless, multiple times, without harmful effects on the child's health. What can objectively cause discomfort and fear in a child are the noise of the device and the stay inside the machine's tun-

nel. Therefore, the child's companion must be a parent or guardian (5).

Quality indicators in the healthcare system not only describe the level of performance in standards but also provide a fundamental dimension to healthcare that relates to: efficiency, accessibility, safety, effectiveness, justification, patient-centeredness, timeliness, appropriateness, quality improvement, and others, with efficiency and effectiveness being key in every definition of healthcare quality.

In line with the above, the Children's Disease Clinic 'Klaićeva' continuously strives to ensure the availability of MRI services by systematically improving accessibility to MRI exams through reducing official waiting lists for MRI diagnostics and maximizing the use of available MRI equipment. Parents of pediatric patients are promptly reminded of their scheduled appointments, and confirmation of attendance is requested, so that in case the patient cannot attend the planned examination on time, another patient can be called instead.

Furthermore, the patient is prepared for the examination with additional instructions on which recent results should be presented during the exam (e.g., kidney function parameters), and the parent is reminded of which medical documentation needs to be presented during the examination. Special attention is given to the successful completion of the exam, applying all current norms and standards to avoid the need for repeating the examination, as well as to ensure that the duration of the exam is time-adjusted for young patients. The most important criterion that must be considered is the care for the health of pediatric patients, which must be a top priority in order to ensure that the quality of healthcare is at the highest level.

During the COVID-19 pandemic, wearing protective masks and other protective equipment contributed to an even greater increase in anxiety among 'young' patients, and at the Children's Disease Clinic 'Klaićeva,' a solution to this problem was found.

Instead of a large, gray, intimidating device that even adults can be afraid of, let alone children, the MRI diagnostic room was transformed into a pleasant yellow submarine environment, with elements of dolphins, fish, and an octopus on the walls. Thanks to this intervention in the space, healthcare workers daily witness the joy of children, who no longer perceive the MRI exam as something unpleasant but as a place where they will sail in a submarine among colorful fish. As a result, the stress level in children has been reduced to the minimum possible level.

Aim of the paper

The aim of this paper was to investigate the availability of MRI services for children during the COVID-19 pandemic in relation to the diagnosis of patients.

Methods

This is a retrospective study – conducted at the Children's Disease Clinic Zagreb, within the Department of Pediatric Radiology, MRI diagnostic unit, for a four-year period from January 1, 2018, to December 31, 2021.

The study focuses on the difference in the availability of the diagnostic procedure conducted for patients referred for MRI exams in the pre-pandemic years (from January 1, 2018, to December 31, 2019) and the years of the COVID-19 pandemic (from January 1, 2020, to December 31, 2021), in relation to the patients' diagnoses in the MRI diagnostic unit.

Prior to the study, we received approval from the Ethics Committee of the Children's Disease Clinic Zagreb during an electronic meeting, which decided that there were no ethical objections to conducting this research, and the director's consent for conducting the study was obtained.

The Hospital Information System (HIS) in its functional division recognizes the availability of data in the outpatient clinic (processing patients coming from external institutions and those referred by pediatricians from primary healthcare) and inpatient (patients receiving hospital treatment) (6).

The main input data, or the source of data for this study, was the HIS of the Children's Disease Clinic Zagreb. Data was collected on the total number of days on the



Figure 1. MRI machine at the Zagreb Clinic for Children's Diseases Source: Children's Disease Clinic Zagreb

official waiting list for MRI scans and the total number of patients on the official waiting list for MRI scans from January 1, 2018, to December 31, 2021.

Further review of the database –HIS, for patients who underwent MRI exams, recorded the following data: diagnostic (DG) groups, age, general anesthesia (GA), outpatient clinic, inpatient.

The diagnostic groups according to the International Classification of Diseases (ICD-10) that were singled out and covered by this study were selected based on the most frequent number of performed MRI exams.

Based on the data obtained on the examination date and the date of referral for the examination, the waiting time for the MRI exam at the diagnostic unit was calculated. The standard set by the Agency for Quality and Accreditation in Health and Social Care regarding waiting times for MRI procedures for urgent conditions is up to 24 hours, and for exams that are scheduled in advance, up to 18 weeks (7).

Results

The most frequent diagnostic groups according to the ICD-10 classification in this study are:

- DG group 1: C00 – D48 – Neoplasms
- DG group 2: G00 – G99 – Diseases of the Nervous System
- DG group 3: M00 – M99 – Diseases of the Musculoskeletal System and Connective Tissue
- DG group 4: Q00 – Q99 – Congenital Malformations, Deformations, and Chromosomal Abnormalities
- DG group 5: R00 – R99 – Symptoms, Signs, and Abnormal Clinical and Laboratory Findings, Not Elsewhere Classified
- DG group 6: Other ICD-10 diagnostic groups (6).

Table 1. Proportion of patients referred for diagnostic groups scanned by MRI in the outpatient clinic and inpatient setting during pre-pandemic and pandemic years (Klaićeva Hospital, Zagreb, Croatia).

	2018.		2019.		2020.		2021.	
Proportion (%)	Outpatient clinic	Inpatient departments	Outpatient clinic	Inpatient departments	Outpatient clinic	Inpatient departments	Outpatient clinic	Inpatient departments
Dg. group 1: C00 – D48	9,5	26,3	10,1	27,4	13,7	26,1	11,7	25,6
Dg. group 2: G00 – G99	21	14,5	16,6	17,4	16,8	22,3	16,2	23,7
Dg. group 3: M00 – M99	23,5	4,3	22,9	4,1	20,7	5,3	20,8	3
Dg. group 4: Q00 – Q99	7,4	9	7,5	5	7,7	3,4	6,9	3
Dg. group 5: R00 – R99	16,4	9,8	17,5	13,8	17	10,2	17,9	15,8
Dg. group 6: other dg. group MKB-10	21,8	35,7	25	32,1	23,9	32,5	26,2	28,6

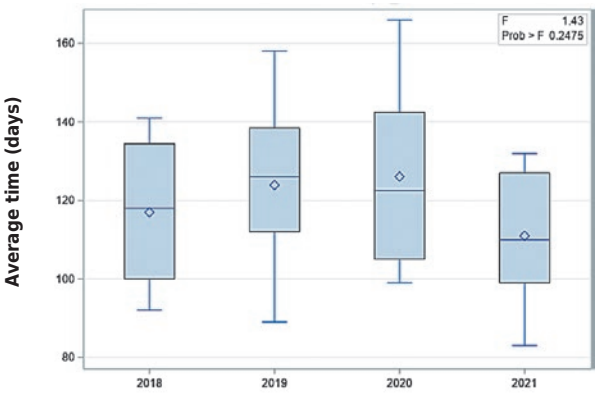
Table 2. Proportion of patients referred for diagnostic groups under GA scanned by MRI in the outpatient clinic and inpatient departments during pre-pandemic and pandemic years (Klaićeva Hospital, Zagreb, Croatia).

	2018.		2019.		2020.		2021.	
Proportion (%)	Outpatient clinic	Inpatient departments	Outpatient clinic	Inpatient departments	Outpatient clinic	Inpatient departments	Outpatient clinic	Inpatient departments
Dg. group 1: C00 – D48	9,9	25,8	9,8	26,3	12,4	29,4	10,7	26,8
Dg. group 2: G00 – G99	22,3	16,4	16,3	16,7	20,4	18,5	17,2	23,9
Dg. group 3: M00 – M99	6,3	1,9	7	3,5	7,6	4,4	7,4	1,4
Dg. group 4: Q00 – Q99	15,5	13,4	14	9,5	12,4	5,1	11,4	5
Dg. group 5: R00 – R99	20,3	5,4	23	10,1	20,1	8,3	23,8	13
Dg. group 6: other dg. group MKB-10	25,4	36,8	29,5	33,5	26,8	33,9	29,2	29,7

Table 3. Average age (years) of patients referred for diagnostic groups scanned by MRI in the outpatient clinic and inpatient departments during pre-pandemic and pandemic years (Klaićeva Hospital, Zagreb, Croatia).

	2018.		2019.		2020.		2021.	
Udio (%)	**Outpatient clinic**	**Inpatient departments**	**Outpatient clinic**	**Inpatient departments**	**Outpatient clinic**	**Inpatient departments**	**Outpatient clinic**	**Inpatient departments**
Dg. group 1: C00 – D48	12	7,4	12,5	7,2	12,7	6,4	12,2	7,6
Dg. group 2: G00 – G99	11,7	5,9	11,7	8,4	11,6	7,2	11,7	7,9
Dg. group 3: M00 – M99	13,6	11,2	13,4	9,3	14	7,9	13,4	10,2
Dg. group 4: Q00 – Q99	9,8	2,3	10,1	2,3	10,8	2,6	9,8	3,1
Dg. group 5: R00 – R99	11	9,3	11,4	8,9	11,6	8,6	11,1	7,8
Dg. group 6: other dg. group MKB-10	11,7	6,4	11,7	6,7	11,7	6	11,2	6,8

Chart 1. Box plot of the average waiting time for all referred patients scanned by MRI between pre-pandemic and pandemic years (Klaićeva Hospital, Zagreb, Croatia).



Pre-pandemic (2018, 2019) and pandemic (2020, 2021) years

The shown chart 1. shows no statistically significant differences in the average waiting time for all referred patients from diagnostic groups scanned by MRI between the pre-pandemic and pandemic years.

In the shown chart 2. the proportion of referred patients for diagnostic group 1 (C00 – D48) – neoplasms, scanned in the outpatient clinic during the pre-pandemic year of 2018 (9.5 ± 0.6 %) was 34% lower (p = 0.0001) than in 2020 (13.7 ± 0.8 %) and 21% lower (p = 0.02) than in 2021 (11.7 ± 0.7 %). Similarly, the proportion of referred patients in the pre-pandemic year of 2019 (10.1 ± 0.7 %) was 30% lower (p = 0.001) than in 2020 (13.7 ± 0.8 %).

In the shown chart 3. the proportion of referred patients for diagnostic group 2 (G00 – G99) – diseases of the nervous system, scanned in the outpatient clinic during the pre-pandemic year of 2018 (21 ± 0.9 %) was 1.31 times higher (p = 0.001) than in 2020 (16.8 ± 0.9

Chart 2. Graphical representation of the odds ratio and 95% confidence interval for the number of referred patients for diagnostic group 1 (C00 – D48) scanned by MRI in the outpatient clinic between pre-pandemic and pandemic years (Klaićeva Hospital, Zagreb, Croatia).

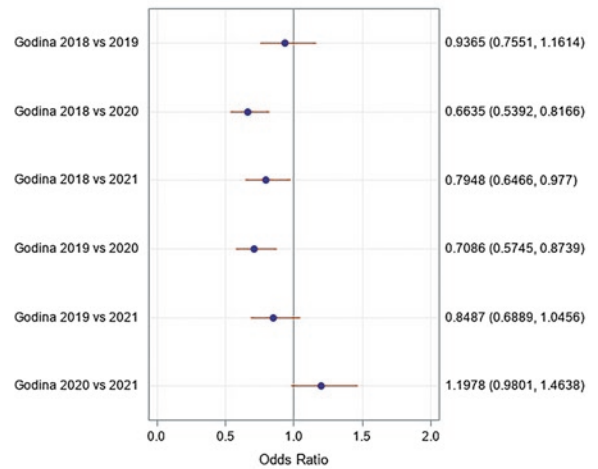


Chart 3. Graphical representation of the odds ratio and 95% confidence interval for the number of referred patients for diagnostic group 2 (G00 – G99) scanned by MRI in the outpatient clinic between pre-pandemic and pandemic years (Klaićeva Hospital, Zagreb, Croatia).

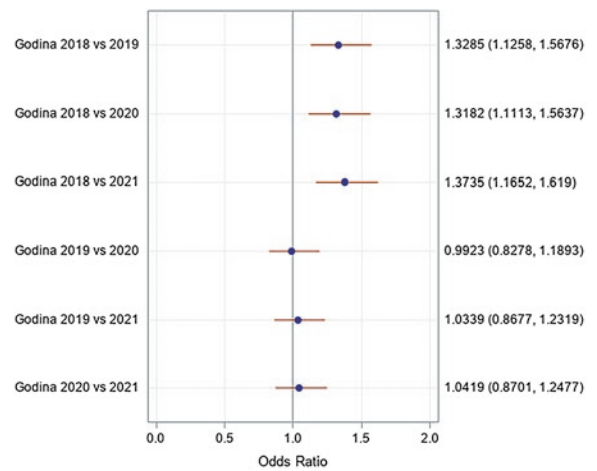


Chart 4. Graphical representation of the odds ratio and 95% confidence interval for the number of referred patients for diagnostic group 3 (M00 – M99) scanned by MRI in the outpatient clinic between pre-pandemic and pandemic years (Klaićeva Hospital, Zagreb, Croatia).

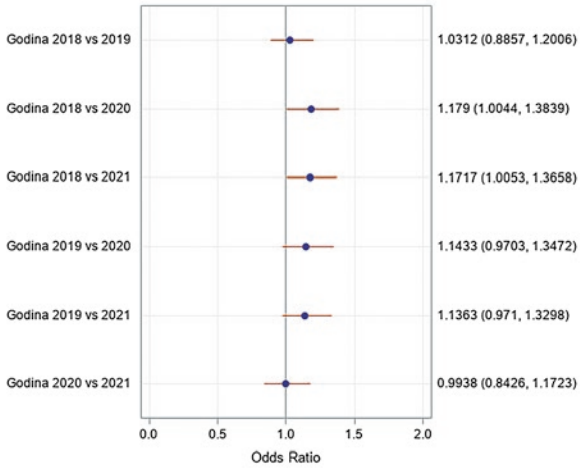
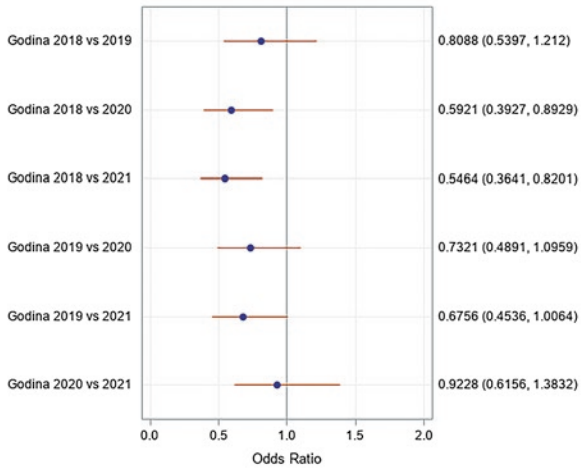


Chart 6. Graphical representation of the odds ratio and 95% confidence interval for the number of referred patients for diagnostic group 2 (G00 – G99) scanned by MRI in the inpatient department between pre-pandemic and pandemic years (Klaićeva Hospital, Zagreb, Croatia).



%) and 1.37 times higher (p = 0.0002) than in 2021 (16.2 ± 0.8 %). Additionally, a statistically significant difference was observed in the proportion of referred patients (p = 0.0008) between the pre-pandemic years, where in 2018 (21 ± 0.9 %) there were 1.32 times more patients compared to 2019 (16.6 ± 0.8 %).

In the shown chart 4. the proportion of referred patients for diagnostic group 3 (M00 – M99) – diseases of the musculoskeletal system and connective tissue, scanned in the outpatient clinic during the pre-pandemic year of 2018 (23.5 ± 0.9 %) was 1.17 times higher (p = 0.04) than in 2020 (20.7 ± 1 %) and 1.17 times higher (p = 0.04) than in 2021 (20.8 ± 0.9 %).

In the shown chart 5. the proportion of referred patients for diagnostic group 6 – other diagnostic groups (ICD-10), scanned in the outpatient clinic during the pre-pandemic year of 2018 (21.9 ± 0.9 %) was 22% lower (p = 0.001) than in 2021 (26.2 ± 1 %). Additionally, a statistically significant difference was observed in the proportion of referred patients (p = 0.02) between the pre-pandemic years, where in 2018 (21.9 ± 0.9 %) there were 16% fewer patients compared to 2019 (25 ± 1 %).

In the shown chart 6. the proportion of referred patients for diagnostic group 2 (G00 – G99) – diseases of the nervous system, scanned in the inpatient department during the pre-pandemic year of 2018 (14.5 ± 1.8 %) was 41% lower (p = 0.01) than in 2020 (22.3 ± 2.5 %) and 46% lower (p = 0.003) than in 2021 (23.7 ± 2.6 %).

In the shown chart 7. the proportion of referred patients for diagnostic group 4 (Q00 – Q99) – congenital mal-

Chart 5. Graphical representation of the odds ratio and 95% confidence interval for the number of referred patients for diagnostic group 6 – other diagnostic groups (ICD-10) scanned by MRI in the outpatient clinic between pre-pandemic and pandemic years (Klaićeva Hospital, Zagreb, Croatia).

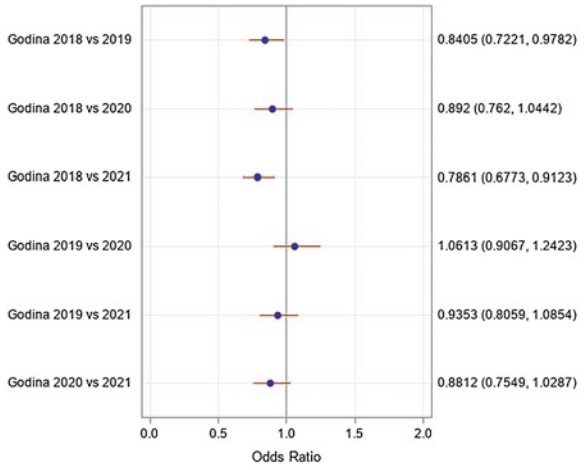


Chart 7. Graphical representation of the odds ratio and 95% confidence interval for the number of referred patients for diagnostic group 4 (Q00 – Q99) scanned by MRI in the inpatient department between pre-pandemic and pandemic years (Klaićeva Hospital, Zagreb, Croatia).

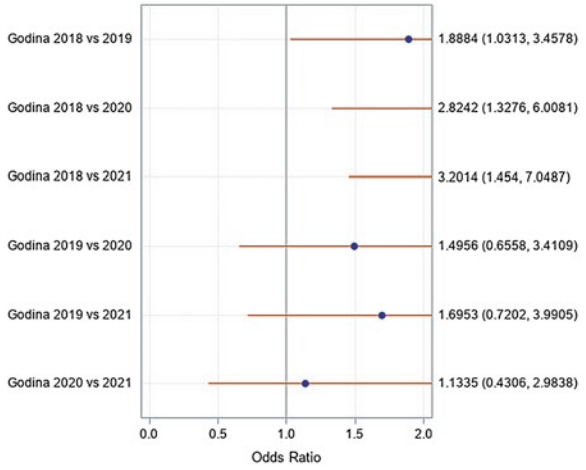
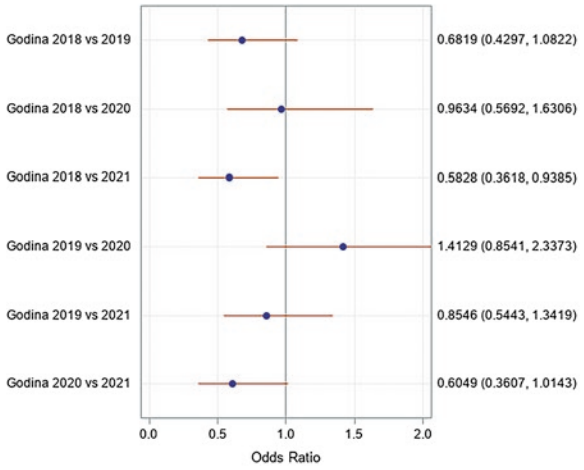


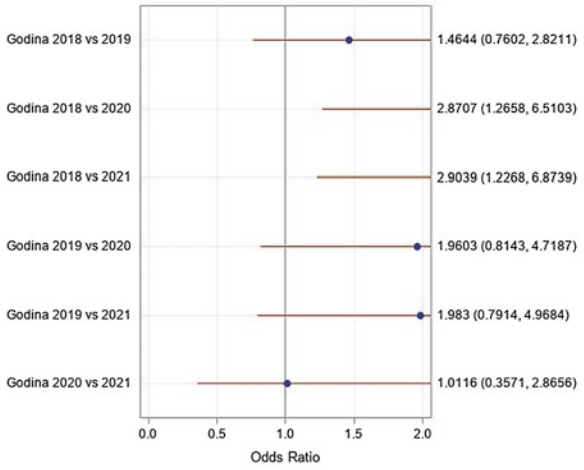
Chart 8. Graphical representation of the odds ratio and 95% confidence interval for the number of referred patients for diagnostic group 5 (R00 – R99) scanned by MRI in the inpatient department between pre-pandemic and pandemic years (Klaićeva Hospital, Zagreb, Croatia).



formations, deformities, and chromosomal abnormalities, scanned in the inpatient department during the pre-pandemic year of 2018 (9 ± 1.5 %) was 2.82 times higher (p = 0.007) than in 2020 (3.4 ± 1.1 %) and 3.2 times higher (p = 0.003) than in 2021 (3 ± 1 %). Additionally, a statistically significant difference was observed in the proportion of referred patients (p = 0.03) between the pre-pandemic years, where in 2018 (9 ± 1.5 %) there were 1.88 times more patients compared to 2019 (5 ± 1.1 %).

In the shown chart 8. the proportion of referred patients for diagnostic group 5 (R00 – R99) – symptoms, signs, and abnormalities of clinical and laboratory findings not classified elsewhere, scanned in the inpatient department during the pre-pandemic year of 2018 (9.8 ± 1.5 %) was 42% lower (p = 0.02) than in 2021 (15.8 ± 2.2 %).

Chart 9. Graphical representation of the odds ratio and 95% confidence interval of the number of patients referred for diagnostic group 4 (Q00 – Q99) – congenital malformations, deformities, and chromosomal abnormalities, scanned under GA in the inpatient department, using MRI between pre-pandemic and pandemic years (Klaićeva Hospital, Zagreb, Croatia).



On the shown graph 9. the proportion of referred patients for diagnostic group 4 (Q00 – Q99) – congenital malformations, deformities, and chromosomal abnormalities, scanned under GA in the inpatient department in the pre-pandemic year of 2018 (13.4 ± 2.4%) was 2.87 times higher (p = 0.01) compared to the year 2020 (5.1 ± 1.7%) and 2.9 times higher (p = 0.01) compared to the year 2021 (5.0 ± 1.8%).

Discussion

The study analyzed archival data collected from the HIS during regular clinical work at the Clinic for Children's Diseases in Zagreb. The impact of the COVID-19 pandemic on the availability of MRI services for pediatric patients was analyzed according to the ICD-10 classification. For the so-called pre-pandemic years, data from 2018 and 2019 were used, while for the so-called pandemic years, data from 2020 and 2021 were used.

Like any other method, MRI scanning also has its drawbacks, such as the duration of the procedure, the cost of the exam, and the confined space of the MRI machine where the child is alone during the scan, which can trigger claustrophobia in children. The main disadvantage of the MRI machine for children is the long duration of the procedure (on average from 20 to 60 minutes), which is especially problematic for very young children, for whom sedation and GA are often required (9). The process is particularly challenging for children with neurodevelopmental disorders, where facing new task demands in an unfamiliar environment can be more difficult due to symptoms-related difficulties.

In 2020, the COVID-19 pandemic emerged, significantly altering the lives of individuals in all aspects of personal, social, work, and life functioning. During the first months of the pandemic, before the advent of an effective vaccine, healthcare professionals faced an especially large challenge in providing care under the new conditions (10). In the world, and also in Croatia, public campaigns urged people to 'stay at home' and avoid unnecessary gatherings and visits to healthcare facilities. In addition to periods of full or partial quarantine, the fear of infection in healthcare facilities discouraged patients from seeking medical services. This resulted in delays in various diagnostic and therapeutic procedures that could be considered less urgent, such as MRI scans for certain indications, either by the healthcare system or by the patients themselves. In some countries, a decrease in the number of MRI procedures was recorded, although to this day, national studies have not been reported (11).

This study found no statistically significant differences in the age of the patients referred for MRI scans in the most common diagnostic groups between the pre-pandemic and pandemic years, either for those scanned in the outpatient clinic or in the hospital at the Clinic for Children's Diseases in Zagreb. Likewise, no statistically significant differences were found in the average waiting time for patients referred for MRI scans between the pre-pandemic and pandemic years.

The proportion of patients referred for MRI scans under GA did not show statistically significant differences between the pre-pandemic and pandemic years for most diagnostic groups. The only exception was for diagnostic

group 4 (Q00 – Q99) – congenital malformations, deformities, and chromosomal abnormalities, where the proportion of patients referred for MRI under GA in the hospital was 2.87 times higher in 2018 compared to 2020 and 2.9 times higher compared to 2021.

Furthermore, it can be determined that for some diagnostic groups, such as diagnostic group 2 (G00 – G99) – diseases of the nervous system, the number of patients referred for MRI scans under GA in the outpatient clinic was higher in the pre-pandemic 2018 compared to 2019. Interestingly, the proportion of referred patients in the pre-pandemic 2018 was 62% lower than in 2021 when considering diagnostic group 5 (R00 – R99) – symptoms, signs, and abnormal findings in clinical and laboratory tests not classified elsewhere, scanned under GA in the hospital.

The total number of patients referred for MRI scans in the outpatient clinic for diagnostic group 1 (C00 – D48) – neoplasms and diagnostic group 6 – other diagnostic groups in the ICD-10 was lower in the pre-pandemic compared to the pandemic years. The proportion of referred patients for diagnostic group 2 (G00 – G99) – diseases of the nervous system and diagnostic group 3 (M00 – M99) – diseases of the musculoskeletal system and connective tissue was higher in the pre-pandemic compared to the pandemic years.

The proportion of patients referred for MRI scans in the hospital for diagnostic group 2 (G00 – G99) – diseases of the nervous system was lower in the pre-pandemic compared to the pandemic years, while the proportion of patients referred for MRI scans in the hospital for diagnostic group 4 (Q00 – Q99) – congenital malformations, deformities, and chromosomal abnormalities was higher in the pre-pandemic compared to the pandemic years.

The negative trend of decreasing the number of scans can be associated with longer intervals between individual scans as a result of the applicable epidemiological guidelines and parental fears of infection, leading them to voluntarily delay elective check-ups, as well as due to their own or their child's PCR test being positive for COVID-19. In the case of an increase in the number of scans, it could be attributed to the referral of more patients from other institutions for MRI scans, particularly oncological patients.

Conclusion

For diagnostic group 1 (C00 – D48) – neoplasms and diagnostic group 6 – other ICD-10 diagnostic groups in the outpatient clinic, a higher number of scans was observed in the pandemic years compared to the pre-pandemic years, while for diagnostic group 2 (G00 – G99) – diseases of the nervous system and diagnostic group 3 (M00 – M99) – diseases of the musculoskeletal system and connective tissue, a lower number of scans was observed in the pandemic years compared to the pre-pandemic years.

For diagnostic group 2 (G00 – G99) – diseases of the nervous system in the hospital, a higher number of scans was observed in the pandemic years compared to the pre-pandemic years, while for diagnostic group 4 (Q00 – Q99) – congenital malformations, deformities, and chromosomal abnormalities, a lower number of scans was observed in the pandemic years compared to the pre-pandemic years.

The number of patients scanned under GA in the pre-pandemic year of 2018 was higher than in the pandemic years for diagnostic group 4 (Q00 – Q99) – congenital malformations, deformities, and chromosomal abnormalities.

The increase in the number of scans can be associated with the referral of a greater number of patients from other institutions for MRI scans, especially oncological patients.

The reduction in the number of some scans can be linked to longer intervals between individual scans as a result of the applicable epidemiological guidelines and the absence of patients due to their parents voluntarily postponing elective check-ups, as well as due to their own or their child's PCR test being positive for COVID-19.

Despite the pandemic and changes in the hospital system due to lockdowns, the average waiting time for diagnostic imaging performed by MRI at the Children's Hospital Zagreb did not increase, remaining at 17 weeks in both the pre-pandemic and pandemic years.

All data in this paper are part of the results of master's thesis „Difference in availability of magnetic resonance imaging diagnostic procedure during the COVID-19 pandemic in relation to patient diagnosis at the Clinic for children's diseases Zagreb" written at the University Department of Health Studies, University of Split (12).

References

1. Republic of Croatia, Ombudsman for Children. Children Waiting – Children's Rights During the Pandemic [Internet]. Zagreb: 2022. Available at: https://dijete.hr/docs/djeca%20na%20cekanju-djecja%20prava%20u%20vrijeme%20pandemije%202020.-2021_prilog%20izvjescu%20pravobraniteljice%20za%20djecu.pdf
2. Frankel J, Wilén J, Hansson Mild K. Assessing Exposures to Magnetic Resonance Imaging's Complex Mixture of Magnetic Fields for In Vivo, In Vitro, and Epidemiologic Studies of Health Effects for Staff and Patients. Front Public Health. 2018 Mar 12;6:66. doi: 10.3389/fpubh.2018.00066.
3. Regulation on Protection from Electromagnetic Fields, Narodne novine, NN 146/2014. [Internet]. Available at: https://narodne-novine.nn.hr/clanci/sluzbeni/2014_12_146_2740.html
4. U.S. Food and Drug Administration. Benefits and Risks [Internet]. Silver Spring: FDA; 2017. Available at: https://www.fda.gov/radiation-emitting-products/mri-magnetic-resonance-imaging/benefits-and-risks
5. Patient Rights Protection Act, Narodne novine, 169/2004. [Internet]. Available at: https://narodne-novine.nn.hr/clanci/sluzbeni/2004_12_169_2953.html
6. Poje I, Braović M. Hospital Information System – Advantages and Disadvantages in Operation [Internet]. Zagreb: Croatian Medical Informatics Society; 2019. Available at: https://hrcak.srce.hr/file/324767
7. Mittermayer R, editor. Handbook on Healthcare Quality Standards and Their Application [Internet].Zagreb:Agency for Quality and Accreditation in Healthcare; 2011. Available at: http://www.aaz.hr/sites/default/files/prirucnik_o_standardima_kvalitete_zdravstvene_zastite_i_nacinu_njihove_primjene_0.pdf
8. Croatian Institute of Public Health. International Classification of Diseases and Related Health Problems – ICD-10. Tenth Revision; Volume 1, 2nd edition [Internet]. Zagreb: Medicinska naklada; 2012. Available at: https://apps.who.int/iris/bitstream/handle/10665/44081/9789241547666_hrv.pdf
9. Edelstein WA, Mahesh M, Carrino JA. MRI: time is dose--and money and versatility. J Am Coll Radiol. 2010 Aug;7(8):650-2. doi: 10.1016/j.jacr.2010.05.002.

10. Rosenbaum L. The Untold Toll – The Pandemic's Effects on Patients without Covid-19. N Engl J Med. 2020 Jun 11;382(24):2368-2371. doi: 10.1056/NEJMms2009984.
11. Luxenburg O, Saban M, Myers V, Vaknin S, Boldor N, Wilf-Miron R. National and regional trends in MRI utilization in the face of the ongoing COVID-19 pandemic. Isr J Health Policy Res. 2021 Jul 15;10(1):40. doi: 10.1186/s13584-021-00
12. Folnožić J. Razlika u dostupnosti dijagnostičkog postupka magnetskom rezonancijom u vrijeme pandemije COVID -19 u odnosu na dijagnozu pacijenata u Klinici za dječje bolesti Zagreb (Diplomski rad). Split: Sveučilište u Splitu, Sveučilišni odjel zdravstvenih studija; 2022 (pristupljeno 10.11.2024.) Available at: https://urn.nsk.hr/urn:nbn:hr:176:668972

Dostupnost magnetske rezonancije tijekom pandemije COVID-19 u Klinici za dječje bolesti Zagreb

Sažetak:

U istraživanju je analiziran utjecaj pandemije bolesti COVID-19 na dostupnost usluge MR-a dječjim pacijentima na pet dijagnostičkih skupina po MKB-10 koje su bile najzastupljenije u pedijatrijskoj dijagnostici Klinike za dječje bolesti Zagreb u razdoblju od 1. siječnja 2018. godine do 31. prosinca 2021. godine.

Statistički značajnih razlika nije bilo prema dobi naručenih pacijenata najčešćih dijagnostičkih skupina snimljenih MR-om u poliklinici i u stacionaru Klinike za dječje bolesti Zagreb između pretpandemijskih (2018., 2019.) i pandemijskih (2020., 2021.) godina. Jednako tako nije bilo statistički značajnih razlika u prosječnom vremenu čekanja, koje iznosi 17 tjedana, u naručenih pacijenata snimljenih MR-om u pretpandemijskim (2018., 2019.) i pandemijskim (2020., 2021.) godinama.

Negativan trend smanjenja broja snimanja može se povezati s većim vremenskim razmacima između pojedinačnih snimanja, kao rezultat važećih epidemioloških smjernica te s bojazni roditelja pacijenata zbog zaraze, koji su samoinicijativno odgađali elektivne kontrole, no i zbog vlastita ili djetetova PCR testa pozitivnog na koronavirus.

U slučaju povećanja broja snimanja možemo govoriti o upućivanju većega broja pacijenata iz drugih ustanova na MR snimanja, posebno onkoloških pacijenata.

Ključne riječi: djeca; kvaliteta; MR; pandemija; snimanje

IZVORNI ZNANSTVENI ČLANAK (ORIGINAL SCIENTIFIC PAPER)

Učinkovitost umjetne inteligencije u razlikovanju malignih od benignih ultrazvučnih osobina tumora dojki

Filip Marković[1], **Damir Štimac**[1,2]

[1] Medicinski fakultet Osijek, Osijek

[2] Nacionalna memorijalna bolnica „Dr. Juraj Njavro“ Vukovar

Corresponding author: Filip Marković, email: fmarkovic24@gmail.com

DOI: https://doi.org/10.55378/rv.49.1.2

Sažetak

U ženskoj populaciji karcinom dojki je najčešća maligna bolest i mortalitet mu je 20 % zbog čega predstavlja veliki društveni i zdravstveni problem, osobito u razvijenim zemljama. Rano otkrivanje karcinoma dojke igra ključnu ulogu u poboljšanju ishoda liječenja. Ultrazvučna dijagnostika predstavlja važan alat za prepoznavanje i razlikovanje sumnjivih lezija, no precizna evaluacija može biti izazovna zbog subjektivnosti interpretacije. U tom kontekstu, umjetna inteligencija (UI), uključujući duboko učenje nude mogućnost standardizacije i unaprjeđenja dijagnostičke točnosti. Ova retrospektivna studija provedena je na Odjelu za radiologiju Nacionalne memorijalne bolnice „Dr. Juraj Njavro“ u Vukovaru, koristeći 257 ultrazvučnih slika pacijentica koje su u razdoblju od studenog 2021. do veljače 2024. obavile ultrazvučni pregled i patohistološku analizu iglenom biopsijom. Prikupljene slike prilagođene su za analizu pomoću neuronske mreže *DenseNet*. Cilj ovog istraživanja bio je ispitati učinkovitost neuronske mreže *DenseNet* u analizi ultrazvučnih slika tumora dojki, s naglaskom na razlikovanje malignih od benignih tvorbi i mogućnost smanjenja broja nepotrebnih invazivnih dijagnostičkih postupaka. Dijagnostička učinkovitost modela procijenjena je usporedbom njegovih rezultata s patohistološkim nalazima, a korišteni su standardni statistički testovi. Model je pokazao točnost od 73%, AUC (*area under the curve*) vrijednost od 0.78, specifičnost od 68.8%, osjetljivost od 80% i F1-score od 70%.

Ključne riječi: tumor dojke; ultrazvuk dojke; umjetna inteligencija

Uvod

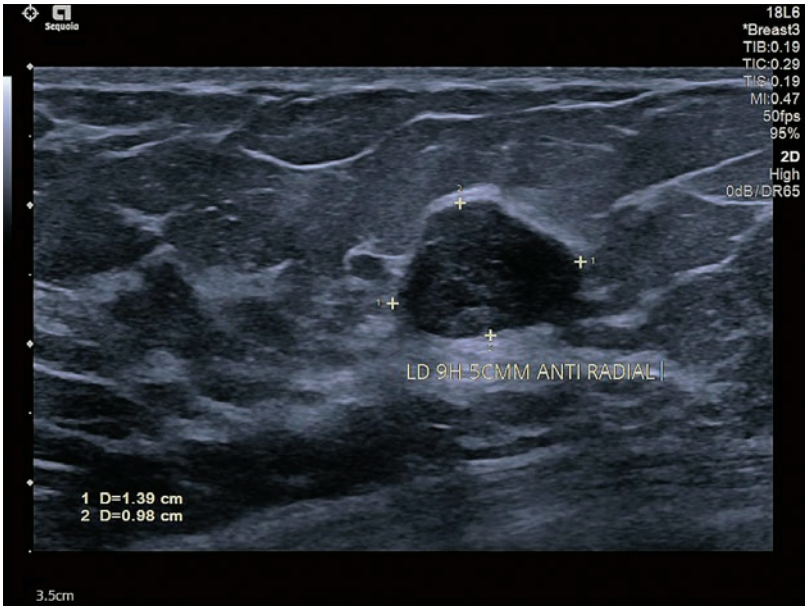
Karcinom dojke najčešća je maligna bolest kod žena, s visokim morbiditetom i mortalitetom, posebno u razvijenim zemljama (1). Pravovremeno i točno razlikovanje benignih od malignih lezija dojke ključno je za učinkovito liječenje i smanjenje broja nepotrebnih invazivnih zahvata. Ultrazvuk je često korištena metoda u dijagnostici promjena u dojci, pružajući detaljan uvid u morfologiju i strukturu lezija. No, interpretacija ultrazvučnih slika može biti subjektivna i ovisi o iskustvu radiologa, što može dovesti do varijabilnosti u dijagnozi.

Razvoj umjetne inteligencije (UI) u medicini, posebno dubokog učenja i neuronskih mreža, pruža nove mogućnosti za automatizaciju i unaprjeđenje točnosti dijagnostike u radiologiji. Neuronska mreža *DenseNet*, poznata po svojoj gusto povezanoj arhitekturi, omogućuje prijenos informacija kroz sve slojeve mreže i precizno prepoznavanje karakteristika tumora. Ova arhitektura omogućuje pouzdano prepoznavanje malignih i benignih karakteristika na temelju medicinskih slika, čime se olakšava donošenje kliničkih odluka i smanjuje potreba za dodatnim dijagnostičkim postupcima.

U ovoj studiji istražena je primjena *DenseNet* mreže u analizi ultrazvučnih slika tumora dojke, s ciljem procjene njene točnosti i potencijala za kliničku primjenu u razlikovanju malignih od benignih lezija, što bi moglo pridonijeti smanjenju broja nepotrebnih invazivnih postupaka te poboljšanju dijagnostičkog procesa.

Materijali i metode

Ovaj rad proveden je kao retrospektivna studija temeljem sekundarnih podataka, s ciljem analize mogućnosti primjene dubokog učenja u razlikovanju benignih i malignih tumora dojki. Studija je provedena na Odjelu za radiologiju Nacionalne memorijalne bolnice „Dr. Juraj Njavro“ u Vukovaru, a uključuje 257 ultrazvučnih slika dojki pacijentica koje su obavile ultrazvučni pregled i patohistološku dijagnostiku iglenom biopsijom između studenog 2021. i veljače 2024. Ovi podaci prikupljeni su iz bolničkog informacijskog sustava (BIS) te su ultrazvučne slike prilagođene za analizu u modelu umjetne inteligencije (UI), s obradom koja uključuje označavanje područja tumora i prilagođavanje veličine piksela kako bi slike bile kompatibilne za obradu

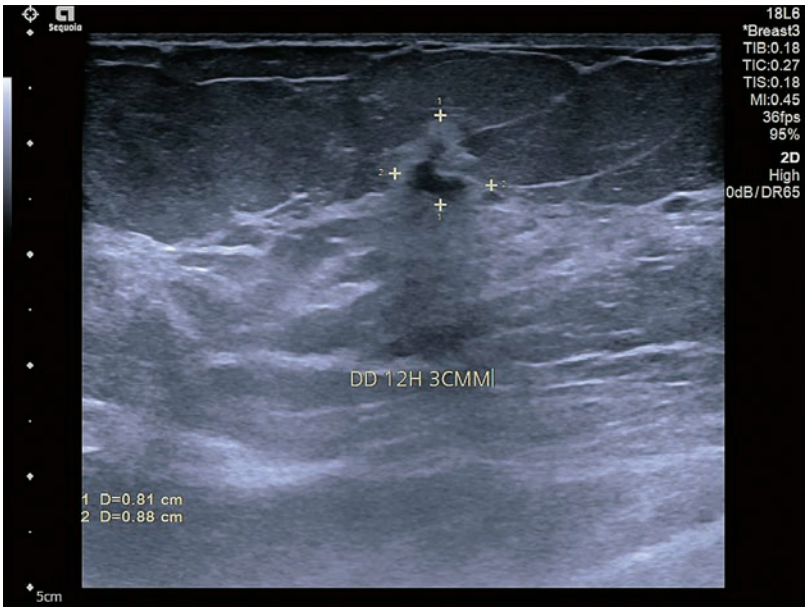


Slika 1. UZV benignog tumora dojke ispravno klasificiran umjetnom inteligencijom

(Slike 1. i 2.). Pacijentice su potpisale informirani pristanak obrade podataka i rad je odobrilo etičko povjerenstvo NMB „Dr. Juraj Njavro" Vukovar.

Za analizu je korišten UI model temeljen na neuronskoj mreži *DenseNet-121*. Ovaj model, s 121 slojem, prethodno je treniran na *ImageNet* skupu podataka, pri čemu su zadnja četiri sloja modela otključana za fino podešavanje. Podaci su podijeljeni na tri skupine: 80% slika korišteno je za trening, 10% za validaciju, a preostalih 10% za testiranje modela. „Trening" skup koristi se za inicijalno učenje modela, gdje model uči prepoznavati obrasce u slikama. „Validacijski" skup pomaže u procjeni općenitosti modela i sprječava prekomjerno učenje, dok je „testni" skup rezerviran za konačnu provjeru modela na potpuno novim podacima, što simulira rad modela u stvarnom kliničkom scenariju. Tijekom treniranja, slike su prolazile kroz model u epohama (jedan prolaz kroz cjelokupni skup za treniranje), a model je treniran tijekom 15 epoha uz primjenu metode ranog zaustavljanja (engl. *early stopping*) kako bi se optimizirao proces učenja i smanjio rizik od prenaučenosti. Praćene su vrijednosti gubitka (engl. *validation loss*) i točnosti na validacijskom skupu (engl. *validation accuracy*) kako bi se prilagodio proces treniranja, dok je brzina učenja postavljena na 0,01, broj koji određuje koliko brzo model ažurira težine tijekom treniranja.

Za evaluaciju modela korišteni su standardni dijagnostički testovi, uključujući točnost (engl. *accuracy*), osjetljivost (engl. *sensitivity*) = TP/(TP + FN), preciznost (engl. *precision*) = TP/(TP + FP), specifičnost = TN/(TN+FP) (specificity), *F1-score* = 2 × (*Precision*× *Sensitivity*) /(*Precision*+ *Sensitivity*) te vrijednost površine ispod



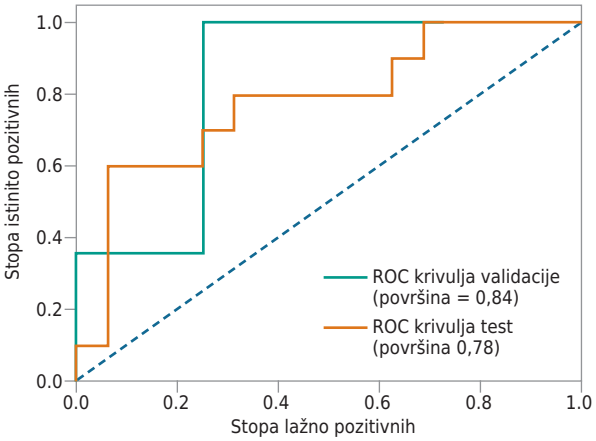
Slika 2. UZV malignog tumor dojke ispravno klasificiran umjetnom inteligencijom

krivulje (AUC). Osjetljivost je određena omjerom istinski pozitivnih (TP) rezultata i zbroja istinski pozitivnih i lažno negativnih (FN), dok je preciznost omjer istinski pozitivnih i zbroja istinski pozitivnih i lažno pozitivnih rezultata (FP). Specifičnost je definirana kao omjer istinski negativnih (TN) i zbroja istinski negativnih i lažno pozitivnih (FP) rezultata. F1-mjera izračunata je kao harmonijska sredina između preciznosti i osjetljivosti kako bi se osigurao uravnotežen pokazatelj uspješnosti modela.

Rezultati

Testiranje modela radilo se na 26 slika, od kojih je 16 slika prikazivalo benigne a 10 maligne lezije. AUC testnog skupa bio je 0.78 (Slika 3.).

Osjetljivost modela za maligne lezije bila je 80%, a točnost 73%. Nešto lošiji rezultati bili su rezultati preciznosti (62%) i *F1-score* (70%). Izračunata specifičnost iz ovih podataka iznosila je 68.8% za skupinu podataka malignih lezija.



Slika 3. Krivulja operativnih karakteristika prijemnika (ROC)

Tablica 1. Tablica klasifikacija

	Preciznost	Osjetljivost	F1- score	Broj slika
Benigno	0.85	0.69	0.76	16
Maligno	0.62	0.80	0.70	10
Točnost			0.73	26

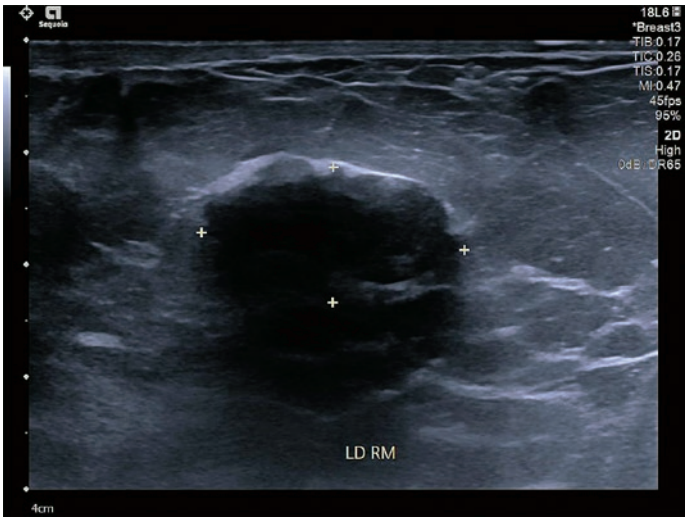
U klasifikaciji tumora, model je ispravno identificirao 11 benignih i 8 malignih uzoraka (Tablica 2., Slika 1., Slika 2., Slika 4., Slika 5.).

Tablica 2. Matrica zabune

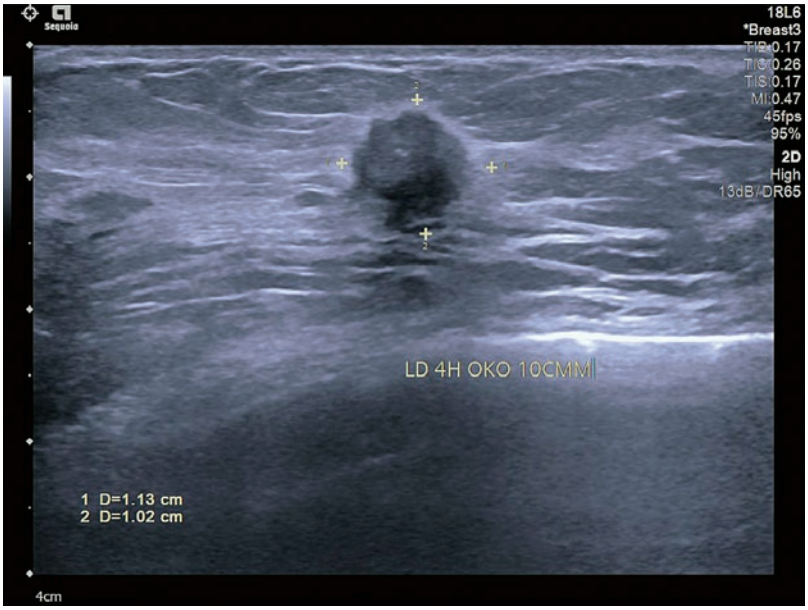
	Benigno	Maligno
Stvarno benigno	11	5
Stvarno maligno	2	8

Rasprava

U našem istraživanju obuhvaćena su 126 benigna i 131 maligni tumor, što je dobar preduvjet za kvalitetno treniranje modela zbog balansiranja ispitivanih grupa. U ostalim istraživanjima raspored grupa znao je varirati pa u jednom istraživanju raspored je bio ujednačen s 93 maligne i 102 benigne lezije (2) dok neka druga istraživanja imaju velike razlike između grupa kao npr. 575 benignih i 326 malignih promjena (3). To znači da se program može istrenirati i na nebalansiranim grupama, ali potrebno je obratiti pažnju na ostale hiperparametre treniranja i evaluacije. Jedna je od čestih zabluda potreba za velikim brojem slika kako bi se pravilno i što bolje istrenirao UI model. Veći broj slika je prednost u treningu i provjeri učinkovitosti, ali iz našeg istraživanja vidimo da se i sa 200 slika može napraviti model i istrenirati da pokazuje vjerodostojne rezultate. Kvaliteta slika korištenih za treniranje UI modela igra ključnu ulogu u njegovoj preciznosti i sposobnosti razlikovanja različitih karakteristika. Model treniran na slikama visoke kvalitete, koje su jasno definirane i pravilno označene, ima veću šansu za postizanje boljih rezultata. Niska rezolucija, šum ili loša kontrastnost mogu otežati modelu prepoznavanje relevantnih obilježja, što izravno utječe na njegovu učinkovitost i pouzdanost u stvarnim scenarijima. U ovom istraživanju korištene su ultrazvučne slike u B-modu dostupne na odjelu, različitih rezolucija i kontrasta (Slika 6.). U istraživanju Starena i suradnika, sve pacijentice se snimalo u istom položaju i isključivalo nejasne slike UZV dojke, kako bi se osigurao dobar trening i učinkovitost UI modela (4). Istraživanja su isto tako koristila različite pristupe od isključivo B-mod ultrazvučnih slika dojke do dodatnih mogućnosti npr. power Doppler analize ili ultrazvuka s kontrastom za poboljšanje klasifikacije malignih promjena dojke (5, 4). Testiranjem modela dobili su se dobri, ali ne i izvrsni rezultati, što se vidi iz AUC testnog skupa koji je iznosio je 0.78. Model ima dobru sposobnost razlikovanja između benignih i malignih tumora. Dobivena AUC vrijednost testnog skupa je slična drugim istraživanjima, gdje je kod korištenja multimodalnih ultrazvuka AUC bio 0.85 ili gdje je kod korištenja 3D power Doppler ultrazvuka najmanja vrijednost bila 0.782.



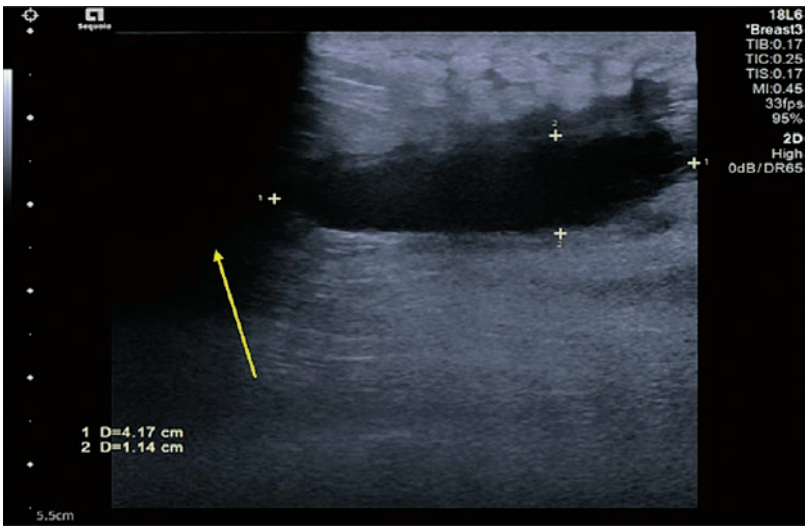
Slika 4. Benigni tumor klasificiran kao maligni.



Slika 5. Maligni tumor klasificiran kao benigni

U jednom istraživanju autori su koristili multimodalni UZV u poboljšanju točnosti procjene sentinelnih limfnih čvorova u slučajevima raka dojke (7). U tom istraživanju za dvodimenzionalni (2D) UZV, AUC je iznosio 0.678 što je znatno manje od dobivene AUC u ovome istraživanju, ali bitno je naglasiti da UI modeli nisu jednako klasificirali (6, 7).

Točnost ovog modela na testnom skupu bila je 73% što je vjerojatno zbog različitih kvaliteta i rezolucija slika. Točnost u istraživanjima znatno varira od točnosti kao što je 70.5% na B-mod ultrazvuku pa sve do točnosti od preko 90% korištenjem multimodalnih ultrazvuka (6, 8, 9). U nekim istraživanjima koja su koristila modulacije slike prije prolaska kroz modeltočnost je iznosila čak i 96% (10). Iako još uvijek postoje modeli istovjetne točnosti kao što je naš model, ipak mislimo da ima prostora za poboljšanje. Primjenom dodatnih ultrazvučnih tehnika ili dodatnim procesiranjem slika očekujemo da bi točnost ovog modela rasla. Preciznost u ovom modelu bila je 62%. U istraživanju preciznost na analizi 3D ultrazvučne slike iznosila je 84.7% dok na običnoj ultrazvučnoj slici 75.9%, što govori da UI modeli još uvijek nisu dovoljno precizni u određivanju malignih lezija i to u tom su segmentu potrebna daljnja istraživanja (8). Ovaj model pokazuje znatno nižu specifičnost (68.8%) od modela koji su analizirali slike multimodalnih UZV-a, gdje je specifičnost bila 92.4%, nešto manju specifičnost od modela koji su koristili analizu slika 3D UZV (75.6%), ali ima veću specifičnost od modela koji je analizirao 2D UZV slike (64.9%) (6, 8, 9). U usporedbi s modelom koji je analizirao iste slike ovaj model točnije prepoznaje benigne slučajeve. Ovaj je model osjetljiviji (80%) u komparaciji s modelom koji je koristio multimodalne UZV slike (77.4%) (6). Model testiran na 3D UZV slikama pokazuje najveću osjetljivost (90.4%), a jedan od modela koji je istraživao samo B-mod UZV slike ima nešto višu osjetljivost od našeg (81.7%) (8, 9). Model iz ovog istraživanja konkurentan je u usporedbi s drugim modelima, ali model na 3D UZV slikama pokazuje



Slika 6. UZV slika sa šumom iz istraživanja

znatno bolju osjetljivost što znači da postoji dosta prostor za napredovanje. *F1-score* (0.70) je niži u usporedbi s drugim istraživanjima, gdje istraživanje s nebalansiranim grupama ima F1-score od 0.87, a istraživanje s približnom istom razlikom u broju malignih i benignih tumora ima F1-score 0.97 (3, 10).

Na temelju provedenog istraživanja, može se zaključiti da je razvijeni model učinkovit u razlikovanju benignih od malignih tumora dojke. Iako postoje određena ograničenja, model pokazuje potencijal za unaprjeđenje dijagnostičkog procesa UZV-a dojke. Iako ne može potpuno eliminirati upotrebu invazivnih dijagnostičkih metoda, rezultati ukazuju na to da može značajno poboljšati razlikovanje benignog od malignog tumora. Daljnje istraživanje i optimizacija modela, uključujući primjenu dodatnih tehnika i poboljšanje kvalitete slika, mogla bi dodatno povećati njegovu točnost i pouzdanost.

References

1. Ivan Damjanov, Sven Seiwerth, Stanko Jukić, Marin Nola, Patologija, 5 izd. Zagreb: Medicinska naklada; 2018.
2. Xu Z, Wang Y, Chen M, Zhang Q. Multi-region radiomics for artificially intelligent diagnosis of breast cancer using multimodal ultrasound. Comput Biol Med. 2022 Oct;149:105920. doi: 10.1016/j.compbiomed.2022.105920. Epub 2022 Aug 6. PMID: 35986969.
3. Wei Q, Yan YJ, Wu GG, Ye XR, Jiang F, Liu J, Wang G, Wang Y, Song J, Pan ZP, Hu JH, Jin CY, Wang X, Dietrich CF, Cui XW. The diagnostic performance of ultrasound computer-aided diagnosis system for distinguishing breast masses: a prospective multicenter study. Eur Radiol. 2022 Jun;32(6):4046-4055. doi: 10.1007/s00330-021-08452-1. Epub 2022 Jan 23. PMID: 35066633.
4. Staren ED, O'Neill TP. Breast ultrasound. Surg Clin North Am. 1998 Apr;78(2):219-35. doi: 10.1016/s0039-6109(05)70310-8. PMID: 9602844.
5. G. Huang, Z. Liu, L. Van Der Maaten and K. Q. Weinberger, "Densely Connected Convolutional Networks," 2017 IEEE Conference on Computer Vision and Pattern Recognition (CVPR), Honolulu, HI, USA, 2017, pp. 2261-2269, doi: 10.1109/CVPR.2017.243. keywords: {Training;Convolution;Network architecture;Convolutional codes;Neural networks;Road transportation},
6. Xu Z, Wang Y, Chen M, Zhang Q. Multi-region radiomics for artificially intelligent diagnosis of breast cancer using multimodal ultrasound. Comput Biol Med. 2022 Oct;149:105920. doi: 10.1016/j.compbiomed.2022.105920. Epub 2022 Aug 6. PMID: 35986969.
7. Su S, Ye J, Ke H, Zhong H, Lyu G, Xu Z. Multimodal ultrasound imaging: a method to improve the accuracy of sentinel lymph node diagnosis in breast cancer. Front Oncol. 2024 Mar 25;14:1366876. doi: 10.3389/fonc.2024.1366876. PMID: 38590661; PMCID: PMC10999636.
8. Xiao X, Gan F, Yu H. Tomographic Ultrasound Imaging in the Diagnosis of Breast Tumors under the Guidance of Deep Learning Algorithms. Comput Intell Neurosci. 2022 Feb 28;2022:9227440. doi: 10.1155/2022/9227440. PMID: 35265119; PMCID: PMC8901319.
9. Ma H, Tian R, Li H, Sun H, Lu G, Liu R, Wang Z. Fus2Net: a novel Convolutional Neural Network for classification of benign and malignant breast tumor in ultrasound images. Biomed Eng Online. 2021 Nov 18;20(1):112. doi: 10.1186/s12938-021-00950-z. PMID: 34794443; PMCID: PMC8600702.
10. Chen H, Ma M, Liu G, Wang Y, Jin Z, Liu C. Breast Tumor Classification in Ultrasound Images by Fusion of Deep Convolutional Neural Network and Shallow LBP Feature. J Digit Imaging. 2023 Jun;36(3):932-946. doi: 10.1007/s10278-022-00711-x. Epub 2023 Jan 31. PMID: 36720840; PMCID: PMC10287618.

The Efficiency of Artificial Intelligence in Distinguishing Malignant from Benign Ultrasound Features of Breast Tumors

Abstract

In the female population, breast cancer is the most common malignant disease, with a mortality rate of 20%, making it a significant social and health problem, especially in developed countries. Early detection of breast cancer plays a crucial role in improving treatment outcomes. Ultrasound diagnostics represent a significant tool for identifying and differentiating suspicious lesions, but accurate evaluation can be challenging due to the subjectivity of interpretation. In this context, artificial intelligence (AI) and deep learning offer the potential for standardization and enhancement of diagnostic accuracy. This retrospective study was conducted at the Radiology Department of the National Memorial Hospital "Dr. Juraj Njavro" in Vukovar, using 257 ultrasound images from patients who underwent ultrasound examinations and pathohistological analysis via needle biopsy from November 2021 to February 2024. The collected images were adjusted for analysis using the DenseNet neural network. The aim of this research was to examine the effectiveness of the DenseNet neural network in analyzing ultrasound images of breast tumors, focusing on distinguishing malignant from benign formations and the potential to reduce the number of unnecessary invasive diagnostic procedures. The diagnostic efficacy of the model was assessed by comparing its results with pathohistological findings, utilizing standard statistical tests. The model demonstrated an accuracy of 73%, an AUC (area under the curve) value of 0.78, a specificity of 68.8%, a sensitivity of 80%, and an F1-score of 70%.

Keywords: artificial Intelligence; breast tumor; breast ultrasound

Redefine what is possible in pulmonology

The world's first photon-counting CT



Courtesy of Uniklinikum Augsburg, Augsburg, Germany



NAEOTOM Alpha® with Quantum Technology

NAEOTOM Alpha is nothing less than the reinvention of computed tomography. Explore more.

siemens-healthineers.com/NAEOTOM-Alpha

SIEMENS Healthineers

REVIEW ARTICLE (PREGLEDNI RAD)

Radiological Management of Infections in Immunocompromised Patients

Domagoj Babić[1,2], **Sanja Lovrić Kojundžić** [2, 3, 4]

[1] Univeristy Hospital for Infectious Diseases „Dr Fran Mihaljević"; Zagreb, Croatia

[2] University Department of Health Studies, Univeristy of Split, Split, Croatia

[3] Department of Diagnostic and Interventional Radiology, University Hospital of Split, Split, Croatia

[4] School of Medicine, University of Split, Split, Croatia

Corresponding author: Domagoj Babić, e-mail: domagojbabic@hotmail.com

DOI: https://doi.org/10.55378/rv.49.1.3

Summary

Immunocompromised status is defined as a condition of impaired or dysfunctional immune system, which is unable to protect the body from external pathogens. The causes of immunocompromised status can be congenital or acquired, with the most notable example worldwide being the human immunodeficiency virus. An immunocompromised patient has an increased susceptibility to infections, which can be caused by pathogens such as fungi, parasites, bacteria, or viruses.

The use of appropriate radiological methods in diagnostic purpose plays an important role in the early detection and treatment of various infections and other diseases characteristic for immunocompromised patients.

Immunocompromised patients most commonly develop opportunistic infections of the neurological system. Since neurological changes in the early stages of development can be undetectable on CT scans, magnetic resonance imaging is primarily used for promt disease detection, as it is the most specific and sensitive method for these conditions. During MRI imaging, it is crucial to use multiple different pre-contrast and additional post-contrast sequences to reliably confirm highly specific neurological infections and differentiate them based on the type of etiological factor. Besides neurological complications, immunocompromised patients are also highly prone to developing respiratory infections. The method of choice for such complications is undoubtedly multislice CT, which can detect even the smallest changes within the respiratory system in the early stages of the disease. After the initial detection of the disease, radiographic imaging of the thoracic region represents an extremely powerful and accessible tool for further monitoring, with significant sensitivity that can guide the subsequent course of treatment.

Key words: HIV; immunodeficiency, infections, radiology

Abbreviations and acronyms: ADC (Apparent Diffusion Coefficient), AIDS (Acquired Immunodeficiency Syndrome), CE-T1 WI (Contrast-Enhanced T1-Weighted Imaging), CNS (Central Nervous System), CMV (Cytomegalovirus), CSF (Cerebrospinal Fluid), CT (Computed Tomography), DWI (Diffusion-Weighted Imaging), FLAIR (Fluid Attenuated Inversion Recovery), HAND (HIV-Associated Neurocognitive Disorders), HIV (Human Immunodeficiency Virus), HRCT (High-Resolution Computed Tomography), HSV (Herpes Simplex Virus), MRI (Magnetic Resonance Imaging), NK (Natural Killer), PCNSL (Primary Central Nervous System Lymphoma), PID (Primary Immunodeficiency Disease), PJP (Pneumocystis Jiroveci Pneumonia), SCID (Severe Combined Immunodeficiency), SPECT (Single Photon Emission Computed Tomography), SWI (Susceptibility Weighted Imaging), T1 WI (T1-Weighted Imaging), T2 WI (T2-Weighted Imaging)

Introduction

Immunocompromised patients may have a compromised immune system due to acquired (primary) factors, iatrogenic factors or hereditary factors. Causes of immunodeficiency can be infectious, such as the human immunodeficiency virus (HIV), which causes acquired immunodeficiency syndrome (AIDS). Also, there are solid organ or bone marrow transplants, cancer, chemotherapy, radiotherapy, lymphoma, glucocorticoid therapy, splenectomy, and traumatic injuries. Immunocompromised patients are at an increased risk of life-threatening infections, which must be treated as early as possible in their development (1).

Congenital forms of immunodeficiency are often associated with acquired immunodeficiency syndrome (AIDS), caused by the HIV. Malignant diseases, particularly

hematopoietic and lymphoid cancers, lead to immune dysfunction by causing a deficiency in immune effector cells or dysfunction in antibody synthesis. Additionally, the use of cytostatics in chemotherapy, as well as radiotherapy used in the treatment of cancer patients, has a negative impact on the immune system, leading to a state of immunodeficiency (2).

The risk of infection in immunocompromised patients can be classified as high, moderate, or low, depending on the cause of the immunodeficiency. Infections in these patients can be caused by a variety range of pathogens, which are generally divided into fungal, parasitic, bacterial, and viral pathogens.

Aim of the paper

The aim of the paper is to provide a detailed explanation of the types of immunocompromised conditions and the opportunistic infections that may develop. The role of radiology in diagnosis, treatment, and monitoring of such patients is defined. Each relevant radiological method in diagnosis of these conditions is explained and further supported with illustrative examples. The article was written using available articles from the PubMed platform, as well as professional books in both physical and digital formats. When searching the literature on the internet, the terms *radiology, infectology, immunodeficiency,* and *immunocompromised* were used, with the operators *AND* or *OR*. All results found online were presented in a narrative and descriptive form in English, and each article or paper was publicly available in its entirety.

Discussion

1. Immunocompromised host

Immunocompromised state, immunodeficiency, or immunosuppression are synonymous terms that describe a condition of impaired immune function and an increased risk of infections. This condition can manifest due to a congenital or acquired disorder affecting one or more immune components of the the organism. It most commonly refers to patients with some form of congenital immune deficiency, such as primary immunodeficiency, as well as those who have become immunocompromised to other conditions, including individuals infected with the HIV. Acquired immunocompromised states may result from malignant diseases or can be iatrogenic, meaning they occur as a consequence of certain treatments, such as cytostatic therapy, organ transplantation, splenectomy, chemotherapy, or radiotherapy (3).

1.1. Causes of immunosuppression in patients

Primary immunodeficiency disease (PID) refers to a highly diverse group of disorders characterized by severely weakened or absent immune system function, either fully or partially. Such immunological impairments in individuals lead to an increased risk of developing severe infections, autoimmune diseases, or malignant conditions. Patients with specific T-cell defects may have abnormally low levels of lymphocytes and neutrophils, known as lymphopenia and neutropenia. In the most severe forms of severe combined immunodeficiency (SCID), T-cell deficiency is frequently observed, often accompanied by a corresponding B-cell deficiency (4). Antibody deficiency, or B-cell dysfunction, is the most common type of immunodeficiency, accounting for 50% of all PID cases (5).

Solid Organ Transplantation is the definitive therapy for many severe organ diseases that can no longer be effectively treated by medication or surgery. However, the transplanted organ (allograft) triggers an immune response from the recipient, which, without adequate systemic immunosuppression, would lead to allograft rejection, then procedure failure, and potentially fatal outcomes. While immunosuppression has significantly improved graft survival, it also left patients more susceptible to pathogens and infectious complications. Glucocorticoids were the first agents used for immunosuppression in solid organ transplantation. They are considered highly potent but non-selective, affecting multiple cell types, including T and B cells, macrophages, granulocytes, and monocytes, leading to systemic immunosuppression (6).

Advancements in radiotherapy techniques have led to increased precision in dose delivery and better protection of surrounding healthy tissue. However, radiotherapy treatments not only affect adjacent tissues but also have systemic adverse effects. The most pronounced harmful effects of ionizing radiation occur in the tumor microenvironment. In general, lymphocytic cells, particularly B cells and natural killer (NK) cells, are among the most radiosensitive cells in the body. Their destruction directly correlates with immune system weakening. The effects of radiation on the tumor microenvironment and the overall immune system can be modulated by fractionating of radiation doses. Numerous studies have reached a universal conclusion: the use of hypofractionated high doses instead of high single doses significantly reduces the immunosuppressive effects of radiation on healthy tissue (7).

2. Human immunodeficiency virus (HIV)

The human immunodeficiency virus belongs to the family of human retroviruses. The virus first emerged in 1981 when it was described as an unexplained pneumonia affecting several homosexual patients. By 1983, the virus had been discovered, when a group of French scientists successfully isolated it. And the following year, it was confirmed that HIV is the main and only cause of AIDS (8).

Over the years, HIV has remained one of the major global health challenges. More than 40 million people worldwide are currently infected with some subtype of the virus. Some countries even reporting an increase in the number of cases (9). The virus is transmitted through three primary routes: sexual contact, blood exposure, and maternal-fetal transmission.

There are two main types of HIV: HIV-1, the dominant and more easily transmissible form, it is responsible for the global pandemic (Figure 1). The second one is HIV-2, which is mostly localized in West and Central Africa, has lower virulence. HIV treatment is highly challenging due to the virus's constant mutation. As the immune response and antiretroviral drugs exert pressure on the virus, its population within the body continuously evolves. This means that the initial virus, which was responsible for the infection can completely change within just a few days (3).

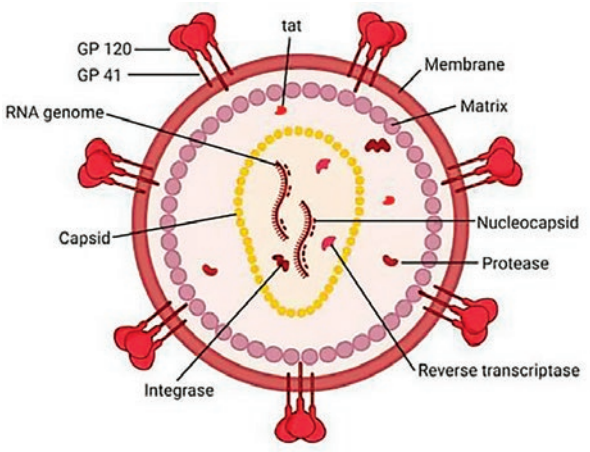


Figure 1. Illustration of human immunodeficiency virus (HIV-1).
Source: https://pubmed.ncbi.nlm.nih.gov/33572761/

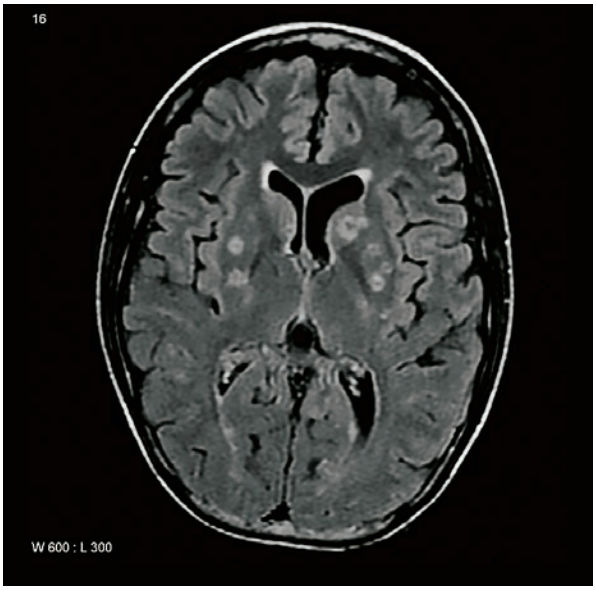


Figure 2. MRI, axial image of brain in FLAIR sequence, ring-enhancing lesions caused by toxoplasmosis infection (HIV patient).
Source: https://radiopaedia.org/articles/toxoplasmosis-vs-lymphoma

2.1. Imunopathogenesis

During the first week of infection, the virus remains undetectable but is highly destructive, leading to the irreversible loss of 80% of the total T helper cells in organism. The virus infects monocytes/macrophages as well as active $CD4^+$ cells and also T lymphocytes, which are in adults predominantly located in the lymph nodes (3).

Once the virus enters the bloodstream, it initially spreads to the spleen and other lymphoid organs**,** where the primary infection begins. After a certain period, HIV establishes itself in lymphoid organs and disseminates into various organ systems, including the central nervous system, where it is protected from the systemic immune response. The virus evades both cellular and humoral immunity, not immediately killing its host but instead actively replicating and progressing toward chronic infection. Persistent viremia also depletes B lymphocytes, leading to weakened humoral immunity (3).

In untreated patients, approximately 10 years after the initial infection**,** HIV disease progresses to an advanced stage. The $CD4^+$ cells count is critically low, leading to significant immunosuppression, making individuals highly susceptible to opportunistic infections and malignancies. Thanks to antiretroviral therapy, even patients in advanced stages of the disease can live long lives with HIV (3).

2.2. Neuroimaging of HIV-associated disorders

Neurological manifestations caused by the human immunodeficiency virus are very common. Around 20% of HIV-infected patients notice their first symptoms through neurological abnormalities, while 30-40% of patients in the advanced stage of HIV infection develop some form of neurological impairment. The term HIV-associated neurocognitive disorders (HAND) is used to describe a spectrum of various asymptomatic disorders that can only be detected through neuropsychiatric testing. It is estimated that around 50% of infected patients (even those receiving antiretroviral therapy) exhibit some form of HAND (3).

Among opportunistic diseases associated with HIV infection, cerebral toxoplasmosis is very common. It presents with ring-enhancing lesions in the basal ganglia region or at the corticomedullary junction (the boundary between gray and white matter), often surrounded by significant edema (Figure 2) (3).

Another frequently observed condition is primary central nervous system lymphoma (PCNSL), which appears on CT and MRI scans as a periventricular lesion with irregular contrast enhancement (Figure 3). In addition to diagnostic radiology, lymphoma patients are often examined using nuclear medicine imaging techniques, such as single-photon emission computed tomography (SPECT). This method utilizes thallium-201 to analyze its accumulation in the brain, reflecting increased metabolic activity (3,4).



Figure 3. MRI, axial image of brain in T2 sequence, brain lymphoma caused by HIV infection.
Source: https://radiopaedia.org/articles/toxoplasmosis-vs-lymphoma

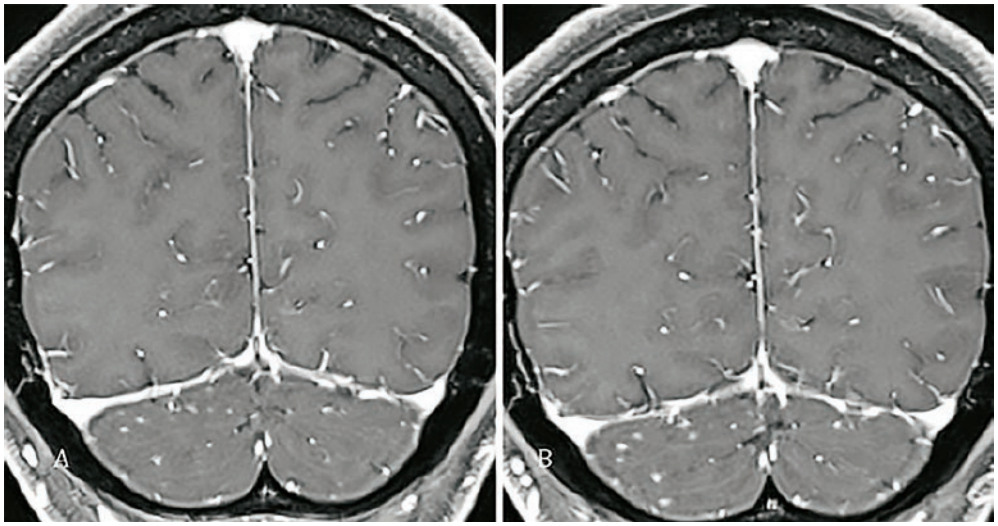


Figure 4. MRI, coronal contrast-enhanced brain images, show nodular leptomeningeal enhancement in the posterior fossa in the HIV patient with cryptococcus meningitis.
Source: https://link.springer.com/referenceworkentry/10.1007/978-3-319-61423-6_48-1

3. The radiological diagnosis of infetcions

3.1. Fungal infections

Fungi are widespread organisms, but only a few species are actually pathogenic and capable of causing pathological disorders in the body. Several different types of fungal forms are distinguished based on their morphological structure. Fungi represent a significant medical problem in patients with various forms of immunosuppression, as they cause invasive infections that are a frequent cause of mortality in such patients. It is estimated that more than 80% of patients with fungal infections are fundamentally immunocompromised (10).

3.1.1. Cryptococcosis

Meningitis caused by Cryptococcus occurs as a secondary reaction to the spread of the Cryptococcus fungus into the meningeal microcirculation. It is considered as the most common fungal infection of the central nervous system (CNS) (10,11). Magnetic resonance imaging is the method of choice for visualizing pathological changes affecting the meninges. FLAIR (Fluid Attenuated Inversion Recovery) sequences show high signal intensity of the the subarachnoid spaces, which is also confirmed by contrast-enhanced T1-weighted imaging (CE-T1 WI), highlighting the leptomeningeal space. Post-contrast enhancement can appear smooth or thick, nodular and irregular, long and coninuous or asymmetric (Figure 4). FLAIR contrast sequences are often used for detecting pathological changes, and in cryptococcosis, ventricular space dilation is frequently observed (10).

Meningitis caused by cryptococcosis also leads to the formation of pseudocysts outside the Virchow-Robin space, which appear on MRI scans as asymmetrical cystic lesions with a “soap-bubble” appearance. These lesions have the same intensity as cerebrospinal fluid (CSF) and do not show diffusion restriction on diffusion-weighted imaging (DWI) sequences (10).

3.1.2. Aspergillosis

Aspergillosis often presents with multiple abscesses located near the gray-white matter junction, but they can also appear in the deep gray matter nuclei, which is not typically the case with abscesses caused by bacterial infections. On T2-weighted MRI scans, these abscesses most commonly present as a centrally localized hypointense signal surrounded by hyperintense perifocal edema. On contrast-enhanced T1-weighted images, fungal abscesses appear with a thin ring-shaped capsule that also has an irregular outer margin (Figure 5). On T2-weighted sequences, a hypointense signal zone with a thin contrast-enhancing rim can be differentiated, which is significantly thicker than the contrast rim seen on post-contrast T1-weighted images (10).

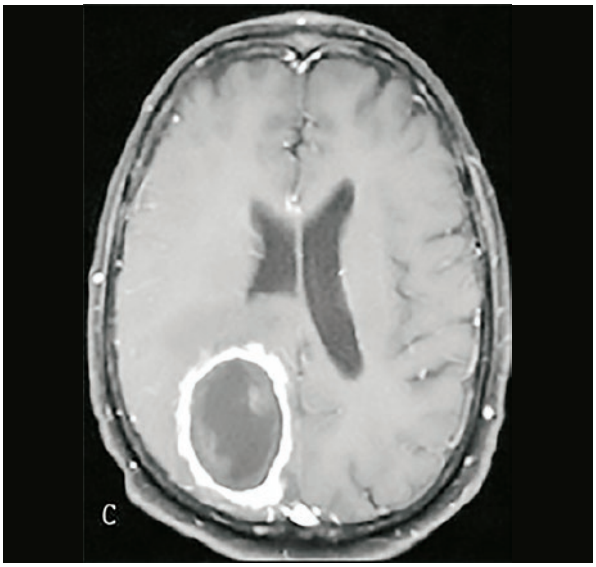


Figure 5. CE-T1 WI, abscess with peripheral contrast enchancment.
Source: https://link.springer.com/referenceworkentry/10.1007/978-3-319-61423-6_48-1

The DWI sequence is crucial for differentiating fungal abscesses from bacterial ones. Both bacterial and fungal abscesses in the brain show diffusion restriction within the abscess cavity, but unlike bacterial abscesses, fungal abscesses exhibit an inhomogeneous signal within the cavity on DWI sequences. The SWI (Susceptibility-Weighted Imaging) sequence is also used to differentiate fungal infections from bacterial infections. On SWI sequences, fungal abscesses manifest with a thick, single, dark rim, and in immunocompromised hosts, multiple dark areas within the abscess cavity are frequently observed (10).

Aspergillosis can also develop within the respiratory system and may exhibit a highly invasive nature. In the semi-invasive type of aspergillosis, CT scans of the thoracic region highlight unilateral or bilateral segmental areas of consolidations. In the angioinvasive type of aspergillosis, the most common manifestation is the Halo sign, which represents multiple nodules surrounded by a ground-glass opacities in the lung parenchyma. Additionally, this type of aspergillosis may present with consolidations and even hemorrhagic infarctions (14).

3.1.3. Candidiasis

Candida albicans is one of the most common fungal infections and is particularly prevalent in immunocompromised patients. Candida has the ability to transform into hyphal forms, which leads to a significantly more invasive parenchymal disease. It most commonly manifests as multiple small brain abscesses (<3 mm) or exhibits angioinvasive behavior, causing thrombosis or hemorrhages (11).

Cerebral microabscesses caused by Candida sometimes can be very small and may not be visible on CT brain scans. Therefore, MRI is the preferred method for detecting these small abscesses. These abscesses are typically seen as small ring-enhancing lesions at the gray-white matter junction and in the basal ganglia. On FLAIR images, areas of hypointense signal are observed in parenchymal regions affected by Candida abscesses. On T2-weighted images, these areas appear ring-shaped with a higher signal intensity. In SWI sequences, the abscesses present with a dark peripheral rim. The DWI sequence is particularly useful for early disease detection, as post-contrast T1-weighted images may initially show no abnormalities. On DWI, Candida abscesses appear as multiple punctate zones of restricted diffusion, bilaterally localized in the basal ganglia and cerebral cortex (Figure 6) (10).

3.1.4. Pneumocystis jiroveci pneumonia (PJP)

In immunocompromised patients infected with the fungus Pneumocystis jirovecii, abnormalities develop within the respiratory system. In these patients, chest radiography can differentiate various pathological changes in more than 90% of cases. Typical findings include bilateral inflammatory processes, usually diffusely distributed, with a predominant perihilar localization (14).

On CT scans, a characteristic ground-glass opacity is observed, along with interlobular septal thickening (14). The absence of ground-glass opacity on CT imaging can, with high probability, exclude Pneumocystis jirovecii as major cause of described pneumonia (3). Additionally, it is important to emphasize that clinical experience has shown that in immunosuppressed patients, particularly those HIV-positive, Pneumocystis jirovecii pneumonia (PJP) is a very common comorbid diagnosis (14).

3.2. Parasitic infections

Various pathogenic species, when and if they colonize a host organism, can establish different types of relationships with it: mutualistic, symbiotic, or parasitic. The parasitic relationship is the most detrimental to the host, as the colonizing pathogen benefits at the host's expense. Although, in theory, every infectious pathogen can be considered as a type of parasite due to its relationship with the host, only certain eukaryotic subtypes (which do not belong to viruses, bacteria, or fungi) have been classified specifically as parasites.

3.2.1. Toxoplasmosis

Toxoplasmosis is a condition caused by the parasite Toxoplasma gondii, which is considered the most common opportunistic infection of the central nervous system in patients with AIDS. Once it enters the human body, T. gondii settles in the brain, retina, striated muscles, and cardiac muscle. If the infected individual has a functional immune system, the parasite remains in a dormant state. However, in immunocompromised individuals, T. gondii begins to proliferate. Initially, the infected person may

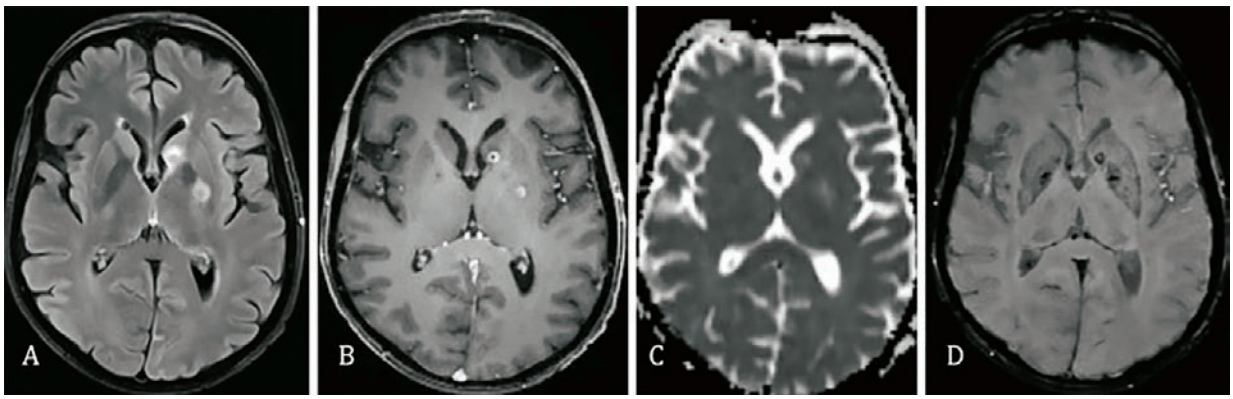


Figure 6. Microabscesses caused by Candida on MRI FLAIR, T2 weighted, DWI and SWI images.
Source: https://link.springer.com/referenceworkentry/10.1007/978-3-319-61423-6_48-1

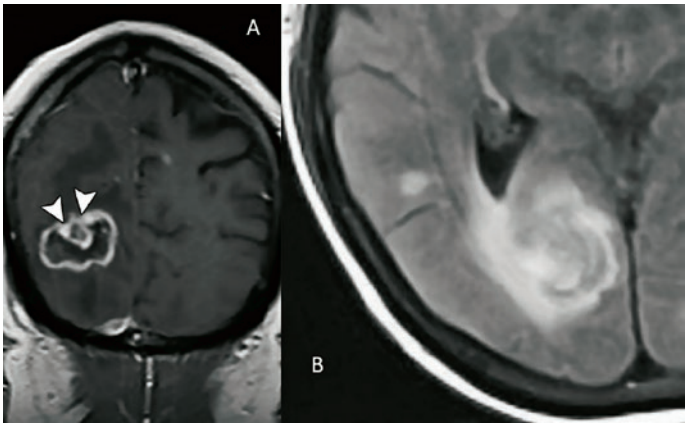


Figure 7. Image A displays brain MRI, coronal view, CE-T1 WI, „eccentric target sign". Image B displays brain MRI, axial view, FLAIR, „concentric target sign".
Source: https://link.springer.com/referenceworkentry/10.1007/978-3-319-61423-6_48-1

experience symptoms such as seizures, microcephaly, fever, and lymphadenopathy. Once the central nervous system is affected, symptoms such as headaches, convulsion and others follow (11).

Neuroradiological imaging of patients with toxoplasmosis reveals multiple abscesses in the basal ganglia, cortex, thalamus and cerebellum (10). The vast majority of lesions identified through CT scans exhibit a ring-like pattern with a surrounding zone of perifocal edema (13). Lesions can be further differentiated using MRI with a contrast-enhanced T1 weighted sequence, which highlights peripheral enhancement of the lesion that may appear nodular, ring-shaped, or irregular (10).

There are two characteristic imaging patterns that distinguish toxoplasmosis lesions from others causes. The first is the „eccentric target sign", which presents as a ring-like zone of a peripheral contrast-enhancment with small eccentic nodule along the wall (Figure 7). Although considered highly indicative of toxoplasmosis, it is observed in only about 30% of cases. The second common pattern is the "concentric target sign" on T2-weighted MRI images, which shows alternating concentric layers of hypo- and hyperintensity (Figure 7) (10).

3.2.2. Echinococcosis

The disease caused by the Echinococcus parasite manifests in two common forms in the human body. Cystic echinococcosis (hydatid disease) is caused by Echinococcus granulosus, a canine tapeworm that is most commonly transmitted via the fecal-oral route (11). The second type, alveolar echinococcosis, is a much more severe and dangerous condition. It is caused by Echinococcus multilocularis, with foxes being the primary carriers. This tapeworm primarily affects the liver, while brain and lung involvement is extremely rare. The advanced stage of alveolar echinococcosis is characterized by intrahepatic lesions that infiltrate the vascular structures of the liver, ususally extend to the diaphragm, and may spread even further (14).

Radiological diagnosis of intrahepatic lesions is relatively straightforward due to their characteristic appearance. On a X-ray image of abdominal region, ring-like hepatic calcifications may be observed, suggesting the presence of such a lesion. For confirmation, additional imaging such as ultrasound and CT scan can be performed (15).

3.2.3. Malaria

Malaria is considered the most significant parasitic disease worldwide, primarily due to its high incidence, with 300–500 million new cases each year, and an estimated 2 million deaths annually (11). It is transmitted by the Anopheles mosquito and caused by the Plasmodium parasite. With timely treatment, malaria can be effectively managed and symptoms resolve quickly. However, in untreated patients, severe complications may arise, including cerebral malaria, anemia, and ultimately death (16).

On MRI scans, cerebral malaria may present as diffuse brain edema caused by micro-occlusions. DWI sequences reveal cortical infarcts and there is non-specific hyperintense signals on T2 weighted images, along with hemorrhagic infarcts in the corticomedullary junction and deep white matter. Additionally, there have been detailed reports of cases showing hyperintense signals in T2 and FLAIR sequences, localized in the splenium of the corpus callosum, accompanied by diffusion restriction on DWI sequences and ADC maps, though without contrast enhancement of the described lesion (Figure 8) (11).

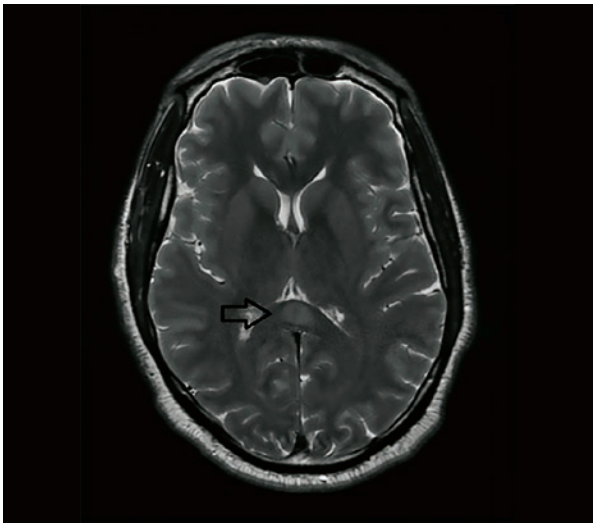


Figure 8. MRI, T2 WI, axial view of brain, display of hyperintense signal localized in the splenium of the corpus callosum.
Source: https://radiopaedia.org/cases/cerebral-malaria

3.3. Bacterial infections

3.3.1. Pyogenic meningitis

Meningitis is an inflammatory condition of the meninges that includes inflammatory processes divided into two categories: leptomeningeal (pia mater and arachnoid) and pachymeningeal (dura mater). The most common causes of pyogenic meningitis are Neisseria meningitidis,

Streptococcus pneumoniae, and Haemophilus influenzae. It most commonly develops in patients with chronic illnesses and immunocompromised individuals (17).

Computed tomography is frequently used in the early stages of the disease, primarily as a native CT scan of the head, performed before a lumbar puncture to rule out the presence of pathological changes causing increased intracranial pressure, which would ultimately be a contraindication for lumbar puncture. Occasionally, during such CT examinations, mild hyperdense reductions in the subarachnoid spaces may be observed as incidental findings. These changes represent a typical sign of pyogenic meningitis but are very difficult to detect, often leading to false-negative results (11).

During MRI scans, at some patients diagnosed with pyogenic meningitis, images may show abnormal hyperintensities within the cerebral sulci on T2, FLAIR, and diffusion-weighted sequences (Figure 9). Another very common sign is an abnormal increase in signal intensity in the pia mater and subarachnoid space. A thin linear hyperintense signal in the cerebral sulci is highly characteristic of acute bacterial meningitis. Additional MRI sequences that can be used to confirm leptomeningeal disease include post-contrast FLAIR and delayed post-contrast T1 weighted sequences. (11)

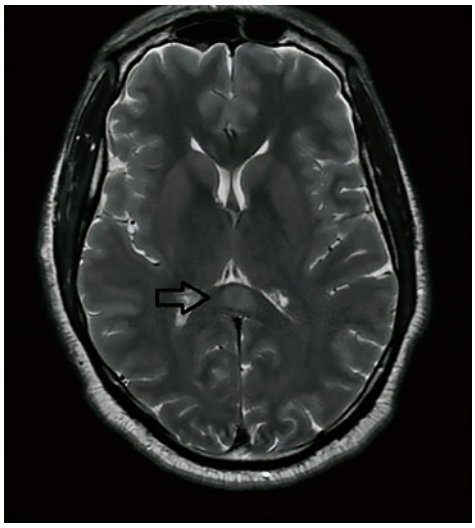


Figure 9. Brain MRI, axial view, FLAIR sequence, display of hyperintense signal distributed diffusely within cerebral sulci.
Source: https://radiopaedia.org/cases/bacterial-meningitis-1

3.3.2. Pyogenic spondilitis

Infections affecting the spinal cord often originate from the vertebral bodies, which are richly supplied with blood, and then spread through the intervertebral discs to the medulla. The most commonly affected region is the lumbosacral spine, followed by the thoracic and cervical regions. These infections are most frequently caused by the bacterium Staphylococcus aureus (55–90%), followed by Streptococcus, Pneumococcus, Enterococcus, E. coli, and others (18).

During the inflammatory process, spondylitis typically involves two vertebrae, the intervertebral disc, and part of the spinal cord, which is why this condition is often referred to as spondylodiscitis. On T1-weighted MRI sequences, the affected vertebrae appear as hypointense signals with an unclear distinction between the two affected vertebrae (Figure 10). The same area on T2-weighted images shows a high-intensity signal (Figure 10). The affected disc exhibits a signal similar to fluid on both T1- and T2-weighted images. After application of gadolinium-based contrast medium, the infected disc enhances with it. This enhancement can be homogeneous throughout the disc, partially affecting the disc or be present as thicker or thinner peripheral linear zones. The bone marrow within the infected vertebra also enhances with contrast, which is best visualized on fat-saturated sequences. The spread of infection into the paravertebral or epidural spaces may present as an abscess, which appears isointense or hypointense compared to the medulla on T1-weighted images and hyperintense on T2-weighted images (18).

3.3.3. Bacterially caused respiratory infections

The most prevalent bacterial cause of community-acquired infections is Streptococcus pneumoniae. It typically manifests as lobular pneumonia and often leads to bilateral consolidations. Staphylococcus aureus is a notable pathogen frequently found in hospital-acquired infections. Radiographic findings often reveal a bronchopneumonia pattern, while CT scans provide a more detailed depiction of centrilobular nodules with bronchial wall thickening (23). Nocardiosis, a Gram-positive bacterial infection, primarily affects immunocompromised patients, especially those who have undergone solid organ transplantation (most commonly lung transplants). Though rare, the infection has an extremely high mortality rate of up to 80% (12). Radiographic imaging of nocardiosis typically shows multiple consolidations as a reaction to abscess formation. In chronic cases, pleural thickening, bronchospasm, and fluid collections may be present (23).

3.4. Viral infections

3.4.1. Infections caused by cytomegalovirus (CMV)

Cytomegalovirus (CMV) is a DNA virus belonging to the herpesvirus family. Once it enters the human body, it remains dormant until the host enters an immunosuppressive state, triggering its reactivation (10). CMV most commonly manifests as infections of the neurological and respiratory systems.

CMV-induced encephalitis almost exclusively occurs in severely immunocompromised patients. On MRI scans, there are presentation of cortical atrophy and hyperintensities of white matter localized diffusely on T2 and FLAIR sequences (Figure 11). If periventricular or subependymal signal enhancement is noted in immunocompromised patients, CMV infection or the presence of lymphoma should be suspected. Additionally, solitary brain masses are very rare. It is important to note that MRI alone cannot confirm or exclude CMV infection, and because of that lumbar puncture and analysis of cerebrospinal fluid are necessary for definitive diagnosis (10).

More than 50% of virally induced pneumonias in immunocompromised patients are caused by CMV, making

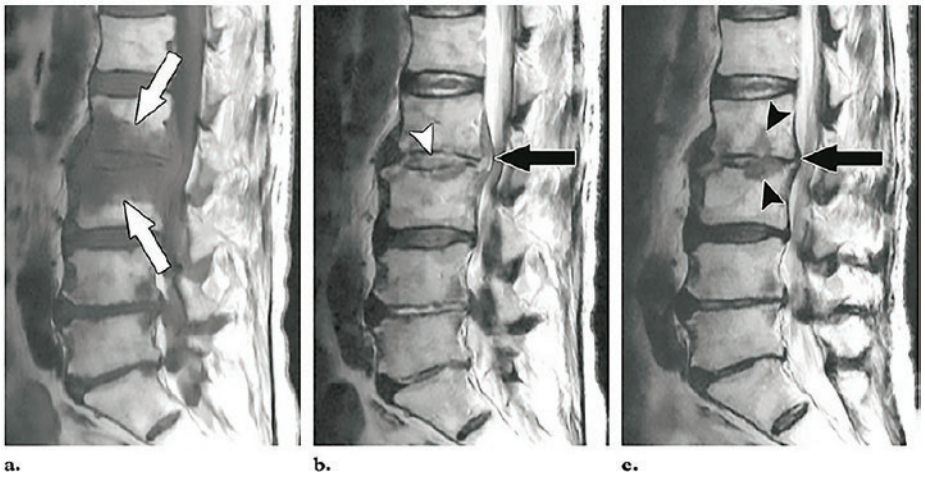


Figure 10. Image A displays MRI T1 WI, sagittal view; arrows indicate a hypointense signal in the vertebral bodies of L2 and L3, along with the corresponding disc. Image B displays MRI T2 WI, showing increased signal intensity in the affected disc, accompanied by an epidural abscess. Image C displays MRI T2 WI, taken two months after image B, demonstrating a reduction of the abscess, but progression of vertebral erosion.
Source: https://pubmed.ncbi.nlm.nih.gov/19325068/

it one of the most prevalent pathogens. On radiographic images, CMV pneumonia typically presents as unilateral or bilateral interstitial infiltrates, alveolar consolidations, and a ground-glass opacities. Some radiological signs of CMV infection may overlap with those of Pneumocystis jirovecii pneumonia; however, pleural effusions are more common in CMV pneumonia (12). CT imaging reveals consolidations, a ground-glass opacities, and centrilobular nodules. Additionally, in HIV-positive patients, discrete pulmonary masses ranging from 1 to 3 cm in size may also be present (23).

3.4.2. Infections caused by herpes simplex virus (HSV)

The herpes simplex virus is divided into two types: the first type is HSV-1, which causes encephalitis in older children and adults and is one of the most common causes of sporadic encephalitis worldwide. The second type, HSV-2, primarily causes encephalitis in neonates and immunocompromised hosts (20).

CT imaging is often the first method used for disease detection, helping to confirm or rule out conditions such as hemorrhage or increased intracranial pressure. Due to its lower sensitivity, CT frequently produces false-negative results in the early stages of the disease. It takes 3 to 4 days for the first abnormalities to be seen on CT images in the temporal or frontal lobes. The abnormalities commonly include areas of hypodensity, hemorrhage, or edema. Contrast changes may not be visible until a week after onset (20).

Unlike CT, MRI is significantly more sensitive in detecting encephalitic changes caused by the herpes simplex virus. The presence of brain lesions manifests as hypointense signals on T1-weighted sequences and hyperintense signals on T2-weighted and FLAIR sequences. Initial abnormalities appear as changes in white matter, primarily localized in the temporal lobe before spreading frontally (Figure 12). FLAIR sequences show thalamic involvement, which is not evident on DWI sequences. Contrast-enhanced T1 sequences often do not show changes in the early stages of the disease, but in advanced stages, there is an increased signal in the gyri, leptomeningeally, or diffusely throughout the brain (21). In immunocompromised patients, the affected area of cerebrum is larger and may include the medulla oblongata and cerebellum (20).

3.4.3. Infections caused by influenza A virus (H1N1)

An immunocompromised host has a very high tendency to get infected with influenza A virus, and the resulting symptoms are significantly more severe, with an increased possibility of complications compared to individuals with a stable immune system. The most common complication in immunocompromised patients infected with influenza A virus is pneumonia, while neurological complications

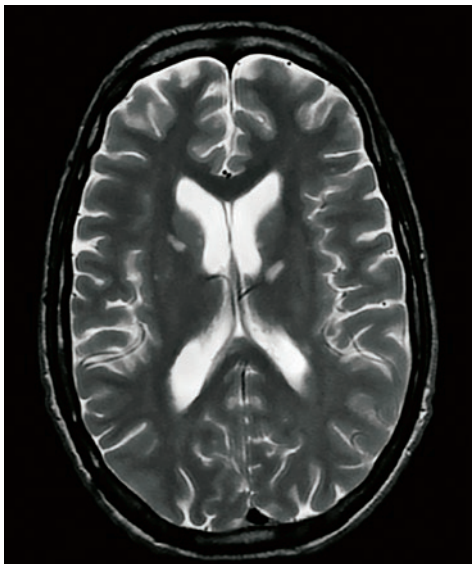


Figure 11. MRI of brain, axial view in T2 WI. Display of multiple periventricular areas of hyperintense signal at patient with CMV infection.
Source: https://radiopaedia.org/cases/cmv-ventriculitis-and-encephalitis

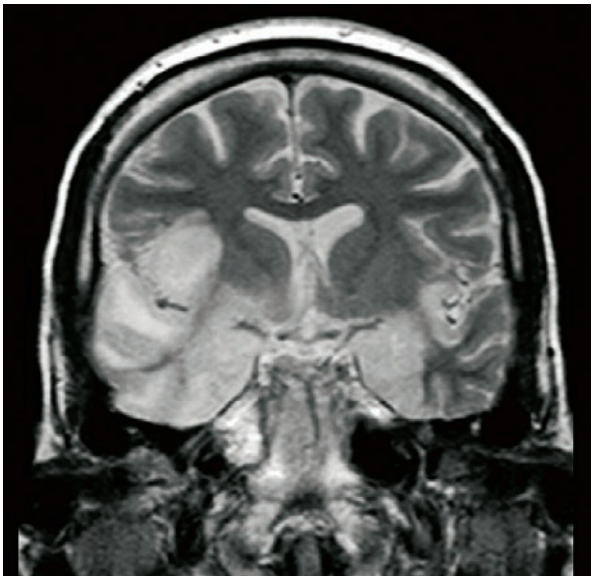


Figure 12. MRI of brain, coronal view in T2 WI. Display of hyperintense signal in the temporal lobes, extending to the hippocampus and the lower right frontal gyrus.
Source: https://radiopaedia.org/cases/hsv-encephalitis-2

are rarer and include epilepsy, encephalitis, meningitis, and Guillain-Barré syndrome. In addition to these, other inflammatory conditions affecting different organs may also occur. In immunocompromised patients, influenza A often develops as a co-infection with bacterial and fungal pathogens (22).

Influenza A virus most commonly presents with abnormalities in the lower respiratory tract. In a study by Amorim et al., which retrospectively analyzed 71 patients with H1N1 infection in 2009, high-resolution computed tomography (HRCT) findings of respiratory changes were presented. According to the study, the most frequently detected finding was a ground-glass opacities, followed by consolidations, which often appeared in combination. Additionally, bronchial wall thickening, interlobular septal thickening, and a crazy-paving pattern were relatively common. Pleural effusion was rarely observed, and when present, it was minimal (Table 1) (23).

Table 1. Distribution of HRCT findings in 71 patients with influenza A virus. (23).

Finding	Frequency	
	No of patients	Percentage (%)
Ground-glass opacities	60	85
Consolidations	46	64
Airspace nodules	18	25
Bronchial wall thickening	18	25
Interlobular septal thickening	15	21
Crazy-paving pattern	11	15
Perilobular pattern	2	3
Air trapping	2	3

Conclusion

Radiological imaging methods are a essential tools for establishing an accurate diagnosis, which leads to the prompt initiation of patient treatment. This is particulary crucial for immunocompromised patients, where time is a decisive factor in implementing an appropriate therapeutic approach.

Since immunocompromised patients are exposed to a wide range of aggressive pathogens that can cause highly specific infectious changes, it is essential to select their diagnosis method appropriately. For detecting infectious changes within the neurological system, MRI has proven to be an exceptionally reliable method. In addition to standard T1 WI and T2 WI sequences, DWI sequence should also be performed to clearly differentiate etiological factors and identify the causative pathogen. Alongside these pre-contrast sequences, post-contrast T1 and FLAIR sequences should also be conducted to determine the localization and extent of any inflammatory processes within the cerebrum, medulla oblongata or cerebellum. When diagnosing spondylitis or spondylodiscitis, fat-saturated sequences additionally highlight inflammatory processes within the discs and vertebrae.

Fungal and viral pathogens that cause infectious changes within the respiratory system can be reliably detected through HRCT, due to its extremely high sensitivity and specificity. Once the diagnosis is successfully established and the extent of inflammatory processes within the system is determined, follow-up diagnostics at shorter intervals can be conducted using a standard chest X-ray.

Radiology provides a comprehensive imaging overview of all infectious conditions that develop within the human body. Depending on the type of pathogen and the disease's localization, radiology offers an appropriate diagnostic method that can timely detect and differentiate the condition and its causative agent.

All data in this paper are part of the results of master's thesis "Radiological approach to immunocompromised patient" written at the University Department of Health Studies, University of Split (24).

Reference

1. Thurnher, M.M. (2018). Infections in Immunocompromised Individuals. In: Barkhof, F., Jager, R., Thurnher, M., Rovira Cañellas, A. (eds) Clinical Neuroradiology. Springer, Cham. https://doi.org/10.1007/978-3-319-61423-6_48-1
2. Meidani M, Naeini AE, Rostami M, Sherkat R, Tayeri K. Immunocompromised patients: Review of the most common infections happened in 446 hospitalized patients. J Res Med Sci. 2014 Mar;19(Suppl 1):S71-3.
3. Begovac J. i sur. Klinička infektologija. Zagreb: Medicinska naklada; 2019. Stranice 321-432.
4. McCusker C, Upton J, Warrington R. Primary immunodeficiency. Allergy Asthma Clin Immunol. 2018 Sep 12;14(Suppl 2):61. doi: 10.1186/s13223-018-0290-5.
5. Bonilla, Francisco A.Bonilla, Francisco A.Khan, David A.Bernstein, David I.Bonilla, Francisco A. et al.; Practice parameter for the diagnosis and management of primary immunodeficiency; Journal of Allergy and Clinical Immunology, Volume 136, Issue 5, 1186 – 1205.e78
6. Duncan MD, Wilkes DS. Transplant-related immunosuppression: a review of immunosuppression and pulmonary infections. Proc Am Thorac Soc. 2005;2(5):449-55. doi: 10.1513/pats.200507-073JS.

7. Carvalho HA, Villar RC. Radiotherapy and immune response: the systemic effects of a local treatment. Clinics (Sao Paulo). 2018 Dec 10;73(suppl 1):e557s. doi: 10.6061/clinics/2018/e557s.
8. Sharp PM, Hahn BH. Origins of HIV and the AIDS pandemic. Cold Spring Harb Perspect Med. 2011 Sep;1(1):a006841. doi: 10.1101/cshperspect.a006841.
9. World Health Organisation [Internet], HIV and AIDS, (updated 22 July 2024., accessed 21 Feb 2025.) Dostupno na: https://www.who.int/news-room/fact-sheets/detail/hiv-aids
10. Thurnher, M.M. (2018). Infections in Immunocompromised Individuals. In: Barkhof, F., Jager, R., Thurnher, M., Rovira Cañellas, A. (eds) Clinical Neuroradiology. Springer, Cham. https://doi.org/10.1007/978-3-319-61423-6_48-1
11. Shih Robert Y., Koeller Kelly K., Bacterial, Fungal, and Parasitic Infections of the Central Nervous System: Radiologic-Pathologic Correlation and Historical Perspectives, 2015, 35:0000-0000.
12. Xiangpeng Zheng, Guozhen Zhang, Imaging pulmonary infectious diseases in immunocompromised patients, Radiology of Infectious Diseases, Volume 1, Issue 1, 2014, Pages 37-41, ISSN 2352-6211. https://doi.org/10.1016/j.jrid.2014.11.001
13. Višković K., Hertl V., Mirt M., Tota M., Frković M., Zekan Š., Begovac J., Radiološka diferencijalna dijagnostika prstenastih imbibiranih lezija središnjeg živčanog sustava u bolesnika zaraženih HIV-om., Croatian Journal of Infection 34:3, Pages 157-162, 2014. ISSN 1331-2820
14. Qu B, Guo L, Sheng G, Yu F, Chen G, Wang Y, Shi Y, Zhan H, Yang Y, Du X. Management of Advanced Hepatic Alveolar Echinococcosis: Report of 42 Cases. Am J Trop Med Hyg. 2017 Mar;96(3):680-685. doi: 10.4269/ajtmh.16-0557.
15. Shah U. Infections of the Liver. Diseases of the Liver in Children. 2013 Aug 23:285–312. doi: 10.1007/978-1-4614-9005-0_15.
16. Buck E, Finnigan NA. Malaria. [Updated 2023 Jul 31]. In: StatPearls [Internet]. Treasure Island (FL): StatPearls Publishing; 2024 Jan-. Available from: https://www.ncbi.nlm.nih.gov/books/NBK551711/
17. Di Muzio B, Elfeky M, Kumar K, et al. Pyogenic meningitis. Reference article, Radiopaedia.org (Accessed on 18 Mar 2024) https://doi.org/10.53347/rID-36907
18. Hong SH, Choi JY, Lee JW, Kim NR, Choi JA, Kang HS. MR imaging assessment of the spine: infection or an imitation? Radiographics. 2009 Mar-Apr;29(2):599-612. doi: 10.1148/rg.292085137.
19. Garg M, Prabhakar N, Gulati A, Agarwal R, Dhooria S. Spectrum of imaging findings in pulmonary infections. Part 1: Bacterial and viral. Pol J Radiol. 2019 Apr 18;84:e205-e213. doi: 10.5114/pjr.2019.85812.
20. AK AK, Bhutta BS, Mendez MD. Herpes Simplex Encephalitis. [Updated 2024 Jan 19]. In: StatPearls [Internet]. Treasure Island (FL): StatPearls Publishing; 2024 Jan-. Available from: https://www.ncbi.nlm.nih.gov/books/NBK557643
21. Gaillard F, Sharma R, Glick Y, et al. Herpes simplex encephalitis. Reference article, Radiopaedia.org (Accessed on 24 Mar 2024) https://doi.org/10.53347/rID-1410
22. Harish MM, Ruhatiya RS. Influenza H1N1 infection in immunocompromised host: A concise review. Lung India. 2019 Jul-Aug;36(4):330-336. doi: 10.4103/lungindia.lungindia_464_18.
23. Amorim VB, Rodrigues RS, Barreto MM, Zanetti G, Hochhegger B, Marchiori E. Influenza A (H1N1) pneumonia: HRCT findings. J Bras Pneumol. 2013 May-Jun;39(3):323-9. doi: 10.1590/S1806-37132013000300009.
24. Babić D., Radiološki pristup imunokompromitiranom pacijentu [Master Thesis]. Split: Univesrity of Split; 2024 [Accessed 14.02.2025.] Available from: https://urn.nsk.hr/urn:nbn:hr:176:350965

Radiološka Obrada Infekcija kod Imunokompromitiranih Pacijenata

Sažetak

Imunokompromitiranost se definira kao stanje narušenog ili disfunkcionalnog imunološkog sustava, koji nije u stanju obraniti organizam od vanjskih patogena. Uzroci imunokompromitiranosti mogu biti prirođeni ili stečeni, a najogledniji primjer u svijetu jest virus humane imunodeficijencije. Imunokompromitirani bolesnik ima povećanu sklonost za razvoj infekcije, koja može biti uzrokovana patogenima poput gljivica, parazita, bakterija ili virusa.

Primjena odgovarajućih radioloških metoda u okviru dijagnostičke upotrebe ima važnu ulogu u ranom otkrivanju i liječenju različitih infektivnih i drugih bolesti koje su svojstvene imunokompromitiranim bolesnicima.

Imunokompromitirani pacijenti najčešće razvijaju oportunističke infekcije neurološkog sustava. S obzirom da neurološke promjene u početnom stadiju razvoja često ne budu uočene na CT pregledima, ponajviše se za pravovremenu detekciju bolesti koristi magnetska rezonancija, kao metoda najveće specifičnosti i osjetljivosti za navedena stanja. Prilikom snimanja MR-om bitno je koristiti više različitih predkontrastnih i dodatno postkontrastnih sekvenci, kako bi se sa sigurnošću mogle dokazati izrazito specifične neurološke infekcije, te njihova diferencijacija u odnosu na vrstu etiološkog čimbenika. Osim neuroloških komplikacija, imunokompromitirani pacijenti su vrlo skloni i razvoju respiratornih infekcija. Metoda izbora kod takvih komplikacija je svakako višeslojni CT, koji u ranoj fazi bolesti može detektirati i najmanje promjene unutar respiratornog sustava. Nakon inicijalne detekcije bolesti, za njeno daljnje praćenje, radiografska obrada torakalne regije predstavlja izuzetno snažan i pristupačan alat, koji sa svojom značajnom osjetljivošću može usmjeravati daljnji tijek liječenja.

Ključne riječi: HIV, imunodeficijencija, infekcija, radiologija

REVIEW ARTICLE (PREGLEDNI RAD)

Present and future role of MRI in radiotherapy

Endira Al-Khazae[1,2], **Frane Mihanović**[2]

[1] UPMC Hillman Cancer Center Croatia

[2] University of Split, University Department of Health Studies, Split, Croatia

Corresponding author: Frane Mihanović, frane.mihanovic@ozs.unist.hr

DOI: https://doi.org/10.55378/rv.49.1.4

Abstract

This paper explores the integration of MRI into modern clinical radiotherapy practice, examining its potential to enhance treatment precision, efficiency, and improve patient outcomes. The study offers an overview of MRI applications, including radiotherapy planning, image registration, quality assurance with an emphasis on reducing geometric distortions, and real-time adaptive MRI-guided radiotherapy. The introduction covers the use of MRI in treatment planning, followed by a description of its role during therapy, emphasizing functional imaging techniques and motion control. Dosimetric requirements, CT replacement techniques, and adaptive MRI-guided real-time radiotherapy are also discussed. The paper also presents early results obtained from MRI-linear accelerators, discussing technical challenges and the current status of these devices. Finally, by analyzing various scientific articles, the future role of magnetic resonance imaging in radiotherapy is considered, and conclusions are drawn based on the analyses and results collected.

Keywords: Adaptive Radiotherapy; MRIgRT; MR-linear accelerator; modern radiotherapy

Abbreviations and acronyms: ART – Adaptive Radiotherapy, **CBCT** – Cone Beam Computed Tomography, **CT** – Computed Tomography, **CTV** – Clinical Target Volume**, DVH –** Dose-Volume Histogram, **FOV** – Field of View, **GTV** – Gross Tumor Volume, **MRI** – Magnetic Resonance Imaging, **MRIgRT** – Magnetic Resonance Image-guided Radiotherapy, **MRI-LINAC –** MRI-Linear Accelerator system, **OAR** – Organs at Risk, **PTV** – Planning Target Volume**, QA –** Quality Assurance, **RF** – Radiofrequency, **RT** – Radiotherapy, **RTP** – Radiation Treatment Planning**, SBRT** – Stereotactic Body Radiation Therapy, **SCT** – Synthetic Computed Tomography, **SNR** – Signal-to-Noise Ratio, **SRS** – Stereotactic Radiosurgery

Introduction

Over the past century, a significant decline in cancer mortality rates has been observed [1], with the exception of certain aggressive malignancies such as glioblastoma and pancreatic cancer. This trend is closely associated with advances in treatment, particularly in the field of radiotherapy (Figure 1), which has become very important, often in combination with chemotherapy. Radiotherapy is applicable to approximately 60% of oncology patients and continues to evolve through technological advancements and innovations in treatment planning and delivery [1]. In modern oncology, Magnetic Resonance Imaging is gaining an increasingly prominent role, not only in the treatment planning but also during the execution of therapy (Figure 2) [2]. Advances in high-resolution imaging, superior soft tissue contrast, and real-time monitoring capabilities contribute to more precise dose delivery, reduced toxicity, and improved patient quality of life [3,4]. The radiotherapy workflow begins with patient preparation, including education about the procedure, immobilization, and positioning, followed by simulation using CT or MRI [2] (Figure 3). Based on these images, a radiation treatment plan



Figure 1: Linear accelerator
Source: https://trends.medicalexpo.com/varian-oncology/project-70440-414038.html



Figure 2. MRI Simulator for Radiotherapy Treatment Planning
Source: https://www.siemens-healthineers.com/radiotherapy/MR-for-rt

is developed, integrating previous diagnostic data. During therapy, image verification is ensured through CBCT comparing current images with those acquired during simulation. This process ensures the correct positioning of the clinical target volume (CTV) and maintains the radiation dose within prescribed limits [2]. In this context, the role of MRI is not merely supplementary but increasingly serves as a primary modality in radiotherapy planning, because of its capacity to provide detailed anatomical and functional information [5,6].

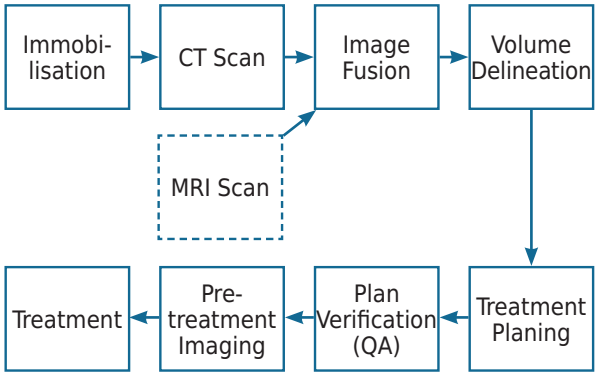


Figure 3. Radiotherapy Workflow
Source: https://pubmed.ncbi.nlm.nih.gov/30194794/

Radiotherapy planning workflow

Treatment Planning Systems (TPS): Core of planning, integrating imaging, dose calculations, and optimization [6,7].
Imaging & Simulation: High-quality CT, MRI, and PET imaging for accurate tumor and organ-at-risk (OAR) delineation [4,7].
Target Volume Definition:

- *GTV:* localize the tumor, guide the dose distribution, minimize the exposure to surrounding healthy tissues [4,7]
- *CTV*: includes microscopic spread
- *PTV*: adds margins for uncertainties

Dose Prescription & Constraints: Balancing dose to targets while minimizing exposure to OARs [3,7].
Treatment Techniques:

- *3D-CRT*, *IMRT*, *VMAT* for dose conformity
- *SRS/SBRT* for precision in small targets [4,7]

Motion Management: Techniques like gating, breath-hold, and adaptive planning for organ motion [4,7].
Quality Assurance: Ensuring treatment accuracy with conformity and safety checks [7].
Adaptive Radiotherapy: Adjusting plans based on anatomical changes during treatment [7].

MRI in radiotherapy treatment planning

Radiotherapy treatment planning requires precise delineation of the target volume and identification of critical structures to be protected. Advances in technology have led to the development of techniques such as SRS and SBRT, which improve treatment outcomes by reducing side effects and enhancing therapeutic efficacy [4]. The use of MRI in RTP offers multiple advantages [4,7]. Unlike CT, MRI provides superior soft tissue contrast, allowing more accurate contouring of tumors and surrounding healthy organs [7,8]. Despite initial challenges, such as reduced bone imaging capability and the lack of electron density information needed for dosimetric calculations, new MRI techniques including the use of dynamic contrast and diffusion sequences have improved tissue segmentation and therapy individualization [6]. In specific body regions, particularly the head, neck, and brain, MRI is already used independently (Figure 6). MRI images can serve as a secondary modality alongside CT during planning; however,

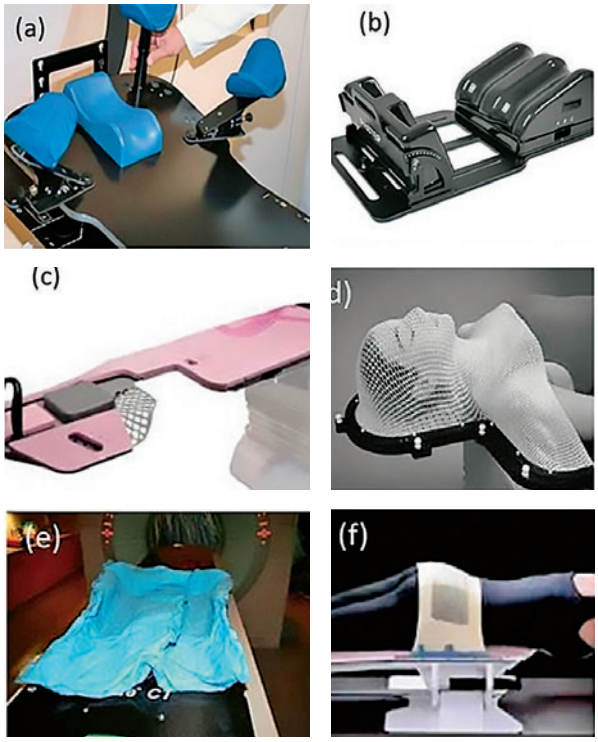


Figure 4. Immobilization devices in radiotherapy
Source: https://pubmed.ncbi.nlm.nih.gov/30194794/

more recently, planning is increasingly being performed only based on MRI images (Figure 5). A growing number of clinical studies confirm its utility and reliability [9]. Over the last decade, MRI has been increasingly utilized in radiotherapy, not only for planning but also for assessing treatment response. To streamline workflow, reduce patient

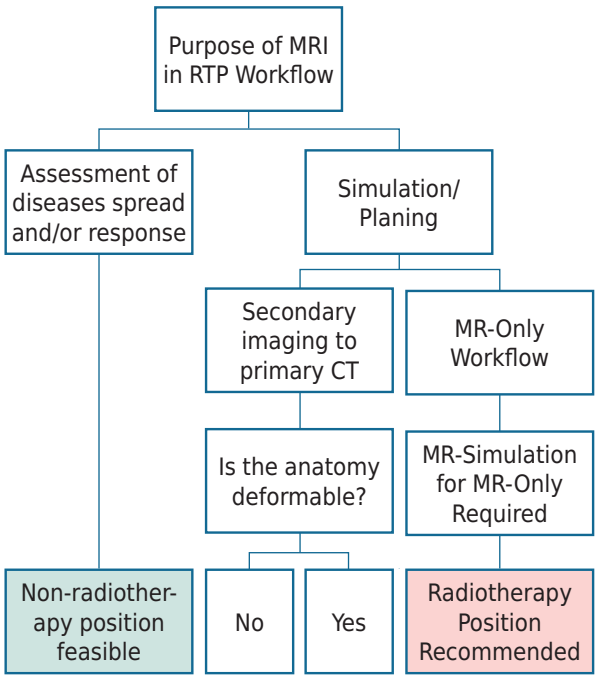


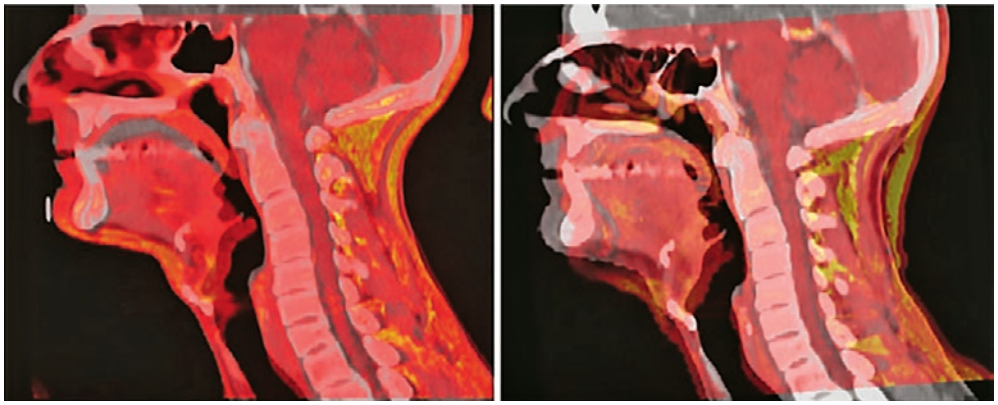
Figure 5. Guide for the use of the different imaging positions in RTP workflow
Source: Tijssen RHN, Paulson ES, Rai R. Implementation and Acquisition Protocols. MRI for Radiotherapy [Internet]. 2019;3–19.



Figure 6. Example of a head and neck setup with the patient immobilisied using a thermoplastic mask and vacuum bag
Source: Jonsson, J.H., Karlsson M.G., Karlsson M., *et al.* Treatment planning using MRI data: an analysis of the dose calculation accuracy for different treatment regions. Radiat. Oncol. 2010 Jun 30;5:62. doi: 10.1186/1748-717X-5-62

dose, and ensure cost-effectiveness, it is logical to aim for a treatment planning process entirely based on MRI [10]. Radiotherapy planning also requires specific protocols for MRI equipment placement [11]. Rooms housing MRI equipment must meet strict criteria, including vibration protection and minimal electromagnetic interference. Safety protocols involve dividing spaces into zones (from Zone I—free access, to Zone IV—the highest risk area), ensuring only educated staff access specific zones [11]. Additionally, immobilization sets must be tailored to MRI devices, and their compatibility tested through internal protocols to minimize artifacts and ensure optimal image quality [6,11] (Figure 4). Successful integration of MRI into radiotherapy planning relies on collaboration between radiation oncologists, radiation therapists, and medical physicists [6,11]. Ongoing staff education and training are crucial to adapting to new technologies and maintaining safety standards. This approach facilitates effective use of MRI in planning, achieving more accurate target volume definition and reducing the risk of adverse side effects [6,7,11].

The integration of MRI into radiotherapy protocols presents challenges related to patient safety [6]. Before each MRI procedure, a thorough assessment of the patient's compatibility with the device is performed, including a review of implanted devices such as pacemakers and ICD [11]. Strict adherence to manufacturer guidelines is necessary for these patients to avoid adverse reactions such as overheating or current induction [11]. The use of contrast, particularly gadolinium, adds another level of complexity to safety protocols. Gadolinium enhances T1 contrast, but different types of contrast vary in their retention dynamics within the body. Therefore, laboratory tests, including an assessment of renal function, are required before contrast administration, and patients must be informed about potential side effects [11]. Another critical aspect of radiotherapy implementation is QA, which is of paramount importance. Specific requirements, such as patient positioning using flat table inserts and immobilization devices, directly impact MRI image quality [12]. QA protocols involve daily, weekly, monthly, and annual reviews. For radiotherapy imaging, a larger FOV is often required to encompass tumor volumes, organs at risk, and the external body contours. QA procedures typically uti-



Treatment position MRI **Diagnostic position MRI**

Figure 9. Images of a patient with an oropharyngeal squamous cell carcinoma, grey overlay images are CT, and red overlay are MRI. MRI images acquired in the treatment and diagnostic position
Source: Speight R., MRI to CT Image Registration. In: Liney G, van der Heide U, editors. MRI for Radiotherapy [Internet]. Springer International Publishing; 2019.

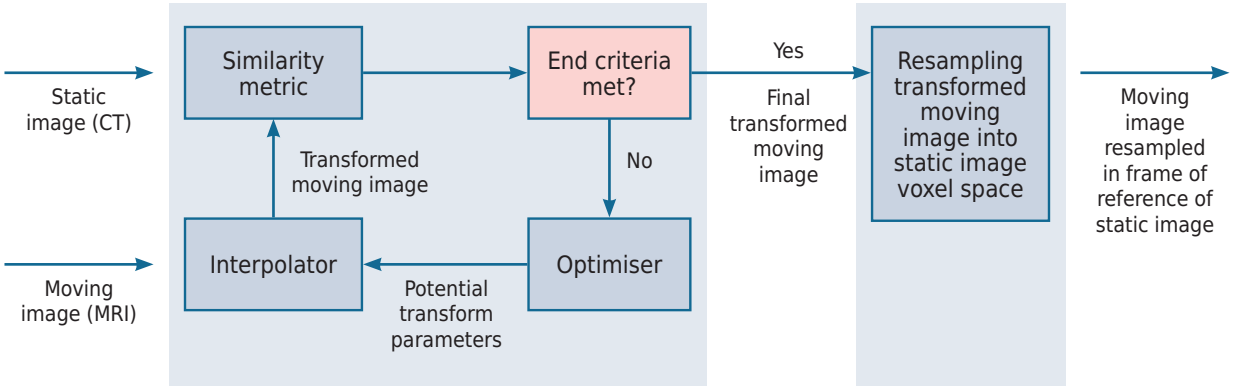
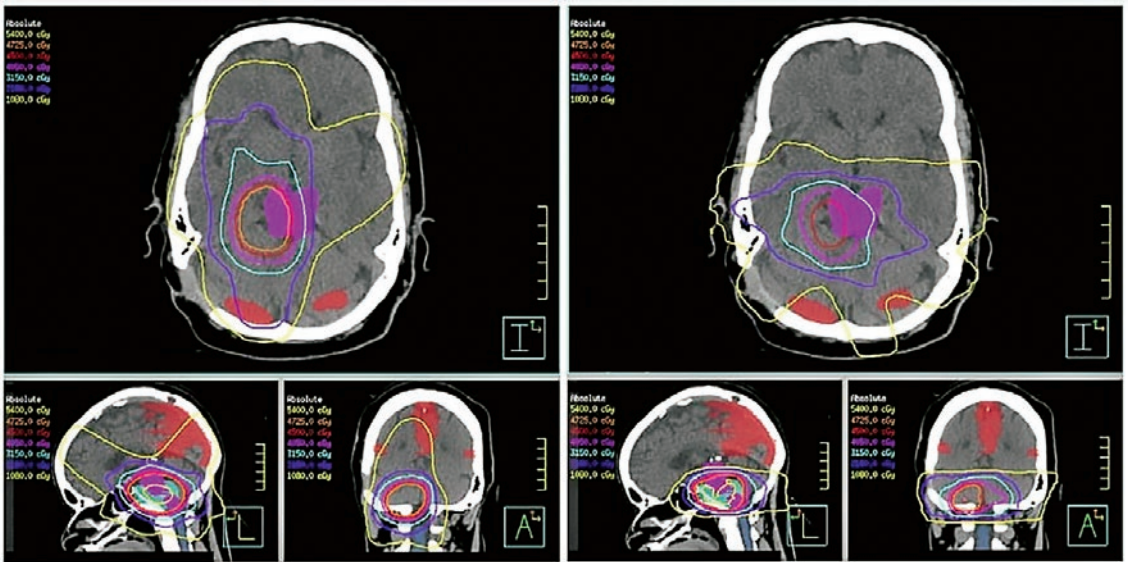


Figure 10. Schematic of the automatic image registration process
Source: Speight R., MRI to CT Image Registration. In: Liney G, van der Heide U, editors. MRI for Radiotherapy [Internet]. Springer International Publishing; 2019.



Standard care plan **fMRI DWN avoidance plan**

Figure 11. Comparison of standard radiotherapy (left) vs. fMRI-guided DMN avoidance (right), highlighting differences in dose distribution to protect brain function
Source: https://physicsworld.com/a/resting-state-fmri-fine-tunes-brain-radiotherapy-plans/

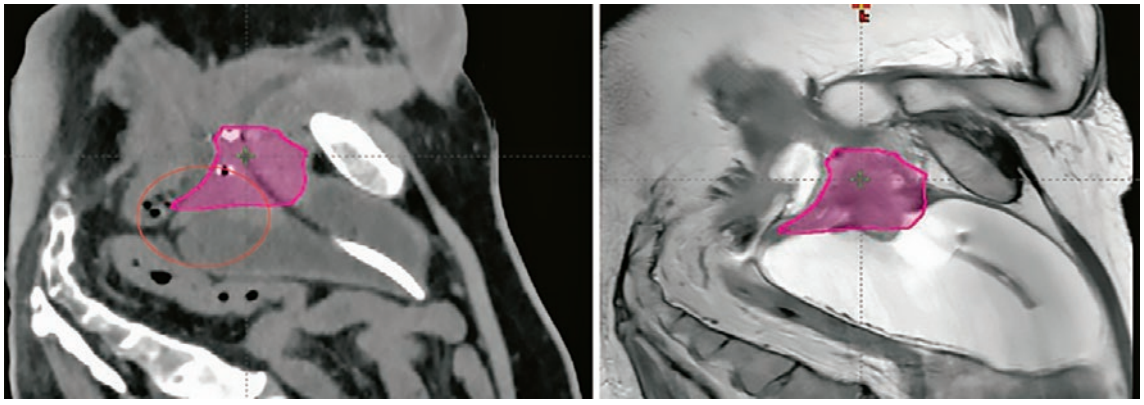


Figure 12. An example case when MRI is used as a secondary imaging modality
Source: Tyagi N., Challenges and Requirements, in: Liney G, van der Heide U, editors. MRI for Radiotherapy [Internet]. Springer International Publishing; 2019.

lize the ACR MR QA phantom along with commercial large FOV phantoms with geometric accuracy to assess image quality [12].

MRI during treatment

For effective implementation of MRI in radiotherapy, it is necessary to establish strict protocols for image registration [6]. The registration of MRI and CT images, or the fusion of data from both modalities, enables the transfer of specific structures from one image to another. Figure 9 displays MRI images obtained in both radiotherapy and diagnostic positions, where significant variations in the positioning of the neck and chin are visible [6]. However, due to the fundamental differences between MRI (which maps proton signals) and CT (which maps electron density), this process requires advanced algorithms and manual or automatic adjustments to achieve high precision [6]. Automated registration algorithms use optimization loops that adjust translations and rotations of the moving image, while manual registration depends on experienced staff who can further refine the results. This hybrid approach ensures that the registration is within acceptable error margins, thereby minimizing the risk of errors in dose delivery [6] (Figure 10).

The application of MRI in radiotherapy delivery opens up opportunities for monitoring anatomical changes in patients during treatment [6]. Functional MRI (fMRI) imaging provides visualization of physiological tissue characteristics, including vascularization, cell density, and metabolism, which is particularly valuable in assessing tumor response to radiation [13]. For instance, in the case of brain tumors, the integration of fMRI data enables more precise delineation of the tumor volume and allows for real-time dose adjustment, thereby enhancing disease control [13]. Figure 11 compares standard radiation therapy planning (left) with fMRI-guided DMN avoidance planning (right), showing differences in radiation dose distribution to preserve critical brain networks [13].

One of the most important challenges in radiotherapy delivery is organ motion during treatment [13]. In Figure 12, an example is shown where MRI is used as a secondary imaging modality. Variations in the bladder and rectum between CT and MRI resulted in different positions of the seminal vesicles [14]. Traditional CT techniques, due to their limited soft tissue contrast, often cannot accurately track patient movements, which may lead to deviations in

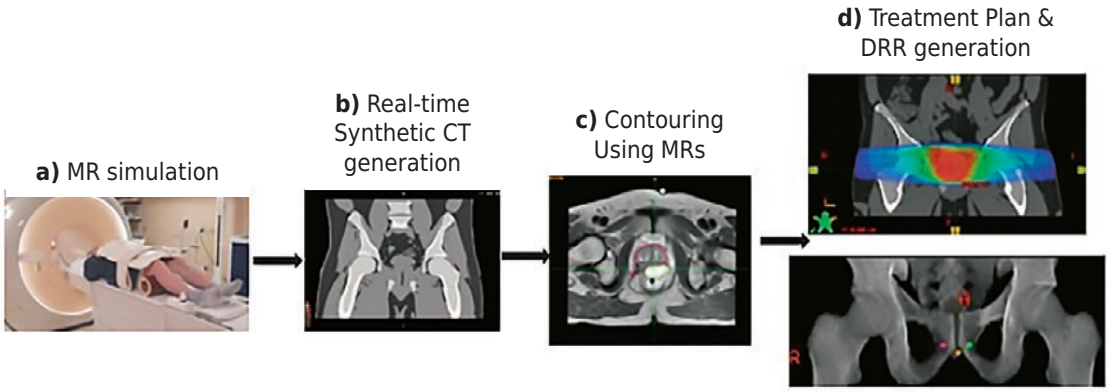


Figure 13. MRI-only workflow: (a) MR simulation. (b) Real-time synthetic CT generation. (c) Contouring using MRI. (d) Treatment plan and DRR generation
Source: Tyagi N., Challenges and Requirements, in: Liney G, van der Heide U, editors. MRI for Radiotherapy [Internet]. Springer International Publishing; 2019.

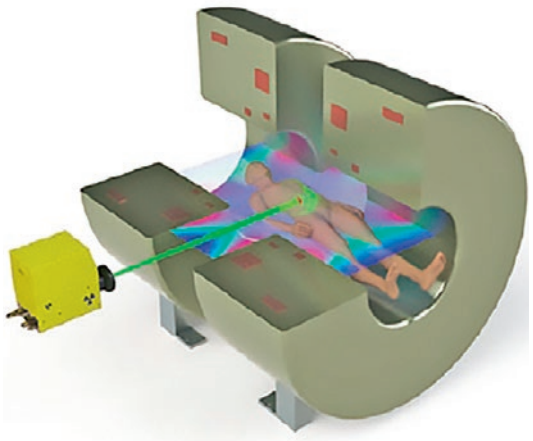
dose delivery. MRI, on the other hand, enables real-time motion tracking through high-frequency imaging, facilitating treatment adaptation during each fraction [14]. This approach, known as MRIgRT enables continuous verification of the position of the target volume and adjustment of plans in case of changes in anatomy [6,12,14,15].

Innovative approaches in radiotherapy delivery also include method where planning and treatment are based on MRI only modality [6,15] (Figure 13). This approach eliminates the need for additional MRI and CT image registration, thereby reducing the potential for errors, saving time, and decreasing patient exposure to radiation from CT devices [6,15]. Clinical experiences indicate that using an MRI-only protocol can enhance dose delivery precision and allow for dynamic treatment plan adaptation, particularly in tumors prone to changes during therapy. MRIgRT requires precise monitoring of the CTV [6,7-9,14-16]. MR-linear accelerators enable continuous high-frequency imaging, facilitating the detection and compensation of motion during therapy. Monitoring is typically performed in the sagittal plane, with parameters such as boundary expansion (defining the permissible space outside the target volume) and the region of interest for monitoring being established [7,16]. Incorporating audio or visual feedback further assists patients in maintaining a stable position, thus enhancing the accuracy of therapy [16].

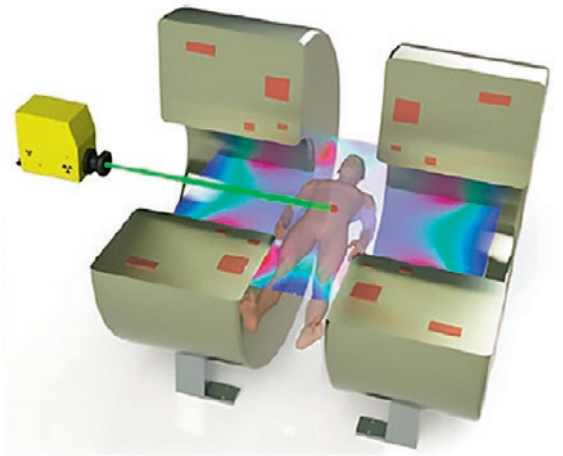
MRI-linac integration challenges

While MRI technology offers numerous advantages in radiotherapy, its integration into clinical practice presents a range of technical and logistical challenges [6,16,17]. One of the most significant challenges is synchronizing the MRI system with the linear accelerator. Operating a linear accelerator in proximity to an MRI device is particularly difficult due to electromagnetic interference between the two subsystems (MRI and linear accelerator) [16-22]. The magnetic fields generated by the MRI affect the electron trajectories in the accelerator according to the Lorentz law:

$$\vec{F} = q(\vec{E} + \vec{v} \times \vec{B}),$$



a) Perpendicular configuration



b) In-line configuration

Figure 14. MRI-Linac systems in two possible configurations
Source: Whelan B., Oborn B., Liney G., Keall P., RI Linac Systems, In: Liney G, van der Heide U, editors. MRI for Radiotherapy [Internet]. Springer International Publishing; 2019.

System	Radiation type	Field strength	Magnet type	Orientation	Source-isocentre distance	First patient Tx
Elekta Unity	7 MV FFF	1.5 T	Closed superconducting	Perpendicular	1.47 m	May 2017
View Ray MRIdian	6 MV or ^{60}Co FFF	0.35 T	Split superconducting	Perpendicular	0.9 m	February 2014 (^{60}Co) July 2017 (Linac)
Magnet Tx Aurora	6MV	0.5 T	High temperature superconducting with steel yoke	In-line	1.4 m	Has not yet occurred
Australian MRI-Linac	4 & 6 MV FFF	1.0 T	Open superconducting	In- line with perpendicular option	1.8 m	Has not yet occurred

FFF flattening filter free, *MV* megavoltage, *Tx* treatment

Figure 15. Specifications of the existing MRI-Linacs
Source: Whelan B., Oborn B., Liney G., Keall P., RI Linac Systems, In: Liney G, van der Heide U, editors. MRI for Radiotherapy [Internet]. Springer International Publishing; 2019

where q is the electron charge, v is the velocity, B is the magnetic field, and F is the force acting on the electron [22]. These systems facilitate the simultaneous use of MRI imaging and radiation, enabling real-time therapy adaptation [21-23]. The configurations of MRI-linear accelerators can be either perpendicular or parallel, depending on the orientation of the magnetic field relative to the radiation beam [22]. In the perpendicular configuration, the magnetic field influences the electron path within the accelerator, potentially reducing the beam energy if the magnetic field is not adequately shielded [22]. In the parallel configuration, negative effects occur only at much higher magnetic field strengths (Figure 14). Therefore, it is essential to position the linear accelerator in a region where the magnetic field is minimal or apply appropriate shielding measures to ensure beam stability [11,22].

Adaptive radiotherapy

ART is a methodology that modifies patient treatment based on changes in target volumes and organs at risk (OARs) [23]. This approach enhances dose delivery precision to the tumor while simultaneously sparing the OARs from unnecessary exposure to the same dose. ART involves real-time image guided radiotherapy, accurate image registration, re-contouring of targets and OARs, treatment plan evaluation and re-optimization, as well as dosimetry andQA [23-26]. Adaptation can be performed offline, where new data is collected, and a new treatment plan is generated over hours or days, or online, where adjustments are made while the patient is on the treatment table during radiotherapy (Figure 16) [23-26].

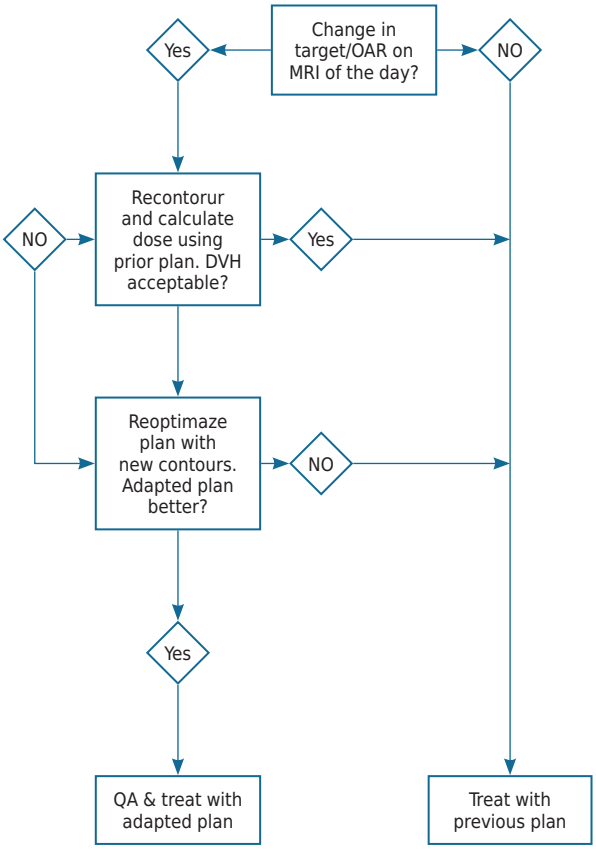


Figure 16. Example online adapted workflow: OAR, DVH, QA
Source: Roach M., Glide-Hurst C.K., MR at the time of External Beam Treatment In: Liney G, van der Heide U, editors. MRI for Radiotherapy [Internet]. Springer International Publishing; 2019.

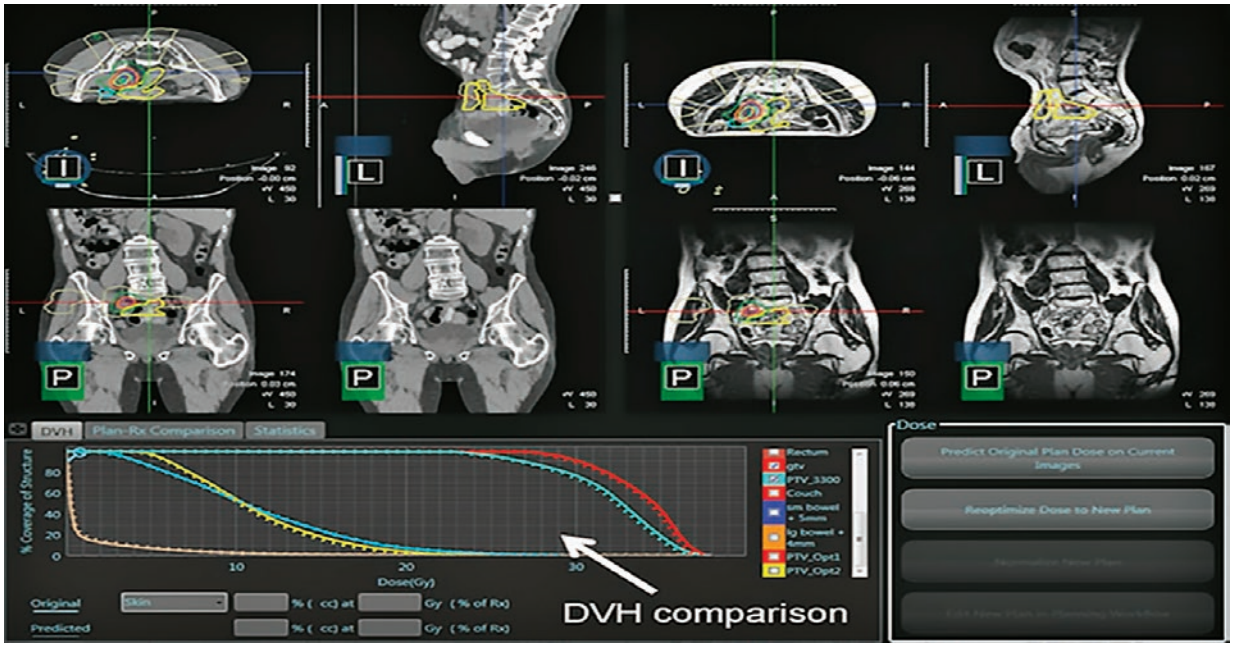


Figure 17. Comparison of original plan (four upper left CT images) on the original CT simulation scan, and the original plan's beams when calculated on the first day's MRI scan on ViewRay. The lower half of the panel shows a DVH showing the percent of structures receiving a certain dose
Source: Roach M., Glide-Hurst C.K., MR at the time of External Beam Treatment In: Liney G, van der Heide U, editors. MRI for Radiotherapy [Internet]. Springer International Publishing; 2019.

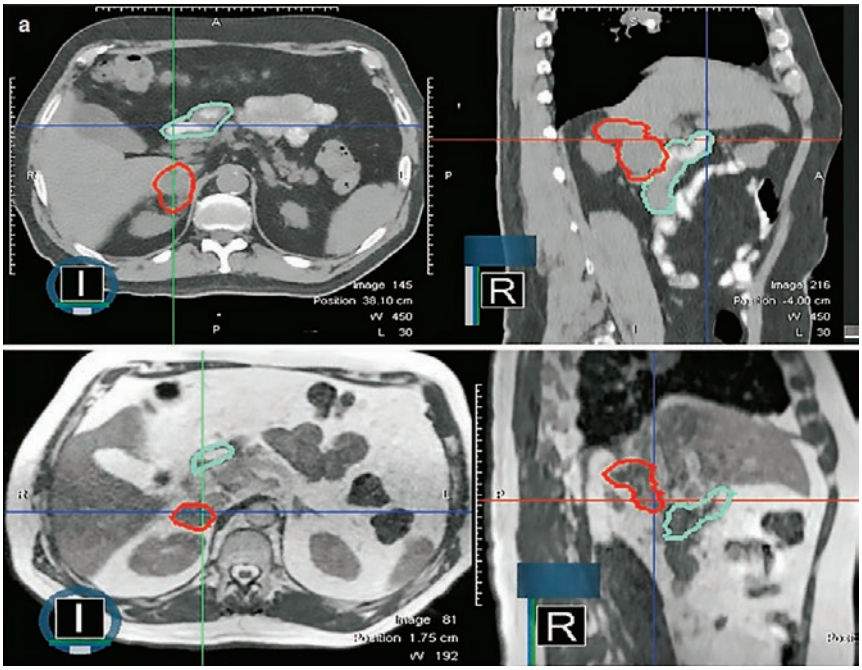


Figure 18. Online/on-table adaptation of a right adrenal target (red) on ViewRay. The top two panels are axial and sagittal slices of the simulation CT scan where nearby duodenum (cyan) is nearby. The bottom panels show that on the set-up MRI for the first day of treatment, the duo denum has shifted further away from the target, poten tially allowing for better dose coverage of the target

Source: Roach M., Glide-Hurst C.K., MR at the time of External Beam Treatment In: Liney G, van der Heide U, editors. MRI for Radiotherapy [Internet]. Springer International Publishing; 2019.

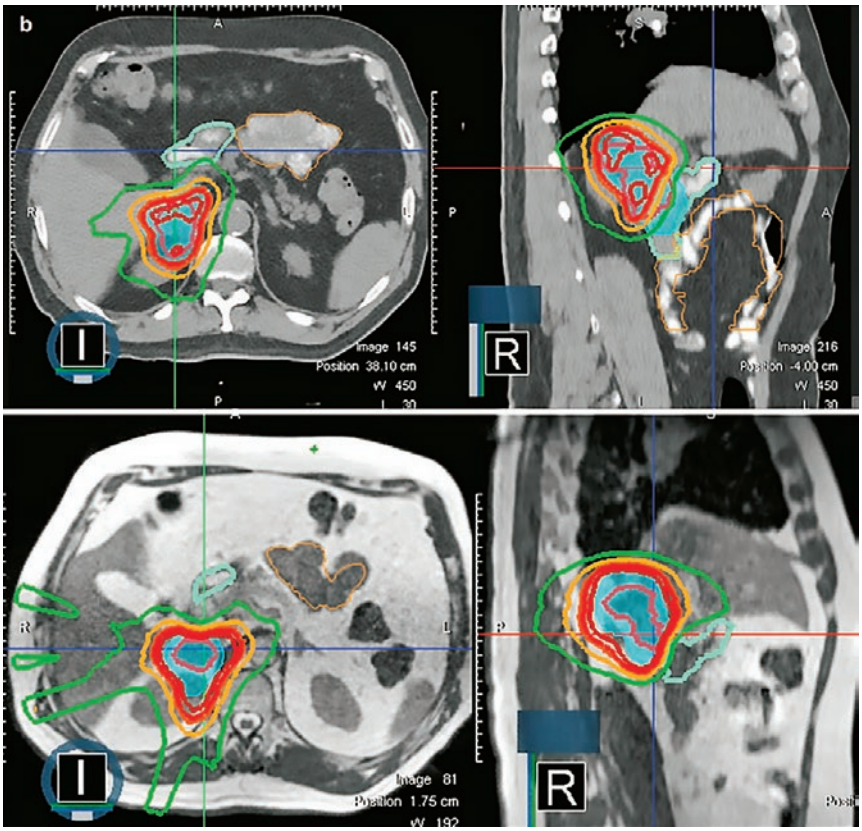


Figure 19. Online adaptation of a right adrenal target (blue color wash) on ViewRay. On the top panels, the original plan is shown where high dose coverage (orange and red) is limited due to target proximity to the duodenum (cyan). On the bottom panels, the plan has been adapted to increase coverage of the target

Source: Roach M., Glide-Hurst C.K., MR at the time of External Beam Treatment In: Liney G, van der Heide U, editors. MRI for Radiotherapy [Internet]. Springer International Publishing; 2019.

Study objective

The objective of this study is to evaluate the role of MRI in modern radiotherapy by examining its clinical application, technical considerations, and impact on treatment outcomes. Additionally, the study aims to investigate the clinical feasibility, dosimetric accuracy, and patient outcomes associated with MRI-guided radiotherapy across different tissue sites. Through the analysis of various scientific articles, this study seeks to contribute to the optimization and standardization of MRI-guided radiotherapy protocols, ultimately enhancing treatment precision, improving therapeutic efficacy, and reducing adverse effects.

Discussion

The analysis of scientific articles demonstrates improved treatment outcomes with the use of MRI in radiotherapy, enabling adaptive MRI-guided real-time therapy and increasing the curative potential for patients with malignant diseases [4-19,21-25]. This paper presents the advancements, challenges, and benefits of magnetic resonance imaging (MRI) in future radiotherapy practices, critically examining the role of MRI in modern radiotherapy and its implications for the future of cancer treatment [6,9,11-18].

The integration of MRI into the radiotherapy workflow has shown promise as an approach to enhance treatment accuracy and efficiency [7-14]. By offering superior soft tissue contrast and real-time imaging capabilities, MRI provides unique advantages over traditional modalities such as CT in radiotherapy applications [8-14,26]. The use of MRI for radiotherapy planning and execution has led to significant progress in recent years [5,6,23]. High-resolution MRI systems, combined with advanced image registration and fusion techniques, allow for precise delineation of tumors and critical structures, facilitating personalized treatment plans tailored to the patient's individual anatomy [7-15]. Moreover, real-time MRI imaging during dose delivery enables dynamic tumor tracking and adaptation, ensuring optimal dose coverage while minimizing radiation exposure to surrounding healthy organs [7,11,13-16,23-25]. Despite these potential benefits, integrating MRI into the radiotherapy workflow presents several challenges and limitations [6,11,12,15,16]. The integration of MRI with existing radiotherapy equipment requires substantial infrastructure and financial investment, posing a barrier to widespread adoption, particularly in resource-limited settings [6,22].

Addressing these challenges necessitates collaborative efforts within the radiotherapy team to optimize MRI-based radiotherapy and enhance its accessibility [27,28]. Looking ahead, the synergy between MRI and radiotherapy promises to advance cancer treatment paradigms. Emerging technologies, such as MRI-guided linear accelerators, offer the potential for real-time adaptive radiotherapy with unprecedented precision and tumor-tracking capabilities [22-26,29,31-34]. Furthermore, ongoing research efforts suggest the use of imaging biomarkers to predict treatment responses and optimize therapeutic outcomes [29]. As MRI technology continues to evolve and seamlessly integrates into radiotherapy workflows, it is poised to improve cancer care by ushering in an era of personalized, image-guided radiotherapy [23-25]. Certain future developments in the field of MRI-linear accelerators are foreseeable. The number of MRI-linear accelerators is expected to increase, along with the potential emergence of innovative designs with varying capabilities and strengths. These devices will enhance therapeutic efficiency by improving local control and reducing toxicity [23-25, 26,28,29,32-34].

The precision of the linear accelerator can improve approaches to anatomy and tissue preservation, such as maintaining small neurovascular bundles associated with erectile dysfunction during prostate cancer radiotherapy [33]. Additionally, considering immunotherapy, the MRI-linear accelerator can provide an ideal environment for targeted, personalized therapies in synergy with adjuvant pharmacological treatment. In summary, MRI-linear accelerators enhance radiotherapy by offering real-time visualization of target and normal tissues, enabling adaptive radiation dose delivery to optimize tumor control and reduce side effects [23,24,26,28,29,32-34]. They hold potential for physiological targeting, focusing the radiation dose on the most resistant tumor regions. With the continued evolution of this technology, its direct impact on treatment outcomes, quality of life, and broader social implications remains a topic of active interest and research [29]. MRI-linear accelerators can expand the management of internal and external anatomical changes, providing the ability to adapt the treatment plan and dose according to the patient's current anatomy and directly monitor tumor movement during treatment through continuous MRI imaging.

Online adaptive therapy offers safe, precise, and rapid treatment, supported by the application of artificial intelligence for MRI use in image segmentation, synthetic CT reconstruction, and automatic (online) planning [23,24,26,28,29,32-35]. Despite this progress, the broad application of MRI in radiotherapy is not without challenges. The need for specialized staff educated in MRI for radiotherapy also presents a challenge [6,12,17,22,27]. Moreover, developing standardized protocols for using MRI in radiotherapy remains a continuous challenge, as variability in MRI systems and techniques can affect treatment consistency [6,12,17,22,27,30]. Overcoming these issues requires a coordinated effort by the radiotherapy team to develop solutions and educational programs that can facilitate broader access to MRI-based radiotherapy [6,11,27]. Looking forward, the evolution of MRI technology is expected to continue driving advances in cancer treatment. The development of the next generation of MRI-linear accelerators with enhanced imaging capabilities and more powerful linear accelerators is likely to further improve the precision and efficiency of radiotherapy [22,26,28,29,32-35]. Additionally, integrating advanced imaging biomarkers within MRI could enable the prediction of treatment responses, allowing for even more personalized treatment plans that optimize therapeutic outcomes while minimizing side effects [7,23,24,28]. The combination of MRI with other therapeutic modalities, such as immunotherapy, offers even greater potential for treating malignant diseases [36-41]. This combination of technologies could be particularly beneficial for cancers that are difficult to treat, where conventional therapies have limited effectiveness [31,36-41].

Conclusion

Radiotherapy, alongside other treatment modalities, provides a critical approach to cancer management, enabling effective tumor control while minimizing damage to healthy tissues. Technological advancements, particularly in the use of MRI, have significantly improved radiotherapy methods, enhancing treatment precision for patients with malignant diseases. The integration of MRI into the radiotherapy workflow reveals numerous benefits, including superior soft tissue visualization, clear delineation of the CTV, real-time imaging capabilities that facilitate adaptive treatment planning, and functional and molecular imaging that offers insights into tumor biology. Additionally, the use of MRI reduces inter- and intra-fractional motion, improving dose delivery accuracy and leading to better clinical outcomes while simultaneously reducing toxicity. Ongoing research and technological progress will ensure the continued development of these advantages, providing a foundation for new therapeutic approaches in oncology.

All data in this paper are part of the results from the master's thesis titled 'Magnetic Resonance Imaging in Modern Radiotherapy ', written at the University Department of Health Studies, University of Split [42].

Literature

1. Jonsson, J.H., Karlsson M.G., Karlsson M., *et al*. Treatment planning using MRI data: an analysis of the dose calculation accuracy for different treatment regions. Radiat. Oncol. 2010 Jun 30;5:62. doi: 10.1186/1748-717X-5-62
2. Torresin A, Brambilla MG, Monti AF, Moscato A, Brockmann MA, Schad L, Attenberger UI, Lohr F. Review of potential improvements using MRI in the radiotherapy workflow. Z Med Phys. 2015 Sep;25(3):210-20. doi: 10.1016/j.zemedi.2014.11.003.
3. Schmidt MA, Payne GS. Radiotherapy planning using MRI. Phys Med Biol. 2015 Nov 21;60(22):R323-61. doi: 10.1088/0031-9155/60/22/R323.
4. Herbert T, Scurr E. Immobilization and patient positioning considerations when using MRI for radiotherapy treatment planning. In: Advances in Magnetic Resonance Technology and Applications. Vol. 8. Academic Press; 2023. p. 123-151. doi:10. 1016/b978-0-323-91689-9.00007-8
5. Liney G, van der Heide U, editors. MRI for radiotherapy: planning, delivery, and response assessment. Cham: Springer International Publishing; 2019. doi:10.1007/s00259-021-05223-4.
6. Tijssen RHN, Paulson ES, Rai R. Implementation and Acquisition Protocols. MRI for Radiotherapy [Internet]. 2019;3–19. Available from: http://dx.doi.org/10.1007/978-3-030-14442-5_1
7. Glide-Hurst, C. K., & Chetty, I. J. (2014). Improving radiotherapy planning, delivery accuracy, and normal tissue sparing using cutting edge technologies. Journal of thoracic disease, 6(4), 303–318. https://doi.org/10.3978/j.issn.2072-1439.2013.11.
8. Khoo VS, Dearnaley DP, Finnigan DJ, Padhani A, Tanner SF, Leach MO. Magnetic resonance imaging (MRI): considerations and applications in radiotherapy treatment planning. Radiotherapy and Oncology [Internet]. 1997 Jan;42(1):1–15. Available from: http://dx.doi.org/10.1016/s0167-8140(96)01866-x
9. VS, Joon DL. New developments in MRI for target volume delineation in radiotherapy. The British Journal of Radiology [Internet]. 2006 Sep;79(special_issue_1):S2–15. Available from: http://dx.doi.org/10.1259/bjr/41321492
10. Chandarana H, Wang H, Tijssen RHN, Das IJ. Emerging role of MRI in radiation therapy. Journal of Magnetic Resonance Imaging [Internet]. 2018 Sep 8;48(6):1468–78. Available from: http://dx.doi.org/10.1002/jmri.26271
11. Speight R., MRI to CT Image Registration. In: Liney G, van der Heide U, editors. MRI for Radiotherapy [Internet]. Springer International Publishing; 2019. Available from: http://dx.doi.org/10.1007/978-3-030-14442-5
12. Adjeiwaah M, Garpebring A, Nyholm T. Sensitivity analysis of different quality assurance methods for magnetic resonance imaging in radiotherapy. Physics and Imaging in Radiation Oncology [Internet]. 2020 Jan;13:21–7. Available from: http://dx.doi.org/10.1016/j.phro.2020.03.001
13. Bahig H., Koay E., Barkati M., Fuller M. C., Menard C., Clinical Applications of MRI in Radiotherapy Planning.. In: Liney G, van der Heide U, editors. MRI for Radiotherapy [Internet]. Springer International Publishing; 2019. Available from: http://dx.doi.org/10.1007/978-3-030-14442-5
14. Philippens M., García-Álvarez R., Functional MRI Imaging, In: Liney G, van der Heide U, editors. MRI for Radiotherapy [Internet]. Springer International Publishing; 2019. Available from: http://dx.doi.org/10.1007/978-3-030-14442-5.
15. Owrangi, A. M., Greer, P. B., & Glide-Hurst, C. K. (2018). MRI-only treatment planning: benefits and challenges. Physics in medicine and biology, 63(5), 05TR01. Available from: https://doi.org/10.1088/1361-6560/aaaca4
16. Paulson E.S., Tijssen R. H. N., Motion Management, In: Liney G, van der Heide U, editors. MRI for Radiotherapy [Internet]. Springer International Publishing; 2019. Available from: http://dx.doi.org/10.1007/978-3-030-14442-5
17. Tyagi N., Challenges and Requirements, In: Liney G, van der Heide U, editors. MRI for Radiotherapy [Internet]. Springer International Publishing; 2019. Available from: http://dx.doi.org/10.1007/978-3-030-14442-5
18. Keall, P. J., Barton, M., Crozier, S. (2014). The integration of MRI in radiation therapy. Australian Physical & Engineering Sciences in Medicine**,** 37(1), 1–6. Available from: https://doi.org/10.1007/s13246-014-0252-5
19. Wen, N., Kim, J., Doemer, A., Huang, Y., Qin, Y., Kong, F. M., Movsas, B. (2018). Evaluation of a magnetic resonance guided linear accelerator for stereotactic radiosurgery treatment planning and delivery. Radiotherapy and Oncology**,** 127(3), 460–466. Available from: https://doi.org/10.1016/j.radonc.2018.04.021
20. Raaymakers, B. W., Jürgenliemk-Schulz, I. M., Bol, G. H., Glitzner, M., Kotte, A. N. T. J., van Asselen, B., Lagendijk, J. J. W. (2017). First patients treated with a 1.5 T MRI-linac: clinical proof of concept of a high-precision, high-field MRI guided radiotherapy treatment. Physics in Medicine & Biology**,** 62(23), L41–L50. Available from: https://doi.org/10.1088/1361-6560/aa9517
21. Dowling A., Korhonen J., MRI-Only Methodology, In: Liney G, van der Heide U, editors. MRI for Radiotherapy [Internet]. Springer International Publishing; 2019. Available from: http://dx.doi.org/10.1007/978-3-030-14442-5
22. Whelan B., Oborn B., Liney G., Keall P., RI Linac Systems, In: Liney G, van der Heide U, editors. MRI for Radiotherapy [Internet]. Springer International Publishing; 2019. Available from: http://dx.doi.org/10.1007/978-3-030-14442-5
23. Roach M., Glide-Hurst C.K., MR at the time of External Beam Treatment In: Liney G, van der Heide U, editors. MRI for Radiotherapy [Internet]. Springer International Publishing; 2019. Available from: http://dx.doi.org/10.1007/978-3-030-14442-5
24. Hunt, A., Hansen, V. N., Oelfke, U., Nill, S., Hafeez, S. (2018). Adaptive Radiotherapy Enabled by MRI Guidance. Clinical oncology (Royal College of Radiologists (Great Britain), 30(11), 711–719. https://doi.org/10.1016/j.clon.2018.08.001
25. Brock K. K. (2019). Adaptive Radiotherapy: Moving Into the Future. *Seminars in* radiation oncology, 29(3), 181–184. https://doi.org/10.1016/j.semradonc.2019.02.011
26. Kerkmeijer LGW, Fuller CD, Verkooijen HM, Verheij M, Choudhury A, Harrington KJ, et al. The MRI-Linear Accelerator Consortium: Evidence-Based Clinical Introduction of an Innovation in Radiation Oncology Connecting Researchers, Methodology, Data Collection, Quality Assurance, and Technical Development. Frontiers in Oncology [Internet]. 2016 Oct 13;6. Available from: http://dx.doi.org/10.3389/fonc.2016.00215

27. Corradini S, Alongi F, Andratschke N, Belka C, Boldrini L, Cellini F, et al. MR-guidance in clinical reality: current treatment challenges and future perspectives. Radiation Oncology [Internet]. 2019 Jun 3;14(1). Available from: http://dx.doi.org/10.1186/s13014-019-1308-y
28. Henke L, Kashani R, Robinson C, Curcuru A, DeWees T, Bradley J, et al. Phase I trial of stereotactic MR-guided online adaptive radiation therapy (SMART) for the treatment of oligometastatic or unresectable primary malignancies of the abdomen. Radiotherapy and Oncology [Internet]. 2018 Mar;126(3):519–26. Available from: http://dx.doi.org/10.1016/j.radonc.2017.11.032
29. Boldrini L, Cusumano D, Chiloiro G, Casà C, Masciocchi C, Lenkowicz J, et al. Delta radiomics for rectal cancer response prediction with hybrid 0.35 T magnetic resonance-guided radiotherapy (MRgRT): a hypothesis-generating study for an innovative personalized medicine approach. La radiologia medica [Internet]. 2018 Oct 29;124(2):145–53. Available from: http://dx.doi.org/10.1007/s11547-018-0951-y
30. Tijssen RHN, Philippens MEP, Paulson ES, Glitzner M, Chugh B, Wetscherek A, et al. MRI commissioning of 1.5T MR-linac systems—a multi-institutional study. Radiother Oncol. 2019;132:114-20. doi:10.1016/j.radonc.2018.12.010
31. Smith J, Doe A, Johnson K, Lee T. The evolving role of MRI in modern radiotherapy: Enhancing precision and personalization in cancer treatment. Radiother Oncol. 2023;150:75-85.doi:10.1016/j.radonc.2023.03.01
32. Tetar, S. U., Bruynzeel, A. M. E., Lagerwaard, F. J., Slotman, B. J., Bohoudi, O., & Palacios, M. A. (2019). Clinical implementation of magnetic resonance imaging guided adaptive radiotherapy for localized prostate cancer. Physics and imaging in radiation oncology, 9, 69–76. https://doi.org/10.1016/j.phro.2019.02.002
33. Raaymakers, B. W., Jürgenliemk-Schulz, I. M., Bol, G. H., Glitzner, M., Kotte, A. N. T. J., van Asselen, B., Lagendijk, J. J. W. (2017). First patients treated with a 1.5 T MRI-linac: Clinical proof of concept of a high-precision, high-field MRI guided radiotherapy treatment. Physics in Medicine and Biology, 62(23), L41–L50. Available from: https://doi.org/10.1088/1361-6560/aa9517
34. Keall, P. J., Nguyen, D. T., O'Brien, R., Caillet, V., Hewson, E., Poulsen, P. R., Bromley, R., Bell, L., Eade, T., Kneebone, A., Martin, J., & Booth, J. T. (2018). The first clinical implementation of real-time image-guided adaptive radiotherapy using a standard linear accelerator. *Radiotherapy and oncology : journal of the European* Society for Therapeutic Radiology and Oncology, 127(1), 6–11. Available from: https://doi.org/10.1016/j.radonc.2018.01.001
35. van Houdt, P. J., Li, S., Yang, Y., & van der Heide, U. A. (2024). Quantitative MRI on MR-Linacs: Towards Biological Image-Guided Adaptive Radiotherapy. Seminars in radiation oncology, 34(1), 107–119. Available from https://doi.org/10.1016/j.semradonc.2023.10.010
36. Pointer, K. B., Pitroda, S. P., & Weichselbaum, R. R. (2022). Radiotherapy and immunotherapy: open questions and future strategies. Trends in cancer, 8(1), 9–20. Available from: https://doi.org/10.1016/j.trecan.2021.10.003
37. Bang, A., Schoenfeld, J. D. (2019). Immunotherapy and radiotherapy for metastatic cancers. Annals of palliative medicine, 8(3), 312–325. Available from: https://doi.org/10.21037/apm.2018.07.10
38. Mondini, M., Levy, A., Meziani, L., Milliat, F., & Deutsch, E. (2020). Radiotherapy-immunotherapy combinations – perspectives and challenges. Molecular oncology, 14(7), 1529–1537. Available from: https://doi.org/10.1002/1878-0261.12658
39. Aupérin, A., Le Péchoux, C., Pignon, J. P., Koning, C., Jeremic, B., Clamon, G., Einhorn, L., Ball, D., Trovo, M. G., Groen, H. J., Bonner, J. A., Le Chevalier, T., Arriagada, R., & Meta-Analysis of Cisplatin/carboplatin based Concomitant Chemotherapy in non-small cell Lung Cancer (MAC3-LC) Group (2006). Concomitant radio-chemotherapy based on platin compounds in patients with locally advanced non-small cell lung cancer (NSCLC): a meta-analysis of individual data from 1764 patients. Annals of oncology : official journal of the European Society for Medical Oncology, 17(3), 473–483. Available from: https://doi.org/10.1093/annonc/mdj117
40. Pasqualetti, F., Gonnelli, A., Orlandi, P., Palladino, E., Giannini, N., Gadducci, G., Mattioni, R., Montrone, S., et al. (2021). Association of XRCC3 rs1799794 polymorphism with survival of glioblastoma multiforme patients treated with combined radio-chemotherapy. Investigational new drugs, 39(4), 1159–1165. Available from: https://doi.org/10.1007/s10637-021-01075-9
41. Narvaez, C. A., Schild, S. E., Janssen, S., Schroeder, U., Bruchhage, K. L., Hakim, S. G., & Rades, D. (2021). Accelerated Fractionation With Concomitant Boost *vs*. Conventional Radio-chemotherapy for Definitive Treatment of Locally Advanced Squamous Cell Carcinoma of the Head-and-Neck (SCCHN). Anticancer research, 41(1), 477–484. Available from: https://doi.org/10.21873/anticanres.14798
42. Al-Khazae E. Magnetska Rezonancija u Suvremenoj Radioterapiji (Diplomski rad). Split: Sveučilište u Splitu, Sveučilišni odjel zdravstvenih studija; 2024 (pristupljeno 11.3.2025.) Available at: https://urn.nsk.hr/urn:nbn:hr:176:036240

Trenutna i buduća uloga magnetske rezonancije u radioterapiji

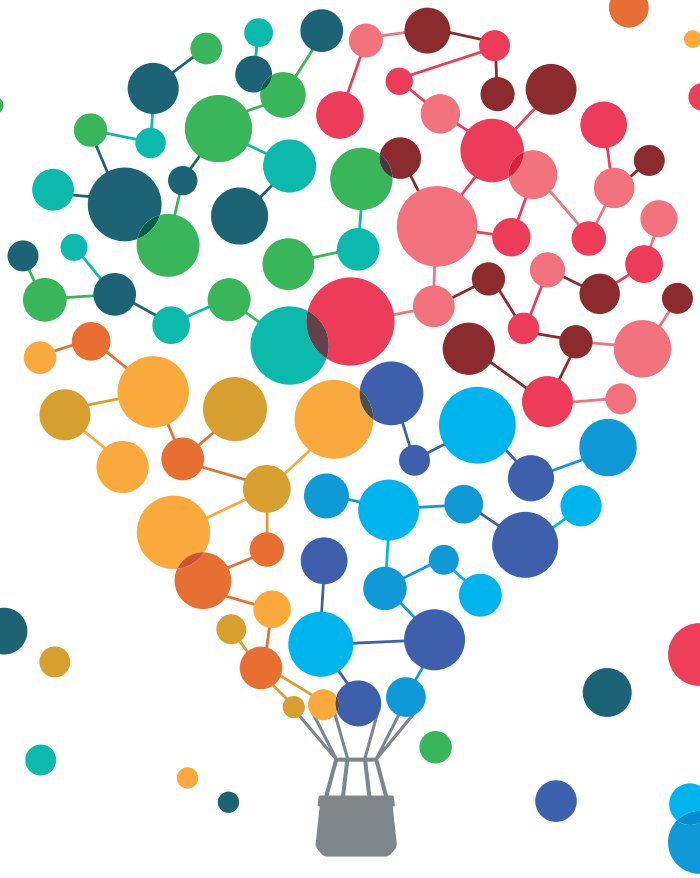
Sažetak

Ovaj rad istražuje integraciju magnetske rezonancije u suvremenu kliničku praksu radioterapije, istražujući njen potencijal za poboljšanje preciznosti i učinkovitosti liječenja te unaprjeđenje ishoda pacijenata. Rad pruža pregled primjene MR-a, uključujući planiranje radioterapije, registraciju slika, osiguranje kvalitete s naglaskom na smanjenje geometrijskih distorzija te prilagođenu MR-slikom vođenu radioterapiju u stvarnom vremenu. Uvodni dio rada obuhvaća ulogu MR-a u planiranju liječenja, nakon čega slijedi opis primjene MR-a tijekom terapije, s posebnim naglaskom na funkcionalne tehnike snimanja i kontrolu pokreta. Razmotreni su dozimetrijski zahtjevi, tehnike zamjene CT-a i adaptivna MR-slikom vođena radioterapija u stvarnom vremenu. Rad prikazuje i prve rezultate dobivene korištenjem MR-linearnog akceleratora, uz analizu tehničkih izazova i trenutačnog stanja ovih uređaja. Na kraju, kroz analizu raznih znanstvenih radova, razmatra se buduća uloga magnetske rezonancije u radioterapiji te se donose zaključci temeljeni na prikupljenim analizama i rezultatima.

Ključne riječi: Adaptivna radioterapija; MRIgRT; MR-linearni akcelerator; suvremena radioterapija

SHIMADZU
Excellence in Science

150 YEARS ANNIVERSARY



150 Years of Innovation

- **Founded in 1875 by Genzo Shimadzu Sr. in Kyoto, Japan,** Shimadzu Corporation was manufacturing physics and chemistry instruments.
- **The company grew significantly under the leadership of Genzo Jr.,** one of Japan's most remarkable inventors.
- **Shimadzu's product portfolio of medical systems, analytical instrumentation and more enables** its customers to protect people's health and lives as well as the environment.
- **Shimadzu's culture of "Contributing to Society through Science and Technology"** has been inherited by each new generation of employees worldwide.

www.shimadzu.eu/150-years

Learn more!

REVIEW PAPER (PREGLEDNI RAD)

Comparison of magnetic resonance imaging of the prostate 1.5T and 3T

Goran Kutlić[1,2], **Krešimir Dolić**[2,3,4]

[1] University Hospital "Holy Spirit", Zagreb, Croatia

[2] University Department of Health Studies, University of Split, Split, Croatia

[3] Department of Diagnostic and Interventional Radiology, University Hospital of Split,Split, Croatia

[4] School of Medicine, University of Split, Split, Croatia

Corresponding author: Goran Kutlić, e-mail: gorankutlic@proton.me

DOI: https://doi.org/10.55378/rv.49.1.5

Abstract

With its excellent display of soft tissues and the possibilities of three-dimensional display, magnetic resonance has become one of the fundamental diagnostics in the display of prostate and its pathological conditions since its beginnings 40 years ago. Although there is greater availability of devices for magnetic resonance with a field strength of 1.5T, the recommendation of the European Association of Urogenital Radiologists is that imaging of the prostate with magnetic resonance is performed on devices with a field strength of 3T. 3T devices were introduced due to the increased signal-to-noise ratio (SNR), which can be used to shorten recording time or increase resolution, i.e. improve image quality. There is more and more research into the application of quantitative techniques such as Magnetic resonance fingerprinting, T2 mapping, BOLD, which could improve the detection and quantification of prostate cancer lesions, and by optimizing the protocol at 1.5T and 3T it is possible to perform exam of equal diagnostic value.

Keyword: MRI; prostate; 1.5T; 3T

Introduction

Magnetic resonance imaging (MRI) of the prostate is a diagnostic method for detecting and assessing the extent of benign and malignant changes in the prostate. The examination is performed on 1.5T and 3T devices with an abdominal coil or with the use of an endorectal coil (ERC).

Although 1.5T and 3.0T field strength devices for prostate imaging can provide adequate and reliable diagnostic examinations when acquisition parameters are optimized and appropriate modern technology is used, according to the Prostate Imaging-Reporting and Data System (PI-RADS) v2.1 document, it is recommended that MRI of the prostate, if possible, be performed on 3T field strength devices due to better signal-to-noise ratio (SNR), spatial and temporal resolution. Devices with a field strength of 1.5T are recommended in cases where the patient has implants that are conditioned for a field strength of 1.5T. They are also recommended in cases where the implants are safe for the 3T field strength, but are anatomically located in such a way that they will cause artifacts that will affect the quality of the examination. Performing the search on devices with a field strength of less than 1.5T is not recommended [1].

In prostate imaging, biparametric (bpMRI) or multiparametric (mpMRI) protocols are used, which include: T1 weighted image (T1W), T2 weighted image (T2W), diffusion weighted images (DWI), sequences with dynamic contrast (DCE) and in some cases spectroscopy.

Over the last 10 years, advances in mpMRI have made it possible to accurately detect and characterize lesions suspected of prostate cancer. The widespread use of prostate mpMRI has resulted in high variability in scan quality for each sequence, and especially for DWI and DCE sequences [2].

In the last 5 years, several debates have been initiated about the best protocol for prostate MRI to obtain adequate diagnostic quality with good spatial resolution and high signal-to-noise ratio for each sequence. Currently, the recommendation of the PI-RADS v2.1 document is a minimum T2W sequence in the axial plane and additionally in the sagittal or coronary plane, DWI sequences and DCE sequences (Figure 1.) [3].

Aim

The aim of this paper is to present the current research of prostate MRI in clinical practice on devices with a field strength of 1.5T and 3T.

The paper was made by searching scientific papers in the PubMed database in the period from year 2012 till 2023. The terms MRI, prostate, 1.5T, 3T were used for the examination. The search yielded 305 published scientific

	T2-weighted imaging (T2-WI)	Diffusion-weighted imaging (DWI)	Dynamic contrast-enhanced (DCE)
Imaging planes	Same used for DUT and DCE	Same used for T2-UT and DCE	Same used for T2- UT and DUT
Slice thickness	3 mm no gap	<4 mm. no gap	3 mm no gap
Field of new	12–20 cm	16–22 cm	12–20 cm
In-plane dimension	<0.7 mm (phase)x≤ 0.4 mm (frequency)	<2.5 mm (phase and frequency)	<2 mm (phase and frequency)
Specific recommendations			
T2-WI acquisition	Axial plane: either straight axial to the patient or in an oblique axial plane matching the long axis of the prostate	–	–
	At least one additional orthogonal plane (sagittal and/or coronal)	–	–
	3D axial as an adjunct to 2D acquisitions	–	–
Low *b*-value	–	0 (preferably 50)–100 sec/mm^2	–
Intermediate *b*-value	–	800–1000 sec/mm^2	–
High *b*-value	–	● Dedicated (≥1,400 sec/mm^2) • Synthesised (from other *b*-values)	–
Temporal resolution	–	–	≤15 s
Total observation rate	–	–	>2 min
Dose of GBCA	–	–	0.1 mmol/kg
Injection rate	–	–	2 – 3cc/s
Fat suppression/subtraction	–	–	Recommended

Figure 1. Minimum technical requirements for mpMRI according to PI-RADS v2.1 guidelines
Source: https://www.acr.org/-/media/ACR/Files/RADS/Pi-RADS/PIRADS-v2-1.pdf

papers, whereby 23 of them were selected based on predetermined criteria and were used in the writing of this paper.

Methods

According to the current recommendations of the American College of Radiology (ACR) and the European Society of Urogenital Radiology (ESUR) published in the guidelines PI-RADS v2.1, T1W, T2W, DWI sequences are required for all MRI examinations of the prostate and, if necessary, DCE sequence and spectrometry are used [1].

T1W sequences are primarily used to determine the presence of bleeding inside the prostate and seminal vesicles and to show, i.e. outline of the prostate (Figure 2.).

T1W sequences may also be useful for detecting nodal and skeletal metastases, especially after intravenous administration of a gadolinium-based contrast agent (Figure 2.). Axial T1W images of the prostate can be obtained with or without fat suppression using spin echo or

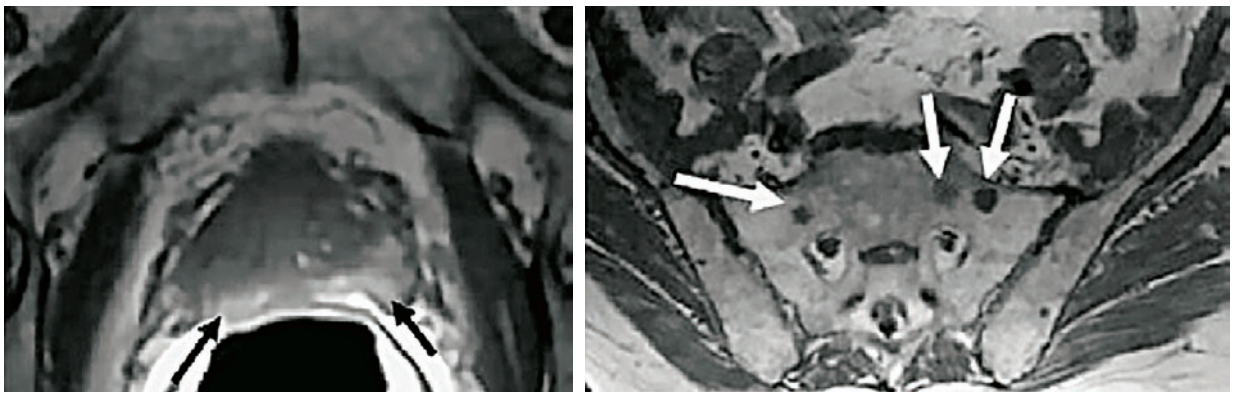


Figure 2. on the left is T1W image of bleeding after biopsy and right is T1W image of metastases in the sacrum
Source:https://www.researchgate.net/publication
6352762_Prostate_cancer_detection_Magnetic_resonance_MR_spectroscopic_imaging/figures?lo=1

gradient echo sequences. The recording planes should be the same as those used for DWI and DCE. Unlike the T2W sequence, in which spatial resolution is important, in the T1W sequence, temporal resolution is more important. Thus, in the T1W sequence, we can reduce spatial resolution and use this to increase anatomical coverage [4].

In MRI examination of the prostate, T2W images are used to discern the zonal anatomy of the prostate, assess abnormalities within the gland, and assess the involvement of seminal vesicles and node involvement.

On T2W images, carcinomas in the peripheral zone usually appear as round and poorly defined hypointense focal lesions. Also, hypointense displays can have conditions such as prostatitis, bleeding, atrophy of the glands, benign hyperplasia, scars associated with biopsy and after therapy (hormonal, ablation, etc.). Transitional zone carcinomas can be difficult to identify on T2W images because the transition zone often consists of varying amounts of intermixed glandular (T2-hyperintense) and stromal (T2-hypointense) tissue, which shows a heterogeneous signal intensity. Areas where benign stromal elements predominate may mimic and/or mask clinically significant cancers.

T2W images should always be obtained in the axial plane and at least one additional orthogonal plane (i.e., sagittal and/or coronary). T2W images are usually obtained using two-dimensional (2D) FSE or TSE techniques.

According to the recommendation of PI-RADS v2.1, the parameters that should be followed are as follows:

- slice thickness: 3 mm, without gaps,
- The recording planes must be identical to those of the DWI and DCE sequences,
- FOV: generally 12-20 cm to cover the entire prostate and seminal vesicles,
- In-plane: ≤0.7 mm (phase) x ≤0.4 mm (frequency).

Also, further improvement of T2W sequences is achieved by optimizing parameters such as: TSE factor, TSE spacing and choice of image filters [5].

Three-dimensional (3D) imaging can be used in addition to two-dimensional (2D) imaging. If recorded using isotropic voxels, 3D images can be particularly useful for visualizing detailed anatomy and distinguishing between true lesions and partial volume averaging effects. However, the contrast of the soft tissue is not identical and, in some cases, may be worse than that seen in 2D T2W images, and the resolution in the plane may be lower than the 2D image taken with the same technique (Figure 3.).



Figure 3. T2W axial showing prostate cancer
Source: https://radiologyassistant.nl/abdomen/prostate/prostate-cancer-pi-rads-v2

Diffusion-weighted imaging (DWI) reflects the random movement of water molecules and is a key component of the mpMRI prostate imaging protocol. Most clinically significant cancers have limited diffusion as compared to normal tissues, hence they appear hypointense on the greyscale ADC maps. Although ADC values have been reported to be inversely correlated with histological grades, there is significant overlap between BPH, low-grade cancer, and high-grade cancer.

According to the recommendations of PI-RADS v2.1, an ADC map and images with a high b-value (b>1400 s/mm2) should be included. An ADC map is a representation of the ADC value for each voxel in an image. In most current clinical implementations, two or more b-values and a mono exponential signal attenuation model with increasing b-values are used to calculate ADC values. ADC calculations are influenced by the selection of b-values and are not standardized among device manufacturers. Independent of devices, qualitative visual assessment is most commonly used as the primary method for assessing ADCs. If we use ADC values of 750-900 μm2/sec, we can differentiate a benign lesion from prostate cancer. Images with a high b-value are considered to be those with at least 1400 s/mm2. They show signal conservation in areas of limited/prevented diffusion compared to normal tissues. Normal tissues show a reduced signal due to greater diffusion between the application of gradients with different b-values. Compared to the basic ADC maps alone (b-value 0-100 s/mm2 and 800-1000 s/mm2), the visibility of clinically significant cancers is sometimes improved in high-b-value images. Especially on those that are adjacent to the anterior fibromuscular stroma [6]. Increasing the b-value above 3000 s/mm2 has been shown to better suppress the background signal, but does not contribute to improved prostate cancer detection [7]. High-b-value images can be obtained in one of two ways: directly by obtaining a high-b-value DWI sequence, or by calculating a high-b-value image from the collected data of lower b-value DWI sequences.

Recommended parameters for DWI sequences according to PI-RADS v2.1:

- SE EPI sequence without retention of breathing and fat saturation,
- TE: ≤90 msec; TR: ≥3000 msec,
- slice thickness: ≤4 mm, without gaps,
- the image planes should match or be similar to those used for T2W and DCE sequences,
- FOV: 16-22 cm,
- plane dimensions: ≤2.5 mm phase and frequency,
- in case of time or technical limitation of the MRI device, it is recommended to use two values, one low b-value of 50-100 s/mm2 and one medium b-value of 800-1000 s/mm2,
- it is recommended that the maximum b-value used for the calculation of the ADC be ≤1000 s/mm2 in order to avoid the diffusion kurtosis effect that is described at higher b-values,
- Images with a high B-value (≥1400 s/mm2) are also mandatory and should preferably be obtained through a separate acquisition.

DCE MRI is defined as obtaining T1W gradient echo scans before, during, and after intravenous administration of a gadolinium-based contrast agent. After contrast administration, prostate cancer tissue shows an early im-

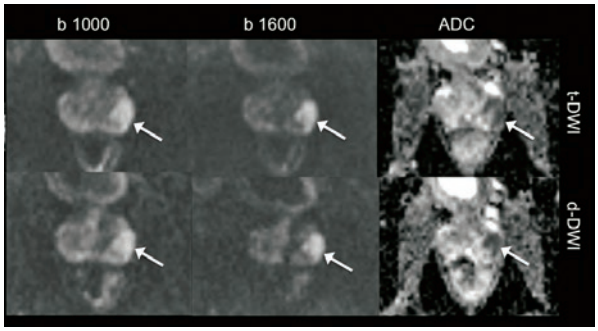


Figure 4. Example of DWI sequences and ADC maps of prostate cancer
Source: https://onlinelibrary.wiley.com/doi/10.1002/jmri.25705

provement in signals compared to normal tissue. DCE is performed in multiple repeated series of signal acquisition to show early lesions compared to surrounding prostate tissue. It is carried out for several minutes in order to evaluate the characteristics of signal improvement. DCE sequences should have a time resolution of <15 seconds per recording to show focal early signal gain. Likewise, a faster temporal resolution can be selected if we maintain sufficient spatial resolution and diagnostic image quality. The diagnostic quality of the image can be further improved by suppression of fat signals or subtraction. 3D T1W sequences on the new devices have reached the quality of 2D T1W sequences and it is recommended to use them in order to shorten the review time.

Parameters for DCE sequences are:

- TR/TE: <100 msec/ <5 msec
- layer thickness: 3 mm, no gaps
- acquisition planes identical to DWI
- FOV: covers the entire prostate and seminal vesicles
- total recording duration: >2 min,
- Dose: 0.1 mmol/kg standard contrast based on gadolinium,
- Contrast application speed: 2-3 cc/s, and the start of administration correlates with the initiation of the sequence.

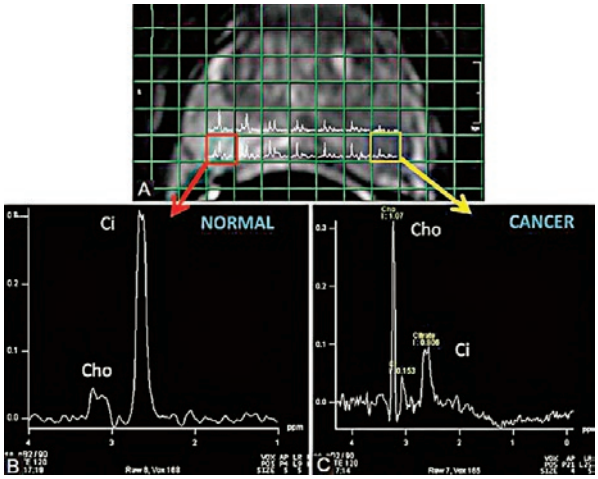


Figure 5. An example of MR spectroscopy where the left is the spectroscopy of the normal prostate and the right is the prostate cancer spectroscopy
Source: https://mriquestions.com/prostate-spectra.html

Spectroscopy is a non-invasive method based on spectroscopic analysis of tissue metabolism and as such is used to characterize metabolic changes associated with prostate cancer. Prostate spectroscopy is based on measurements of citrate, choline and creatinine concentrations. Although it used to be the standard method for MRI imaging of the prostate, today spectroscopy is according to PI-RADS v2.1. auxiliary method [1]. MRI prostate spectroscopy was the first method of choice for detecting aggressive cancers. By improving DWI sequences, we can now collect the same information in a shorter time and in a more technically simpler way (Figure 5.) [6].

New paths in MRI prostate

3D T2W Sequence

Three-dimensional imaging allows visualization of the prostate in any arbitrarily determined anatomical plane, without loss of image quality, and can be obtained in a shorter time compared to separate multiplanar 2D imaging [8]. High-resolution 3D T2W MRI with adequate volumetric coverage can improve sensitivity for cancer detection [9]. It allows for a more accurate image-guided biopsy and improves surgical planning or targeted treatment. The 3D sequence can be optimally used in the latest technologies such as PET-MR, whereby fast 3D T2W MRI sequences are used to fuse the image with 3D PET (Figure. 6.) [10].

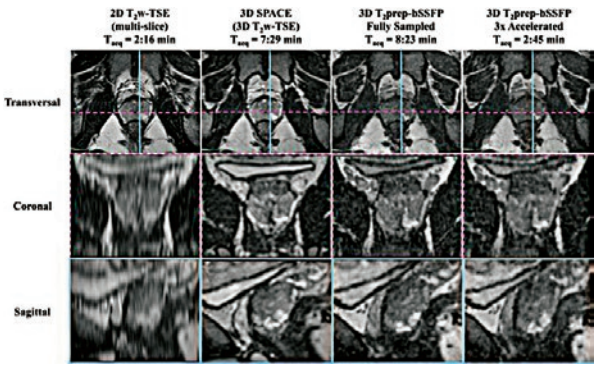


Figure 6. Comparison of 2D T2W and 3D T2W sequences with acquisition time
Source: https://www.ncbi.nlm.nih.gov/pmc/articles/instance/6563534/bin/MRM-82-721-g004.jpg

Functional magnetic resonance imaging (fMRI)

fMRI is a rapid MRI technique that obtains images of organs in the activity phase and then in the resting phase. In prostate imaging, the Blood oxygenation level dependent (BOLD) sequence is based on the difference in magnetic sensitivity of oxyhemoglobin and deoxyhemoglobin due to increased blood flow in the vessels and reduced or no increase in local oxygen consumption that occurs during activity [11]. In the case of prostate cancer, it is known that in solid fast-growing tumors, there is a decrease in oxygen levels in the tissues due to inadequate blood supply and too rapid tumor growth. If we apply the BOLD

technique, we can quantify the distribution of cancer in the prostate. Since deoxyhemoglobin is paramagnetic, the vessels containing a significant amount of this molecule generate local field inhomogeneities causing dephasing and, therefore, signal loss. During activity, there is an increase in blood supply to the prostate tissue, and thus the level of deoxyhemoglobin decreases, resulting in an increase in signal intensity. These changes in the phases of activity are short-lived and require extremely rapid sequences. In order to take advantage of the effect of fast dephasing, T2W FSE sequences are used for the 1.5T and 3T field strength magnets for the BOLD technique, from which R2* maps are calculated (Figure 7.) [12].

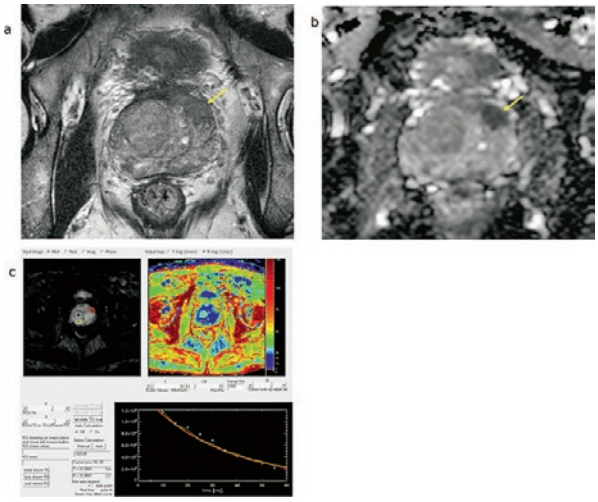


Figure 7. MRI of the prostate T2W (a.), DWI (b.), BOLD (c.)
Source:https://pubmed.ncbi.nlm.nih.gov/34235962/#&gid=article-figures&pid=figure-1-uid-

T2 mapping

T2 mapping is a technique that allows the quantification of T2W signals. The technique is based on mapping the T2 time of relaxation of prostate tissue. The biophysiological basis for T2 mapping is based on the relative percentages of stromal and glandular tissue, and the water component that varies between benign and cancerous prostate tissue. Using a series of SE sequences, a relaxation curve is obtained and the T2 relaxation time of each voxel can be determined [13,14].

Sathiadoss et al. [15] conducted a study aimed at assessing the image quality and the possibility of detecting prostate cancer by T2 mapping and DWI sequence in men with hip prostheses. The study involved 30 men with hip prostheses, undergoing MRI of the prostate gland read by 5 radiologists, independent of each other. The study showed that images obtained by T2 mapping were of better quality than images of DWI sequences. They concluded that T2 mapping should be included in the MRI of the prostate in men with an implanted hip prosthesis.

Magnetic resonance Fingerprinting (MRF)

MRF is a quantitative imaging technique that enables the rapid and simultaneous generation of T1 and T2 maps with a unique value of each tissue. The data is collected so that different tissues have unique signal fingerprints. The tissue signal fingerprint database contains a subset of all expected tissue signals generated by simulations. The resulting impressions are compared with simulated impressions from the base (pattern recognition) to identify the tissue under each voxel. Based on the identified tissue from the base, each voxel is assigned a tissue property to generate an impression map (Figure 8.) [16,17]. The advantages of MRF over standard mapping techniques are multi-site repeatability and significantly shorter acquisition time. Given the current trend, shorter acquisition time also allows for shorter imaging protocols, while maintaining the diagnostic quality of the examination [18].

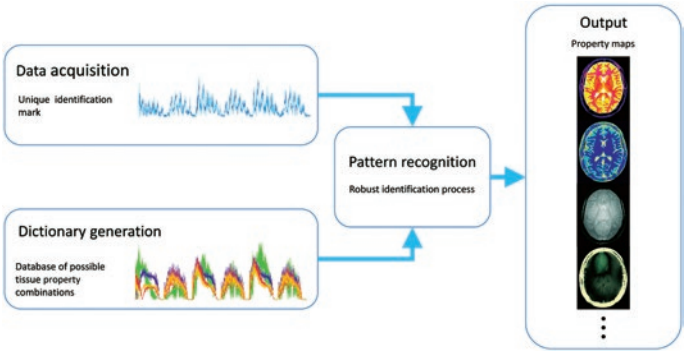


Figure 8. Example of how MRF works
Source: https://onlinelibrary.wiley.com/cms/asset/6fd61ec4-d3b6-4403-9cbd-d81bce16f50e/mrm27403-fig-0001-m.jpg

Results

MRI is one of the basic diagnostic tests for detecting pathological conditions of the prostate gland. Thanks to bpMRI and mpMRI protocols, it has found its indispensable place in diagnosing and monitoring prostate cancer, benign prostatic hyperplasia, diagnosing and monitoring inflammatory conditions, conducting targeted prostata cancer biopsies, assessing the effect of radiotherapy and chemotherapy [19]. The basis of the protocol for MRI of the prostate is made up of T2W, DWI and DCE sequences. When imaging the prostate, it is important to clearly distinguish between the central, peripheral and transitional zones. A successful diagnostic test requires the acquisition of high-resolution images and contrast in the shortest possible time without losing their quality. MRI of the prostate gland is recorded on devices with a field strength of 1.5T or 3T. The main advantage of 3T field power devices over 1.5T field power devices is manifested in the field strength that gives a higher SNR. Twice the SNR is obtained by inducing an MR signal in the receiving coil that is proportional to the strength of the main magnetic field (B0) and by noise that has a linear dependence on the strength of the magnetic field > 1.0T. The resulting difference in SNR can be used to reduce search time or increase spatial resolution. The fundamental advantage of MRI 1.5T is the lower sensitivity to metal-induced artifacts in the imaging area (e.g. hip arthroplasty) and the greater range of MRI-conditioned medical devices, primarily pacemakers [20].

Table 1. Sequence parameters for MR 1.5T and MR 3T [21]

	Axial T2W TSE		Axial DWI	
Parameters	1.5T	3T	1.5T	3T
Coil	6-channel phased-array	6-channel phased-array	6-channel phased-array	6-channel phased-array
TR(ms)/TE (ms)	10130/113	10630/117	4800/93	4600/90
Voxel size (mm)	0.7 x 0.7 x 3.0	0.5 x 0.5 x 3.0	1.5 x 1.5 x 3.0	1.5 x 1.5 x 3.0
Gap (%)	10	10	10	10
Field of View (mm)	128	128	204	204
Matrix	192x192	256x256	136x136	136x136
Number of Signal averages	3	2	9	8
b-values			0, 500, 1000	0, 500, 1000
Number of slices	30	30	30	30
Acquisition Time	8:48	8:21	5:18	4:31

From the first issuance of the PI-RADS guidelines in 2015 until today, the guidelines state that 1.5T and 3T field strength MRI devices can provide adequate and reliable MRI of the prostate. Nonetheless, the majority of PI-RADS Board members prefer, use, and recommend that prostate MRI be performed on 3T field strength devices.

Taking all this into account, Ulrich et al. [21] conducted a study comparing the quality of MRI images of the prostate on 1.5T and 3T field strength devices. The primary objective of the study was to prove that the SNR and CNR between MR 1.5T and MR 3T when performing T2W and DWI sequences is equal to or less than 10%. The secondary objectives of the study were to evaluate the subjective assessment of image quality, using a rating scale of 1 to 5, and then to score according to PI-RADS v.2. This assessment refers to benign prostate lesions and prostate cancer and the definition of different prostate zones. The study included 63 patients with elevated PSA levels referred for MRI of the prostate. It was carried out in the period from September 2013 to May 2014. All patients underwent mpMRI on MRI 3T and bpMRI on MRI 1.5T (maximum interval 33 days) 7 days apart. No intervention was made between the two examinations. After mpMRI, 59 patients underwent prostate biopsy and the samples were histopathologically evaluated.

The mpMRI protocols of the prostate were performed on a 3T MRI scanner (Magnetom Trio A TIM System, Siemens Healthcare GmbH), and bpMRI examinations on a 1.5T MRI scanner (Magnetom Avanto, Siemens Healthcare GmbH). Six-channel phase coils for the body were used on both devices. BpMRI on MRI 1.5T was done to avoid unnecessary administration of contrast medium to the patient, since temporal, not spatial, resolution is crucial for DCE. In order to obtain the best image quality for each MRI and for each sequence, the parameters are optimized. (Table 1.) The images did not contain information on which device

Table 2. SNR and CNR values on 3T and 1.5T devices, with statistically significant differences in bold [21]

Signal-Noise-Ratio (SNR) (mean±SD)			3T	1.5T	p-value
T2W	Muscle	1.4±0.4	1.4±0.3	0.7	
	Prostate	8.5±2.5	8.5±2.6	0.9	
	PC	5.9±2.5	6.0±1.8	0.7	
DWI	High b-value images	Muscle	11±1.8	7.9±1.4	**<0.001**
		Prostate	16±2.1	11±1.4	**<0.001**
		PC	20±4.4	14±2.5	**<0.001**
	ADC map	Muscle	1.4±0.5	1.2±0.3	**0.03**
		Prostate	12±2.9	9.0±2.0	**<0.001**
		PC	7.3±3.0	6.4±1.7	0.2
Contrast-Noise-Ratio (CNR) (mean±SD)			**3T**	**1.5T**	**p-value**
T2W	Prostate-PC	2.3±1.7	2.7±2.5	1	
	PZ-TZ	2.6±2.0	2.7±2.2	0.8	
DWI	High b-value images	Prostate -PC	4.1±3.2	2.1±1.8	**0.05**
		PZ-TZ	0.8±0.8	0.4±0.4	**<0.001**
	ADC map	Prostate -PC	3.7±2.4	3.0±1.8	0.4
		PZ-TZ	1.9±1.8	1.4±1.3	0.2

they were taken and were evaluated by two independent radiologists (R1 and R2).

The primary objective of the study showed that differences in normalized signal strength (nSI) in T2W and in ADC maps obtained on MRI 3T and MRI 1.5T were not statistically significant for ROI in prostate cancer lesions or for ROI in benign prostate tissue. In images with a high b-value, there were significant differences between the nSI data obtained MR 3T and MR 1.5T measured for ROI in the whole prostate and peripheral and transition zone (MR 3T: nSI = 1.3 ± 0.5 and MR 1.5T: nSI = 1.2 ± 0.1). In the obtained T2W images, there was no significant difference in SNR between MR 3T and MR 1.5T for ROI in muscle (lat. m. obturator internus) and prostate, regardless of the localization of prostate cancer in the peripheral or transition zone (Table 2).

Significant differences between MR 3T and MR 1.5T were measured in images with a high b-value for all selected ROIs in muscle, prostate and prostate cancer. In the ADC maps, the SNR varied significantly for muscle and the entire prostate. For SNR measurements in ADC maps, ROI was set exclusively in prostate cancer lesions

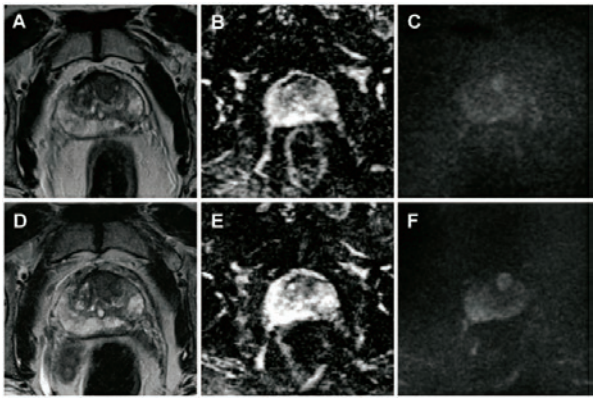


Figure 9. An example of the quality of the images used in the research. Images of A (T2W), B (ADC map) and C (DWI) obtained on MRI 1.5T and D (T2W), E (ADC map) and F (DWI) obtained on MRI 3T. High b-value images (1000 s/mm2) obtained on the 3T MRI (F) are qualitatively superior to the obtained image on the 1.5T MRI.
Source: https://www.sciencedirect.com/science/article/pii/S0720048X17300967#fig0005

Table 3. Subjective quality (scale 1-5) and PI-RADS v2. evaluation by two radiologists (R1, R2) for images collected on MRI 3T and MRI 1.5T [21]

Subjective IQ (mean ± SD)			**3T**	**1.5T**	**p-value**
Patients	Number		63	63	MWU
R1	T2W		4.2±1.0	3.8±0.8	**0.01**
	DWI	High b-value images	4.1±0.8	3.5±0.8	**<0.001**
		ADC map	4.1±0.7	3.8±0.6	**0.01**
R2	T2W		4.2±0.9	3.8±0.8	**0.01**
	DWI	High b-value images	4.2±0.8	3.6±0.8	**<0.001**
		ADC map	4.2±0.7	3.9±0.6	**0.01**
PI-RADS Score (mean ± SD)			**3T**	**1.5T**	**p-value**
R1	T2W		2.9±1.0	2.9±1.0	0.8
	DWI		2.9±1.0	2.8±1.0	0.2
	Overall		3.3±1.0	3.3±1.0	0.7
R2	T2W		3.0±0.9	3.0±0.9	1
	DWI		3.9±0.9	3.9±0.9	0.7
	Overall		3.4±1.0	3.4±0.9	0.9
PI-RADS Score (PCa) n = 15					
R1	T2W		4.4±0.8	4.4±0.8	1
	DWI		4.5±0.7	4.3±0.8	0.5
	Overall		4.5±0.6	4.5±0.6	1
R2	T2W		4.3±0.8	4.3±0.8	0.9
	DWI		4.4±0.7	4.4±0.7	0.9
	Overall		4.5±0.6	4.4±0.6	0.8
PI-RADS Score (benign) n = 44					
R1	T2W		2.6±0.8	2.7±0.7	0.7
	DWI		2.6±0.7	2.5±0.7	**0.05**
	Overall		2.9±0.8	2.8±0.8	0.6
R2	T2W		2.7±0.7	2.7±0.7	0.9
	DWI		2.7±0.7	2.7±0.7	0.6
	Overall		3.0±0.8	3.0±0.7	1

Author	Number	3.0 T scanner	3.0 T MRI sequences	1.5 T scanner	1.5 T MRI sequences	Objective	Subjects and primary findings
Beyersdorff [14]	22	Signa 3.0 T (GE Healthcare) using a torso phased-array coil (USA Instruments)	After a localizer scan, at least a T2W angulated axial FSE sequence with a TR/TE of 4,500/102 and an ETL of 8 or 16 and an angulated coronal FSE sequence (3,800/78.3; ETL, 8) with a FOV of 16 × 16 cm and a matrix of 256 × 256 were acquired. Four acquisitions were performed with each sequence at a slice thickness of 4 mm and a gap of 1 mm*.	Magnetom Vision or Magnetom Symphony (Siemens Medical Solutions) using a combination of an endorectal coil (Medrad) and a body phased-array coil.	T2W TSE sequence in angulated axial (3,500/96; ETL, 13; 3 acquisitions) and coronal (4,522/112; ETL, 13; 2 acquisitions) slice orientations with a FOV of 16 × 16 cm. The matrix was 256 × 256. In addition, an angulated axial T1W spin-echo sequence (680/14; ETL, 3) was acquired. The FOV was 16 × 16 cm, and the matrix was 256 × 256. The slice thickness was 3 mm and the interslice gap, 0.9 mm*.	To compare the image quality, tumour delineation, and depiction of staging criteria on MRI of PCa at 1.5 and 3.0 T.	No statistically significant differences in the visualization of staging criteria.
Torricelli [15]	29	Intera 3.0 T magnet, operating at 3.0 T (Philips Medical System), using a 6-channel external phased-array cardiac receiver coil	TSE T2W (TR/TE: 5504/120 ms) in the axial and coronal plane with ETL: 21, NSA: 4, FOV: 210 mm, slice thickness: 3 mm, gap: 0.5 mm, scan matrix: 320 × 320, and scan reconstruction: 512 × 512. TSE T1w (TR/TE: 445/11 ms) in the axial plane with ETL: 3, NSA: 2, FOV: 210 mm, slice thickness: 3 mm, gap: 0.5 mm, scan matrix: 320 × 320, and scan reconstruction: 512 × 512.	Intera 1.5 T Philips magnet, operating at 1.5 T (Philips Medical System), using an Ecca 64 MHz endocavitary coil (Philips Medical System).	TSE T2W (TR/ TE: 4750/130 ms) in the axial and coronal plane with ETL: 18, NSA: 6, FOV: 180 mm, slice thickness: 3 mm, gap: 0.5 mm, scan matrix: 320 × 320, and reconstruction matrix: 512 × 512. TSE T1W (TR/TE: 445/11 ms) in the axial plane with ETL: 3, NSA: 2, FOV: 180 mm, slice thickness: 3 mm, gap: 0.5 mm, scan matrix: 320 × 320, and reconstruction matrix: 512 × 512.	To compare the image quality and the diagnostic accuracy of endorectal coil 1.5 T MRI and phased-array coil 3.0 T MRI in staging of PCa.	3.0 T MRI had worse image quality but can provide similar diagnostic information compared with 1.5 T MRI.
Park [13]	108	Intera Achieva 3.0 T (Philips Medical System); examination was performed using a 6-channel external phased-array cardiac receiver coil (USA Instruments)	TSE using a SENSE technique (factor = 2) was used for T2W imaging with the following parameters: TR, 3300 to 4000 ms; TE, 80 to 100 ms; TSE factor, 12; FOV, 15 cm (17 cm for sagittal images); matrix number, 304 × 304; one acquisition; slice thickness, 3 mm; gap, 0.3 mm. Second, axial T1W imaging in a large FOV (24 cm) at both 3.0 and 1.5 T.**	Genesis Signa; GE Healthcare with endorectal coil (Medrad).	FSE was used for T2W imaging with the following parameters: TR, 3300-4000 ms; TE, 80-100 ms; ETL, 13; FOV, 18 cm; matrix number, 512 × 256; one acquisition; slice thickness, 3 mm; gap, 1 mm. Second, axial T1W imaging in a large FOV (24 cm) at both 3.0 and 1.5 T.**	To evaluate local staging accuracy for PCa at 3.0 T MRI compared with 1.5 T MRI.	3.0 T phased-array MRI is equivalent to the 1.5 T endorectal MRI in evaluating local staging accuracy for PCa without significant loss of imaging quality.
Ryznarova [16]	103 (1.5 T: 41, 3 T: 63)	Trio, Siemens, using 8-channel phased-array surface coils.	T1W TSE sequence in axial plane T2W TS sequences were performed in axial (orthogonal to the urethra), coronal, and sagittal planes. Echo-planar DWI was obtained in transverse plane parallel to the transverse T2W to construct ADC maps using the standard Siemens software. DCE 3D T1-spoiled gradient echo images were acquired during an intravenous bolus injection of paramagnetic contrast medium (gadobenate dimeglumine) at a dose of 0.1 mmol/kg of body weight for examination at 3.0 T. A MRS was also obtained by using a point-resolved 3D spectroscopic imaging sequence.	Avanto Siemens, Erlangen, Germany using 8 channels phased-array surface coils.	T1W TSE sequence in axial plane; T2W TSE sequences were performed in axial (orthogonal to the urethra), coronal, and sagittal planes. Echo-planar DWI was obtained in transverse plane parallel to the transverse T2W to construct ADC maps using the standard Siemens software. DCE 3D T1-spoiled gradient echo images were acquired during an intravenous bolus injection of paramagnetic contrast medium (gadobenate dimeglumine) at a dose of 0.2 mmol/kg of body weight for examination at 1.5 T. MRS was also obtained by using a point-resolved 3D spectroscopic imaging sequence.	To compares the results of MRI obtained by the 1.5 T and 3.0 T scanners using surface coils in patients with PCa.	Highest accuracy of local PCa staging with 3.0 T MRI scanner was seen when the protocol included DCE. No significant difference was found in tumour localization assessment between 3.0 T and 1.5 T MRI scanners.

Figure 10. An overview of accepted studies with their characteristics
Source:https://www.ncbi.nlm.nih.gov/pmc/articles/PMC9373864/table/T1/?report=objectonly

and did not differ significantly between MR 3T and MR 1.5T. For CNR measurements on MRI 3T and MRI 1.5T T2W sequences and ADC maps, ROI was set in benign prostate tissues and prostate cancer lesions. In high-b-value images, the CNR for ROI placed in benign prostate tissue and prostate cancer lesions was 4.1 ± 3.2 on MRI 3T and 2.1 ± 1.8 on MRI 1.5T. For the peripheral and transition zones, the 3T MRI was 0.8 ± 0.8, and 0.4 ± 0.4 respectively on the 1.5T MRI. Therefore, with sequence optimization on both MR 1.5T and MRI 3T, images of approximate SNR and CNR values can be obtained. (Table 3). For both radiologists, the average subjective image quality (Figure 9.) estimated on a scale of 1 to 5 was significantly better for the T2W sequence on MRI 3T compared to the sequence on MRI 1.5T (R1:4.2 ± 1.0 and 3.8 ± 0.8, respectively; R2: 4.2 ± 0.9 and 3.8 ± ± 0.8), as well as for high-b-value images (R1: 4.1 ± 0.8 and 3.5 ± 0.8, R2: 4.2 ± 0.8 and 3.6 respectively ± 0.8) and ADC maps (R1: 4.1 ± 0.7 and 3.8 ± 0.6, respectively; R2: 4.2 ± 0.7 and 3.9 ± 0.6, respectively). (Table 3.)

A total of 170 MRI lesions were defined for PI-RADS assessment. The individual results of both radiologists according to the PI-RADS classification for T2W and DWI images obtained on MRI 3T and MRI 1.5T were similar to the overall result in both radiologists. Patients with prostate cancer had significantly higher PI-RADS scores compared to patients with benign histopathological findings (total PI-RADS scores of 4.5 ± 0.6 and 2.9 ± 0.8 for R1 and 4.5 ± 0.6 and 3.0 ± 0.8 for R2, respectively). (Table 3.)

Although subjectively the quality of the images was rated significantly better on MRI 3T for all imaging sequences and in both radiologists, PI-RADS scoring was similar for MR 3T and MR 1.5T. None of the patients diagnosed with histologically proven prostate cancer received a total PI-RADS score below 4, either with images obtained on 3T MRI or 1.5T MRI.

In July 2022, Virarkar et al. [22] published a systematic review of studies with a meta-analysis aimed at determining the optimal field strength for prostate cancer MRI. The initial search yielded 24 articles and after applying the given selection criteria, 8 of them were reviewed. Of these, 4 studies included MRI of prostate cancer at both 3T and 1.5T and were selected for the study. All studies found a low risk of systemic bias in participant selection, except in Parker's study. The study by Torriceli et al. did not identify a low risk of systemic error for reference standards. All studies were rated as low risk for flow, time and index test. For MR 3T, the group sensitivity was 69.5%, with a 95% confidence interval (CI) of 56.4 to 80.1%. The group specificity for MR 3T was 48.8%, with a 95% CI of 6 to 93.4%. The group diagnostic odds ratio (DOR) for MRI 3T was 3%, with a 95% CI of 0 to 26%. The area under the curve (AUC) was 0.684. The collective sensitivity for MR 1.5T was 70.6%, with a 95% CI of 55.0 to 82.5%. The group sensitivity for MR 1.5T was 70.6%, with a 95% CI of 55.0 to 82.5%. The group specificity for MR 1.5T was 41.7%, with a 95% CI of 6.2 to 88.6%. The group DOR for MR 1.5T was 2, with a 95% confidence interval of 0 to 18. AUC was 0.679. (Figure 10.)

A meta-analysis of MRI comparison on 3T and 1.5T field strength devices for determining the stage of prostate cancer did not find significant relationships between magnet strength, sensitivity, specificity, or DOR values (p = 0.91, 0.88, and 0.89, respectively). (Figure 11.)

Parameter	3.0 T	1.5 T	p
TP	68	67	–
TN	47	28	–
FP	19	21	–
FN	26	23	–
Sensitivity (95% CI)	69.5% (56.4–80.1%)	70.6% (55.0– 82.5%)	0.91
Specificity (95% CI)	48.8% (6.0–93.4%)	41.7% (6.2–88.6%)	0.88
DOR (95% CI)	3 (0–26)	2 (0–18)	0.89
AUC	0.684	0.679	–

Figure 11. Results of a meta-analysis of diagnostic efficacy of 3.0 T versus 1.5 T MRI in determining the stage of prostate cancer
Source: https://www.ncbi.nlm.nih.gov/pmc/articles/PMC9373864/table/T3/?report=objectonly

Conclusion

Prostate cancer is the second most common cancer in the male population in the world and the fifth most fatal. Despite the fact that PI-RADS recommendations state that MRI of the prostate is performed on 3T power devices, more and more studies emphasize the equal diagnostic value of prostate MRI on 1.5T devices in diagnosing and monitoring diseases. The study was limited by the small amount of available studies comparing the quality of prostate MRI with 1.5T and 3T field strength devices, but monitoring over a 10-year period, from 2012 to 2022, can conclude that there was a significant improvement in the quality of 1.5T field strength devices. By comparing studies, it was found that due to SNR, sequences, primarily DWI, have technically better performance, but without a significant diagnostic difference in the detection of prostate cancer compared to MRI performed on 1.5T devices. By introducing 3D and MRF sequences, we can further shorten the duration of prostate MRI, and by introducing BOLD sequences, T2 mapping and MRF sequences, we can quantify the signal and get a better ability to assess the spread of prostate cancer, as well as improve differentiation in relation to BPH and prostatitis. As mentioned at the beginning, the relatively small proportion of comparative studies of MR 1.5T and MR 3T, the absence of analysis of other parameters that affect the quality of the sequence (matrix size, bandwith, additional analysis of coil selection, FOV selection, etc.) and the heterogeneity of the studies require that the results of this meta-analysis be taken with a grain of salt.

Taking into account the above, further research is needed in this area to determine whether the diagnostic value of MRI of the prostate depends on the strength of the magnetic field.

All data in this paper are part of the results from the master's thesis titled "Comparison of magnetic resonance imaging of the prostate 1.5T and 3T", written at the University Department of Health Studies, University of Split [23].

Literature:

1. PI-RADS v2.1. (preuzeto 12.2.2023.) Dostupno na https://www.acr.org/-/media/ACR/Files/RADS/Pi-RADS/PIRADS-v2-1.pdf
2. Giganti F., Rosenkrantz B. A., Villeirs G., Panebianco V., Stabile A., Emberton M., Moore C. M. The Evolution of MRI of the Prostate: The Past, the Present, and the Future. AJR Am J Roentgenol. 2019 Aug; 213(2): 384-396.
3. Giganti F, Allen C. Imaging quality and prostate MR: it is time to improve. Br J Radiol. 2021 Feb 1;94(1118):20200934. doi: 10.1259/bjr.20200934.
4. Westbrook C., Talbot J. MRI in Practice, 5th Edition. Wiley-Blackwell, 2018.
5. Jambor I. Optimization of prostate MRI acquisition and post-processing protocol: a pictorial review with access to acquisition protocols. Acta Radiol Open. 2017 Dec 8;6(12):2058460117745574. doi: 10.1177/2058460117745574.

6. Maier SE, Wallström J, Langkilde F, Johansson J, Kuczera S, Hugosson J, Hellström M. Prostate Cancer Diffusion-Weighted Magnetic Resonance Imaging: Does the Choice of Diffusion-Weighting Level Matter? J Magn Reson Imaging. 2022 Mar;55(3):842-853. doi: 10.1002/jmri.27895.
7. Tamada T, Kido A, Ueda Y, Takeuchi M, Fukunaga T, Sone T, Yamamoto A. Clinical impact of ultra-high b-value (3000 s/mm2) diffusion-weighted magnetic resonance imaging in prostate cancer at 3T: comparison with b-value of 2000 s/mm2. Br J Radiol. 2022 Mar 1;95(1131):20210465. doi: 10.1259/bjr.20210465.
8. Polanec SH, Lazar M, Wengert GJ, Bickel H, Spick C, Susani M, Shariat S, Clauser P, Baltzer PAT. 3D T2-weighted imaging to shorten multiparametric prostate MRI protocols. Eur Radiol. 2018 Apr;28(4):1634-1641. doi: 10.1007/s00330-017-5120-5.
9. Vidya Shankar R, Roccia E, Cruz G, Neji R, Botnar R, Prezzi D, Goh V, Prieto C, Dregely I. Accelerated 3D T2 w-imaging of the prostate with 1-millimeter isotropic resolution in less than 3 minutes. Magn Reson Med. 2019 Aug;82(2):721-731. doi: 10.1002/mrm.27764.
10. Caglic I, Povalej Brzan P, Warren AY, Bratt O, Shah N, Barrett T. Defining the incremental value of 3D T2-weighted imaging in the assessment of prostate cancer extracapsular extension. Eur Radiol. 2019 Oct;29(10):5488-5497. doi: 10.1007/s00330-019-06070-6.
11. Alonzi R, Taylor NJ, Stirling JJ, d'Arcy JA, Collins DJ, Saunders MI, Hoskin PJ, Padhani AR. Reproducibility and correlation between quantitative and semiquantitative dynamic and intrinsic susceptibility-weighted MRI parameters in the benign and malignant human prostate. J Magn Reson Imaging. 2010 Jul;32(1):155-64. doi: 10.1002/jmri.22215.
12. Kim Y, Park JJ, Kim CK. Blood oxygenation level-dependent MRI at 3T for differentiating prostate cancer from benign tissue: a preliminary experience. Br J Radiol 2022; 95: 20210461.
13. Klingebiel M, Schimmöller L, Weiland E, Franiel T, Jannusch K, Kirchner J, Hilbert T, Strecker R, Arsov C, Wittsack HJ, Albers P, Antoch G, Ullrich T. Value of T2 Mapping MRI for Prostate Cancer Detection and Classification. J Magn Reson Imaging. 2022 Aug;56(2):413-422. doi: 10.1002/jmri.28061.
14. Mai J, Abubrig M, Lehmann T, Hilbert T, Weiland E, Grimm MO, Teichgräber U, Franiel T. T2 Mapping in Prostate Cancer. Invest Radiol. 2019 Mar;54(3):146-152. doi: 10.1097/RLI.0000000000000520.
15. Sathiadoss P, Schieda N, Haroon M, Osman H, Alrasheed S, Flood TA, Melkus G. Utility of Quantitative T2-Mapping Compared to Conventional and Advanced Diffusion Weighted Imaging Techniques for Multiparametric Prostate MRI in Men with Hip Prosthesis. J Magn Reson Imaging. 2022 Jan;55(1):265-274. doi: 10.1002/jmri.27803.
16. Al-Bourini O, Seif Amir Hosseini A, Giganti F, Balz J, Heitz LG, Voit D, Lotz J, Trojan L, Frahm J, Uhlig A, Uhlig J. T1 Mapping of the Prostate Using Single-Shot T1FLASH: A Clinical Feasibility Study to Optimize Prostate Cancer Assessment. Invest Radiol. 2022 Dec 8. doi: 10.1097/RLI.0000000000000945.
17. Sushentsev N, Kaggie JD, Slough RA, Carmo B, Barrett T. Reproducibility of magnetic resonance fingerprinting-based T1 mapping of the healthy prostate at 1.5 and 3.0 T: A proof-of-concept study. PLoS One. 2021 Jan 29;16(1):e0245970. doi: 10.1371/journal.pone. 0245970.
18. Shiradkar R, Panda A, Leo P, Janowczyk A, Farre X, Janaki N, Li L, Pahwa S, Mahran A, Buzzy C, Fu P, Elliott R, MacLennan G, Ponsky L, Gulani V, Madabhushi A. T1 and T2 MR fingerprinting measurements of prostate cancer and prostatitis correlate with deep learning-derived estimates of epithelium, lumen, and stromal composition on corresponding whole mount histopathology. Eur Radiol. 2021 Mar;31(3):1336-1346. doi: 10.1007/s00330-020-07214-9..
19. Tamada T, Kido A, Yamamoto A, Takeuchi M, Miyaji Y, Moriya T, Sone T. Comparison of Biparametric and Multiparametric MRI for Clinically Significant Prostate Cancer Detection With PI-RADS Version 2.1. J Magn Reson Imaging. 2021 Jan;53(1):283-291. doi: 10.1002/jmri.27283.
20. Felisi M, Monti AF, Lizio D, Nici S, Pellegrini RG, Riga S, Bortolato B, Brambilla MG, Carbonini C, Abujami M, Carsana C, Sibio D, Potente C, Vanzulli A, Palazzi MF, Torresin A. MRI only in a patient with prostate cancer with bilateral metal hip prostheses: case study. Tumori. 2021 Dec;107(6):NP41-NP44. doi: 10.1177/0300891621997549.
21. Ullrich T, Quentin M, Oelers C, Dietzel F, Sawicki LM, Arsov C, Rabenalt R, Albers P, Antoch G, Blondin D, Wittsack HJ, Schimmöller L. Magnetic resonance imaging of the prostate at 1.5 versus 3.0T: A prospective comparison study of image quality. Eur J Radiol. 2017 May;90:192-197.
22. Virarkar M, Szklaruk J, Diab R, Bassett R, Bhosale P. Diagnostic value of 3.0 T versus 1.5 T MRI in staging prostate cancer: systematic review and meta-analysis. Pol J Radiol. 2022 Jul 29;87:e421-e429.
23. Kutlić G. Usporedba oslikavanja prostate magnetskom rezonancijom 1.5 T i 3 T (Diplomski rad). Split: Sveučilište u Splitu, Sveučilišni odjel zdravstvenih studija; 2023 (pristupljeno13.01.2025.) Dostupno na: https://urn.nsk.hr/urn:nbn:hr:176:919786

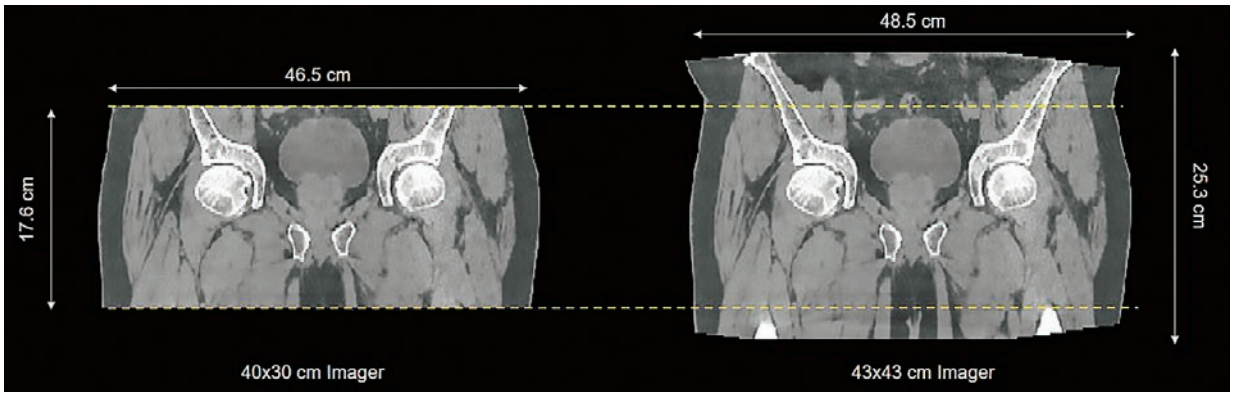
Usporedba oslikavanja prostate magnetskom rezonancijom 1.5T i 3T

Sažetak

Izvrsnim prikazom mekih tkiva i mogućnostima trodimenzionalnog prikaza magnetska rezonancija od svojih je početaka prije 40 godina do danas postala jedna od temeljnih dijagnostika u prikazu prostate i njezinih patoloških stanja. Iako je veća dostupnost uređaja za magnetsku rezonanciju snage polja 1.5T, preporuka Europskog udruženja urogenitalnih radiologa je da se snimanje prostate magnetskom rezonancijom vrši na uređajima snage polja 3T. Uređaji snage 3T nametnuli su se zbog povećanog omjera signala i šuma (SNR) koji se može iskoristi za skraćenje vremena snimanja ili povećanja rezolucije, tj. poboljšanja kvalitete slike. Sve je više istraživanja primjene kvantitativnih tehnika, kao što su engl. *Magnetic resonance fingerprinting,* T2 mapiranje, BOLD, kojima bi se mogla poboljšati detekcija i kvantificiranje lezija kracinoma prostate, a optimizacijom protokola na 1.5T i 3T moguće je učiniti pretrage jednake dijagnostičke vrijednosti.

Ključne riječi: MRI; prostata; 1.5T; 3T

HyperSight Spotlight: Larger Field of View



Images acquired on TrueBeam, courtesy of UH Seidman Cancer Center, Cleveland, Ohio.

Varian's HyperSight imaging solution, available as an optional feature on the Halcyon, Ethos, TrueBeam, and Edge radiotherapy systems, allows clinicians to acquire high-quality cone-beam CT (CBCT) images comparable to that of a CT simulation image. The larger images, high soft tissue contrast, and faster image acquisition are designed to improve the ability to target tumor volumes more precisely while sparing healthy tissue.

Below, we're highlighting key benefits offered by the HyperSight imaging solution's larger field of view (FOV).

Thanks to the larger kV imaging panel and software innovations that are exclusive with HyperSight, clinicians now have the ability to see more anatomy, in both the axial and transverse planes, that may have previously been cut off or out of view. This may be particularly beneficial when working with larger anatomy, off-center targets, and disease sites where there is extensive nodal involvement. The larger FOV can reduce the need to acquire multiple CBCT images and it may give clinicians the information they need to proceed with off-line adaptation.

The ability to see the entire target is essential for having confidence in the patient's alignment both for imaging and planning, helping enable clinicians to reduce target margins. For patients, this may translate into reduced time on the treatment couch. Here are examples where the larger FOV translates into clinical impact.

Head and Neck

In this head and neck case with extensive disease involvement, the larger FOV delivered by HyperSight on a Varian TrueBeam system provides greater visibility of the structures and organs surrounding the target to enable a more accurate positional alignment. In this case, the clinician is able to visualize all pertinent anatomy without the need to acquire additional images. This potentially means less



Image courtesy of University of Maryland Medical Center, Baltimore, Maryland.

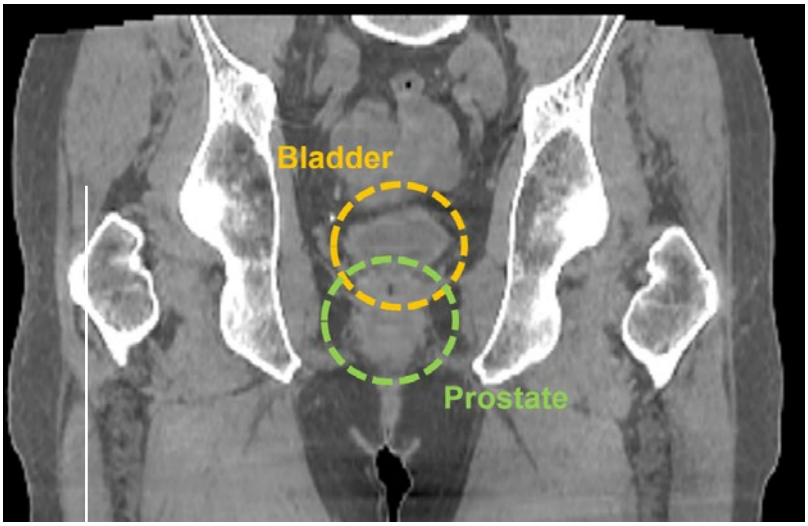


Image courtesy of University Hospitals Seidman Cancer Center, Cleveland, Ohio.

time on the treatment couch, less time in the immobilization device, and less imaging dose to the patient.

Prostate

In this prostate case, the larger FOV provided by the HyperSight image, taken using a Varian TrueBeam system, enables a clinician to see the entire treatment area including the lymphatic region, which may also require treatment. It also enables the clinician to visualize the relevant anatomy without acquiring multiple CBCT images.

Breast

This HyperSight cone-beam CT for planning (CBCTp*) image, taken using a Varian Halcyon system,** encompasses the entire breast and body, giving clinicians the information they need to generate the initial treatment plan. During treatment, the larger FOV also enables clinicians to see and assess changes in adjacent anatomical structures and landmarks. If the change is deemed significant enough that offline adaptive is needed, they may be able to replan using the latest HyperSight CBCT image.



Image courtesy of Northeastern Oklahoma Cancer Institute, Claremore, Oklahoma.

* CBCTp is an image-only workflow only available on the Halcyon system.

** HyperSight on Halcyon has different specifications than HyperSight on TrueBeam, as the system configuration for Halcyon allows for a larger kV imaging panel.

QR700020026

© 2025 VARIAN MEDICAL SYSTEMS, INC. All trademarks are the property of their respective owners.

REVIEW ARTICLE (PREGLEDNI RAD)

Advantages and limitations of artificial intelligence tools in the analysis of thoracic computed tomography images in patients with COVID-19 pneumonia – a review

Nina Mrvoš[1], **Melita Kukuljan**[1,2], **Maja Karić**[1,2], **Klaudija Višković**[1,3]

[1] Faculty of Health Studies, University of Rijeka, Rijeka, Croatia

[2] Clinical Hospital Center Rijeka, Department of Diagnostic and Interventional Radiology, Rijeka, Croatia

[3] University Hospital for Infectious Diseases „Dr. Fran Mihaljević", Department of Radiology and Ultrasound, Zagreb, Croatia

Corresponding author: Nina Mrvoš, email: ninamrvos@gmail.com

DOI: https://doi.org/10.55378/rv.49.1.6

Abstract

Coronavirus disease 2019 (COVID-19) is a systemic viral infection caused by the highly infectious SARS-CoV-2 virus, which can lead to pneumonia and other complications. It first appeared at the end of 2019 in China and spread rapidly around the world causing authorities to declare a pandemic at the start of 2020. People infected with this virus usually present with symptoms such as cough, fever and shortness of breath. This respiratory disease causes changes in lung parenchyma that can be analysed on a CT scan. CT became one of the most accurate diagnostic methods for confirmation of COVID-19 in patients as well as a tool for estimating the stage of infection. Since identifying the disease from radiological scans is quite time-consuming and complex, the development of artificial intelligence (AI) models has emerged as a potential solution to enhance diagnostic speed and accuracy. Most common AI models were based on deep learning and machine learning and were able to correctly identify COVID-19 pneumonia on CT scans. The main problem in developing these models proved to be the lack of databases on which these models could be trained. This review analysed the results of twenty-one papers published on the topic of AI use in detecting COVID-19 on CT scans. The results of analysis show that AI is significantly accurate in detecting COVID-19 pneumonia, but it still needs to be developed further.

Key words: COVID-19, SARS-CoV-2, computed tomography of the chest, artificial intelligence, deep learning, machine learning

Introduction

As of February 2, 2025, the World Health Organization (WHO) has published a report according to which there have been 777,368,929 recorded cases of COVID-19 in the world since December 2019 (1). Since its beginning in Wuhan, China, this severe respiratory disease has spread rapidly globally, leading to the declaration of a pandemic on March 11, 2020 (1).

The high speed of expansion and the growing number of patients have created enormous pressure on the healthcare system and its employees. One of the main health specialties that actively worked on the early detection and control of the development of COVID-19 was radiology. Radiological methods used in the diagnosis of COVID-19 are: chest radiographs, computed tomography (CT) of the chest, thorax ultrasound and magnetic resonance imaging (MRI) of the chest (2, 3, 4). Given that patients infected with COVID-19 required urgent hospital admission, there was a shift in long waiting lists for examinations of patients not infected with COVID and an additional workload of radiology department employees.

In order to perform examinations as quickly and efficiently as possible and make a diagnosis, the idea of introducing new systems and technologies in healthcare appeared. One of the most commonly implemented technologies was artificial intelligence (AI) (2). At the starting stages of the pandemic, AI models were still under development, so their precision and accuracy were low. In order to achieve better results, it was necessary to create large databases with numerous radiological images, especially CT scans of patients who had proven disease by PCR (Polymerase Chain Reaction) test (5).

The goal of this review paper is to determine the advantages in the application of artificial intelligence tools i.e. machine learning and deep learning, in the analysis of images of patients with COVID-19 pneumonia using computed tomography compared to the analysis of images read exclusively by radiologists.

Methods

Databases Google Scholar, MedRix, IEEE, PubMed and Scopus were searched using the following keywords: artificial intelligence, computed tomography of the chest, COVID-19, deep learning, machine learning, SARS-CoV-2.

Study inclusion criteria was set that included review articles and original scientific papers according to the above keywords published from January 1, 2020 to December 31, 2024. In addition, all articles had to be published in English. Articles without peer review, duplicate articles, articles that dealt with other radiological diagnostic methods except CT (X-ray, ultrasound, MR), case reports and studies which involved CT protocols of the thorax with contrast were not included in the analysis.

Articles selected for further analysis, after separating those that met exclusion criteria, were divided into review articles and original scientific articles. The next step was to group articles that deal with the use of AI tools in CT and thorax in patients with COVID-19 pneumonia by the deep learning method and by the machine learning method. The articles highlighted in the previous step were reviewed, with a focus on the title and abstract to ensure the relevance of the topic. After that, the selected articles were analysed in detail in their entirety with an assessment of whether the research goals were clearly stated, whether the research methodology was elaborated in detail, and whether the research results were presented in accordance with the research question. In the last phase of filtering, in accordance with the hypotheses, studies were separated into two groups, one which showed that the use of AI tools such as machine learning and deep learning in the diagnosis of COVID-19 using CT, allow for faster detection of diseases compared to images read exclusively by radiologists and the group with studies that showed that AI tools did not contribute to faster and more accurate detection of diseases.

A total of 59 papers on the application of artificial intelligence in the diagnosis of COVID-19 using computed tomography of the thorax were reviewed. Out of 59 reviewed papers, 40 articles were excluded according to the given criteria, and 12 review papers and 9 original scientific papers were included.

Papers that were finally selected for detailed analysis were divided into several thematic groups: pathophysiology and epidemiology of COVID-19 infection, CT-scan protocols, opacification and other radiological signs of COVID-19 infection on CT, the significance of the use of AI tools in COVID-19 pneumonia in CT of thorax, the advantages and limitations of the use of deep learning tools, the advantages and limitations of the use of machine learning tools, guidelines for further research of artificial intelligence tools.

Finally, the limitations of the study were listed, and in the conclusion, the supporting arguments of the study highlighted with a summary of key evidence.

Table 1. Review articles included in the analysis on the application of artificial intelligence in the diagnosis of COVID-19 disease using computed tomography of the thorax

Article no.	Name of the first author and year of publication	Methodology explored	Imaging method	Research goals	Research results	Limitations of the study
1.	Serena Low W.C. et al., 2021 (6)	Deep learning	CT & X-ray	A review of deep learning techniques in imaging of COVID-19 pneumonia patients	The development of deep learning techniques is limited due to the limited number of databases.	Different formats, forms of archiving and quality are used in image databases so it makes comparison of images difficult
2.	Fusco R. et al., 2021 (7)	Machine learning and deep learning	CT & X-ray	Overview of deep learning and machine learning techniques in the diagnosis and treatment of COVID-19 pneumonia, comparison of sensitivity and specificity of CT and X-ray images	There was no statistically significant difference in the median value of accuracy between X-ray and CT (Chi square test; p value > 0.05).	The analysis of the images could not be performed for patients who were in critical condition, as they could not be involved in the imaging process.
3.	Alassiri R. et al., 2022 (8)	Deep learning and transferable learning	CT	Retrospective analysis of deep learning algorithms to improve the results of pre-trained models with and without data augmentation	The rate of improvement in the accuracy of pre-trained models after data augmentation was 3%.	A small number of CT studies of patients were used (349, of which only 10% were used for validation). Clinical patient data were not considered.

Article no.	Name of the first author and year of publication	Methodology explored	Imaging method	Research goals	Research results	Limitations of the study
4.	Heidari A. et al., 2022 (9)	Deep learning	CT & X-ray	Comparison of modern systems that use deep learning for the detection of COVID-19 disease by systematic review of the literature.	The effectiveness of different models varies.	Unavailability of non-English articles, and articles published by certain publications, insufficiently clear description of the algorithms used.
5.	Roberts M. et al., 2021 (10)	Machine learning	CT & X-ray	To compare the quality of the methodology and the possibility of repeating the use of methods of different machine learning models for the detection of COVID-19 disease.	None of the included machine learning models is good enough to be used in diagnosis of COVID-19.	Lack of documentation on proposed algorithmic approaches, high risk of model bias due to training on a small number of COVID-19 positive images
6.	Aggarwal P. et al., 2022. (11)	Deep learning	CT & X-ray	Summarize significant deep learning-based studies that can help in the future of developing models for the rapid and accurate diagnosis of COVID-19	Summary of the latest achievements (state of art) of deep learning techniques used in CT and X-ray technology. Most of the studies used smaller datasets, and there is a lack of comparison with existing studies, and there are no codes and data available to verify clinical use.	They are not highlighted.
7.	Komolafe T. E. et al., 2021 (12)	Deep learning	CT	Summarize all available evidence through systematic review and meta-analysis to quantitatively assess the accuracy of the diagnostic test (DTA) of the deep learning algorithm for detecting COVID-19 disease on chest CT scans.	Three studies reported higher accuracy of the deep learning algorithm's diagnostic test (DTA) compared to the radiologist's interpretation, 4 studies showed that the deep learning algorithm helped DTA performance, 6 studies showed that sensitivity was higher than specificity, 9 studies showed that specificity was higher than sensitivity.	They are not highlighted.
8.	Ozsahin I. et al., 2020 (3)	Deep learning and machine learning	CT	To review studies that address the use of AI in the diagnosis of COVID-19 using CT.	Widely trained networks can be very successful at every stage of CT scan classification.	The data used in the studies could come from different institutions and different devices. Lack of demographic and clinical information about patients.

Article no.	Name of the first author and year of publication	Methodology explored	Imaging method	Research goals	Research results	Limitations of the study
9.	Alzubaidi M. et al., 2021 (14)	Deep learning	CT, X-ray and UTZ	Identify and demonstrate the role of deep learning algorithms during the COVID-19 pandemic.	Most studies used a deep learning algorithm to detect COVID-19 through radiological images, but did not use the algorithm for the purpose of tracking infected cases or applications in robotics.	The number of data sets is small and uniform. The analysed studies were suggestions and have not been empirically tested.
10.	Wang Q. et al., 2022 (13)	Deep learning	CT	To analyse the performance of deep learning models in the diagnosis of COVID-19 disease from chest CT scans.	Deep learning models have great potential in accurately diagnosing COVID-19 and distinguishing them from other inflammatory lung diseases.	Source of data from different countries and from different CT machines. Too little literature is included.
11.	Kataoka Y. et al., 2024 (14)	Deep learning	CT	To examine whether the central-peripheral distributions of ground glass opacity and consolidation were associated with severe outcomes in patients with SARS-CoV-2 pneumonia independent of the whole-lung extents of these abnormal shadows.	Higher ratio of GGOs in the central regions to those in the peripheral regions was associated with severe outcomes in patients with severe SARS-CoV-2 pneumonia.	CT protocols vary among institutions, images with pleural effusion, pneumothorax, and pulmonary lung tumors were not included, associations of the CT findings with short-term outcomes, but not long-term outcomes.
12.	Bumm R. et al., 2024. (16)	Machine learning	CT	Determine the accordance of computer vs. human analysis to demonstrate the feasibility of computer analysis with Lung CT Analyzer and to elaborate on the existing differences in lung involvement between the severity-scored groups, to evaluate whether tissue affection in severe cases could be attributed to the side of lungs, lung regions or lung lobes and to predict patients requiring intensive care unit treatment.	The extent of lung involvement, particularly in the lower lobes, dorsal lungs, and lower half of the lungs, may be associated with the need for ICU admission in patients with COVID-19. Computer analysis showed a high correlation with expert rating.	An inherent component of the design in the preceding study, subjective variables.

Table 2. Original scientific articles included in the analysis on the application of artificial intelligence in the diagnosis of COVID-19 using computed tomography of the thorax

Article no.	Name of the first author and year of publication	Methodology explored	Imaging method	Research goals	Research results	Limitations of the study
1.	Abdulsalam Hamwi W., et al 2022 (17)	Machine learning (convolutional neural network)	CT & X-ray	Develop an integrated machine learning model to reduce misdiagnosis and late diagnosis of COVID-19, and compare research with other research.	An overall accuracy and an F1 score of 99.73% was achieved by applying meshes in the analysis of CT scans in PNG format. Most of the scans are accurately diagnosed.	They are not highlighted.
2.	Türk V. et al., 2022 (18)	Deep learning	CT	To compare four models of a deep learning algorithm for classifying positive and negative COVID-19 findings.	The best result and the highest accuracy were achieved by the MobileNet architecture.	Limited number of COVID-19 patients, different sizes and resolutions of CT scans.
3.	Vaidyanathan A. et al., 2022 (19)	Deep learning	CT	Propose an artificial intelligence framework based on a three-dimensional convolutional neural network intended for the classification of CT scans of patients with COVID-19 disease, influenza/ pneumonia acquired in the community and without infection.	The tested model showed excellent results in an external validation system with an area under the curve of 0.90, 0.92 and 0.92 for COVID-19 disease, community-acquired influenza/pneumonia and no infection.	The presence of only cases of community-acquired pneumonia in the division for influenza/community-acquired pneumonia, the origin of shots from only two different suppliers.
4.	Yousefzadeh M. et al., 2021 (20)	Deep learning	CT	Present and evaluate the diagnostic performance of *the ai-corona model* on multiple databases, and compare it with the findings of radiologists, RT – PCR tests and two other scientific studies.	The *ai-corona* model has learned to diagnose COVID-19, and distinguish it from other lung diseases from CT scans. It also showed better performance compared to the other two models.	The model was built to be as powerful and accurate as possible, but on a simpler database. They did not separate other types of pneumonia separately to make the model as accurate as possible. They did not enter data on cases that were RT-PCR negative and CT positive.
5.	Anwar T. et al., 2021 (21)	Deep learning	CT	Test the EfficientNet model using a five-fold cross-check strategy to verify the accuracy of the model and compare the performance with other articles.	An accuracy score and an F1 score of 0.90 were obtained on the same database where the other articles received an accuracy score of 0.86 and an F1 score of 0.85.	They are not highlighted.

Article no.	Name of the first author and year of publication	Methodology explored	Imaging method	Research goals	Research results	Limitations of the study
6.	Chamberlin J. H. et al., 2022 (22)	Deep learning	CT	To assess the ability of a deep convolutional neural network to predict the outcome of COVID-19 disease, and to analyse the success of an algorithm for grading disease progression.	The tested algorithm proved to be a precise and diagnostically accurate tool in the assessment of COVID-19 disease.	A single institution source of data, the retrospective nature of this study that includes repeated waves of COVID-19, vaccines, and strains, the study did not include current demographics and comorbidities as risk factors in scope.
7.	Chrzan R. et al., 2022 (23)	Deep learning	CT (High Resolution HRCT)	To analyse the performance of artificial intelligence models in estimating the degree of COVID – 19 disease progression on CT scans with high resolution.	Artificial intelligence has proven to be a simple and reliable way to diagnose COVID-19, as for prediction of the degree of advancement of the disease.	Retrospective design, no specific estimate was used to measure the volume of inflammation therefore the model cannot estimate the volume of inflammation, it could not distinguish between inflammatory consolidations and changes in the lungs caused by diseases other than COVID-19.
8.	Gunraj H. et al., 2022 (24)	Deep learning (deep neural network)	CT	To present the new COVID – Net CT – 2 algorithm intended for the diagnosis of diseases COVID-19 from CT scans.	This algorithm has been trained on a large, diverse and multinational group of patients and provides precise and accurate quantitative results.	The algorithm is not entirely ready for widespread use, but it can be used as a basis for new research.
9.	Nguyen D. et al., 2021 (25)	Deep learning	CT (3D)	To evaluate deep learning classification models trained to identify COVID-19 disease based on 3D CT data from different countries.	Deep learning models correctly identify patients who are COVID-19 positive with high accuracy, but only when the model was used on the database on which it was trained.	Models fail when applied to an unknown database (possible consequence of different protocols and methods of data collection from different countries and different patient demographics), lack of generalization in patient identification.

Respiratory disease COVID-19

COVID-19 is one of the inflammatory diseases of the respiratory system caused by the Severe Acute Respiratory Syndrome Coronavirus 2 (SARS-CoV-2). This type of virus causes diseases in animals in most cases, but through mutations in wild animals, it can come into contact with humans and infect them. This is how the SARS-CoV-2 virus was transmitted from bats to humans, giving rise to a new respiratory disease, COVID-19, transmitted by aerosol from person to person in close contact and presenting with symptoms such as high body temperature, cough and respiratory difficulties (26).

Structure of the SARS-CoV-2 virus

The SARS-CoV-2 virus belongs to the coronavirus family *Coronaviridae*, its particle size ranges from 60 to 140 nm, and it contains single-stranded ribonucleic acid (RNA). It contains 14 open-read frameworks encoding 16 non-structural, 9 auxiliary, and 4 structural proteins (27). Non-structural proteins are involved in regulating the replication and transcription of RNA viruses as enzymes. Helper proteins are not essential for coronavirus replication and transcription, but they make it easier for the virus to adapt to the host and defend against the host's immune system (Figure 1).

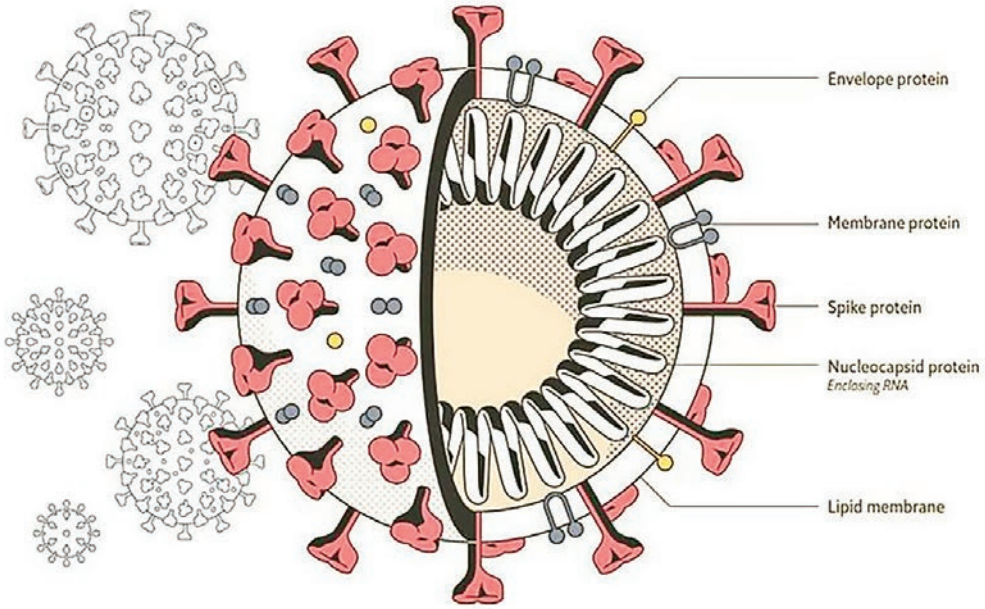


Figure 1. Structure of SARS-CoV-2 virus
Source: https://www.researchgate.net/publication/354266318/figure/fig1/AS:1063078342950912@1630469036040/The-structure-of-COVID-19.jpg

Transmission of SARS-CoV-2 virus and protection measures

After the virus mutated enough to be able to jump from animal to human, it became highly infectious to humans. Infected people are most contagious before they develop the first symptoms (approximately 2 days before the onset of symptoms) and in the early stages of the disease. The disease caused by this virus can be transmitted between people in different ways (1).

It is most often spread among people who are in close contact, at a short distance. The virus is transmitted by liquid particles, i.e. aerosol from the mouth or nose of an infected person when the person speaks, breathes or coughs. A person can become infected this way if the particles come into contact with the mucous membranes of the eyes, mouth or nose (1). Infection can also occur if people touch their mouth, nose, or eyes after touching a contaminated surface or object. It is also possible to be infected in poorly ventilated rooms or in closed spaces where there are many people where the aerosol full of infectious particles lingers for a long time (1).

During the pandemic, the WHO gave detailed guidelines for adherence to the population to reduce the spread of the disease (1). To reduce the possibility of infection with the virus, it is important to keep a physical distance of at least one meter from others. It is desirable to avoid crowds, but if it is unavoidable, it is necessary to wear medical face masks properly. Frequent washing and disinfecting of hands also reduces the likelihood of transmission of infection.

Preventive action is achieved by vaccination. With the rapid development of the disease, scientists tried to develop vaccines that would be successful in defending against the disease. At the very beginning of the disease, over 100 types of vaccines were developed based on previous knowledge of *Coronaviruses* (28). The use of vaccines was primarily recommended for the elderly population and people with comorbidities or immunocompromised, in order to protect them from infection or to mitigate the severity of the disease if infection occurs. Today, it is recommended that the entire population should be vaccinated with at least one dose of the vaccine in order to alleviate possible symptoms and to reduce mortality (1).

Symptomatology and clinical picture of COVID-19

The incubation period of COVID-19, the period of time from exposure to the virus to the manifestation of the first symptoms, lasts on average 5 to 6 days, but can last up to 14 days (29). This period is also called the presymptomatic period, it is characterized by high contagiousness of people who can easily transmit the virus to other healthy individuals.

The age group most often affected by this disease is from 40 to 70 years of age (30). The main symptoms include fever, body aches, shortness of breath, dry cough and sometimes gastrointestinal symptoms such as abdominal pain, vomiting and changes in stool. The severity of the disease can vary from asymptomatic so that patients do not even notice that they are infected, through a mild form to very severe disease (30).

Initially, it may be an infection of the upper respiratory system, but in some patients the disease can develop into a more severe form such as pneumonia with shortness of breath and can progress to acute respiratory distress syndrome (ARDS) and in the most severe cases can lead to death (31). The at-risk part of the population consists of elderly people with comorbidities, pregnant and premature babies, newborns and people who are immunocompromised (30).

Methods of diagnosing COVID-19

Timely detection of the SARS-CoV-2 virus is important to help control the spread and progression of COVID-19. Thanks to modern molecular medicine techniques, there

are several ways and tests that can detect the SARS-CoV-2 virus. One of the tests that has become the gold standard in the diagnosis of COVID-19 is reverse transcriptase-polymerase chain reaction (RT-PCR) (32). This infectious disease of the lungs can also be detected by radiological methods, the most accurate of which is the CT method (32).

RT-PCR test

RT-PCR is the most commonly used test to determine COVID-19 disease. It is mainly used to quickly diagnose patients who have developed symptoms of the disease, or to screen asymptomatic patients. It works on the principle of highly sensitive technology that detects the presence of genetic material of the virus in a sample. A sample for analysis is taken with a swab of the nasal or nasopharyngeal area (33).

Once the sample is taken for analysis, it is treated with several chemical solutions to extract the RNA and remove other substances such as proteins and fats. The RNA extracted in this way is a mixture of the patient's genetic material and the RNA of the virus, if present (33). In the next step, RNA is converted into DNA through a reverse transcription process with the help of enzymes. Then, the mixture with DNA is placed in an RT-PRC machine that works on the principle of heating and cooling the mixture in order to initiate chemical processes that create copies of certain parts of the viral DNA (33). In addition to the process of creating copies of viral DNA, marker tags are attached to the new parts, which release a fluorescent dye. The computer measures the release of fluorescent dye and displays the result on the screen (33).

The result is positive, i.e. the presence of the virus is confirmed, when the fluorescence level exceeds a certain measure (33). Scientists also track how many cycles of viral DNA copy formation it took for fluorescence to occur, as this is how they determine the severity of the disease and how advanced it is. The fewer cycles it takes, the more severe the disease is (33).

This test is accurate in most cases, but false negative and false positive results can also occur. This is due to sampling at different times from the onset of symptoms. Ideally, the patient should be tested on the third or fourth day after the onset of the first symptoms (33).

Computed tomography (CT) of the thorax

CT is a layering imaging technique that uses a collimated X-ray beam directed perpendicular to the longitudinal axis of the body resulting in an axial cross-section of the selected layer thickness. The image is obtained in such a way that the detectors measure the intensity of attenuated radiation after passing through the body. Due to its high sensitivity, this radiological method is used to confirm the presence of COVID-19 disease and determine the stage of advancement (3).

The chosen protocol for imaging a patient suspected of having COVID-19 disease is the standard protocol for imaging the thorax, but it can also be recorded using a high-resolution protocol (HRCT) (34). The topogram determines the field of view, usually from the apex of the lungs

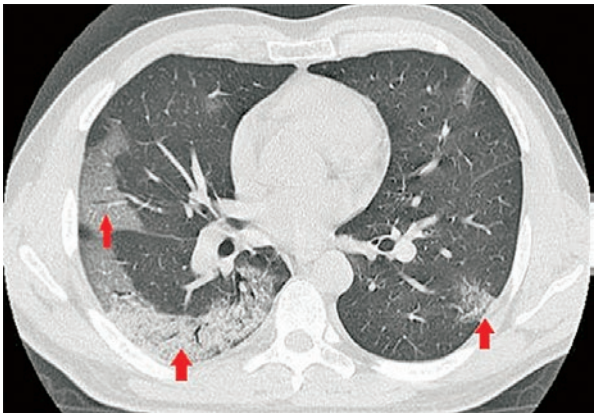


Figure 2. Chest CT in a patient with COVID-19 pneumonia on the third day of illness. Visible peripherally located ground glass opacifications (red arrows).
Archive of the University Hospital for Infectious Diseases „ Dr. Fran Mihaljević" Zagreb

to the base of the lungs, without including the adrenal glands. The use of a contrast agent is not necessary for this examination because COVID-19 pneumonia is mainly localized in the lungs and does not spread to the pleura and mediastinum. It is desirable that the imaging is done when the patient takes a deep breath in order to have a better view of the lungs. However, given that COVID-19 is a lung disease that causes coughing and breathing difficulties, it is necessary for the imaging protocol to last as short as possible to avoid artefacts. Therefore, single-phase CT imaging is suggested – with a faster case rotation time (0.5 s or less) and a higher value *pitch* (more than 1:1) (34).

Radiomorphological signs of COVID-19 disease that are presented on CT scans are consolidations, air bronchogram, ground-glass opacities (GGO), crazy-paving, reverse halo sign and perilobular pattern (3). Observing these radiomorphological signs, it can be roughly concluded at what stage of development the disease is.

In the early stage, which lasts from the onset of the disease to four days, GGO can be seen on CT scans (Figure 2). The next, progressive phase, which lasts five to eight days, is presented on CT scans by opacification of crazy paving, GGO and minor consolidations. The peak phase lasts for nine to thirteen days, which is manifested on CT scans by consolidations of the lung parenchyma surrounded by a halo or GGO sign (Figure 3). The last or absorption phase occurs after the fourteenth day of the disease when the lung parenchyma begins to recover, which is seen on CT scans as GGO and linear consolidation (35).

The most common sign of COVID-19 pneumonia are multifocal GGO that are located bilaterally. The lesions are most often located in the basal, peripheral and posterior parts of the lungs. The signs of COVID-19 that are presented on CT scans can be quite similar to the signs of other viral pneumonia. What distinguishes COVID-19 from some viral pneumonia (e.g., caused by adenovirus or influenza virus) is the peripheral localization of the lesions, the permeation of all five lung lobes, and the presence of narrow reticulations and peribronchovascular thickenings (36).

It is also possible that COVID-19 pneumonia is atypically presented on CT scans, in which case pseudonodular consolidations can be seen on the scans, and an inverted

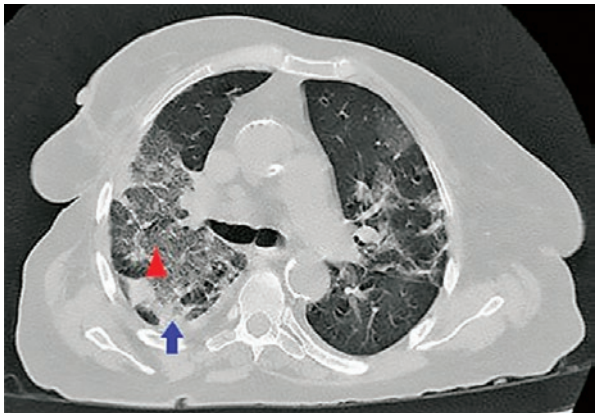


Figure 3. Chest CT in a patient with COVID-19 pneumonia on the tenth day of illness. Ground glass opacifications (red triangle) and peripheral consolidations are visible in the lung parenchyma of the right lung (blue arrow). *Archive* of the University Hospital for Infectious Diseases „ Dr. Fran Mihaljević“ Zagreb

halo sign. If the disease is in its early stages, i.e. there is no involvement of both lungs, signs may be visible only unilaterally (usually for the first four days from the onset of symptoms). The localization of pathological patterns in the pulmonary tips or peribronchovascular can also be highlighted (37).

Artificial intelligence (AI)

AI is a field of science that is classified as a branch of computer science that aims to imitate human behavior by copying human thinking and intelligence and thus solving complex tasks (38). This domain of computer science builds systems that have the ability to receive, analyze, and respond to various stimuli that are presented to them in the form of data. Based on the data entered, the program based on AI technology can learn from the given data and act independently. The two main tools by which an AI-based program can update its database are machine learning and deep learning (38).

Machine learning

In a similar way to humans, AI systems can learn from past experiences and thus improve. This is made possible by a concept of work called machine learning. Namely, machine learning is a domain of artificial intelligence that deals with the construction of algorithms by which a computer independently studies given databases and learns from them and builds experience (38). With this method, the computer studies the available database (usually a training database) and uses the given algorithms to analyse it and decide what the outcome might be. The accuracy of predictions and better performance of the computer itself are the result of training on databases as large as possible (38). This model is advantageous in industries that process large amounts of complex data, as it makes people's work easier and reduces the time required to process data (38).

Machine learning can be divided into three main categories depending on what kind of learning signal or response the computer received (38). The categories are supervised, unsupervised and reinforcement learning (38).

Supervised learning works in such a way that algorithms are trained using annotated data (38). This approach provides the system with a database that contains both a known input and output dataset, and the analysis trains the model for prediction. In this way, the algorithm compares its actual output with the given correct outputs and is thus actualized to achieve sufficiently good results. According to this way of learning, algorithms can be divided into two categories, regression and classification (38).

Unsupervised learning is a method in which a computer trains itself without a supervisor (38). The system is provided with a database that is not labelled or classified. The algorithm must independently analyse the data and determine the degree of similarity between them in order to be able to conclude and lead to an accurate output for a given problem. In this way of learning, algorithms can use two techniques, grouping and association (38).

Reinforcement learning is a learning method based on the feedback that an algorithm receives after solving a given problem (38). It works by analysing previous performances. For each correct result, the computer receives a reward, and for each incorrect result, it is punished. In this way, the algorithm is set the goal of collecting as many rewards as possible, and thus improving correctness (38).

The main advantage of this method is the ability to repeat the process until it finds the correct output and thus builds on its own. But on the other hand, the problem with the machine learning method is that training requires a heterogeneous database with a large number of data (38).

Algorithms that are upgraded and learned by the machine learning method have a wide range of applications, most often in medical diagnostics, photo processing, in the marketing and financial sectors, and many others.

Deep learning

Deep learning is categorized as a subgroup of machine learning that is more advanced than others because the system by which it works is similar to the human nervous system and tries to mimic the work of neurons (38). This model works based on the architecture of neural networks that are inspired by the human brain. Neural networks consist of numerous nodes that are located in hidden layers whose task is to connect the input and output layers (38). The number of hidden layers varies from network to network, and because of their number, which is usually large, it comes from the name deep learning (Figure 4). The "deeper" the network, i.e. the more hidden layers there are, the greater the possibility of better display and processing of data. The deep learning process begins with the computer understanding the given problem and identifying the data and selecting the correct algorithm, after which the training and testing of the model begins (38).

The advantage of this learning model is that it can learn without predefined data and does not require detailed programming like machine learning. The biggest challenge faced by this model is the collection of large amounts of data and their accurate classification (38).

AI has found application in medicine in various parts of the healthcare system, from data storage to aid in di-

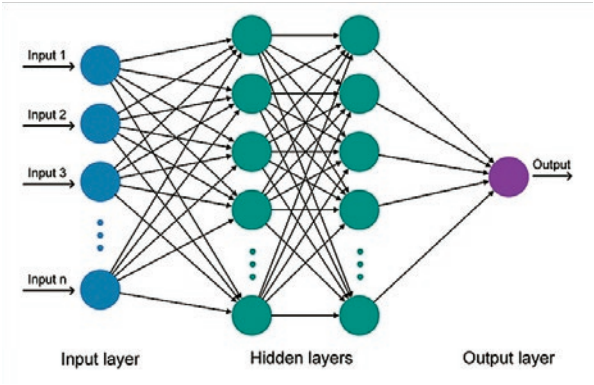


Figure 4. Structure of deep neural network
Source: https://www.researchgate.net/publication/352111703/figure/fig4/AS:1030797767237634@1622772747886/Schematic-diagram-of-an-Artificial-Neural-Network-ANN.png

agnosis. The branch of medicine that has always led the way in the digitalization of medicine has been radiology. Radiology is still one of the leading drivers in the introduction of AI into the healthcare system in order to work on accuracy and speed in diagnosis.

Every year, more and more radiological examinations are performed, which creates a high workload for radiologists. Regardless of the scope of knowledge and experience of the radiologist, with such a workload, inevitable errors can occur when diagnosing. Therefore, in order to help radiologists and reduce their workload, AI technology began to be introduced in radiology. The application of AI was particularly prominent during the COVID-19 pandemic, when the wide scope of work had already become extremely large (38).

Application of artificial intelligence in the diagnosis of COVID-19

With the onset of the COVID-19 pandemic, various new challenges for the healthcare system have emerged. There were difficulties with timely diagnosis due to the fact that the tests were sometimes unavailable and of lower quality, which would lead to false results. Also, due to the high speed of the spread of the disease, many people were infected at the same time, which resulted in delays in the processing of samples. Due to the very nature of the disease, it was necessary for COVID-19 to be accurately and quickly diagnosed.

In order to address the challenges brought by the COVID-19 pandemic, AI technology has begun to be implemented in the healthcare system. The benefit of AI has been particularly highlighted by its application in diagnostic radiology in the reading of radiological images such as CT scans and digital thoracic radiographs. In this way, the accuracy and speed of the time required to process the footage is increased. Studies have shown that today's AI models are very successful in diagnosing COVID-19, and that their accuracy in predicting the diagnosis is on par with radiologists and in some cases even more accurate (39).

Healthcare professionals use AI technology to analyse radiological images as quickly and accurately as possible and reach a diagnosis without the need for long-term analysis of images. Also, when reviewing a large number of images, radiologist fatigue can occur and subjectivity in interpreting the findings, which can result in errors in diagnosis (39).

In order to reduce the rate of diagnostic errors, deep learning models are used with the aim of developing tools for image analysis that work on the principle of automatism (Figure 5). These tools lead to more accurate results and diagnoses more quickly, and ultimately reduce the workload on radiologists. It is characteristic of deep learning models that by identifying individual structures and parts, they can learn from radiological images and thus upgrade the neural network and expand the database (40).

To build software for the diagnosis of COVID-19, in most cases, deep learning models were used that function by using the transfer learning method (40). This combination has achieved high precision and accuracy of the model in distinguishing COVID-19 from other lung diseases (40). Several classification algorithms have played an important role in classification in research related to the diagnosis of COVID-19 disease (40). Some of these are neural networks, vector support machines, random forest

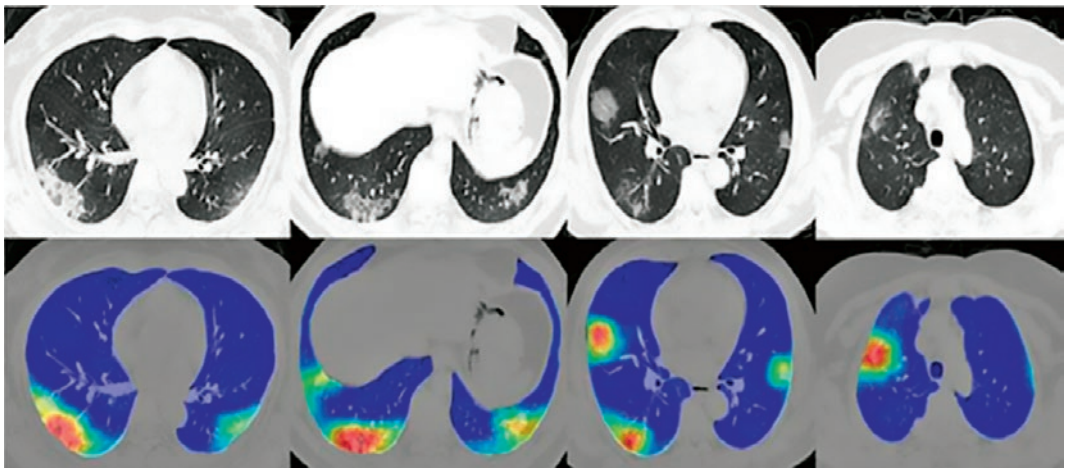


Figure 5. The top row shows unmarked CT scans of a patient with COVID-19 pneumonia, and the bottom row shows "heat maps" with marked characteristic lesions for COVID-19 pneumonia marked by an artificial intelligence algorithm.
Archive of the University Hospital for Infectious Diseases „ Dr. Fran Mihaljević" Zagreb

algorithm, and decision trees (40). These algorithms have shown high performance in performing tasks, but they still need to be optimized (40).

Radiological signs of COVID-19 infection on computed tomography and scanning protocols

The authors of all analysed papers, both review and original, listed in Tables 1 and 2, are unique in the use and classification of radiological signs that occur on CT scans in patients with COVID-19 pneumonia. In the acute phase, ground-glass opacifications (GGO), consolidation of the lung parenchyma, or combinations occur most often (7). The terminology is standardized and defined according to the Fleischner Society glossary of terms (36).

Of the 9 original scientific papers (Table 2), only three groups of authors provided a detailed protocol for scanning patients (19, 22, 23). These protocols were performed on 64 or 128-layer CTs, in the inspiratory phase, without the use of an intravenous contrast agent, during a single breath hold. The thickness of the layers ranged from 0.5 to 2 mm, and the fixed pipe voltage was set at 120 kVp with automatic tube modulation. From the raw data, CT images were reconstructed with a 512x512 matrix in axial cross-section, with iterative reconstruction. The data was then archived in a Picture Archiving and Communications System (PACS) and transferred to interfaces for different algorithms for the use of AI tools.

The authors of the other analysed scientific papers from Table 2 (17, 18, 20, 21, 24, 25) did not precisely specify the scanning protocols. Some used globally publicly available databases that they named and defined. For example, Nguyen et al. used three databases: 1) China Consortium of Chest CT Image Investigation (CC – CCII) Dataset (China), 2) COVID – CTset (Iran) and 3) MosMedDat (Russia) (25). Other authors did not specify the names of the databases, but only stated that they were publicly available databases (19) or data collected within their hospitals (20).

The fact that different databases of imaging data and unknown or uneven scanning protocols are used in different studies points to one of the major problems in the development and integration of AI in the process of analysing CT scans in COVID-19 patients, and that is the lack of data standardization. Therefore, the comparison of results is difficult.

Training the algorithm on high-quality data that is representative of the target population, with external validation, provides the best estimate of model performance (26).

In order to collect high-quality imaging data, researchers must be familiar with local guidelines related to the use and distribution of patient data, and protocols for anonymizing and securely storing data in PACS are also crucial. Getting large amounts of CT scans with quality images and labelled lesions that have been tagged by experienced thoracic radiologists is difficult, especially when dealing with small databases. There are discrepancies between research standards in medicine and machine learning. Researchers in the field of machine learning should be familiar with standard regulations for evaluating model features. On the other hand, medical standards must be updated to support deep learning rules.

Significance of the application of artificial intelligence tools in COVID-19 pneumonia in computed tomography of the thorax

During the COVID-19 pandemic, numerous studies have proven that CT is the primary imaging modality and the "gold standard" in patients with suspected infection (9, 21, 23). CT scans have significantly better spatial resolution compared to X-rays and show the distribution of opacifications and their forms in more detail. High spatial resolution in three-dimensional representation is particularly important, which allows for precise quantification of opacifications (9). Given the large number of patients faced by hospitals around the world during the pandemic, the limited number of radiologists, and the time that could be devoted to readings, AI experts put a lot of effort into developing tools and implementing them to automate the diagnostic process and speed up the reporting process, which would be equivalent in quality and reliability to the findings of an experienced radiologist.

The Radiologic Society of North America (RSNA) and the Imaging COVID-19 AI Initiative in Europe have made public access to databases of imaging materials, in order to enable the training of deep learning tools on proven cases (7). If there is not enough image data, the models cannot be generalized enough. In order to eliminate this shortcoming, the data augmentation method has been introduced, which is effective in training discriminatory deep learning models (3). Examples of data augmentation techniques include rotation, color fluctuation, random cropping, elastic distortions, and Generative Adverse Networks (GAN) for synthetic data generation (3, 41). They consist of two networks that conflict with each other. The first is called a generator, and the second is called a discriminator. Traditional augmentation methods that make simple image changes are less effective than advanced ones (3). In overcoming data gaps, GAN is used to develop effective data augmentation strategies for image recognition (3). This refers to complex and specialised algorithms and deep learning systems that produce dynamic image data according to predictions and data transformation from one system to another (7).

Part of the review and original studies listed in Tables 1 and 2 showed high accuracy of deep learning methods in the analysis of CT scans in patients with COVID-19 pneumonia (8, 12, 18, 19, 20). Most of these studies divided the dataset into 70–80% for training and 30–20% for testing, while other studies divided the dataset into 50% for training and 50% for testing (14). A study that divided the dataset into 40% for training and 60% for testing achieved high sensitivity and the best results (14).

Ortiz and colleagues developed two ways to automatically extract clinically relevant features from CT of the thorax within limited data and combined these features with demographic data to develop a prognosis model for COVID–19 outcomes. With the help of MIP reconstructions (Maximum Intensity Projection) they created 3D CT volume maps, which can be used in a COVID-19 diagnostic model without the need for lesion segmentation.

The model then identified four lung lesions specific to COVID-19 infection and calculated the location and extent of each type of lesion. This approach has made it possible to identify 3D pathological imaging data that can be combined with other clinical data. In this way, the authors created a predictive approach that analysed the most relevant CT findings—combined with demographic data to accurately predict outcomes compared to models based only on intensity mapping or segmented features (42).

Advantages and limitations of using deep learning tools

Datasets

To implement convolutional neural networks, it is necessary to introduce a dataset and the necessary libraries, prepare the data, build a CNN, train it, and get the final prediction. The advantage of large, publicly available databases is the possibility that they can be used by numerous researchers indefinitely in creating and testing deep learning tools. However, it is necessary to take into account that most datasets have a limited number of clinical cases of COVID-19 infection. Before data can be analysed with a deep learning tool, most of the available datasets require "pre-processing," such as resizing, matching image formats, and segmenting the lung parenchyma image from other body parts (18). Due to problems with "unclean" raw data, such as repetitive and unsegmented lung images, selecting the best image for a model is often very challenging (18).

The ability to 'refine' datasets allows repetitive images to be removed from datasets (18). In this way, it is ensured that there are no repeating images before the dataset is handed over to the model. Repetitive images will generate inaccurate results if they appear in datasets that are used for both training and testing. The test set must not "see" the data beforehand, in order to test the effectiveness of the model (18). By dividing the data into three categories of sets: training, test and validation based on patient demographics, it prevents the same patient from appearing in two sets (18).

Segmentation method

Lung segmentation is the separation of images of parts of the lungs from other parts of the chest. This initial step is required for the analysis of CT scans of the lungs and plays a key role in the performance of the classification model (7). "Raw" CT scans contain noise and vary, depending on the types of devices and variations in the constitution of patients. Segmentation also resolves the heterogeneity of data among different subsets of data, if combined into a single set. Segmentation allows the model to focus on the characteristic COVID-19 opacification of the input image. The most common and widely accepted method is to mark the boundaries of the lungs that separate them from the surrounding organs, using special tools (10).

The segmentation results are annotated and the results are controlled by at least two experienced thoracic radiologists. Compared to radiologist opacification annotations, segmentation networks achieve better results in terms of obtaining high accuracy and sharper and clearer lesion separation boundaries (10).

Pre-Trained Deep Learning Models

Pre-trained deep learning models have shown promising results in solving many problems in various research areas, such as computer vision, pattern recognition, natural language processing, and medical image classification. The superior capabilities of pre-trained networks stem from their extensive training on large datasets. To improve the diagnostic capabilities of the COVID–19 classification model, some researchers performed pre–training using an external dataset of CT scans on a large public dataset (26). Many models of convolutional neural networks have been trained on the ImageNet dataset.

Distinguishing COVID-19 from other viral pneumonias

Opacifications that occur on CT scan in patients with COVID-19 pneumonia are similar to various forms of pneumonia caused by other viruses, such as influenza, adenovirus, syncytial respiratory virus, etc. Therefore, distinguishing COVID-19 from other viral pneumonias is a key challenge in multiclass classification studies compared to binary classification studies. A multiclass classification model is used to differentiate normal lung findings from COVID-19 pneumonia and pneumonia from the general population (26).

Advantages and limitations of using machine learning tools

The machine learning process in the detection of COVID-19 pneumonia on CT scans of the lungs consists of data collection, data preparation, model selection, model training, evaluation, parameter adjustment, and prediction or inference (26).

CapsNet is a machine learning system that represents a type of artificial neural network that can be used to better model hierarchical relationships (7). It mimics a biological neural organization. "Capsules" are added to the convolutional neural network and then the output from several "capsules" is used to form more stable representations (7).

Using CapsNet is one of the practical solutions for limited COVID-19 data sets, as it can handle small data sets. Alaufi et al. used CapsNet without applying any methods to augment the datasets or pre-train the model (26). They achieved 95.7% accuracy, 95.8% specificity, 90% sensitivity and 97% AUC (26). They modified the loss function to highlight the problem of unbalanced classes due to the lack of available images of COVID-19.

Guidelines for further research on AI tools

Advanced AI algorithms still need to be developed, especially for detection, segmentation and classification of lesions in the diagnosis of COVID-19 pneumonia by CT. Our analysis of original and review scientific papers listed in Tables 1 and 2 has highlighted the following guidelines for further research of artificial intelligence tools in the analysis of CT thorax images in patients with COVID-19 pneumonia.

Anwar et al. who used the deep learning algorithm (EfficientNet) on a set of 253 CT scans of patients with COVID-19 pneumonia and 291 scans of patients who did not have COVID-19 pneumonia, believe that its further development will be achieved by testing the model on a different dataset, since they did not use a separate validation dataset in this study (21).

Alaufi et al. believe that binary classification has reached high performance, but it is necessary to improve the model of multiclass classification of CT scans in COVID-19 pneumonia by creating high-performance matrices (26). Deep learning models can be applied in the categorization of different stages of COVID-19 infection, such as pre-symptomatic, asymptomatic, mild and severe (26).

Chamberlain et al. who tested the deep convolutional network (dCNN) algorithm in the categorization of CT opacifications in patients with COVID-19 pneumonia and used a scoring system based on the expert assessment of three thoracic radiologists as the gold standard, believe that future research must focus more on the outcomes of multivariate predictive analysis than on reconciliation among radiologists (22).

Gunray et al. used amplified deep neural networks to detect COVID-19 pneumonia in two different, large international cohorts of 4500 subjects from 16 countries (24). They concluded that future research should focus on the use of pre-trained networks for tasks such as predicting lung function, assessing the severity of the disease, and creating personalized treatments for patients with COVID-19 pneumonia (24).

In the research of Pan et al., the evaluation of new deep learning methods for quantifying COVID-19 and pacification showed a good correlation with conventional CT scoring (36). They believe that in the future, the quantification of opacification based on deep learning methods in the assessment of the severity of COVID-19 pneumonia will be applicable to other forms of viral pneumonia (36).

Turk et al. evaluated four different deep learning algorithm architectures using a publicly available database on a total of 360 images of COVID-positive patients, and found that the MobilNet algorithm had the highest accuracy (18). They believe that in order to develop deep learning algorithms in the future, much larger databases must be publicly available (18).

Vaidyanathan et al. demonstrated the excellent performance of the deep learning algorithm in distinguishing opacification in COVID-19 pneumonia from influenza pneumonia in external validation on a dataset from another healthcare institution (19). They believe that such an algorithm will be very useful in clinical practice in the near future and will be able to separate the relevant layers of CT scans that contain abnormalities and are important for the disease being investigated. Such a development requires more intensive collaboration between clinicians and computer scientists who specialise in AI (19).

Verma et al. tested a mobile application of an algorithm that has high precision (99.58%) and specificity (99.46%) in labeling opacifications in patients with COVID-19 pneumonia (41). They believe that the development of mobile applications will accelerate significantly, because they are more accessible to radiologists, especially in parts of the world with less developed health care, and will enable the assessment of disease severity, and thus adequate treatment in a much larger number of patients (41).

Yousefzadeh and colleagues concluded that in the future, AI algorithms that combine clinical information, laboratory findings including PCR and CT-based diagnosis will have the most accurate diagnosis of COVID-19 pneumonia (20).

Conclusion

AI is taking the leading role in almost every aspect of modern life today, so it is necessary to apply this technology for the best possible purposes. Its application in medicine, particularly in radiology, can greatly help and facilitate radiologists, especially in crisis situations such as the COVID-19 pandemic. The emergence of the pandemic has created an urgent need to develop AI models that would help detect COVID-19 pneumonia on CT scans.

Greater accuracy in detecting COVID-19 pneumonia has been demonstrated by deep learning models based on convolutional neural networks. These models are of significant importance for diagnosing and monitoring the progression of the disease and allow radiologists to detect infection more quickly. In addition to the advantages in the application of AI tools, there are also certain limitations. To develop a model, large databases are needed on which algorithms train. Due to the uneven size of publicly available databases, there are variations in the success of the model. Datasets can be in different formats, standards, and different qualities, making it difficult to compare results. Some research models were only experimental, and CT scans of critically ill patients with COVID-19 pneumonia were missing from the databases, due to the severity of the medical condition and the inability to transport due to connection to various devices necessary for life support.

By overcoming these limitations, AI tools can significantly improve in their precision, speed and clinical applicability in the near future and can be an excellent tool for the analysis of thoracic CT images in patients with COVID-19 infection and thus expedite and facilitate the work of radiologists.

Literature

1. World Health Organization. Coronavirus Disease (COVID-19) Pandemic [Internet]. World Health Organization. 2020 [cited 2025 Feb 2]. Available from: https://www.who.int/emergencies/diseases/novel-coronavirus-2019
2. Khanna VV, Chadaga K, Sampathila N, Prabhu S, Chadaga R, Umakanth S. Diagnosing COVID-19 using artificial intelligence: a comprehensive review. Netw Model Anal Health Inform Bioinforma. 2022;11:25. doi: 10.1007/s13721-022-00367-1
3. Ozsahin I, Sekeroglu B, Musa MS, Mustapha MT, Uzun Ozsahin D. Review on Diagnosis of COVID-19 from Chest CT Images Using Artificial Intelligence. Comput Math Methods Med. 2020;2020:9756518. doi: 10.1155/2020/9756518.
4. Wang Q, Ma J, Zhang L, Xie L. Diagnostic performance of corona virus disease 2019 chest computer tomography image recognition based on deep learning: systematic review and meta-analysis. Medicine (Baltimore). 2022;101(42):e31346.doi: 10.1097/MD.0000000000031346.

5. Harmon SA, Sanford TH, Xu S, Turkbey EB, Roth H, Xu Z, et al. Artificial intelligence for the detection of COVID-19 pneumonia on chest CT using multinational datasets. Nat Commun. 2020;11(1):4080. doi: 10.1038/s41467-020-17971-2.
6. Serena Low WC, Chuah JH, Tee CATH, Anis S, Shoaib MA, Faisal A, et al. An Overview of Deep Learning Techniques on Chest X-Ray and CT Scan Identification of COVID-19. Comput Math Methods Med. 2021;2021:5528144. doi: 10.1155/2021/5528144.
7. Fusco R, Grassi R, Granata V, Setola SV, Grassi F, Cozzi D, et al. Artificial Intelligence and COVID-19 Using Chest CT Scan and Chest X-ray Images: Machine Learning and Deep Learning Approaches for Diagnosis and Treatment. J Pers Med. 2021;11(10):993. doi: 10.3390/jpm11100993.
8. Alassiri R, Abukhodair F, Kalkatawi M, Khashoggi K, Alotaibi R. COVID-19 diagnosis from chest CT scan images using deep learning. Rom J Inf Tech Aut C. 2022;30;32(3):65-72. doi:10.33436/v32i3y202205.
9. Heidari A, Jafari Navimipour N, Unal M, Toumaj S. The COVID-19 epidemic analysis and diagnosis using deep learning: A systematic literature review and future directions. Comput Biol Med. 2022;141:105141. doi: 10.1016/j.compbiomed.2021.105141.
10. Roberts M, Driggs D, Thorpe M, Gilbey J, Yeung M, Ursprung S, et al. Common pitfalls and recommendations for using machine learning to detect and prognosticate for COVID-19 using chest radiographs and CT scans. Nat Mach Intell. 2021;3(3):199-217. doi: doi.org/10.1038/s42256-021-00307-0
11. Aggarwal P, Mishra NK, Fatimah B, Singh P, Gupta A, Joshi SD. COVID-19 image classification using deep learning: Advances, challenges and opportunities. Comput Biol Med. 2022;144:105350. doi:10.1016/j.compbiomed.2022.105350.
12. Komolafe TE, Cao Y, Nguchu BA, Monkam P, Olaniyi EO, Sun H, et al. Diagnostic Test Accuracy of Deep Learning Detection of COVID-19: A Systematic Review and Meta-Analysis. Acad Radiol. 2021;28(11):1507-1523. doi: 10.1016/j.acra.2021.08.008.
13. Alzubaidi M, Zubaydi HD, Bin-Salem AA, Abd-Alrazaq AA, Ahmed A, Househ M. Role of deep learning in early detection of COVID-19: Scoping review. Comput Methods Programs Biomed Update. 2021;1:100025. doi: 10.1016/j.cmpbup.2021.100025.
14. Wang Q, Ma J, Zhang L, Xie L. Diagnostic performance of corona virus disease 2019 chest computer tomography image recognition based on deep learning: Systematic review and meta-analysis. Medicine (Baltimore). 2022; 101(42):e31346. doi: 10.1097/MD.0000000000031346.
15. Kataoka Y, Tanabe N, Shirata M, Hamao N, Oi I, Maetani T, et al. Artificial intelligence-based analysis of the spatial distribution of abnormal computed tomography patterns in SARS-CoV-2 pneumonia: association with disease severity. Respir Res. 2024;25(1):24. doi: 10.1186/s12931-024-02673-w.
16. Bumm R, Zaffino P, Lasso A, Estépar RSJ, Pieper S, Wasserthal J, et al. Artificial intelligence (AI)-assisted chest computer tomography (CT) insights: a study on intensive care unit (ICU) admittance trends in 78 coronavirus disease 2019 (COVID-19) patients. J Thorac Dis. 2024;16(2):1009-1020. doi: 10.21037/jtd-23-1150.
17. Abdulsalam Hamwi W, Almustafa MM. Development and integration of VGG and dense transfer-learning systems supported with diverse lung images for discovery of the Coronavirus identity. Inform Med Unlocked. 2022;32:101004. doi: 10.1016/j.imu.2022.101004.
18. Turk V, Çatal Reis H, Kaya S. Automatic prediction of covid-19 from chest- computed tomography (CT) images using deep learning architectures. GUFBD. 2022; IOCENS'21 Konferansı Ek Sayısı: 76-88. doi: 10.17714/gumusfenbil.1002738
19. Vaidyanathan A, Guiot J, Zerka F, Belmans F, Van Peufflik I, Deprez L, et al. An externally validated fully automated deep learning algorithm to classify COVID-19 and other pneumonias on chest computed tomography. ERJ Open Res. 2022;8(2):00579-2021. doi: 10.1183/23120541.00579-2021.
20. Yousefzadeh M, Esfahanian P, Movahed SMS, Gorgin S, Rahmati D, Abedini A, et al. ai-corona: Radiologist-assistant deep learning framework for COVID-19 diagnosis in chest CT scans. PLoS One. 2021;16(5):e0250952. doi: 10.1371/journal.pone.0250952.
21. Anwar T, Zakir S. Deep learning based diagnosis of COVID-19 using chest CT-scan images. 2020 IEEE 23rd International Multitopic Conference (INMIC), Bahawalpur, Pakistan, 2020, pp. 1-5, doi: 10.1109/INMIC50486.2020.9318212.
22. Chamberlin JH, Aquino G, Schoepf UJ, Nance S, Godoy F, Carson L, et al. An Interpretable Chest CT Deep Learning Algorithm for Quantification of COVID-19 Lung Disease and Prediction of Inpatient Morbidity and Mortality. Acad Radiol. 2022;29(8):1178-1188. doi: 10.1016/j.acra.2022.03.023.
23. Chrzan R, Wojciechowska W, Terlecki M, Klocek M, Rajzer M, Popiela T. The role of artificial intelligence technology analysis of high-resolution computed tomography images in predicting the severity of COVID-19 pneumonia. Pol Arch Intern Med. 2022;132(12):16332. doi: 10.20452/pamw.16332.
24. Gunraj H, Sabri A, Koff D, Wong A. COVID-Net CT-2: Enhanced Deep Neural Networks for Detection of COVID-19 From Chest CT Images Through Bigger, More Diverse Learning. Front Med (Lausanne). 2022;8:729287. doi: 10.3389/fmed.2021.729287.
25. Nguyen D, Kay F, Tan J, Yan Y, Ng YS, Iyengar P, et al. Deep Learning-Based COVID-19 Pneumonia Classification Using Chest CT Images: Model Generalizability. Front Artif Intell. 2021;4:694875. doi: 10.3389/frai.2021.694875.
26. Alaufi R, Kalkatawi M, Abukhodair F. Challenges of deep learning diagnosis for COVID-19 from chest imaging. Multimed Tools Appl. 2024;83: 14337–14361. doi: 10.1007/s11042-023-16017-1
27. Bai Y, Ning K. How does severe acute respiratory syndrome coronavirus 2 (SARS-CoV-2) achieve immune evasion?: A narrative review. Medicine (Baltimore). 2024;103(16):e37780. doi: 10.1097/MD.0000000000037780.
28. Ndwandwe D, Wiysonge CS. COVID-19 vaccines. Curr Opin Immunol. 2021;71:111-116. doi: 10.1016/j.coi.2021.07.003.
29. Cha Y, Jung W, Seo M, Rahmati M. The emerging pandemic recent: SARS-CoV-2. Life Cycle. 2023;3:e2. doi: 10.54724/lc.2023.e2
30. Tsai PH, Lai WY, Lin YY, Luo YH, Lin YT, Chen HK. Clinical manifestation and disease progression in COVID-19 infection. J Chin Med Assoc. 2021;84(1):3-8. doi: 10.1097/JCMA.0000000000000463.
31. Keni R, Alexander A, Nayak PG, Mudgal J, Nandakumar K. COVID-19: Emergence, Spread, Possible Treatments, and Global Burden. Front Public Health. 2020;8:216. doi: 10.3389/fpubh.2020.00216.
32. Long C, Xu H, Shen Q, Zhang X, Fan B, Wang C, et al. Diagnosis of the Coronavirus disease (COVID-19): rRT-PCR or CT? Eur J Radiol. 2020;126:108961. doi:10.1016/j.ejrad.2020.108961.
33. Teymouri M, Mollazadeh S, Mortazavi H, Naderi Ghale-Noie Z, Keyvani V, Aghababaei F, et al. Recent advances and challenges of RT-PCR tests for the diagnosis of COVID-19. Pathol Res Pract. 2021;221:153443. doi: 10.1016/j.prp.2021.153443.
34. Kalra MK, Homayounieh F, Arru C, Holmberg O, Vassileva J. Chest CT practice and protocols for COVID-19 from radiation dose management perspective. Eur Radiol. 2020;30(12):6554-6560. doi: 10.1007/s00330-020-07034-x.
35. Vince A, Papić N, Židovec Lepej S, Kutleša M, Stemberger Marić L, Tešović G, Višković K. Molekularna biologija SARS – CoV – 2, patogeneza, klinička slika, liječenje i profilaksa bolesti. Zagreb: Medicinski fakultet Sveučilišta u Zagrebu; 2023.
36. Pan F, Ye T, Sun P, Gui S, Liang B, Li L, et al. Time Course of Lung Changes at Chest CT during Recovery from Coronavirus Disease 2019 (COVID-19). Radiology. 2020;295(3):715-721. doi: 10.1148/radiol.2020200370.
37. Jalaber C, Lapotre T, Morcet-Delattre T, Ribet F, Jouneau S, Lederlin M. Chest CT in COVID-19 pneumonia: A review of current knowledge. Diagn Interv Imaging. 2020;101(7-8):431-437. doi: 10.1016/j.diii.2020.06.001.
38. Ghosh M, Thirugnanam A. Introduction to Artificial Intelligence. Studies in Big Data. 2021;23-44. doi: 10.1007/978-981-16-0415-7_2
39. Albatoul A, Abdulrahman M, Sherin A, Thamer N, Bassam M, Salameh L, et al. COVID-19 detection and classification: key AI challenges and recommendations for the way forward. J Pulmonol Respir Res. 2023;7(1):10–14. doi: 10.29328/journal.jprr.1001044

40. El-Bouzaidi YEI, Abdoun O. Advances in Artificial Intelligence for Accurate and Timely Diagnosis of COVID-19: A Comprehensive Review of Medical Imaging Analysis. Scientific African. 2023;22:e01961. doi: 10.1016/j.sciaf.2023.e01961
41. Verma A, Amin SB, Naeem M, Saha M. Detecting COVID-19 from chest computed tomography scans using AI-driven android application. Comput Biol Med. 2022;143:105298. doi: 10.1016/j.compbiomed.2022.105298.
42. Ortiz A, Trivedi A, Desbiens J, Blazes M, Robinson C, Gupta S, et al. Effective deep learning approaches for predicting COVID-19 outcomes from chest computed tomography volumes. Sci Rep. 2022;12(1):1716. doi: 10.1038/s41598-022-05532-0.

Prednosti i ograničenja alata umjetne inteligencije u analizi slika torakalne kompjutorizirane tomografije u bolesnika s COVID-19 upalom pluća – pregled

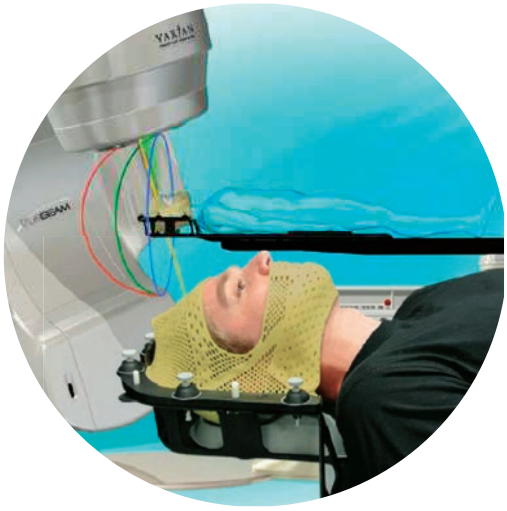
Sažetak

Bolest COVID-19 je sustavna virusna infekcija uzrokovana visokoinfektivnim virusom SARS-CoV-2, koja može dovesti do upale pluća i drugih komplikacija. Prvi put se pojavljuje krajem 2019. godine u Kini i brzo se širi svijetom, zbog čega je početkom 2020. godine proglašena pandemija. Ljudi zaraženi ovim virusom obično imaju simptome kao što su kašalj, groznica i otežano disanje. Ova respiratorna infekcija uzrokuje promjene u plućnom parenhimu koje se mogu analizirati na CT-u, stoga je CT postao jedan od najtočnijih dijagnostičkih metoda za potvrdu COVID-19 kod bolesnika, kao i alat za procjenu stadija razvoja infekcije. Budući da je identifikacija bolesti iz radioloških snimaka dugotrajna i složena, pojavila se ideja da se razviju modeli umjetne inteligencije (UI) kako bi se dobio brži i točniji rezultat. Najčešći modeli UI temeljili su se na dubokom učenju i strojnom učenju i uspjeli su ispravno identificirati COVID-19 na CT snimkama. Glavni problem koji se pojavljuje pri razvoju ovih modela je nedostatak baza podataka na kojima bi se ti modeli mogli trenirati. Ovaj pregledni rad analizirao je rezultate dvadeset i jednog rada na temu korištenja umjetne inteligencije u otkrivanju COVID-19 na CT snimkama. Rezultati analize pokazuju da je umjetna inteligencija visoko precizna i točna u otkrivanju COVID-19 pneumonije, ali ju je potrebno još dodatno razviti.

Encompass SRS Immobilization System

Highly rigid, non-invasive immobilization device designed for precisely targeted treatment to the brain, head & neck.

- Immobilization for treatment of multiple lesions with a single isocenter
- High-precision immobilization with submillimetric accuacy for stereotactic radiosurgery, including trigeminal neuralgia
- Integrated Shim System optimizes workflow efficiencies
- Open view thermoplastic can reduce patient anxiety and allows for intra-fraction positioning verification utilizing optical tracking systems
- Submillimetric immobilization with or without optional IntegraBite



Validated for HyperArc. Image is used courtesy from Varian, a Siemens Healthineers company.

Integrated Shim System

Innovative Integrated Shim allows independent height adjustment at each pin, providing completely customizable immobilization. Each Integrated Shim can be adjusted in discrete 0.5 mm increments, with a total range of 4 mm.

- Adjusting shim height is as easy as simply rotating the pin
- Eliminates the need for mask removal to adjust shim height
- Better workflow and instant setup feedback



2.0 mm



2.5 mm



3.0 mm

IntegraBite

- Decreased head and neck rotation, flexion, and extension
- Repeatable positioning
- Simple, streamlined design makes application and insertion easy





Encompass SRS Fibreplast Masks

Made from the most rigid thermoplastic material available, providing anterior and posterior cranial support.



Fibreplast Variable Perf Open View Mask



Posterior Thermoplastic

visionrt | COMPATIBLE

VIEW THE "BENEFITS OF USING ENCOMPASS SRS IMMOBILIZATION SYSTEM" VIDEO

medical intertrade

Web: www.medical-intertrade.hr
E-mail: medicinska-oprema@medical-intertrade.hr

CQ MEDICAL
Formerly CIVCO RT™ and Qfix®

REVIEW PAPER (PREGLEDNI RAD)

Radiological modalities in the detection, assessment and monitoring of COVID-19 infection

Nives Grepo[1,2], **Maja Marinović Guić**[2,3]

[1] Department of radiological and ultrasound diagnostics; University Hospital for Infectious diseases „Dr. Fran Mihaljevic", Zagreb, Croatia

[2] University Department of Health Studies, University of Split, Split, Croatia

[3] University Hospital of Split, Croatia

Corresponding author: Nives Grepo, email: nivesgrepo@gmail.com

DOI: https://doi.org/10.55378/rv.49.1.7

Summary

The COVID-19 pandemic, caused by the SARS-CoV-2 virus, posed a global health challenge that required rapid reorganization of healthcare systems and the implementation of strict protective measures. The gold standard for diagnosing COVID-19 is certainly the RT-PCR test, along with radiological methods that provide specific visual indications of the disease. The radiological presentation of COVID-19 includes chest radiographs used to evaluate lung changes, CT which offers a detailed view of abnormalities caused by the infection, PET/CT and LUS, which further assist in diagnosis and monitoring, and MRI used for a detailed assessment of complications and post-COVID syndrome. The complications of COVID-19 infection with the highest incidence are pulmonary, neurological, hematological, renal, and cardiac. During the pandemic, their severity and unpredictability became evident, as they further complicated the disease outcome and recovery. Post-COVID syndrome and MIS-C provide particular inspiration and motivation for new scientific research due to their characteristic clinical features.

Keywords: COVID-19; complications; infection; manifestations; radiology

Abbreviations and acronyms: ADEM (Acute Disseminated Encephalomyelitis), ARDS (Acute Respiratory Distress Syndrome), COVID-19 (Coronavirus Disease 2019), CT (Computed Tomography), FAST protocol (Focused, Fast Abbreviated Research Technique), GBS (Guillain-Barré Syndrome), GGO (Ground – Glass Opacity), LUS (Lung Ultrasound), MIS-C (Multisystem Inflammatory Syndrome in Children), MRI (Magnetic Resonance Imaging), PE (Pulmonary Embolism), PET (Positron Emission Tomography), RT-PCR (Reverse Transcription-Polymerase Chain Reaction), 18F-FDG (Fludeoxyglucose F18)

Introduction

The potential dangers of infectious diseases and the exhausting and demanding nature of fighting them, even in modern medicine, were clearly demonstrated during the SARS-CoV-2 pandemic. The history of this novel, previously unknown infectious disease, began in December 2019 in the city of Wuhan, China, when local authorities reported an increased number of cases of acute respiratory syndrome [1]. Given the high genomic similarity between the previously known SARS virus and the new coronavirus, the International Committee on Taxonomy of Viruses (ICTV) named the new virus SARS-CoV-2 (Severe Acute Respiratory Syndrome Coronavirus 2) [1]. Through human-to-human transmission, the virus unexpectedly spread rapidly to other continents, and the World Health Organization officially named the new infectious disease COVID-19 (Coronavirus Disease 2019). On March 11, 2020, the WHO declared the COVID-19 pandemic. The COVID-19 pandemic necessitated an urgent restructuring of healthcare systems worldwide, which faced numerous challenges and burdens, and the development of guidelines to combat the virus, with the aim of reducing the number of cases through responsible adherence to these guidelines.

Aim of the paper

The aim of this paper is to highlight the role and importance of radiology as a medical specialty in the diagnosis and treatment of COVID-19 infection. It also seeks to describe the specificities of the work of radiologic technologists with patients suffering from a previously unknown virus before 2019. Additionally, the paper aims to radiologically illustrate the most common manifestations and complications of COVID-19 disease.

Discussion

Radiological depiction of COVID-19 infection manifestations

The gold standard for diagnosing COVID-19 disease is the viral nucleic acid test, which is performed using reverse transcription polymerase chain reaction (RT-PCR). Alongside the PCR test, radiological methods are also used in the diagnosis of COVID-19, as they provide specific images that indicate the presence of disease.

Chest X-rays in the diagnostic imaging of COVID-19

The basic radiological diagnostic method for confirming and assessing COVID-19 disease is chest X-ray, with the most common abnormalities observed being consolidation and ground-glass opacity. Consolidation (Figure 1) refers to the occupation of air spaces, leading to the filling of alveolar spaces with pathological products such as water, pus, and blood in the lungs [2]. Ground-glass opacity (GGO, Figure 2) represents reduced lung parenchyma aeration while the vascular and bronchial markings remain preserved. GGOs are common in the early stages of infection and may potentially precede the appearance of consolidation [2].

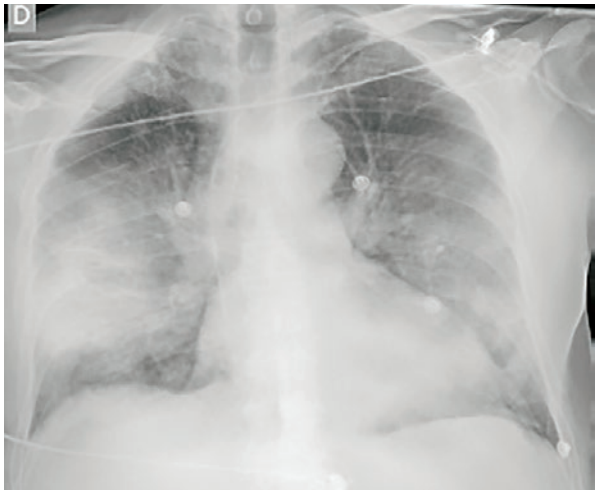


Figure 1. Bilateral ill-defined, patchy alveolar consolidation with peripheral distribution.
Source: https://pubmed.ncbi.nlm.nih.gov/34364071/

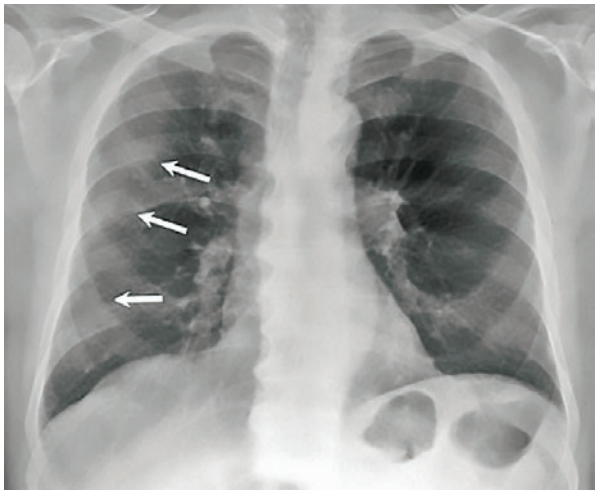


Figure 2. Patchy GGOs with peripheral distribution in the right lung.
Source: https://pubmed.ncbi.nlm.nih.gov/34364071/

Table 1. List of common radiological terms and their explanations used in computed tomography studies [4]

Term	Term explanation
ground-glass opacity - GGO	reduced transparency of lung parenchyma with preserved vascular and bronchial marks
„crazy paving“ opacity	thickening of intra and interlobular septa superimposed on GGO
consolidation	reduced pulmonary transparency which does not preserve vascular and bronchial marks
,,melting sugar sign“	GGO which increases on follow-up images, but decreased in attenuation, should not be interpreted as illness worsening
linear consolidation	thin consolidation situated parallel or perpendicular to pleura; seen in the late phase of organizing pneumonia
parenchymal bands	bands situated parallel or perpendicular to pleura; seen in the late phase of organizing pneumonia
perilobular opacification	opacification seen at the periphery of the secondary pulmonary lobule, may include interlobular septa, visceral pleura, lymphatics and vessels, often seen in any stadium of organizing pneumonia
reticulation	intra and inter-lobular septal thickening; mild form may be seen in the late phase of COVID-19 pneumonia
traction bronchiectasis	bronchal dilatation caused by surrounding fibrosis. The common findings in the late phase of COVID-19 pneumonia
honeycombing	indicative for the end-stage pulmonary fibrosis
bronchial distortion	A more appropriate term for description of the features of CO VID-19 pneumonia than traction bronchiectasis. In this case bronchial geometry is altered in some phase of the illness, but it does not necessarily mean irreversible changes. It may comprise temporary finding in the course of organizing pneumonia, with or without permanent sequelae. In the same way, it is recommended to use terms fissural distortion and blood vessel distortion before the confirmation of irreversible changes on follow-up MSCT scans in a longer time period.
fibrotic-like changes	Reticulation associated with bronchial dilatation and distortion in the areas of GGO and consolidation, may be present in the late phase of COVID-19 pneumonia. It comprises potential precursors of fibrosis, but with high probability of complete resolution in a longer time period (3-6 months or longer).
mosaic attenuation pattern	Abnormal hypodense areas consistent with the secondary pulmonary lobule which alternate with areas of normal parenchyma or GGO. It is described as a late feature of severe COVID-19 pneumonia. It is still unclear if it means residual illness of small airways or microvascular thrombosis.
organizing pneumonia	The pattern of organizing pneumonia on MSCT includes GGO, consolidation, reticulation, and parenchymal distortion.
post-COVID interstitial lung disease	residual pulmonary disease, usually 12 weeks after the onset of symptoms of COVED-19 pneumonia

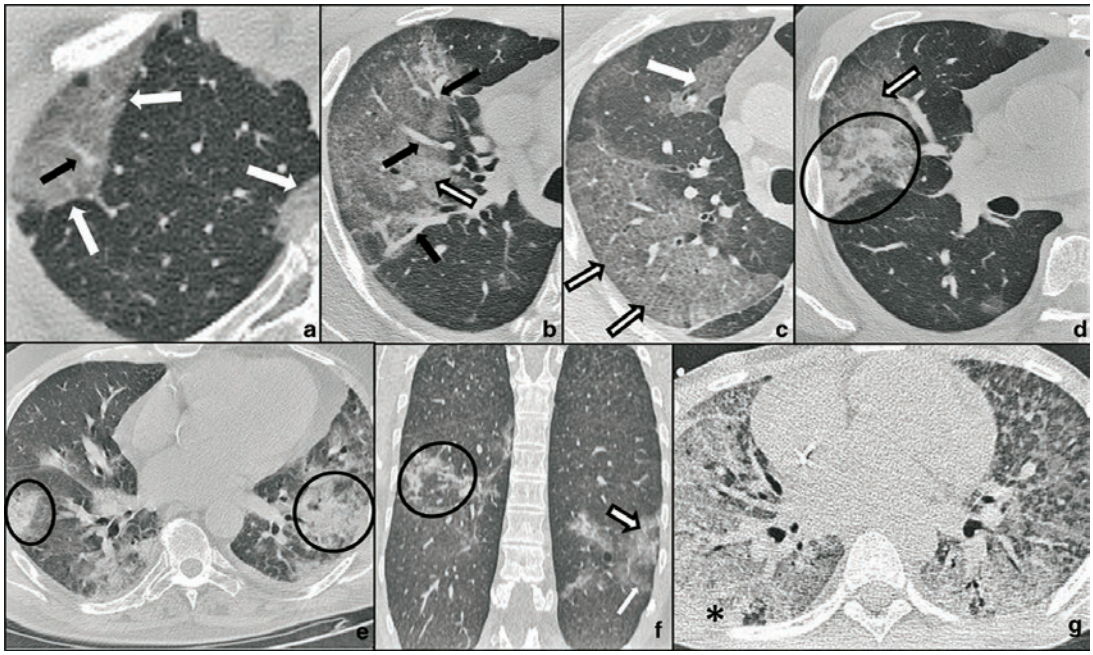


Figure 3. COVID-19 pneumonia phases: a) Stage 1; b,c,d) Stage 2; e) Stage 3; f) Stage 4; g) ARDS – representing a possible complication of COVID-19 pneumonia. Black arrows indicate the dilation of peripheral blood vessels, while white arrows indicate ground-glass opacities. The crazy paving pattern is shown with black-bordered white arrows. Black circles (d, e, f) represent dependent and non-dependent consolidations, while black asterisk in g denote dependent consolidations.
Source: https://doi.org/10.1186/s13244-021-00967-x

CT in the diagnostic imaging of COVID-19

The Fleischner Society has identified three main scenarios in which CT imaging can be the primary radiological diagnostic method: in patients with mild respiratory characteristics consistent with COVID-19 infection but with a significant risk of disease progression, or in patients with moderate to severe symptoms of infection, regardless of the PCR result, and in patients with moderate to severe symptoms in areas of high COVID-19 prevalence and reduced testing capacity [3]. Table 1 shows the most common radiological terms mentioned in MSCT examination reports [4].

Computed tomography has proven to be of exceptional importance in depicting and describing the four stages of COVID pneumonia:

- Stage 1 or early phase (0 – 4 days): opacities resembling “ground-glass” (Figure 3; a)
- Stage 2 or progressive phase (5 – 8 days): opacities with a crazy-paving pattern, GGO, and small consolidations (Figure 3; b, c, d)
- Stage 3 or peak phase (9 – 13 days): consolidations of the lung parenchyma, sometimes surrounded by a “halo” sign or GGO, followed by an atoll sign or reverse “halo” sign (Figure 3; e)
- Stage 4 or absorption phase (≥ 14 days): GGO and linear consolidations, which can be interpreted as a process of repair and reorganization [5] (Figure 3; f).

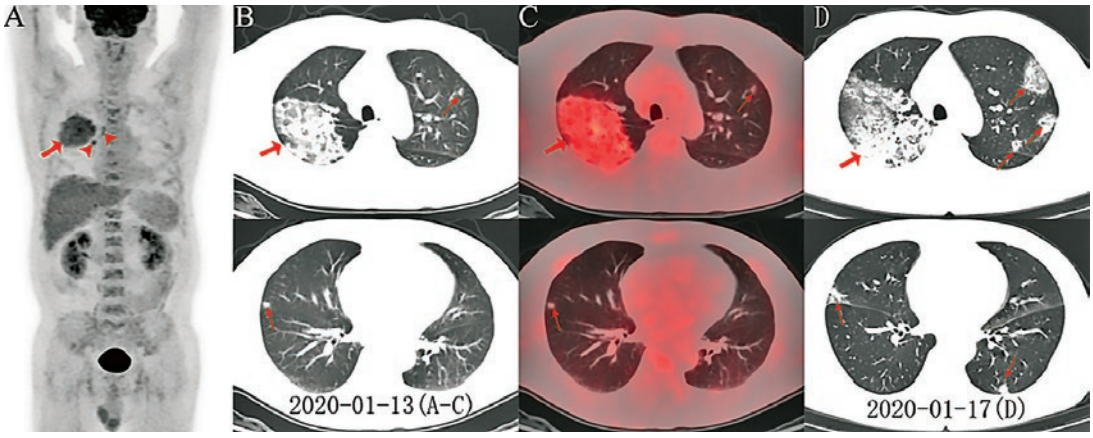


Figure 4. A) FDG PET/CT in a SARS-CoV-2 positive patient, B) Axial CT sections, C) PET/CT fusion showing opacities in the right upper and middle lobes and the left upper lobe, D) Follow-up CT scan showing progression of lesions.
Source: https://pubmed.ncbi.nlm.nih.gov/32142399/

PET/CT in the diagnostic imaging of COVID-19

Studies show that PET/CT is not routinely used in the diagnosis of COVID-19, particularly in emergency cases, but it certainly highlights a potential complementary role in the treatment of the disease. Since advanced disease can damage other organs, such as the kidneys, bone marrow, heart, and gastrointestinal tract 18F-FDG PET/CT can provide a non-invasive whole-body assessment to detect damage [6]. Zou and Zhu [7] observed radiopharmaceutical uptake in the right lung lobe, right hilar, and paratracheal lymph nodes (Figure 4). In the same study, they also discovered FDG accumulation in the bone marrow.

LUS in the diagnostic imaging of COVID-19

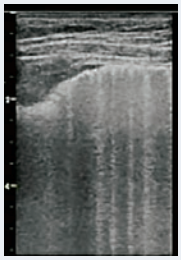
An alternative to standard diagnostic imaging for COVID-19 infection is another radiological method – lung ultrasound (LUS). LUS has proven to be particularly significant in children, pregnant women, and critically ill patients in intensive care units. An ultrasound image of healthy lungs shows the pleural line as a hyperechoic horizontal line (top of the green arrow in Figure 5;a) and multiple horizontal echoes of the pleural line, known as A-lines [8]. In severe interstitial pneumonia, the pleural line becomes irregular, and vertical echoes appear on LUS, indicating multiple blurred lines known as B-lines (Figure 5; b) [8].

One method for assessing lung involvement is a system that differentiates four stages of progressive loss of aeration. This system has shown high diagnostic value in patients with ARDS. Given this, it has been successfully applied to COVID-19 patients as well. The lungs are divided into 12 regions, each of which is examined via ultrasound, and the level of involvement is scored from 0 to 3. Examples of scores from 0 to 3 are shown in Table 2. The lung ultrasound result is then calculated by summing the scores for each region, with a higher total indicating reduced aeration [9].

MRI in the diagnostic imaging of COVID-19

MRI was not the first-choice method for imaging and confirming infection due to the duration of the examination and the challenges of implementing protective measures against potential transmission. However, it has proven to be highly important in imaging and monitoring complications of COVID-19 infection, post-COVID symptoms, and clinical research.

Table 2. LUS scores and representative ultrasound images [9]

Score	Aeration	Characteristics	Representative image
0	Normal	The pleural line is continuous and regular. Horizontal artefacts (A-lines), or two or fewer B-lines are present	
1	Moderate loss	The pleural line is indented. Below the indent, three or more well-spaced, non-confluent vertical artefacts (B-lines) are present	
2	Severe loss	The pleural line is broken. Below the breaking point, small-to-large consolidated areas (subpleural consolidations) appear, with associated areas of multiple confluent vertical artefacts (coalescent B-lines)	
3	Complete loss	The scanned area shows dense and largely extended white lung with tissue-like pattern (consolidation)	

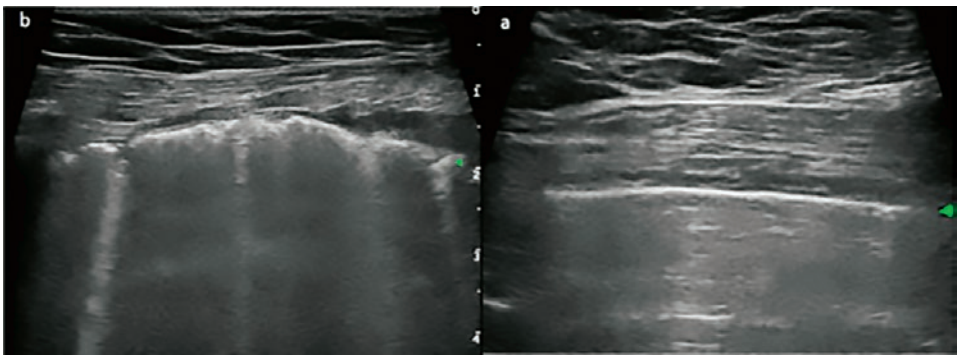


Figure 5. Ultrasound features of healthy lungs (a) and COVID-19 pneumonia (b).
Source: https://pmc.ncbi.nlm.nih.gov/articles/PMC7369598/

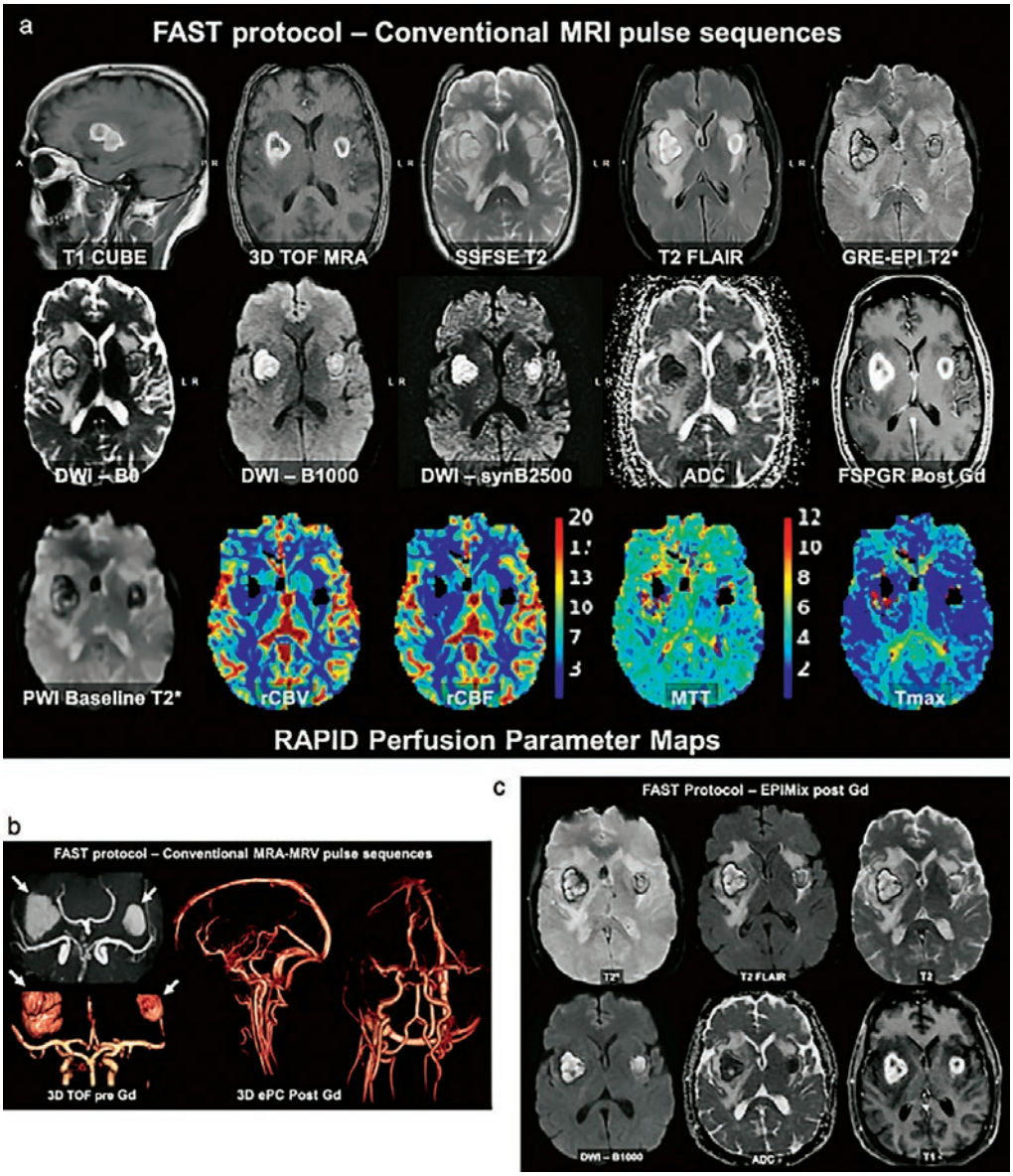


Figure 6. Focused, fast abbreviated survey technique (FAST) stroke protocol: a) By using parallel acceleration techniques, reduced matrices, compressed sensing, and other modifications, all images shown here required less than 15 minutes to acquire, and allowed complete characterization of lesions; b) 3D time-of-flight (TOF) MRA and 3D phase contrast MRA-MRV required 2 minutes, 10 seconds; c) using EPIMix, six high-quality tissue contrasts were acquired in just 75 seconds, with the procedure performed after gadolinium administration.
Source: https://onlinelibrary.wiley.com/doi/10.1002/jmri.28006

A challenge in successfully performing MRI exams was patients who were confirmed positive or suspected of being infected, as their symptoms, whether conscious or unconscious, interfered with the imaging process. It was particularly difficult to scan patients with dyspnea, frequent coughing, involuntary movements, or altered mental status in an MRI environment [10].

Whenever possible, radiologists and radiologic technologists considered the implementation of focused, rapid protocols during the pandemic to reduce the total scan time. An example of such a protocol in neuroradiology is shown in Figure 6. Using the FAST protocol (*Focused, Fast Abbreviated Research Technique*), subacute bilateral hemorrhages of the basal ganglia with surrounding vasogenic edema were observed, attributed to COVID-19 vasculopathy [10].

Most common complications of COVID-19 infection

Pulmonary complications

A well-known complication of COVID-19 infection is acute respiratory distress syndrome (ARDS). Figure 7 shows chest X-ray images of a 64-year-old male with COVID-19 ARDS, demonstrating the rapid progression of the disease [11].

The pathophysiology of ARDS involves damage to the alveolar epithelium, leading to increased permeability of the alveolar epithelial barrier, which causes the formation of a hyaline membrane, interstitial edema, and alveolar edema, resulting in severe hypoxia [12]. Therefore, patients with such complications are placed on non-invasive or invasive mechanical ventilation to improve oxygenation

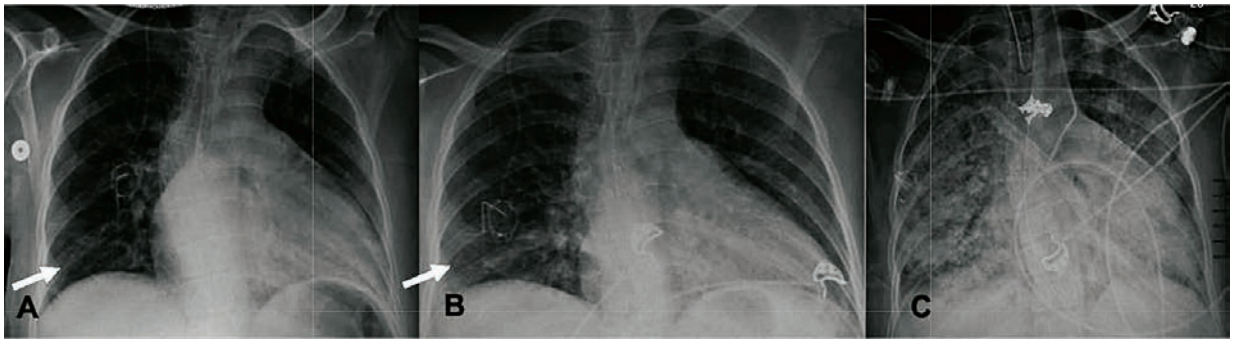


Figure 7. Serial frontal (AP) chest x-rays: A) initial chest x-ray with faint airspace opacities in the right lower lung, B) chest x-ray 2 days later shows increase in the airspace opacities, C) 4 days from the initial exam – rapid progression of bilateral airspace opacities.
Source: http://www.paom.pl/Pulmonary-complications-due-to-COVID-19-a-literature-review,136045,0,2.html

and maintain appropriate blood oxygen levels. Increased intra-alveolar pressure during mechanical ventilation can lead to alveolar rupture, resulting in barotrauma-related injuries such as pneumomediastinum and pneumothorax [12].

Neurological complications

Neurological damage due to COVID-19 infection can occur as a result of the direct effect of the virus or indirectly through the systemic response of the body to the infection [13]. The virus can cause damage to both the central and peripheral nervous systems, as well as muscle damage. The indirect systemic response to the infection is most commonly associated with a paraneoplastic autoimmune effect, known as the *"cytokine storm"*, which was observed in a significant number of patients in intensive care units during the COVID-19 pandemic. Clinical signs of the cytokine storm include elevated inflammatory markers (D-dimer, ferritin), fever, and increased pro-inflammatory cytokines (IL-6, TNF-alpha), which can lead to confusion and altered levels of consciousness [14].

Encephalitis is an inflammatory condition of the brain that has been described in many studies as a severe neurological complication of COVID-19 infection. Typical brain MRI findings in patients with encephalitis (Figure 8) showed diffuse hyperintensity in the white matter of the brain and hemorrhagic lesions on fluid-attenuated inversion recovery (FLAIR) and T2 sequences [15].

Acute Disseminated Encephalomyelitis (ADEM) represents an autoimmune inflammatory disorder of the central nervous system characterized by demyelinating lesions in the white matter of the brain and spinal cord [16]. In most cases, it occurs following an infection or vaccination, which is why it is referred to as post-infectious or post-vaccinal encephalomyelitis. The criteria for diagnosis are based on cerebrospinal fluid analysis and imaging findings from brain and spinal cord MRI (Figure 9).

Guillain-Barré Syndrome (GBS) is an autoimmune peripheral neuropathy whose main symptom is muscle weakness, ranging from slightly impaired gait to complete paralysis of all limbs, facial, bulbar, and respiratory musculature. Symptoms typically begin in the lower extremities and progress upward. Data from the international

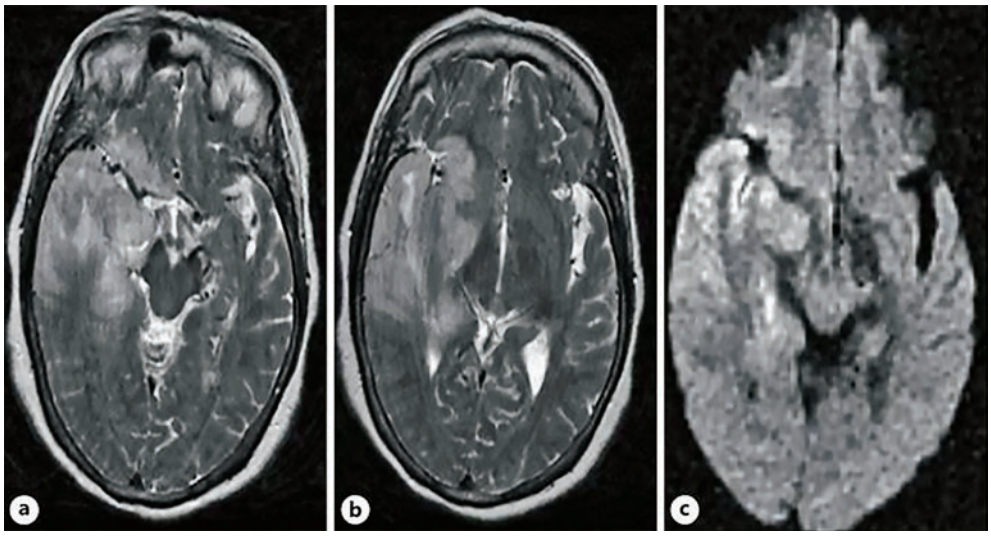


Figure 8. a,b) Axial T2WI shows gyral inflammation and hyperintensities involving the right temporal lobe, posterior aspect of the temporal lobe, and right basal ganglia with restriction of diffusion on the corresponding axial DWI image (c). There is a subtle mass effect on the brainstem with mild leftward midline shift.
Source: https://karger.com/crn/article/15/1/131/845250/Encephalitis-as-a-Clinical-Manifestation-of-COVID

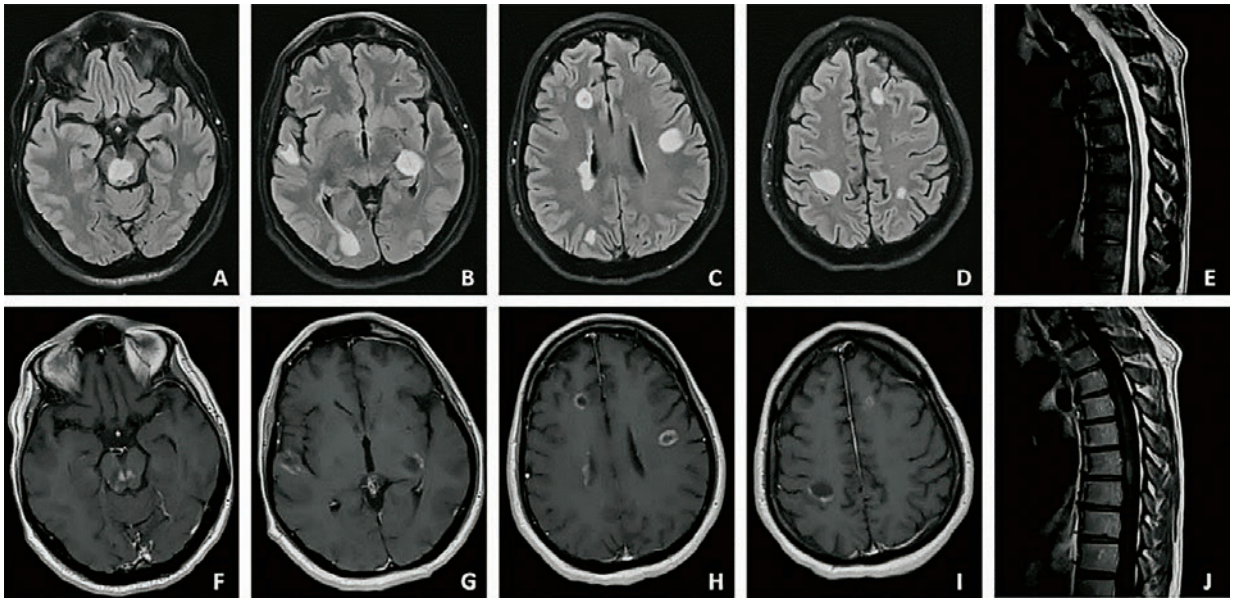


Figure 9. Brain and spinal cord MRI. Brain MRI showing supra- and infratentorial bilateral FLAIR-hyperintense white matter lesions suggestive of ADEM (A–D). In (E) spinal cord MRI documenting a T2-hyperintense dorsal lesion. After gadolinium administration, brain (F–I) and spinal cord (J) are characterized by incomplete contrast enhancement.
Source: https://link.springer.com/article/10.1007/s00415-021-10947-2

IGOS (International GBS Outcome Study) show that 73% of patients experienced sensorimotor symptoms, and 64% had facial nerve palsy [14]. It is believed that in some patients, GBS contributed to difficulties in weaning from mechanical ventilation [17].

In approximately 17.85% of patients who underwent neuroimaging, ischemic changes suggestive of stroke were identified [18]. Many studies confirm the high mortality rate in COVID-positive patients with ischemic stroke, as concluded by Sebastian Fredman and colleagues [19] in a systematic review, where a mortality rate of 45% was observed. The involvement of large blood vessels, particularly the middle cerebral artery (MCA), was most commonly reported. An example of radiological presentation of stroke in a 41-year-old male with COVID-19 infection is shown in Figure 10 [20].

Hematological complications

Changes in hematological parameters can be observed in 20 – 50% of hospitalized COVID-19 patients, who may subsequently develop thrombotic and hemorrhagic complications, more specifically venous and arterial thromboembolisms [21]. In the radiological evaluation of patients suspected of having pulmonary embolism (PE), the CT imaging protocol plays a crucial role, specifically CT pulmonary angiography (CTPA). The imaging protocol, which included the use of an automatic injector to administer 60 ml of contrast at a rate of 4 ml/s and the placement of a trigger to ensure accurate localization with a threshold of 100 HU, resulted in clear visualization of vascular filling defects, which is critical for diagnosing acute pulmonary embolism. Pontone et al. [22] in their study of the role of computed tomography in COVID-19 disease presented the clinical case of an 82-year-old man who presented to the emergency department with symptoms of severe

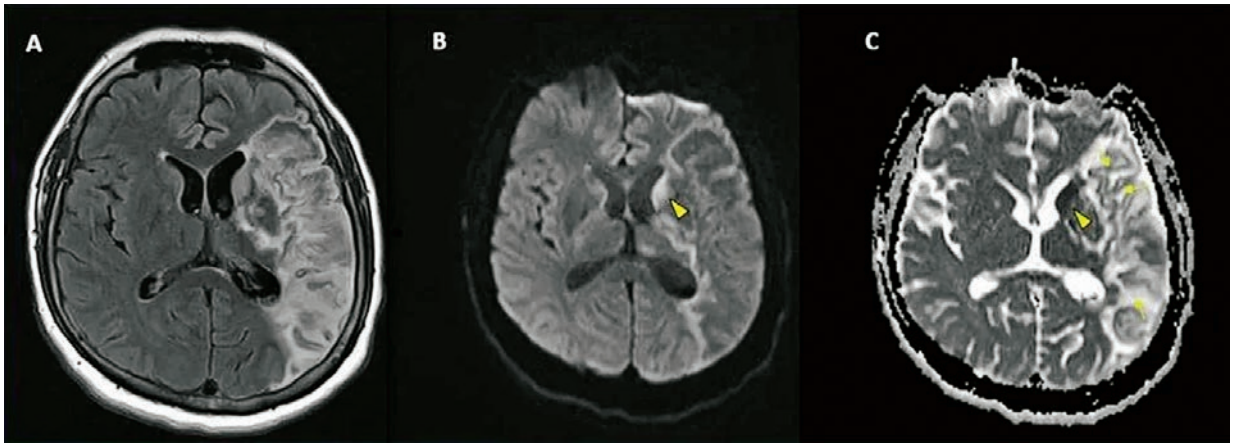


Figure 10. Stroke seen in a 41-year-old male patient with COVID-19 infection.
Source: https://www.itnonline.com/content/large-international-study-reveals-spectrum-covid-19-brain-complications

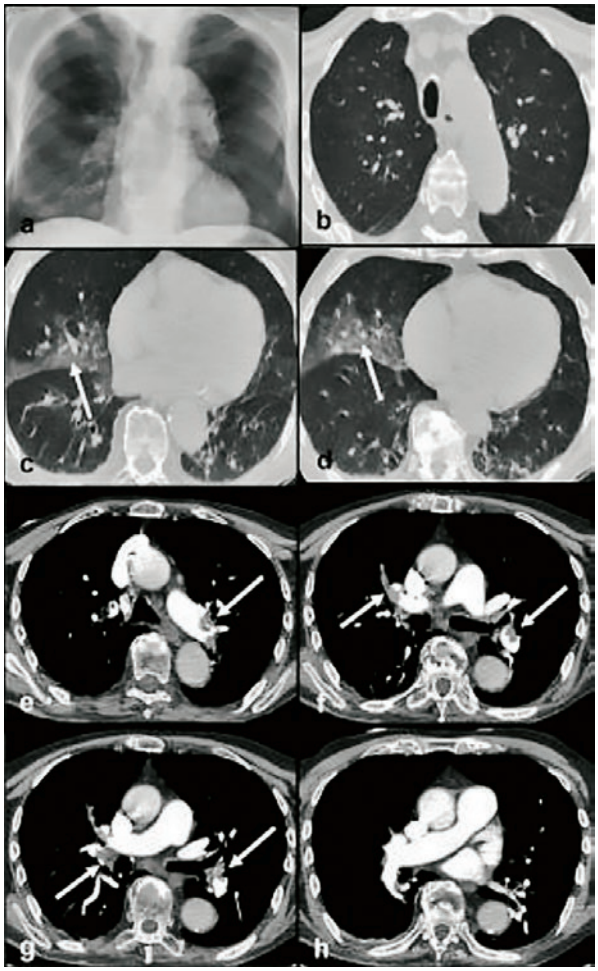


Figure 11. a- AP chest X-ray; b,c,d- axial, non-contrast CT sections show multiple GGO features in both lung fields; e,f,g,h CTPA confirms acute PE.
Source: https://pubmed.ncbi.nlm.nih.gov/32952101/

exertional dyspnea. Blood analysis revealed a significant elevation of D-dimer (7334 ng/ml). The AP chest X-ray showed consolidation in the lower zone of the right lung (Figure 11; a). A CT protocol was performed, consisting of an initial acquisition without contrast (native scan) to evaluate the lung parenchyma, followed by a second acquisition with contrast (contrast-enhanced scan) to assess the pulmonary vasculature (CTPA). Despite the presence of respiratory artifacts that negatively affected image quality, the native CT scan of the chest showed multiple ground-glass opacities (GGO) in both lung fields (Figure 11; b, c, d). The CTPA findings described multiple filling defects in the pulmonary arteries (Figure 11; e, f, g, h), which corresponded to acute PE [22].

Renal complications

The most common renal complications of COVID-19 infection manifest as glomerulonephritis, thrombotic microangiopathy, tubular injury, or interstitial nephritis [23]. Atelj et al. in their professional work described the condition of COVID-19 patients treated in the intensive care unit at the *University Hospital for Infectious Diseases „Dr. Fran Mihaljevic"* and presented data showing that the most frequent complications were shock (66%) and acute renal insufficiency (55%) [24]. The occurrence of renal insufficiency in COVID-19 patients is still not fully understood, and it has been linked to ACE2, the cellular receptor for SARS-CoV-2, which is expressed in both the respiratory epithelium and the kidneys [25]. In cases of renal infarction, ultrasound (US) and contrast-enhanced CT can reveal heterogeneity and hypoperfusion of the renal parenchyma, along with wedge-shaped areas of reduced perfusion (Figure 12) [26].

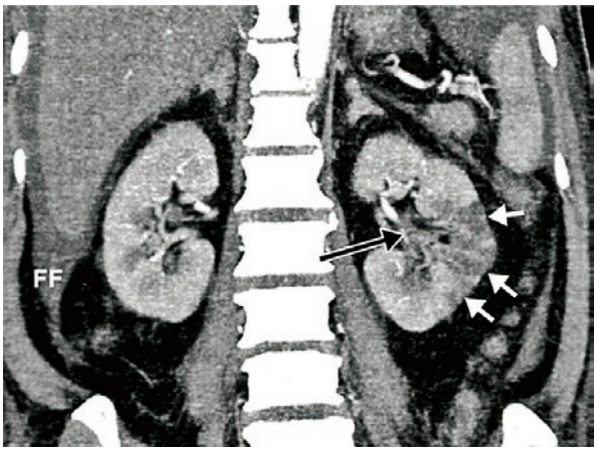


Figure 12. Renal infarction in a 57-year-old male with COVID-19; contrast-enhanced abdominal CT scan shows multiple linear hypoattenuating areas extending from the left renal sinus to the cortical surface (white arrows), with an occlusive thrombus in the segmental left renal artery (black arrow).
Source: https://pubs.rsna.org/doi/full/10.1148/rg.2020200195#fig21

Cardiac complications

The direct vascular effects of the SARS-CoV-2 virus are responsible for myocardial infarction and an increase in the number of sudden out-of-hospital deaths. In addition to myocardial infarction, other damage such as myopericarditis has also been observed. On CT, pericarditis is manifested by the presence of pericardial fluid, accompanied by ground-glass opacity (GGO) opacities characteristic of COVID-19 infection (Figure 13) [27]. An increased incidence of stress cardiomyopathy has also been reported, which is attributed to the indirect involvement of the virus, including the psychological, social, and economic stress associated with the COVID-19 pandemic.

Post-Acute COVID-19 Syndrome

During the ongoing pandemic, persistent symptoms emerged in a large number of patients, becoming characteristic of what is now referred to as "long COVID" (or post-acute COVID-19 syndrome). These symptoms significantly reduce the quality of life, persist for weeks, and can affect nearly every organ system. The most commonly reported symptoms include loss of taste and smell, chronic fatigue, memory and concentration impairments, muscle and joint pain, general weakness, night sweats, headaches, respiratory symptoms such as dyspnea, chest pain, and dry cough, as well as psychiatric issues like asthenia and fatigue.

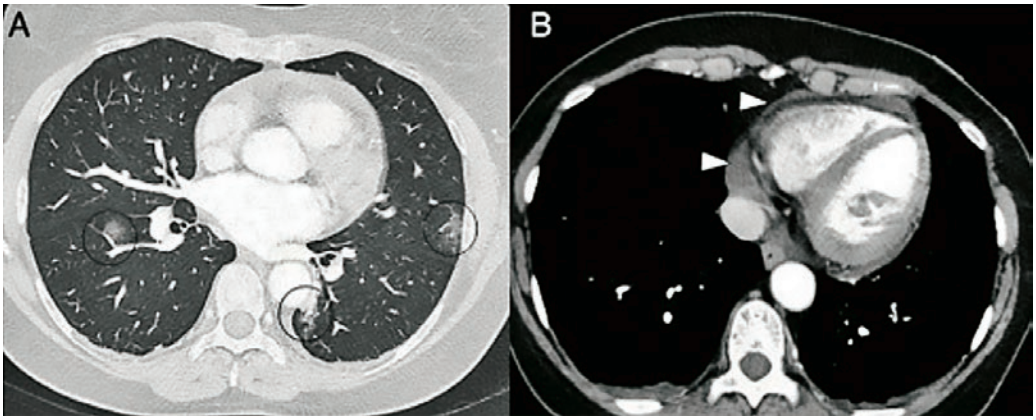


Figure 13. CT scan show GGO opacities (A) and pericardial effusion (tip of the arrows – B).
Source: https://pmc.ncbi.nlm.nih.gov/articles/PMC7687358/

The term "post-acute COVID-19 syndrome," which refers to the previously described condition, was coined by a patient in May 2020 and first used as a hashtag on the social media platform Twitter. On October 6, 2021, the World Health Organization (WHO) defined "Post-COVID condition" as: "a condition in individuals with a history of probable or confirmed SARS-CoV-2 infection, usually three months after the onset of COVID-19 symptoms, that lasts for at least two months and cannot be explained by an alternative diagnosis" [28]. Recent nomenclature categorizes all post-COVID changes into so-called post-acute sequelae, with subdivisions into short-term (one month post-infection), intermediate-term (2 – 3 months post-infection), and long-term (6 months post-disease onset) [29].

The risks for developing post-COVID syndrome are generally related to the severity of the acute illness, age (particularly over 50), and pre-existing comorbidities. In terms of gender differences, studies show that women are less likely to develop severe acute COVID-19 infection but are more likely to develop post-COVID syndrome compared to men. This is believed to be due to hormonal differences and, consequently, varying immune responses [30].

There is no strictly defined diagnostic protocol for post-COVID syndrome, as the diagnosis is based on a combination of clinical signs and symptoms. The greatest experience in detecting both acute and post-acute changes lies in the radiological evaluation of the lungs. Most patients fully recover from pulmonary involvement, while about 10% develop persistent symptoms. In some patients, cystic lung disease with pneumatocele formation develops (Figure 14). Such persistent symptoms mainly arise as a result of barotrauma during mechanical ventilation [31]. "Fibrosis-like changes" (Figure 14) are significant features of post-COVID syndrome, with predisposition factors including ARDS, non-invasive mechanical ventilation, prolonged hospitalization, extensive abnormalities on the initial CT scan, and age over 50 [32].

Complications of COVID-19 infection in children

In general, children tend to experience a milder form of COVID-19 infection that does not require hospitalization. This can be explained by the fact that children have a higher concentration of ACE2 receptors on pneumocytes, their mucosal immune response is generally more effec-

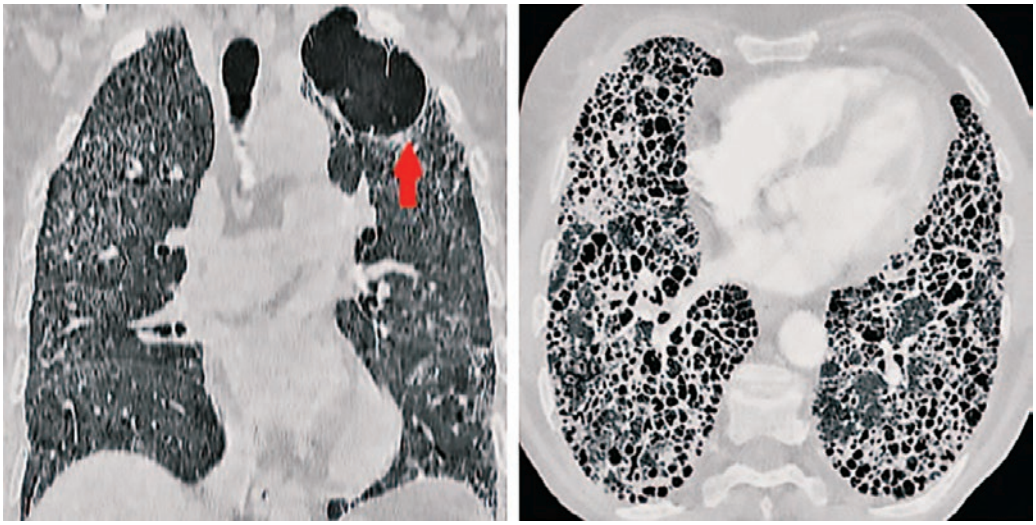


Figure 14. Pneumatocele (red arrow, upper left lobe), six weeks after the diagnosed SARS-CoV-2 infection (left); final stage of fibrosis "honeycombing" after 18 months following recovered COVID pneumonia (right).[29]

tive in preventing infection, and they exhibit a stronger innate antiviral immune response in the upper respiratory tract compared to adults. Hospitalization and admission to intensive care units are necessary for a small percentage of affected children (0.5 – 2%) [4]. Risk factors for developing potential complications of COVID-19 infection in children include neonatal age and comorbidities such as asthma, diabetes mellitus, and obesity.

Extrapulmonary complications are extremely rare, and when they occur, they are typically neurological symptoms such as seizures, Guillain-Barré syndrome (GBS), encephalopathy, or cardiac damage (arrhythmias, myocarditis) of varying severity. Although SARS-CoV-2 typically causes mild clinical symptoms in children, it has led to severe and concerning multisystem inflammatory syndrome in children (MIS-C) in some cases. MIS-C occurs three to six weeks after infection, even if the child was asymptomatic. The incidence of MIS-C is estimated at 1 in 3,000 children, with higher frequencies in children aged 9 to 11 years and in males [4]. The syndrome progresses over several days and involves multisystem involvement, clinically resembling Kawasaki disease. Key MIS-C symptoms include fever, rash, gastrointestinal symptoms, conjunctivitis, and the development of shock due to myocarditis complications. The mortality rate caused by COVID-19 in children is extremely low (0.005 – 0.1%), whereas MIS-C increases the mortality rate to 1.7 – 2% [4].

Conslusion

Radiology played a significant role in the fight against the virus, as its modalities were used for the diagnosis and monitoring of all health changes caused by the infection. Diagnostic modalities such as X-rays, LUS, CT and MRI were tasked with providing patients with timely and appropriate radiological assessment to ensure that potential complications of the disease were identified and treated in a timely manner. To achieve this goal, radiologists and radiologic technologists had to demonstrate a multidisciplinary approach and teamwork to provide the best quality imaging under unusual working conditions, as quickly as possible, while adhering to all protective measures to prevent potential exposure to infection. A special approach was required for patients in intensive care units, whose health status, from an infectious disease perspective, was often insufficiently clear even to modern medicine. Given that severe COVID-19 disease can lead to serious complications, most commonly neurological, treatment in these situations was further complicated by the poorly understood pathophysiological mechanisms of the virus. Published research on the manifestations and complications of COVID-19 highlights the need for further work on comprehensive studies with as much clear, evidence-based data as possible, in order to ensure future results are as precise as possible and to clarify the full range of impacts of the SARS-CoV-2 virus on the human body.

All data in this paper are part of the results from the master's thesis titled 'The role of radiology in the COVID-19 pandemic', written at the University Department of Health Studies, University of Split [33].

Literature:

1. Hrvatski zavod za javno zdravstvo: COVID-19 – Priopćenje prvog slučaja (mrežne stranice). Republika Hrvatska; 24 ožujka 2020. Available at: https://www.hzjz.hr/priopcenja-mediji/covid-19-priopcenje-prvog-slucaja/
2. Sadiq Z, Rana S, Mahfoud Z, Raoof A. Systematic review and meta-analysis of chest radiograph (CXR) findings in COVID-19. Clin Imaging. 2021 Dec;80:229-238. doi: 10.1016/j.clinimag.2021.06.039. Epub 2021 Jul 27. PMID: 34364071; PMCID: PMC8313779.
3. Pontone G., Scafuri S., Mancini M.E., Agalbato C., Guglielmo M., Baggiano A., Muscogiuri G., Fusini L., Andreini D., Mushtaq S., Conte E., Annoni A., Formenti A., Gennari A.G., Guaricci A.I., Rabbat M.R., Pompilio G., Pepi M., Rossi A., Role of computed tomography in COVID-19, Journal of Cardiovascular Computed Tomography, Volume 15, Issue 1, 2021, Pages 27-36, ISSN 1934-5925
4. Vince A., Papić N., Lepej Ž.S., Kutleša M., Stemberger M.L., Tešović G., Višković K. Molekularna biologija SARS-COV-2, patogeneza, klinička slika, liječenje i profilaksa bolesti, Zagreb: Sveučilište u Zagrebu, Medicinski fakultet; 2022./2023.
5. Guarnera, A., Podda, P., Santini, E. *et al.* Differential diagnoses of COVID-19 pneumonia: the current challenge for the radiologist—a pictorial essay. *Insights Imaging* 12, 34 (2021). Available at: https://doi.org/10.1186/s13244-021-00967-x
6. Capitanio S, Nordin AJ, Noraini AR, Rossetti C. PET/CT in nononcological lung diseases: current applications and future perspectives. Eur Respir Rev 2016 Sep 31;25(141):247-258
7. Zou S, Zhu X. FDG PET/CT of COVID-19. Radiology 2020 Aug;296(2):E118-E118
8. Allinovi M., Parise A., Giacalone M., Amerio A., Delsante M., Odone A., Franci A., Gigliotti F.., Amadasi S., Delmonte D., Parri N., Mangia A., Lung Ultrasound May Support Diagnosis and Monitoring of COVID-19 Pneumonia, Ultrasound in Medicine & Biology, Volume 46, Issue 11, 2020, Pages 2908-2917, ISSN 0301-5629
9. Blazic I, Cogliati C, Flor N, et al. The use of lung ultrasound in COVID-19. ERJ Open Res 2023; 9: 00196-2022 [DOI: 10.1183/23120541.00196-2022].
10. Collins, J.D., Rowley, H., Leiner, T., Reeder, S., Hood, M., Dekkers, I., Tha, K., Gulani, V., Kopanoglu, E. and (2022), Magnetic Resonance Imaging During a Pandemic: Recommendations by the ISMRM Safety Committee. J Magn Reson Imaging, 55: 1322-1339. Available at: https://doi.org/10.1002/jmri.28006
11. Pulmonary complications due to COVID-19 – a literature review. Romaszko-Wojtowicz A.M., Doboszynska A., Pol. Ann. Med. 2021;28(2):244-249
12. Gosangi B, Rubinowitz AN, Irugu D, Gange C, Bader A, Cortopassi I. COVID-19 ARDS: a review of imaging features and overview of mechanical ventilation and its complications. Emerg Radiol. 2022 Feb;29(1):23-34. doi: 10.1007/s10140-021-01976-5. Epub 2021 Oct 26. Erratum in: Emerg Radiol. 2022 Feb;29(1):225. doi: 10.1007/s10140-021-01995-2. PMID: 34698956; PMCID: PMC8545770
13. World Health Organization. (2021). Neurology and COVID-19: scientific brief, Available at: https://iris.who.int/handle/10665/345574. License: CC BY-NC-SA 3.0 IGO
14. Bašić Kes V., Grbić N.,Supanc V., Zavoreo I., Zadro Matovina L., Neurološka očitovanja COVID-19, Acta Med Croatica, 75 (2021) 281-288
15. Kremer S, Lersy F, Anheim M, et al. Neurologic and neuroimaging findings in patients with COVID-19: a retrospective multicenter study. Neurology. 2020;95(13):e1868-e1882.
16. Brinar V. Demijelinizacijske bolesti središnjeg živčanog sustava. U: Brinar V, Hajnšek S, Malojčić B, Habek M i sur., ur. Neurologija za medicinare. Zagreb: Medicinska naklada; 2009. Str. 302-337.
17. Nath A. Neurologic Manifestations of Severe Acute Respiratory Syndrome Coronavirus 2 Infection. Continuum (Minneap Minn). 2021 Aug 1;27(4):1051-1065. doi: 10.1212/CON.0000000000000992. PMID: 34623104; PMCID: PMC9527260.

18. Mohan N, Fayyaz MA, Del Rio C, Khurana NKRS, Vaidya SS, Salazar E, Joyce J, Ali AA. Neurological manifestations and neuroimaging findings in patients with SARS-CoV2-a systematic review. Egypt J Neurol Psychiatr Neurosurg. 2021;57(1):68. doi: 10.1186/s41983-021-00322-3. Epub 2021 Jun 2. PMID: 34093004; PMCID: PMC8170868.

19. Fridman S, Bullrich MB, Jimenez-Ruiz A, Costantini P, Shah P, Just C, et al. Stroke risk, phenotypes, and death in COVID-19: systematic review and newly reported cases. Neurology. 2020;95(24):e3373–e3385. doi: 10.1212/WNL.0000000000010851.

20. Faro SH, Manmatharayan A, Leiby B, Jain N, Mohamed FB, Talekar KS, Doshi A, Jambor I, Chang S, Finkelstein M, Kremer S, Lersy F, Lindgren B, Figueiredo NM, Gerevini S, Napolitano A, Jain R, Dogra S, Pillai JJ, Ryan D, Jager R, Carletti F, Mian A, Kaliev A, Anand P, Takahashi C, Murat A, Colen R, Mansueto G, Pizzini F. Neuroimaging findings in 4342 hospitalized COVID-19 subjects: A multicenter report from the United States and Europe. J Neuroimaging. 2023 Sep-Oct;33(5):752-763. doi: 10.1111/jon.13140. Epub 2023 Jun 28. PMID: 37381160.

21. Gómez-Mesa JE, Galindo-Coral S, Montes MC, Muñoz Martin AJ. Thrombosis and coagulopathy in COVID-19. Curr. Probl. Cardiol. 46(3), 100742 (2021).

22. Pontone G, Scafuri S, Mancini ME, Agalbato C, Guglielmo M, Baggiano A, Muscogiuri G, Fusini L, Andreini D, Mushtaq S, Conte E, Annoni A, Formenti A, Gennari AG, Guaricci AI, Rabbat MR, Pompilio G, Pepi M, Rossi A. Role of computed tomography in COVID-19. J Cardiovasc Comput Tomogr. 2021 Jan-Feb;15(1):27-36. doi: 10.1016/j.jcct.2020.08.013. Epub 2020 Sep 4. PMID: 32952101; PMCID: PMC7473149.

23. Farouk SS, Fiaccadori E, Cravedi P, Campbell KN. COVID-19 and the kidney: what we think we know so far and what we don't. *J. Nephrol.* 33, 1213–1218 (2020).

24. Atelj A., Krajinović V., Santini M., Papić N., Vargović M., Kotarski V., Gjurašin B., Krznarić J., Kutleša M., Bolesnici liječeni u Jedinici intezivnog liječenja Klinike za infketivne bolesti „Dr. Fran Mihaljević" u Zagrebu zbog bolesti COVID-19, Infektol glasn 2020; 40 (2);55-63 https://doi.org/10.37797/ig.40.2.3

25. Yu Y, Xu D, Fu S, et al. Patients with COVID-19 in 19 ICUs in Wuhan, China: a cross-sectional study. Crit Care 2020; 24(1): 219.

26. Margarita V. Revzin, Sarah Raza, Neil C. Srivastava, Robin Warshawsky, Catherine D'Agostino, Ajay Malhotra, Anna S. Bader, Ritesh D. Patel, Kan Chen, Christopher Kyriakakos, and John S. Pellerito RadioGraphics 2020 40:7, 1866-1892) Available at: https://pubs.rsna.org/doi/full/10.1148/rg.2020200195#fig21

27. M.L. Parra Gordo, G. Buitrago Weiland, M. Grau García, G. Arenaza Choperena, Radiologic aspects of COVID-19 pneumonia: Outcomes and thoracic complications, Radiología (English Edition), Volume 63, Issue 1, 2021, Pages 74-88, ISSN 2173-5107

28. World Health Organization. A clinical case definition of post COVID-19 condition by a Delphi consensus,. 2021 COVID-19: Clinical care. Available at: https://www.who.int/publications/i/item/WHO-2019-nCoV-Post_COVID-19_condition-Clinical_case_definition-2021.1

29. Vrsaljko N., Višković K., Vince A., Dugi COVID ili postakutne posljedice COVID-19, Liječ Vjesn 2023;15:307-320. Available at: https://doi.org/10.37797/ig.40.2.3

30. Bai F, Tomasoni D, Falcinella C, Barbanotti D, Castodi R, Mule G, et al. Female gender is associated with long COVID syndrome: a prospective cohort study. Clin MicrobiolInfect.2022;28(4):6119–61116. PubMed. Available at: https://doi.org/10.1016/j.cmi.2021.11.002</jrn>

31. Boglione L, Meli G, Poletti F, Rostagno R, Moglia R, Cantone M i sur. Risk factors and incidence of long-COVID syndrome in hospitalized patients: does remdesivir have a protective effect? QJM. 2022;12:865–71.

32. Han X, Fan Y, Alwalid O, Li N, Jia X, Yuan M i sur. Six-month Follow-up Chest CT Findings after Severe COVID-19 Pneumonia. Radiology. 2021;299:E177–E186.

33. Grepo N. Uloga radiologije u COVID-19 pandemiji (Diplomski rad). Split: Sveučilište u Splitu, Sveučilišni odjel zdravstvenih studija; 2024 (pristupljeno 17.2.2025.) Available at: https://repo.ozs.unist.hr/islandora/object/ozs%3A1671/datastream/PDF/view

Radiološki modaliteti u otkrivanju, procjeni i praćenju COVID-19 infekcije

Sažetak

Pandemija COVID-19, uzrokovana SARS-CoV-2 virusom, predstavljala je globalni zdravstveni izazov koji je zahtijevao brzu reorganizaciju zdravstvenih sustava i uvođenje strogih zaštitnih mjera. Zlatni standard kod postavljanja dijagnoze COVID infekcije svakako je RT-PCR test, te uz test, radiološke metode koje svojim specifičnim prikazima ukazuju na oboljenja. Radiološki prikaz manifestacija COVID-19 infekcije uključuje radiograme torakalnih organa koji se koriste za evaluaciju plućnih promjena, CT koji pruža detaljan prikaz abnormalnosti uzrokovanim infekcijom, PET/CT i LUS koji dodatno pomažu u dijagnostici i praćenju, te MRI koja se koristi za detaljnu procjenu komplikacija i post covid sindroma. Komplikacije COVID-19 infekcije s najvećom incidencijom su plućne, neurološke, hematološke, bubrežne i srčane. Tijekom pandemije pokazala se njihova ozbiljnost i nepredvidljivost s obzirom da su ishod bolesti dodatno činile neizvjesnim i otežavale oporavak. Posebnu inspiraciju i motivaciju za nova znanstvena istraživanja daju sindrom post covid-a i MIS-C s obzirom da imaju karakteristične značajke kliničke slike.

Ključne riječi: COVID-19; infekcija; komplikacije; manifestacije; radiologija

RT-SPOT®

Existing skin markers affect dose calculations and must be manually contoured out, increasing the dose planning time per patient.

Manual contouring can be imperfect leading to dose inaccuracies or rework of treatment plans.

RT-SPOT elevated skin markers are designed to minimize dose perturbation and reduce the need for manual contouring.



▲ *The moldable backing allows RT-SPOT Line to bend into various shapes – even small circles.*

RT-SPOT® Line



REF 127 QTY 140cm
2.0mm Diameter
Elevated Non-Metallic Line

THE ELEVATED LINE ONLY FROM BEEKLEY MEDICAL

RT-SPOT® Pellet 2.3



REF 129 QTY 50
2.3mm
Elevated Non-Metallic Pellet

THE ELEVATED PELLET ONLY FROM BEEKLEY MEDICAL

RT-SPOT® Pellet 4.0



REF 130 QTY 50
4.0mm
Elevated Non-Metallic Pellet

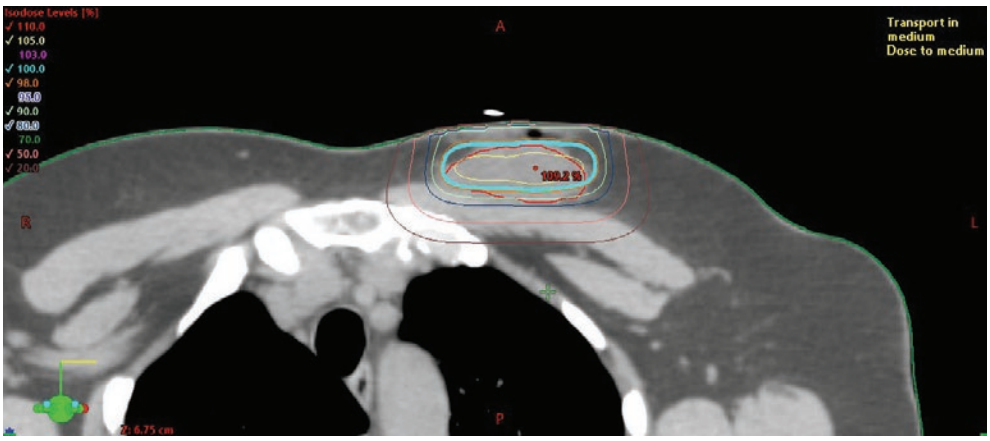
THE ELEVATED PELLET ONLY FROM BEEKLEY MEDICAL

RT-SPOT® Crosshair



REF 135 QTY 30
2.0cm x 2.0cm
Elevated Non-Metallic Crosshair

THE ELEVATED CROSSHAIR ONLY FROM BEEKLEY MEDICAL



◀ *Axial CT Scan of female breast radiation patient with surgical scar identified by RT-SPOT Line. RT-SPOT Line excluded from body contour.*

medical intertrade

Web: www.medical-intertrade.hr
E-mail: medicinska-oprema@medical-intertrade.hr

Beekley Medical®

STRUČNI RAD (PROFESSIONAL PAPER)

Radioterapija kod djece

Marta Pekvarić[1,2], Velimir Karadža[1]

[1] Zdravstveno veleučilište Zagreb

[2] Klinički bolnički centar Sestre Milosrdnice, Klinika za tumore

Corresponding author: Marta Pekvarić, email: martapekvaric2@gmail.com

DOI: https://doi.org/10.55378/rv.49.1.8

Sažetak

Radioterapija u pedijatrijskoj onkologiji donosi specifične izazove i razlike u odnosu na terapiju zračenjem odraslih pacijenata. Djeca su najosjetljivija skupina pacijenata jer su njihovi organi i tkiva i dalje u razvoju, što znači da ionizirajuće zračenje ima puno veći utjecaj i štetnost na zdrava tkiva kod djece nego kod odraslih ljudi.

U pedijatrijskoj onkologiji vrlo često nailazimo na tumore velikih volumena na specifičnim lokalizacijama koji predstavljaju velik izazov u planiranju i provođenju radioterapije. Veliki je rizik zračenja i pojava sekundarnih karcinoma zbog oštećenja zdravog tkiva tijekom liječenja primarnog tumora, a novim metodama taj je rizik moguće smanjiti. Većini djece teško je ili nemoguće objasniti važnost mirovanja tijekom radioterapije, što znači da je većina djece podvrgnuta anesteziji.

Svako dijete i obitelj suočeno s dijagnozom tumora prolazi kroz najteže trenutke života, stoga bi s djecom i njihovim obiteljima trebali raditi stručnjaci specijalizirani u pedijatrijskoj onkologiji i radioterapiji. Djeca se najčešće, tako i u Hrvatskoj, liječe u bolnicama i ustanovama namijenjenima odraslim ljudima.

Kako bi im se olakšao proces liječenja, bitno je objasniti im cijeli proces kroz koji će prolaziti kroz oblik igre i razgovora prilagođenim dobi djeteta. Nakon dijagnoze slijedi priprema i planiranje zračenja, što obavlja liječnik onkolog u dogovoru s radiološkim tehnologom i medicinskim fizičarom. Na kraju slijedi liječenje, odnosno radioterapija, koju provode radiološki/radioterapijski tehnolozi.

Uloga radiološkog/radioterapijskog tehnologa je uputiti, pripremiti i namjestiti dijete u položaj prikladan za zračenje te upravljati uređajem za radioterapiju, linearnim akceleratorom. Današnjim napretkom tehnologije i dolaskom novih metoda liječenja omogućuje se puno bolja isporuka zračenja tumorskom tkivu te puno bolja zaštita okolnog zdravog tkiva.

Ključne riječi: radioterapija, djeca, tumori, zračenje

Uvod

Dječji karcinomi jedan su od vodećih uzroka smrti djece u svijetu. Teško ih je rano otkriti jer često dolaze bez simptoma. Dijagnoza se može postaviti u bilo kojoj dobi, no češća je kod starije djece. Razvojem medicine i radioterapije, sve veći postotak djece preživljava do odrasle dobi (1). Radioterapija može biti vanjska ili unutarnja (brahiterapija). Većina djece prima terapiju vanjskim snopovima 4 do 5 dana tjedno kroz nekoliko tjedana. Male dnevne doze zračenja smanjuju štetu zdravim stanicama, a vikendom se terapija pauzira radi oporavka. Radiološki tehnolog postavlja dijete u pravilan položaj pomoću oznaka i imobilizacije. Roditelji ne smiju biti prisutni u prostoriji tijekom terapije, ali nakon nje su itekako dobrodošli (2). Kasni učinci radioterapije uključuju sekundarne karcinome, probleme rasta, neurokognitivne promjene i hormonalne poremećaje (3). Najčešći dječji karcinomi su leukemija, tumori CNS-a i limfomi, a liječe se terapijom vanjskim snopovima pomoću linearnih akceleratora (4,5).

Tumori dječje dobi

Odrasli obolijevaju od karcinoma često zbog okolišnih faktora, dok je kod djece uzrok često nepoznat. Genetske promjene glavni su uzrok dječjih karcinoma, poput retinoblastoma, a mogu nastati i zbog kromosomskih abnormalnosti (npr. leukemija, limfomi) (6). Najčešći dječji tumori su leukemije, tumori središnjeg živčanog sustava, limfomi, neuroblastomi, Wilmsov tumor te sarkomi kostiju i mekih tkiva (6). Leukemije su najčešće maligne bolesti u djece, a akutna limfoblastična leukemija (ALL) čini 80% svih leukemija. Dijagnoza uključuje biopsiju koštane srži, krvne pretrage, CT, MR i ultrazvuk, a liječenje kemoterapiju, biološku terapiju i transplantaciju koštane srži, dok se radioterapija koristi rijetko. Limfomi se dijele na Hodgkinove i ne-Hodgkinove te se liječe kombinacijom radioterapije, operacije i kemoterapije. Wilmsov tumor liječi se kirurški, kemoterapijom i zračenjem. Osteosarkom se dijagnosticira CT-om, MR-om i biopsijom, a liječi kemoterapijom i operacijom (7). Liječenje dječjih tumora uključuje operaciju,



Slika 1. Protonska terapija
Izvor: IBA (slika je vlasništvo tvrtke Ion Beam Applications S.A.)

kemoterapiju i radioterapiju, pri čemu se najčešće koristi terapija vanjskim snopovima zbog preciznosti i smanjenja nuspojava (8). Radioterapija se najčešće koristi za solidne tumore, dok se za leukemije primjenjuje rjeđe. Napredak tehnologije omogućava smanjenje doze prema zdravom tkivu i nuspojava, čineći radioterapiju sve sigurnijom (9).

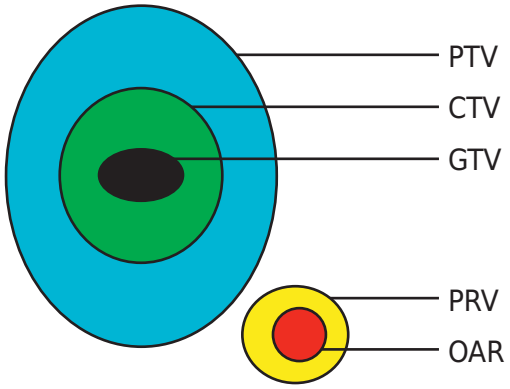
Radioterapija vanjskim snopovima i uređaji u radioterapiji

Radioterapija koristi energetske valove ili čestice za liječenje tumora. Može biti vanjska ili unutarnja, a kod djece se najčešće koristi terapija vanjskim snopovima. Cilj je uništiti stanice raka ili spriječiti njihov rast, smanjujući simptome bolesti. Terapija se provodi linearnim akceleratorom, a provodi je radiološki/radioterapijski tehnolog (7). Kod vanjske radioterapije koriste se fotoni ili čestice, najčešće protoni. Fotoni nastaju u linearnom akceleratoru pri udaru elektrona u metalnu metu, pri čemu se emitira ionizirajuće zračenje (10). Elektromagnetski valovi visoke frekvencije, poput rendgenskih i gama zraka, omogućuju prodiranje u tkivo. Rendgenske zrake nastaju ubrzavanjem elektrona u vakuumskim cijevima, dok gama zrake nastaju radioaktivnim raspadom jezgara nestabilnih izotopa (11). Ionizirajuće zračenje prekida dvostruke lance DNA, uzrokujući staničnu smrt tumorskih stanica. Iako utječe i na zdrave stanice, one se lakše obnavljaju. Međutim, loše planiranje može uzrokovati trajna oštećenja i sekundarne karcinome (10). Radiobiološki zahtjevi nalažu precizno doziranje kako bi se maksimiziralo uništenje tumora uz očuvanje zdravog tkiva. Hiperfrakcioniranje omogućuje primjenu višestrukih manjih doza dnevno, čime se smanjuju kasni učinci zračenja i povećava učinkovitost liječenja (10). Vanjska radioterapija koristi se samostalno ili uz operaciju i kemoterapiju. Kada se primjenjuje uz drugu terapiju, naziva se istodobna radioterapija. Ako slijedi kirurško uklanjanje tumora, to je adjuvantna radioterapija, dok se prije operacije ili kemoterapije naziva neoadjuvantna. Može biti kurativna ili palijativna, za ublažavanje simptoma (12). Napredak u radioterapiji omogućio je bolje ciljanje tumora uz smanjenje oštećenja zdravog tkiva, čime se smanjuje rizik od kasnih učinaka i sekundarnih karcinoma (10). Radioterapija se sastoji od pripreme, planiranja i provođenja terapije. Za planiranje se koriste CT, MR i PET uređaji koji omogućuju preciznu lokalizaciju tumora. Klasični dijagnostički uređaji nisu prilagođeni radioterapiji, pa se koriste CT simulatori s prilagođenim stolom, laserima za pozicioniranje i širim otvorom gantrija. PET-CT kombinira anatomske i funkcionalne informacije o tumoru (13). Za provođenje terapije koristi se linearni akcelerator, složen uređaj koji ubrzava elektrone do visokih energija i stvara fotonski snop za zračenje. Glavne komponente uključuju akceleratorsku cijev, elektronski top, terapijski stol i sustav za praćenje pacijenta. Terapijski stol omogućuje precizno pozicioniranje pacijenta, dok audiovizualni sustav osigurava nadzor tijekom terapije (5). Najpoznatiji proizvođači linearnih akceleratora su Varian, Elekta i Accuray. Njihovi sustavi omogućuju napredne tehnike poput IMRT – radioterapija promjenjivog intenziteta (eng. *Intensity-Modulated Radiation Therapy*), VMAT – lučna terapija promijenjivog intenziteta (eng. *Volumetric Modulated Arc Therapy*), IGRT – slikovno vođena radioterapija (eng. *Image-guided Radiation Therapy*) i SBRT (stereotaksijska radioterapija). Gama nož koristi se za stereotaksijsku radioterapiju, dok spiralna tomoterapija omogućuje kontinuirano zračenje tijekom pomicanja pacijenta (10,14). Protonska terapija veliki je iskorak u liječenju tumora (slika 1.). Njezina najveća prednost je preciznija isporuka doze uz manju štetu okolnom tkivu, odnosno zbog karakteristike Braggova vrha gdje protoni oslobađaju najveću energiju na precizno određenoj dubini unutar tumorskog tkiva. Zbog toga su smanjene nuspojave zračenja i mogućnost pojave sekundarnih karcinoma.

Dodatnu sigurnost i napredak u isporuci zračenja protonima danas pruža slikovno vođena protonska terapija (15,16).

Planiranje i provođenje radioterapije kod djece

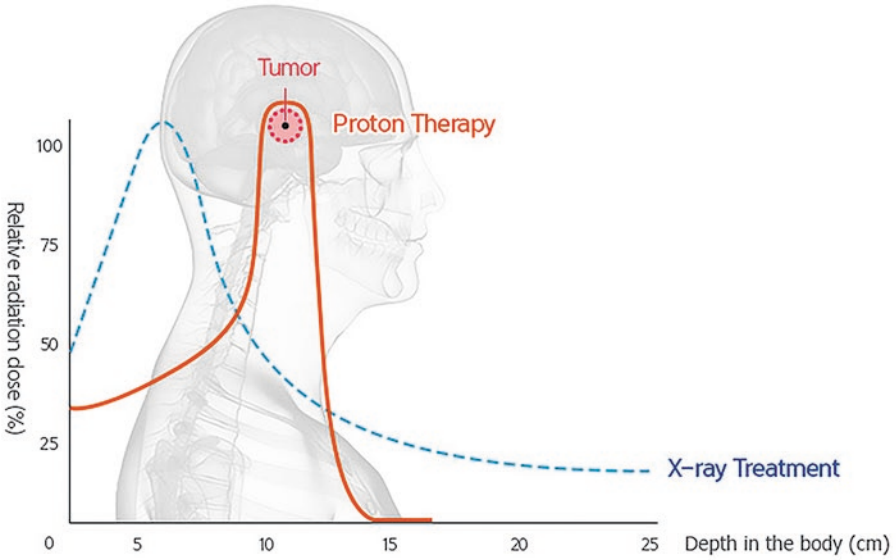
Planiranje radioterapije je proces koji uključuje određivanje ključnih parametara terapije za optimalno liječenje pacijenata. Glavni parametri koji se određuju uključuju GTV (volumen makroskopski vidljivog tumora), CTV (klinički volumen koji uključuje subklinički tumor) i PTV (planirani volumen koji uzima u obzir geometrijske varijacije, poput pomaka pacijenta). Osim toga, označavaju se organi u riziku (OAR), koji su posebno osjetljivi na zračenje i smješteni blizu ciljnih volumena. Ako su organi u riziku mali i pomiču se, koristi se PRV (slika 2.) (10). Planiranje obuhvaća oblikovanje tretmana zračenjem, određivanje doze, frakcioniranje i pozicioniranje pacijenta, a radiološki tehnolog prati cijeli proces u suradnji s onkologom i medicinskim fizičarom (13). Računalno potpomognuto planiranje, uključujući virtualnu 3D rekonstrukciju pomoću CT ili MR uređaja, postalo je standard u radioterapiji. Ova tehnologija omogućuje precizno oblikovanje polja zračenja kako bi se zaštitilo zdravo tkivo, dok se ciljano zrači tumor. Planiranje u dječjoj onkologiji mnogo je zahtjevnije nego kod odraslih jer dječja tkiva puno su osjetljivija na zračenje. Osim toga, u djece su česti veći tumori koji zahtijevaju značajne doze zračenja, dok istovremeno treba poštedjeti rastuće kosti, gonade, mozak i srce (13). Planiranje mora uzeti u obzir i anesteziju za djecu mlađu od 7 godina, budući da je ona često potrebna za precizno postavljanje pacijenta. Također, pri planiranju radioterapije u djece, bitno je razmotriti rizik od nastanka sekundarnih karcinoma uzrokovanih zračenjem. Radioterapija se provodi uz pomoć različitih uređaja, najčešće linearnih akceleratora koji proizvode fotone za zračenje tumora (18). Za svaki dolazak na terapiju, dijete se smješta u isti položaj pomoću malih oznaka ili tetovaža. Za provjeru položaja koristi se uređaj za portalno oslikavanje (EPID) ili uređaj za provjeru kompjutoriziranom tomografijom konusnog snopa (CBCT) koji osigurava da je pacijent u točno istom položaju kao prilikom snimanja CT-a (17). Djeca obično dolaze na terapiju 4 do 5 puta tjedno, a terapija traje nekoliko tjedana. Uz napredne tehnike poput IMRT-a (Intenzitetom Modulirana Radioterapija), omogućuje se precizno prilagođavanje doze zračenja tumoru, smanjujući oštećenje okolnih zdravih tkiva i nuspojave (19). Stereotaktička radiokirurgija (SRS) i stereotaktička radioterapija tijela (SBRT) omogućuju precizno zračenje u velikim dozama, obično u nekoliko tretmana, dok su IMRT i VMAT namijenjeni za veće tumore s ciljem poštede zdravog tkiva (20). Slikovno vođena radioterapija (IGRT), koja koristi slike iz rendgenskih ili ultrazvučnih presjeka, omogućuje visoku preciznost postavljanja pacijenta (5). Ove moderne tehnike zahtijevaju stalno nadograđivanje znanja zdravstvenih djelatnika kako bi mogli sigurno provoditi terapiju (21).



Slika 2. Shematski ciljni volumeni
Izvor: Balenović I. Ocrtavanje organa od rizika u radioterapiji (stručni rad). Radiološki vjesnik 2022/1. Dostupno na: https://hrcak.srce.hr/file/400332, pristupljeno: 2. ožujka 2025.

Terapija zračenjem vanjskim snopovima kod djece

Radioterapija kod djece zahtijeva specifična znanja i suradnju cijelog tima, uključujući onkologe, medicinske fizičare, medicinske sestre, radiološke tehnologe, anesteziologe, a poželjno i psihologa. Ovaj tim mora biti dobro usklađen jer je dječja radioterapija izazovna zbog specifičnih potreba dječjih organizama. Kod djece treba biti izuzetno pažljiv u pogledu njihove dobi, a također treba voditi računa o učincima radioterapije koji će se manifestirati u dugoročnom razdoblju. Na primjer, dječja tkiva imaju manju toleranciju na zračenje od odraslih, a mnogi tumori u dječjoj dobi često zahtijevaju visoke doze terapije. Iz tog razloga, svaki postupak mora biti precizno planiran kako bi se izbjeglo oštećenje zdravih tkiva, što može rezultirati dugoročnim posljedicama, uključujući usporavanje rasta, neplodnost ili smanjenje funkcije vitalnih organa (22). Radioterapija vanjskim snopovima kod djece izazovnija je nego kod odraslih zbog specifičnih karakteristika dječjih tumora. Tumori u djece često su rijetki, veliki i zahtijevaju velike ciljne volumene, a to može uključivati visoke doze zračenja koje mogu imati ozbiljne posljedice. Dječje tkivo, poput jajnika, testisa, hipofize, srca i mozga, zahtijeva posebnu zaštitu jer su ova tkiva osjetljivija na zračenje od onih u odraslih osoba. Na primjer, zračenje veće od 18 Gy može zaustaviti rast kostiju, a ozračivanje jajnika ili testisa iznad 5-10 Gy može prouzročiti neplodnost (23). Očuvanje normalnog moždanog tkiva je također ključno kako bi se izbjegle kognitivne promjene koje mogu nastati zbog zračenja mozga. Za uspješno liječenje, od esencijalne je važnosti odabrati najbolju tehniku liječenja. Najpreporučljivije su IMRT i IGRT tehnike, koje omogućuju maksimalnu dozu zračenja tumoru uz minimalnu štetu zdravim tkivima. Multidisciplinarni tim u dječjoj radioterapiji mora biti kontinuirano obučavan kako bi bio u stanju pratiti napredak u tehnologiji i osigurati najbolju moguću njegu pacijentima. Ovaj tim obuhvaća liječnike, radiološke tehnologe, medicinske fizičare, anesteziologe, medicinske sestre i psihologe (14). Uloga psihologa ili drugih stručnjaka također je ključna u olakšavanju procesa liječenja za djecu i njihove obitelji. Priprema djece za terapiju putem igre, brošura ili video zapisa može značajno smanjiti strahove i tjeskobe te olakšati razumijevanje postupaka liječenja (10). Planiranje radioterapije obično započinje CT simulacijom, pri čemu dijete mirno leži u maski dok se uzimaju rendgenske slike. Nakon toga, specijalisti stvaraju plan radioterapije koji će provesti radiološki tehnologi. Svaka



Slika 3. Shematski prikaz Braggovog vrha
Izvor: Samsung Medical Center. Principles of Proton Therapy. Dostupno na: http://www.samsunghospital.com/home/proton/en/whatIsProtonTherapy/principle.do, pristupljeno: 2. ožujka 2025.

dijagnoza zahtijeva individualizirani pristup, jer različite vrste tumora imaju različite specifičnosti. U liječenju leukemije, radioterapija se koristi kada je likvor ili testisi zahvaćeni malignim stanicama, a često i prije transplantacije koštane srži, u obliku Total Body Irradiation (TBI) (23). Kod meduloblastoma, najčešćeg tumora mozga u djece, doza radioterapije ovisi o riziku. Za visoki rizik predviđa se veća doza, a planiranje se prilagođava specifičnostima svakog pacijenta. Neuroblastom, još jedan čest tumor kod djece, također zahtijeva precizno planiranje. U nekim slučajevima, kirurgija ne može u potpunosti ukloniti tumor, što zahtijeva povećanje doze radioterapije. Novije tehnologije kao što su 3D konformna radioterapija i IMRT omogućuju preciznije planiranje i minimaliziranje rizika za okolne organe poput bubrega, jetre i kralježnice (23). Protonska terapija, koja koristi visoku preciznost protona za liječenje tumora, smatra se važnim dijelom pedijatrijske onkologije. Zbog svoje sposobnosti da zrači samo tumor, smanjuje se rizik od oštećenja okolnih zdravih tkiva, što je osobito važno u dječjoj dobi. (slika 3.) Protonska terapija, iako skuplja, može se pokazati isplativijom dugoročno jer smanjuje nuspojave koje bi zahtijevale dodatno liječenje (29, 13).

Imobilizacija i anestezija

Imobilizacijska sredstva osiguravaju preciznost liječenja i određivanje sigurnosnih granica za planiranje volumena zračenja. Pozicioniranje ovisi o imobilizaciji pomoću maski ili drugih sustava za fiksiranje. Stalan položaj tijekom ozračivanja smanjuje nuspojave zračenja (10). Imobilizacija može biti izazov za djecu, koja često imaju strah od radioterapije i teško razumiju važnost mirovanja. Većina imobilizacijskih sredstava proizvedena je za odrasle pacijente, a prilagođena za djecu, što im može biti neudobno. Za tumore mozga najčešće se koristi termoplastična maska, dok za trupu ili ekstremitete postavljanje tetovaža može biti potrebno (13). Pacijenti se postavljaju na stol pomoću lokalizacijskih lasera i identifikacijskih oznaka, poput tetovaža ili koštanih orijentira. Takav položaj mora biti konstantan kroz cijelo liječenje. Identifikacijske oznake ponekad se iscrtavaju na kalupu, no to nije optimalno zbog pomicanja. Koštani orijentiri su pouzdani, ali preciznost palpacije nije dovoljna za milimetarsku točnost. Pribor za pozicioniranje i imobilizaciju ključan je za preciznost (13). Prilagođavanje imobilizacijskih sredstava djeci zahtijeva strpljenje, osobito pri izradi maski. Maske se oblikuju prema djetetovim crtama lica, a postupak može izazvati stres i strah (24). Istraživanje Children's Oncology Group pokazalo je da modifikacija maske (81%) i njezino ukrašavanje (71%) pomažu djeci da lakše podnesu postupak (25). Uvođenjem 3D konformalne radioterapije, IMRT-a i IGRT-a, tehnologije poput SGRT-a omogućuju precizno praćenje



Slika 4. Priprema za provođenje radioterapije djece sa anestezijom
Izvor: autor

pacijenta, smanjujući potrebu za anestezijom i neudobnim imobilizacijama (26). Priprema djece za postavljanje imobilizacije kroz igru i objašnjenje postupaka smanjuje stres i ubrzava proces (24). Anestezija je često potrebna za djecu mlađu od 7 godina, a anesteziološki tim mora biti dostupan tijekom cijelog liječenja (slika 4.) (10). Sigurnost tijekom anestezije ključno je pitanje, s ciljem minimiziranja rizika i osiguravanja udobnosti djece (27).

Palijativna radioterapija

Palijativna radioterapija koristi se u liječenju djece s malignim bolestima, s ciljem ublažavanja simptoma poput bola ili sprječavanja njihovog nastanka. Obično se primjenjuje kada drugi oblici liječenja, poput kemoterapije, operacije ili radioterapije, nisu dali željene rezultate, ili kod metastatskih bolesti kao što su metastaze u kostima, jetri, mozgu, plućima, glavi i vratu. Cilj ove terapije je poboljšati kvalitetu života djeteta, olakšati simptome bolesti i smanjiti teret liječenja (28). Važno je da pacijenti i njihove obitelji budu dobro informirani o mogućnostima palijativne radioterapije. Istraživanje provedeno na Institutu Dana-Farber otkrilo je da čak 76% roditelja očekuje produljenje života njihove djece uz palijativnu radioterapiju, dok 40% smatra da će terapija izliječiti dijete, što ukazuje na potrebu za boljim objašnjenjem ciljeva palijativne terapije (28). Grupa za dječju onkologiju (Children's Oncology Group) razvila je smjernice za palijativnu radioterapiju djece i adolescenata s neizlječivim zloćudnim tumorima. Smjernice uključuju crtež s indikacijama za liječenje i popis mogućih nuspojava, kao što su alopecija, dermatitis i edemi pri zračenju mozga. Takve smjernice pomažu liječnicima u praćenju i upravljanju nuspojavama te optimizaciji terapije (28).

Nuspojave radioterapije vanjskim snopovima kod djece

Djeca koja su prošla radioterapiju mogu iskusiti razne nuspojave, budući da su njihova tkiva i organi osjetljiviji na zračenje zbog razvoja. Doza zračenja također igra ključnu ulogu u ozbiljnosti nuspojava, a doza od 2-3 Gy prema testisima može uzrokovati azoospermiju, dok doza od 2,5-3 Gy prema srcu može izazvati srčane bolesti. Najčešće nuspojave uključuju probleme u rastu, neurokognitivne promjene, neplodnost, hormonalne promjene i sekundarne karcinome (3). Nuspojave se mogu pojaviti odmah, nekoliko dana nakon tretmana ili čak godinama kasnije. Osim spomenutih, mogu se javiti problemi s apetitom, dehidracija, proljev, umor, alopecija, trombocitopenija, anemija, infekcije i rane na koži (7). Mučnina i povraćanje su česti nakon zračenja glave, dok djeca često doživljavaju probleme s prehranom, zbog kojih je važno pratiti njihovu težinu i opseg tijela, te pružiti dodatke prehrani po potrebi (7). Alopecija, gubitak kose, vrlo je česta nuspojava, osobito kod tumora glave, te može biti vrlo traumatična za djecu, osobito djevojčice (7). Kombinacija radioterapije i kemoterapije povećava rizik od sekundarnih karcinoma, poput akutne mijeloidne leukemije (AML), koja se može javiti čak 20 godina nakon početnog liječenja (7). Kasni učinci zračenja mogu se razviti nakon završetka tretmana, a kod većine preživjelih pacijenata pojavljuju se tijekom godina. Pravovremeno prepoznavanje i liječenje tih učinaka ključno je za poboljšanje kvalitete života i prevenciju ozbiljnih zdravstvenih problema (30).

Zaključak

Terapija zračenjem vanjskim snopovima kod djece složen je proces koji se bitno razlikuje od radioterapije odraslih. Zbog toga što dječji organi i tkiva još uvijek rastu, ionizirajuće zračenje ima snažniji utjecaj. Proces uključuje nekoliko faza: postavljanje dijagnoze, planiranje radioterapije i izvođenje samog tretmana. Liječnik određuje plan, medicinski fizičar ga implementira u računalni sustav, a radiološki tehnolog provodi terapiju putem linearnih akceleratora. Djeca često ne razumiju važnost mirovanja, pa se ponekad koristi anestezija. Napredak tehnologije omogućuje primjenu novih tehnika poput IMRT-a, VMAT-a, IGRT-a i protonske terapije. U Hrvatskoj se primjenjuju sve ove tehnike osim protonske terapije, koja je vrlo precizna, ali još nije dostupna. Tehnologije omogućuju bolji fokus na tumore, minimalno oštećenje zdravih tkiva i smanjenje nuspojava, uključujući sekundarne karcinome. Dugoročni cilj je očuvanje kvalitete života djece nakon liječenja. Dječja radioterapija zahtijeva interdisciplinarni pristup, stalno usavršavanje i edukaciju, a novim tehnikama i tehnologijama postižu se izvrsni rezultati u liječenju dječjih tumora. Svi podaci u ovom radu dio su završnog rada „Terapija zračenjem vanjskim snopovima kod djece" izrađenog na Zdravstveno veleučilište u Zagrebu (31).

Literatura

1. International Atomic Energy Agency. Radiotherapy in cancer care: facing the global challenge. Vienna: IAEA; 2017. 325-338.
2. Sandler ES. Radiation Therapy. Nemours KidsHealth. 2022. Dostupno na: https://kidshealth.org/en/parents/radiation.html Pristupljeno: 25.2.2025.
3. Hariyanto AD, Wijaya HM, Anton J, Yanuarta SE, Octavianus S, Nuryadi E, et al. The Role of Radiotherapy towards Pediatric Cancer. Radioterapi & Onkologi Indonesia. 2020;11(2):57-65.
4. PDQ® Pediatric Treatment Editorial Board. PDQ Retinoblastoma Treatment. Bethesda,MD: National Cancer Institute. 2021. Dostupno na: https://www.ncbi.nlm.nih.gov/books/NBK65754/ Pristupljeno: 25.2.2025.
5. Podgorsak EB. Treatment machines for external beam radiotherapy. U: Podgorsak EB. Radiation Oncology Physics: A Handbook for Teachers and Students. Vienna: IAEA; 2005. 136-160.
6. Constine LS, Tarbell NJ, Halperin EC. Pediatric Radiation Oncology. Philadelphia: Wolters Kluwer; 2016.
7. Estlin E, Gilbertson RJ, Wynn RF. Pediatric Hematology and Oncology. Oxford: Blackwell Publishing Ltd; 2010.
8. Mayo Clinic Staff. Diagnosis and treatment. Pediatric Brain Tumors. 2024. Dostupno na: https://www.mayoclinic.org/diseases-conditions/pediatric-brain-tumor/diagnosis-treatment/drc-20361706, pristupljeno: 24.2.2025.
9. Heike T, Timmermann B. Paediatric proton therapy. The British Journal of Radiology. 2020; 93(1107).
10. Walker D, Perilongo G, Taylor R, Punt J. Brain and spinal tumors of childhood. London: Arnold; 2004.
11. Zdenko Krajina: Radioterapija – radiobiološke i fizikalne osnove, primjena u liječenju raka dojke. Medicinski Vjesnik: 1999; 31(1-4): 97-105.
12. InformedHealth.org. In brief: External radiotherapy. Dostupno na: https://www.ncbi.nlm.nih.gov/books/NBK279300/ Pristupljeno: 25.2.2025.

13. Khan FM, Gibbons JP, Sperduto PW. Khan's Treatment Planning in Radiation Oncology. Fourth edition. Philadelphia: Wolters Kluwer; 2016.
14. Mascarin M, Giugliano FM, Coassin E, Drigo A, Chiovati P, Dassie A, et al. Helical tomotherapy in children and adolescents: dosimetric comparisons, opportunities and issues. Basel:2011;3(4):3972-90.
15. Salem, P.P., Chami, P., Daou, R.; Hajj, J., Lin, H.; Chhabra, A.M., Simone, C.B., II; Lee, N.Y.; Hajj, C. Proton Radiation Therapy: A Systematic Review of Treatment-Related Side Effects and Toxicities. Int. J. Mol. Sci. 2024, 25, 10969. https://doi.org/10.3390/ijms252010969.
16. Lane, S.A., Slater, J.M., Yang, G.Y. Image-Guided Proton Therapy: A Comprehensive Review. Cancers 2023, 15, 2555. https://doi.org/10.3390/cancers15092555
17. KBC Ri. Radioterapija (informativni letak). Dostupno na: https://kbc-rijeka.hr/
18. The European Society for Pediatric Oncology. Dostupnp na: https://siope.eu/
19. Taylor A, Powell ME. Intensity-modulated radiotherapy--what is it? Cancer Imaging. 2004 Mar 26;4(2):68-73.
20. Intensity-Modulated Radiation Therapy (IMRT). Volumetric Intensity Modulated Arc Therapy (VMAT). Radiation Treatments. Dostupno na: https://www.cancercareinstitute.com/, pristupljeno: 26.2.2025.
21. Sibtain A, Morgan A, MacDougall N. Radiotherapy in Practice. Physics for Clinical Oncology. New York: Oxford University Press; 2012.
22. Grah J. Specifičnosti radioterapije u liječenju malignih bolesti, Uloga radioterapije u liječenju tumora dječje dobi. Paediatr Croat. 2013; 57 (Supl 1): 203-209
23. Olch AJ. Pediatric Radiotherapy, Planning and Treatment. New York: Taylor & Francis Group; 2013.
24. Alex-lemodane.org. Dostupno na: www.alexslemonade.org
25. Holt DE, Hiniker SM, Kalapurakal JA, Breneman JC, Shiao JC, Boik N, et al. Improving the Pediatric Patient Experience During Radiation Therapy – A Children's Oncology Group Study. Int J Radiat Oncol Biol Phys. 2021 ;109(2):505-514.
26. Mast M, Perryck S. Introduction to: Surface Guided Radiotherapy (SGRT). Tech Innov Patient Support Radiat Oncol. 2022;22:37-38.
27. Villablanca N, Valls N, González R. Techniques and Complications of Anesthesia in Pediatric Radiotherapy: A Retrospective Cohort Study. J Pediatr Hematol Oncol. 2023;45(7):377-382.
28. Tsang DS, Vargo JA, Goddard K, Breneman JC, Kalapurakal JA, Marcus KJ. Palliative radiation therapy for children with cancer. Pediatr Blood Cancer. 2021:68.
29. MIBS Dr. Berezin Medical Institute. Proton Centers Around the World. Dostupno na: https://protherapy.ru/worldprotoncentres
30. Children's Oncology Group. Late Effects of Treatment for Children's Cancer. Dostupno na: https://childrensoncologygroup.org/lateeffectsoftreatment
31. Pekvarić M. Terapija zračenjem vanjskim snopovima kod djece [Završni rad]. Zagreb: Zdravstveno veleučilište; 2024 (pristupljeno 05.03.2025.) Dostupno na: https://urn.nsk.hr/urn:nbn:hr:139:191624

Radiation Therapy for children

Abstract

Radiotherapy in paediatric oncology brings specific challenges and differences compared to radiation therapy for adult patients. Children are the most sensitive group of patients because their organs and tissues are still developing, which means that ionizing radiation has a much greater impact and harm to healthy tissues in children than in adults. In paediatric oncology, we very often encounter large-volume tumours in specific locations, which pose a great challenge in planning and implementing radiotherapy. The risk of radiation and the occurrence of secondary cancers due to damage to healthy tissue during the treatment of the primary tumour is high, and new methods can reduce this risk. It is difficult or impossible to explain to most children the importance of stillness during radiotherapy, which means that most children are subjected to anaesthesia. Every child and family faced with a tumour diagnosis goes through the most difficult moments of their lives, therefore, children and their families should be treated by professionals specialized in paediatric oncology and radiotherapy. Children are most often, and in Croatia as well, treated in hospitals and institutions intended for adults. To facilitate the treatment process, it is important to explain the entire process that they will go through as a form of play and conversation adapted to the child's age. After the diagnosis follows preparation and planning of radiation therapy, which is carried out by the oncologist in consultation with radiation therapists and medical physicists. Finally, there is treatment, radiation therapy delivery, carried out by radiation therapist (RTT). The role of RTTs is to instruct, prepare and position the child in a way suitable for the treatment and to operate the radiotherapy machine. Today's technological advances and the advent of new treatment methods enable much better delivery of radiation to tumour tissue and much better protection of surrounding healthy tissue.

Keywords: radiotherapy, children, tumours, radiation

Implementation and Practice for Image-guided Stereotactic Body Radiotherapy

Ivan Balentović

KBC Rijeka, Klinika za tumore

E-mail: ibalentovic00@gmail.com, ivan.balentovic@kbc-rijeka.hr

DOI: https://doi.org/10.55378/rv.49.1.9



Slika 1: Kongresna dvorana hotela Ramada by Wyndham Lisbon. Izvor: autor

Uvod

Krajem svibnja 2024. godine prijavio sam se za stipendiju putem ENEN-a (European Nuclear Education Network) kako bih sudjelovao u edukaciji koju organizira ESTRO (European Society for Radiotherapy and Oncology) pod nazivom „Implementation and Practice for Image-guided Stereotactic Body Radiotherapy“. Edukacija se održavala u Lisabonu, Portugal. Početkom kolovoza dobio sam obavijest da je moja prijava za stipendiju prihvaćena, što mi je omogućilo financiranje svih troškova vezanih uz sudjelovanje. U edukaciji je prisustvovalo više od stotinu sudionika, a učesnici su bili uglavnom onkolozi, medicinski fizičari te radiološki tehnolozi (RTT) iz raznih dijelova svijeta.

Projekt ENEN2+

Projekt **ENEN2+** je dio šire inicijative za jačanje nuklearnog obrazovanja i istraživanja u Europi, oslanjajući se na suradnju između akademskih institucija, industrije i istraživačkih centara.

1. Ciljevi projekta

ENEN2+ ima za cilj:

- **Osigurati mobilnost i razmjenu znanja**: Projekt pruža prilike studentima i profesionalcima da sudjeluju u razmjeni unutar EU kako bi stjecali praktično znanje i iskustvo u nuklearnim tehnologijama.



Slika 2: ENEN2+.
Izvor: https://enen.eu/

- **Unificirati obrazovne standarde**: Radi na standardizaciji obrazovanja i obuke u području nuklearnog inženjerstva, što omogućava priznavanje kvalifikacija između zemalja.
- **Razvijati vještine** za rješavanje specifičnih izazova u nuklearnom sektoru, uključujući sigurnost, upravljanje otpadom i nove tehnologije.

2. Ključne aktivnosti

- **Edukacija i trening**: Projekt osigurava edukacijske module, tečajeve i prilike za cjeloživotno učenje.
- **Stipendije i mobilnost**: ENEN2+ nudi programe stipendiranja za studente i mlade stručnjake kako bi sudjelovali u projektima diljem Europe.
- **Suradnja s industrijom**: Povezuje akademsku zajednicu s industrijom kroz zajedničke projekte, čime se osigurava da studenti stječu relevantna znanja za praktičnu primjenu.
- **Radionice i konferencije**: Organizacija događanja usmjerenih na razmjenu najboljih praksi, najnovijih istraživanja i inovacija.

3. Područja interesa

Projekt pokriva široki spektar tema vezanih za nuklearnu energiju, uključujući:

- Nuklearnu sigurnost i zaštitu.
- Upravljanje nuklearnim otpadom i očuvanje okoliša.
- Razvoj naprednih nuklearnih reaktora.
- Fiziku reaktora i materijale za nuklearnu tehnologiju.

4. Korisnici i ciljana skupina

Projekt je namijenjen:

- Studentima preddiplomskih, diplomskih i doktorskih studija iz područja tehničkih znanosti.
- Mladim profesionalcima i istraživačima u industriji.
- Akademskim institucijama i istraživačkim organizacijama koje žele sudjelovati u mreži suradnje.

5. Financiranje i trajanje

Projekt **ENEN2+** (European Nuclear Education Network Plus) financiran je iz programa Euratom za istraživanje i osposobljavanje, koji je dio Okvirnog programa za istraživanje i inovacije. Projekt je započeo 1. lipnja 2022. godine i traje četiri godine, do 31. svibnja 2026. godine.

Kroz ove aktivnosti, ENEN2+ nastoji osigurati održivost i izvrsnost u obrazovanju i osposobljavanju u području nuklearne energije, pridonoseći sigurnoj i učinkovitoj uporabi nuklearnih tehnologija u Europi.

Projekt također osigurava detaljnu analizu ponude i potražnje za stručnjacima u nuklearnom sektoru na razini EU, uključujući industriju, akademsku zajednicu, tehničke sigurnosne organizacije i regulatore. Program mobilnosti podržava više od 100 stručnjaka godišnje i pruža prilike za razvoj karijere za oko 1000 polaznika, s budžetom većim od 2,5 milijuna eura.

Osim toga, uspostavit će se centralizirano središte za pružanje informacija o dostupnim opcijama obrazovanja, treninga i zapošljavanja, uz održavanje veza s projektima koji omogućuju pristup istraživačkim infrastrukturama.

Nakon završetka projekta potrebno je predati izvještaj o sudjelovanju u projektu.

Ovaj je tečaj bio namijenjen stručnjacima iz područja radijacijske onkologije koji sudjeluju u kliničkoj praksi SRT-a (stereotaksijske radioterapije) u bilo kojoj fazi procesa liječenja. Ciljana skupina bili su radijacijski onkolozi, fizičari i radiološki tehnolozi (RTT) s posebnim naglaskom na SBRT i SRS (stereotaksijsku radiokirurgiju). Tečaj je bio namijenjen pojedincima koji su u fazi planiranja uspostave kliničkog stereotaksijskog programa, kao i onima koji već prakticiraju stereotaksijsku radioterapiju. Istaknuta je važnost integracije svih stručnjaka u tim.

Pozitivni ishodi mobilnosti

- Stečeno je znanje o izgradnji multidisciplinarnog tima za provođenje i praksu SRS-a, SRT-a i SBRT-a.
- Dobiveno je jasno razumijevanje tehničkih i fizičkih zahtjeva za SRS, SRT i SBRT.
- Poboljšano je znanje o kliničkim razlozima i ograničenjima SRS-a, SRT-a i SBRT-a.
- Razvijeno je razumijevanje radiobioloških načela iza vrlo visokih doza po frakciji.
- Naučeno je o indikacijama, praksi i ishodima SBRT-a u ranoj fazi NSCLC-a.
- Stečen je uvid u trenutne kliničke dokaze koji podržavaju SRS, SRT i SBRT za različite kliničke indikacije.

Sažetak tečaja „Implementation and Practice for Image-guided Stereotactic Body Radiotherapy“:

1. Pregled IG-SBRT-a

IG-SBRT je precizna tehnika zračenja namijenjena ciljanju tumora u tijelu s točnošću na razini milimetra. Kombinira slikovne tehnologije, poput CT-a ili MR-a, sa stereotaksijskom

radioterapijom kako bi se visokim dozama zračenja tretirali tumori, uz minimalnu izloženost okolnim zdravim tkivima. Ovaj pristup posebno je učinkovit za liječenje malih, lokaliziranih tumora u organima poput pluća, jetre, gušterače ili kralježnice.

2. Tehnike i tehnologije

Slikovne metode: Napredne tehnike oslikavanja u stvarnom vremenu, poput CT-a, fluoroskopije i MR-a, omogućuju preciznu lokalizaciju tumora prije i tijekom tretmana.

Upravljanje pokretima: Pokreti tumora uzrokovani disanjem ili kretanjem pacijenta kontroliraju se tehnikama poput 4D-CT-a, sustava za sinkronizaciju ili praćenje.

Isporuka doze: Visoko fokusirane zrake isporučuju se naprednom opremom poput SRT linearnih akceleratora (LINAC), CyberKnife uređaja ili tomoterapijskih uređaja. Raspored frakcioniranja optimiziran je za maksimalnu kontrolu tumora uz minimalne nuspojave.

3. Tijek rada i osiguranje kvalitete

Planiranje tretmana: Detaljni podaci snimanja koriste se za precizno određivanje granica tumora i optimizaciju distribucije doze.

Simulacija i postavljanje: Točno pozicioniranje pacijenta osigurava se imobilizacijskim sredstvima i verifikacijom putem snimanja.

Verifikacija: Dnevno snimanje prije tretmana osigurava poravnanje pacijenta i tumora unutar polja tretmana.

Isporuka: Tretmani se često završavaju u manje sesija u usporedbi s konvencionalnom radioterapijom (obično 3-5 sesija) aplikacijom većih dnevnih doza.

4. Kliničke primjene

Rak pluća: Visoka učinkovitost u liječenju ranog stadija raka pluća (NSCLC) kod pacijenata koji nisu pogodni za operaciju.

Tumori jetre: Pruža neinvazivnu opciju za neoperabilne lezije jetre.

Metastaze kralježnice: Omogućuje ublažavanje boli i lokalnu kontrolu u jednoj frakciji ili kratkom ciklusu.

Rak prostate: Novi podaci podržavaju SBRT za liječenje raka prostate.

Voditelji tečaja:

- Matthias Guckenberger, *Radiation Oncologist, University Hospital Zurich, Zurich (CH)*
- Dirk Verellen, *Medical Physicist, Iridium Kankernetwerk, University of Antwerp, Antwerp (BE)*



Slika 3: Akreditacija sudionika.
Izvor: autor

Predavači:

- Karin Dieckmann, *Radiation Oncologist, Medical University of Vienna, Vienna (AT)*
- Maria Hawkins, *Clinical Oncologist, University College London, London (UK)*
- Mischa S. Hoogeman, *Medical Physicist, Erasmus Medical Centre-Daniel den Hoed Cancer Centre, Rotterdam (NL)*
- Marta Bogowicz, *Medical Physicist. Maastro Clinic, Maastricht (NL)*
- Pietro Mancosu, *Medical Physicist, Humanitas Research Hospital (IT)*
- Piet Ost, *Radiation Oncologist, Ghent University, Ghent (BE)*
- Stephanie Lang, *Medical Physicist, University Hospital Zurich, Zurich (CH)*
- Suresh Senan, *Radiation Oncologist, VU University Medical Centre, Amsterdam (NL)*
- Sarah Barret, *Assistant Professor Radiation Therapy, Trinty College (IE)*

Implementation and Practice for Image-guided Stereotactic Body Radiotherapy

Abstract

At the end of May 2024, I applied for a scholarship through ENEN (European Nuclear Education Network) to participate in a training organized by ESTRO (European Society for Radiotherapy and Oncology) titled “Implementation and Practice for Image-guided Stereotactic Body Radiotherapy.” The training took place in Lisbon, Portugal. At the beginning of August, I received notification that my scholarship application had been accepted, which covered all expenses related to my participation. The training was attended by over a hundred participants, primarily oncologists, medical physicists, and radiology technologists (RTTs) from various parts of the world.

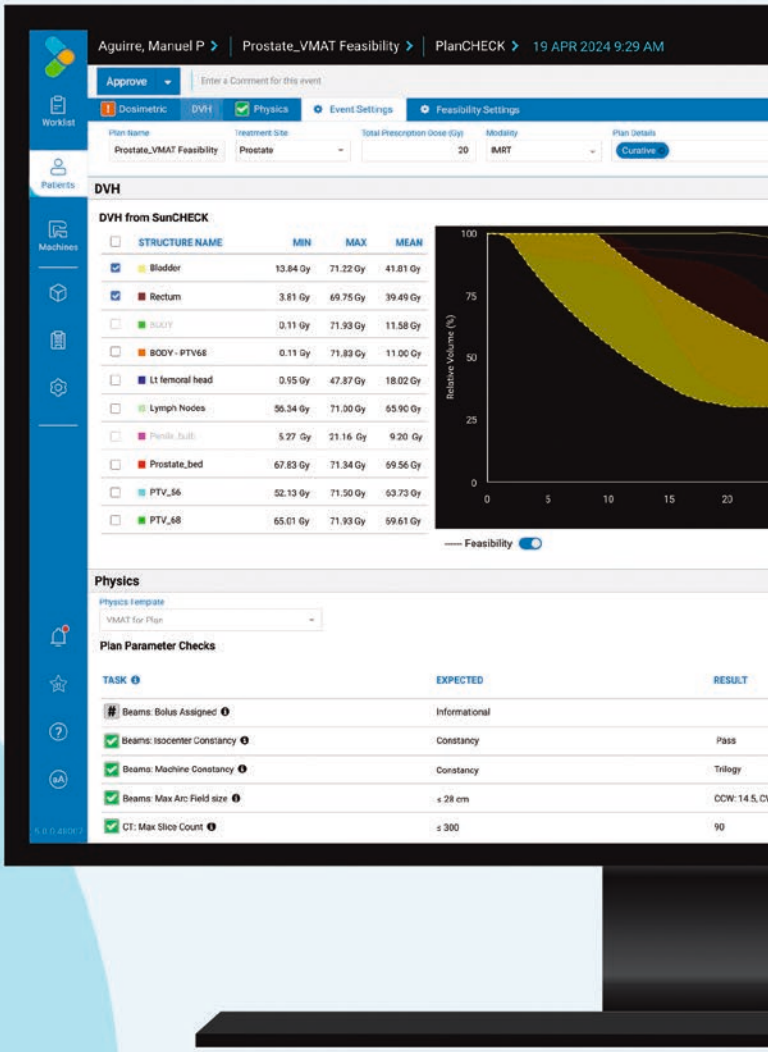
SunCHECK® 5.0

The Connected Workspace for Higher Quality

Aggregate insights, actions, and opportunities to drive continuous improvement in radiation therapy.

Featured enhancements:

- Plan complexity metrics
- Evaluation of plan feasibility per patient
- Enhanced TPS integration
- Refreshed UI with worklist focus



COMING SOON

Monte Carlo Secondary Dose Calculations

sunnuclear.com

SUN NUCLEAR
A MIRION MEDICAL COMPANY

medical intertrade

Web: www.medical-intertrade.hr
E-mail: medicinska-oprema@medical-intertrade.hr

Osvrt na Kongres “Dani radiološke tehnologije” i I. Simpozij studenata radiološke tehnologije

Mirela Buljan, Tanja Ljubić, Mihaela Mihanović, Antonija Mrčela, Magdalena Špar, Merima Zulić

Studenti Sveučilišnog odjela zdravstvenih studija, Sveučilišta u Splitu

Nakon sudjelovanja na našem prvom kongresu i simpoziju studenata odlučile smo napisati naš osvrt na cijeli događaj.

Prije svega bi istaknule da nam je bila velika čast predstaviti sebe i naš SOZS na I. simpoziju studenata radiološke tehnologije. Ovo nam je bio prvi susret sa studentima ostalih fakulteta radiološke tehnologije u Republici Hrvatskoj te smo mogli vidjeti i saslušati njihova izlaganja, ali i kroz razgovore razmijeniti međusobna iskustva o dosadašnjem obrazovanju i iskustvima s praktične nastave. Također bi zahvalile svim profesorima i mentorima koji su pripremali sve studente za ovaj događaj i pružili nam podršku za vrijeme naših izlaganja pred ostalim kolegama.

Što se tiče samog kongresa možemo reći kako smo kroz svaku prezentiranu temu na jedinstven način još više ušli u dubinu našeg budućeg zanimanja. Bilo nam je drago vidjeti da su prezentirali kolege koje rade ne samo na dijagnostičkim modalitetima već i u radioterapiji, nuklearnoj medicini i intervencijama jer je radiološka tehnologija prisutna gotovo u svim granama medicine i nudi nam mogućnost rada u brojnim područjima. Slušajući naše buduće kolege kako iznose svoja istraživanja i radna iskustva definitivno nam se povećala svijest o ozbiljnosti naše profesije. Najviše bi istaknule teme koje su bile usko vezane za nova saznanja, unaprjeđenje dosadašnjih načina rada i inovacija. Vjerujemo kako je to naša ne tako daleka budućnosti te smo si još više osvijestile važnost proučavanja znanstvenih radova i raznih istraživanja, a sve u cilju boljeg razumijevanja svih mogućnosti koje nam naša profesija pruža ponajviše napretkom tehnologije i razvojem umjetne inteligencije.

Za kraj bismo istaknule kako je naše prvo sudjelovanje na ovakvom događaju bilo prekrasno i edukativno te da se veselimo i nadamo ponovnom prisustvovanju na budućim kongresima.



Anela Bistrović, Laura Periša, Lovro Rukelj, Jana Stanivuković, Maja Svjantko

Studenti Zdravstvenog veleučilišta Zagreb



U danima od 25. do 27. listopada 2024. godine imali smo priliku sudjelovati na kongresu „Dani radiološke tehnologije“ i I. simpoziju studenata radiološke tehnologije. Bio je to prvi važan događaj u našem obrazovanju, čije je glavno pitanje „Jesmo li samostalni?“ potaknulo dodatnu želju u nama da budemo dio istog. Ispred studenata Zdravstvenog veleučilišta Zagreb, dobili smo priliku predstaviti, za nas u tom trenutku, bitne teme u okviru naše struke, „Što sve može ionizirajuće zračenje?“ i „Melanom“. Možemo reći kako smo zadovoljni odabirom tema, jer smatramo da su zainteresirale publiku, ali i da je bilo od iznimne važnosti osvijestiti ljude o prevenciji melanoma kao zloćudne bolesti te spomenuti Nacionalni program prevencije i ranog otkrivanja melanoma koji je aktivan u Republici Hrvatskoj. Temom „Što sve može ionizirajuće zračenje?“ iznenadili smo publiku, ali i sami sebe, otkrivajući gdje je ono sve prisutno u našim životima i zadobili brojne pohvale i pozitivne komentare. Isto možemo reći i za temu „Melanom“, unatoč tomu što ju mnogi ne bi direktno povezali sa strukom radioloških tehnologa. Za nas je rad na seminarskim radovima bio izazovan, ali u konačnici uspješno ostvaren uz pomoć mentora Damira Ciprića. Smatramo kako je mentor neizostavan dio tima, budući da je za nas takav događaj bio prvi takav u okviru fakultetskog obrazovanja te nas je netko trebao uputiti u izradu samih radnji, savjetovati nas za javni nastup, a prije svega dati uvijek dobrodošle kritike kako bismo bili što uspješniji. Bila je to za nas iznimna čast i pozitivno iskustvo te smatramo kako bi se takvi događaji trebali nastaviti i u budućnosti. Za nas



studente to je izvrsna prilika da pobliže upoznamo svijet koji nas očekuje tijekom naše poslovne karijere, uvidimo pozitivne i negativne strane naše struke, ali prije svega steknemo nova znanja kojih nikada ne nedostaje. Kongres nas je potaknuo da u budućnosti nastavimo biti dio tako velikih, bitnih i značajnih događanja za struku radioloških tehnologa.

Nina Franki

Sveučilište u Rijeci, Fakultet zdravstvenih studija

Sudjelovanje na simpoziju u Zagrebu bilo je za mene izuzetno pozitivno iskustvo. Kao studentici, bila mi je čast i zadovoljstvo prisustvovati prvom Simpoziju studenata radiološke tehnologije. Na tako važnom događaju bilo mi je uzbudljivo stati za govornicu i prezentirati svoj rad pred velikom publikom iz struke. Također sam imala priliku čuti mnogo novih i zanimljivih informacija, s mnoštvom vrijednih spoznaja iz prezentiranja radova ostalih sudionika Simpozija i Kongresa.” ■





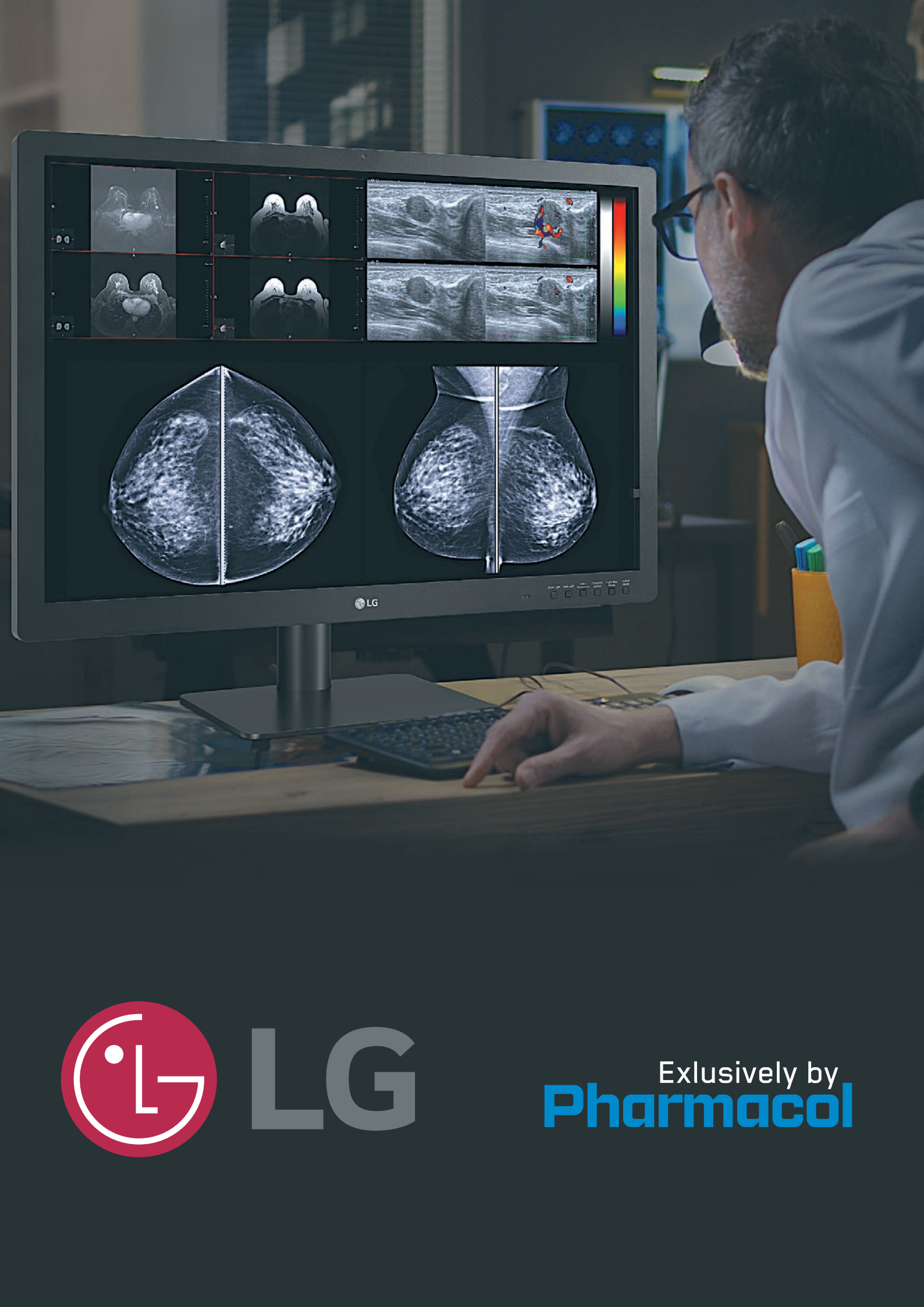


Dotarem®
Gadoteric acid

Optiray®
Ioversol

Xenetix®
Iobitridol

Powered by:
Pharmacol


LG
LG
Exlusively by
Pharmacol

Prevencija infekcije u radiološkoj dijagnostici

Autor: Tomislav Jovanić, mag. rad. techn. (KBC Osijek)

Infekcije povezane sa zdravstvenom skrbi su velik javnozdravstveni problem. U bolnicama, 1/15 pacijenata ima najmanje jednu infekciju povezanu sa zdravstvenom skrbi[1].

U suvremenoj radiološkoj dijagnostici, uz velik broj kompleksnih procedura te simultano snimanje ambulantnih i bolničkih pacijenata, prevencija infekcija i pravilno održavanje opreme su zahtjevan dio svakodnevnog posla. Na primjeru talijanskog istraživanja[2] (Torino, 2014) u 12 odjela za radiologiju, 91.7% uzorkovanih konzola i detektora i 41.7% rendgenskih cijevi bilo je kontaminirano. U istraživanju koje su proveli Balter S., Rodriguez MA., Pike JA. i Kleiman NJ. na olovnoj kontaktnoj zaštiti, dokazana je prisutnost mikroba u 50.8% slučajeva.[3]



ODRŽAVANJE I ČIŠĆENJE UREĐAJA U RADIOLOGIJI

Za dezinfekciju uređaja u radiologiji, kao i većine medicinskih neinvazivnih uređaja i opreme, preporučaju se sredstva na bazi etanola do 70% koncentracije. Svakako treba izbjegavati abrazivna sredstva i sredstva koja sadržavaju aceton, aldehide, silikon, derivate fenola…

Bacticid AF je dermatološki testirano, bezbojno, brzo djelujuće sredstvo na bazi etanola. Ima širok spektar baktericidnog, mikobaktericidnog, virucidnog i fungicidnog djelovanja. Otopina je spremna za uporabu (u bocama sa sprejom od 500 i 1000 ml, te kanister od 5l), a nakon nanošenja na željenu površinu, potrebno je pričekati 30 sekundi radi željenog učinka.

Osjetljive dijelove opreme, kao što su ultrazvučne sonde, monitori, RTG detektori, i sl. potrebno je održavati sredstvima koje ne sadrže alkohol, aldehide i fenole. **STERISEPT WIPES i DETROSAN HP WIPES** su dezinfekcijske maramice širokog spektra protiv bakterija (MRSA, VRE) virusa (HBV, HIV, HCV, Vaccinia, Rota), gljivica i spora. Mogu se koristiti na svim površinama koje toleriraju vodu. Maramice se mogu koristiti za invazivnu i neinvazivnu opremu.

HIGIJENA RUKU

Higijena ruku je najlakše provediva i najekonomičnija mjera sprečavanja infekcija povezanih sa zdravstvenom skrbi. Sukladno smjernicama za higijenu ruku[4], ruke treba prati tekućom vodom i sapunom kad su vidljivo prljave, odnosno kad su vidljivo kontaminirane krvlju ili drugim tjelesnim tekućinama i izlučevinama. Higijenu ruku treba provesti prije i nakon kontakta s bolesnicima, prije rukovanja invazivnim pomagalom za skrb oko pacijenta, nakon kontakta s tjelesnim tekućinama i izlučevinama, sluznicama, oštećenom kožom ili zavojima, nakon kontakta s okolinom (medicinskim uređajima) te nakon skidanja sterilnih odnosno nesterilnih rukavica.

Ecosoft wash lotion sensitive je losion za pranje ruku pod tekućom vodom. Pogodan je za sve tipove kože, pH neutralan, a sadrži alantoin i betain koji sprečavaju prekomjerno isušivanje kože. Ovaj losion nema boje i mirisa, te je zbog svog sastava namijenjen za osobe koje imaju osjetljivu kožu, učestalo peru ruke.

Alkoholni pripravci za utrljavanje su sredstva namijenjena za inaktivaciju mikroorganizama i privremeno sprečavanje njihovog rasta na rukama. Za higijensku dezinfekciju ruku, **Chemisept VIR+** se utrljava na prethodno oprane i osušene ruke, te se trlja dok se ruke ne osuše (30ak sekundi). Ovo sredstvo na bazi etanola sadrži i zaštitne faktore za ruke: pantenol, betain, 2 kokoat, glicerin.

Powered by:
Pharmacol

Popis literature:
1. European antibiotic awareness day. URL: https://antibiotic.ecdc.europa.eu/sites/default/files/documents/infographic-healthcare-associated-infections-patients-safety_HR.pdf
2. Giacometti M, Gualano MR, Bert F, Minniti D, Bistrot F, Grosso M, Siliquini R. Microbiological contamination of radiological equipment. Acta Radiol. 2014 Nov;55(9):1099-103. doi: 10.1177/0284185113512481. Epub 2013 Nov 22. PMID: 24270050.
3. Balter S, Rodriguez MA, Pike JA, Kleiman NJ. Microbial Contamination Risk and Disinfection of Radiation Protective Garments. Health Phys. 2021 Feb 1;120(2):123-130. doi: 10.1097/HP.0000000000001387. PMID: 33369969; PMCID: PMC7872069.
4. Kalenić S, Budimir A, Bošnjak Z, Acketa L, Belina D, Benko I i sur. SMJERNICE ZA HIGIJENU RUKU U ZDRAVSTVENIM USTANOVAMA. Liječnički vjesnik [Internet]. 2011 133(5-6). Dostupno na: https://hrcak.srce.hr/171740



9. RADIONICA OKRT

ZAŠTITA OD ZRAČENJA U RAZLIČITIM PODRUČJIMA RADIOLOŠKE TEHNOLOGIJE U REPUBLICI HRVATSKOJ

Organizator: Hrvatsko društvo radiološke tehnologije

11. – 13. travnja 2025.

Hotel Jezero
Plitvička jezera

Maksimalan broj sudionika: 70

Radionica je organizirana u suradnji sa:

- MUP RH - Ravnateljstvo civilne zaštite, Sektor za radiološku i nuklearnu sigurnost
- HKZR - Strukovni razred za zdravstvenu radiološko-tehnološku djelatnost
- Hrvatsko društvo za medicinsku fiziku i Hrvatsko društvo za zaštitu od zračenja
- Zdravstveno veleučilište u Zagrebu
- Sveučilište u Splitu - Sveučilišni odjel zdravstvenih studija
- Sveučilište u Rijeci - Fakultet zdravstvenih studija

Organizacijski odbor:
Damir Ciprić, Andrija Čop, Velimir Karadža, Maja Karić, Branko Kovalisko, Ivica Lisjak, Tatjana Matijaš, Helena Medvedec, Marija Surić Mihić

Znanstveno-stručni odbor:
Matea Brlošić, Krešimir Dolić, Dražen Horvatinec, Hrvoje Hršak, Matija Hranić, Ivana Kralik, Melita Kukuljan, Frane Mihanović, Vedran Manestar, Goran Roić, Matea Umbehend, Klaudija Višković, Nenad Vodopija

Ciljevi:
Definiranje radiološke sigurnosti i zaštite od zračenja u: dijagnostičkoj radiologiji, intervencijskoj radiologiji, radioterapiji, nuklearnoj medicini; aktualne preporuke i suvremeni standardi u zaštiti od zračenja; rasprava o ulozi djelatnika zaposlenih u zoni ionizirajućeg zračenja u razvoju i provođenju mjera radiološke sigurnosti.

Teme radionice:

1. Trenutno stanje i novosti u zaštiti od zračenja u radiologiji, radioterapiji i nuklearnoj medicini u RH
2. Radiološka sigurnost i korištenje zaštitnih pregača u suvremenoj digitalnoj radiografiji
3. Vrijedi li ALARA (ALADA) još uvijek u digitalnoj radiografiji?
4. Evaluacija online CBCT slika za pacijente s rakom prostate
5. Zaštita od zračenja u nuklearnoj medicini i rad s pripremom i aplikacijom radiofarmaka
6. Klinički audit u radiološkoj tehnologiji

SIEMENS Healthineers
Pharmacol
Swixx BioPharma

PROGRAM RADIONICE

Petak, 11. travnja 2025.

12:00 – 16:00 Registracija

16:30 – 18:00 Sesija I, moderatori: Tatjana Matijaš, Velimir Karadža

16:30 – 16:45 Zaštita od zračenja u različitim područjima radiološke tehnologije u RH, *Tatjana Matijaš*, *Velimir Karadža*

16:45 – 17:00 Radiologija i zaštita od zračenja jučer, danas, sutra, *Maja Karić, Sara Bezak*

17:00 – 17:15 Nuklearna medicina i zaštita od zračenja, *Helena Medvedec*

17:15 – 17:30 Zaštita od zračenja u radioterapiji, *Ivica Lisjak*

17:30 – 17:45 Utjecaj SAR-a na pacijente i osoblje: mitovi i činjenice, *Matija Hranić*

17:45 – 17:55 Sponzorirano predavanje, Contrast safety 2025 – Radiographers' Perspective, *Swixx Biopharma d.o.o.*

17:55 – 18:00 Zaključak prvog dana Radionice

Subota, 12. travnja 2025.

08:00 – 09:00 Registracija

09:00 – 10:00 Sesija II, moderatori: Branko Kovalisko, Matija Hranić

09:00 – 09:20 Fetalne doze pri medicinskom ozračenju: rezultati mjerenja i Monte Carlo simulacija u fantomu trudnice „Tena", *Dario Faj*

09:20 – 09:40 ALARA vs. ALADA, *Ivana Kralik*

09:40 – 10:00 Zaštita od ionizirajućeg zračenja prilikom rada s radioizotopima, *Grgur Šimunić*

10:00 – 10:20 Pauza za kavu

10:20 – 11:20 Sesija III, moderatori: Maja Karić, Damir Ciprić

10:20 – 10:40 Klinički audit - timski prema kvalitetnijem sutra, *Ivana Kralik*

10:40 – 11:00 Preporučena dozna ograničenja u operacijskim salama i kako ih odrediti temeljeno na realističnom radnom opterećenju C-luk uređaja i pozicijama radnika, *Dario Posedel*

11:00 – 11:20 Unaprjeđenje sustava dopunske izobrazbe i obnove znanja o primjeni mjera radiološku sigurnosti, *Antonia Bilić, Sektor za radiološku i nuklearnu sigurnost*

11:20 – 11:40 Pauza za kavu

11:40 – 12:30 Sesija IV, moderatori: Andrija Čop, Dražen Horvatinec

11:40 – 12:00 Primjena europskog konsenzusa o kontaktnoj zaštiti pacijenata u svakodnevnom radu, *Tomislav Jovanić*

12:00 – 12:15 Uloga ovlaštenih stručnih tehničkih servisa u zaštiti od zračenja, *Tea Turkalj*

12:15 – 12:30 Sponzorirano predavanje, *Pharmacol: Kvaliteta dijagnostičkih monitora u RH*

12:30 – 13:30 Panel diskusija – Imamo li suvremene standarde u zaštiti od zračenja u RH? moderatori: Ivana Kralik, Velimir Karadža

13:30 – 14:30 Pauza za ručak

14:30 - 16:00 TTT Radionica - Evaluacija online CBCT slika za pacijente s rakom prostate, moderatori: Ivica Lisjak, Matea Umbehend

14:30 - 14:45 Planiranje i provođenje radioterapije za Ca prostate, *Ivica Lisjak*

14:45 - 15:00 Radijacijska onkologija i zaštita od zračenja, *Goran Marošević*

15:00 - 15:15 Suvremeni pristup oslikavanju i verifikaciji položaja pacijenata za Ca prostate, *Aleksandar Kostovski*

15:15 - 15:30 Adaptivne tehnike za Ca prostate, *Marica Keser*

15:30 - 16:00 Okrugli stol, *moderatori: Aleksandar Kostovski, Vedran Manestar*

Nedjelja, 13. travnja 2025.

10:00 – 11:40 Sesija V, moderatori: Helena Medvedec, Nenad Vodopija

10:00 – 10:10 Sponzorirano predavanje, *AltheaLife: Zaštitna oprema u radiologiji*

10:10 - 10:25 Edukacija za rad na dijagnostičkim radiološkim uređajima - Siemens PEPconnect & SmartSimulator - Budućnost Online školovanja, *Ivica Mikulić*

10:25 - 11:40 Panel diskusija – Imamo li suvremene standarde u zaštiti od zračenja u RH – drugi dio

12.00 Završna riječ

ALTHEA LIFE INTERNATIONAL
SHIMADZU Excellence in Science
eurokontakt



Poštovani članovi Hrvatske komore zdravstvenih radnika i cijenjeni suradnici!

Osobito nam je zadovoljstvo i čast najaviti 6. Kongres radiološke tehnologije s međunarodnim sudjelovanjem u organizaciji Strukovnog razreda za zdravstvenu radiološko-tehnološku djelatnost Hrvatske komore zdravstvenih radnika. Kongres će se održati od 07. do 09. studenog 2025. godine u hotelu Olympia u Vodicama.

Vođeni idejom da prilikom odabira mjesta održavanja Kongresa radiološke tehnologije obiđemo cijelu Hrvatsku te na taj način učinimo sudjelovanje na kongresima podjednako dostupnim svim članovima, a sudionicima iz okolnih zemalja i svijeta približimo kulturna bogatstva i raznolikost naše zemlje, ove godine odabir je pao na predivne Vodice.

Nastavljajući tradiciju održavanja Kongresa diljem Hrvatske, s ciljem osiguravanja jednake dostupnosti stručnih skupova svim članovima te približavanja naše struke i kulture sudionicima iz regije i svijeta, ovogodišnji Kongres donosi još bogatiji i svestraniji program.

Svjesni smo činjenice da sve grane u kojima naša profesija djeluje doživljavaju stalne promjene u tehnološkom, stručnom, znanstvenom i organizacijskom smislu, što iziskuje kontinuirano učenje i primjenu novih spoznaja u svakodnevnoj praksi. Stoga smo ovogodišnji kongres koncipirali oko aktualnih i ključnih tema:

- **Dijagnostička radiologija**
- **Intervencijska radiologija**
- **Dentalna radiologija**
- **Radioterapija**
- **Nuklearna medicina**
- **Osiguranje kvalitete u radiološkoj tehnologiji**
- **Zaštita od zračenja**
- **Medicinsko pravo**
- **Menadžment u zdravstvu**

Smatramo da su susreti ovog tipa od velikog značaja u razmjeni iskustava te usvajanju novih spoznaja, ali i učvršćivanju položaja profesije u zdravstvenom sustavu. Stoga vas pozivamo da svojom nazočnošću i aktivnim sudjelovanjem doprinesete ovom značajnom stručnom događaju. . Aktivnim sudjelovanjem u predavanjima, panel diskusijama i radionicama, svi sudionici imat će priliku steći nova znanja i vještine, kao i doprinijeti daljnjem razvoju struke.

Očekivano međunarodno sudjelovanje kolega iz različitih zemalja dodatno obogaćuje program Kongresa te pruža priliku za uvid u globalne trendove i inovacije u radiološkoj tehnologiji.

Očekujemo, značajan odaziv kolega iz okolnih zemalja i regije te se radujemo razmjeni iskustava na međunarodnoj razini.

Radujemo se vašem dolasku u Vodice i vidimo se na 6. Kongresu radiološke tehnologije!

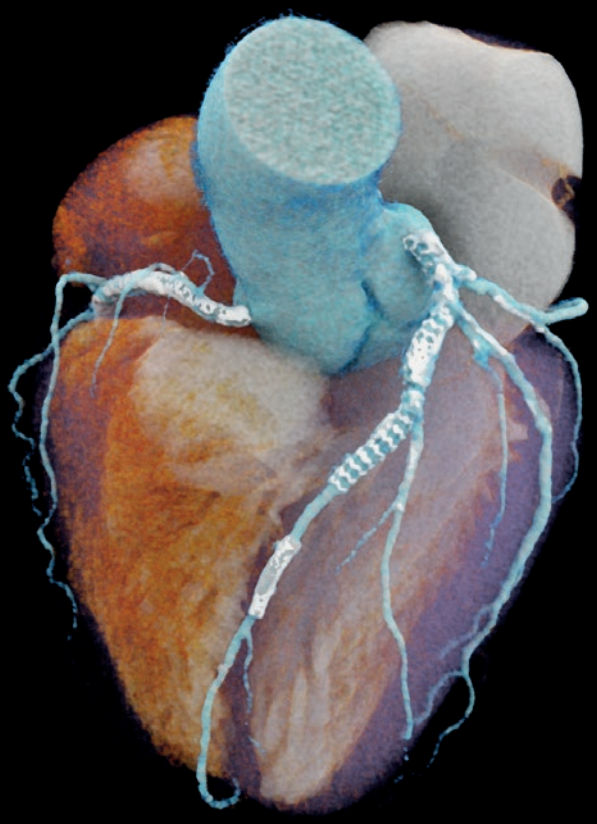
S poštovanjem,

Dopredsjednik Hrvatske komore zdravstvenih radnika,
Voditelj Strukovnog razreda za zdravstvenu radiološko tehnološku djelatnost

Miroslav Bašić, bacc.radiol.techn.

Redefine what is possible in cardiology

The world's first photon-counting CT



Courtesy of Universitätsspital Zürich, Zurich, Switzerland



NAEOTOM Alpha® with Quantum Technology

NAEOTOM Alpha is nothing less than the reinvention of computed tomography. Explore more.

siemens-healthineers.com/NAEOTOM-Alpha

SIEMENS Healthineers

SIEMENS Healthineers

Pharmacol

medical intertrade

SHIMADZU
Excellence in Science

Hrvatsko društvo
radiološke tehnologije

www.hdrt.hr